An investigation of the translocator protein as a biomarker of disease activity in rheumatoid arthritis



Nehal Narayan
Balliol College

Thesis submitted to the University of Oxford
for the degree Doctor of Philosophy

Trinity 2017

Supervisors:
Professor Afsie Sabokbar
Professor Peter Taylor

Abstract

It is now widely accepted that musculoskeletal imaging has a useful role to play in the early diagnosis of inflammatory arthritis, as well as providing a rapid and sensitive means of assessing treatment response, not only for individual patients in clinical practice, but also in clinical trials. However, the most frequently employed imaging modalities assess morphological changes in inflamed tissues. In contrast, Positron Emission Tomography (PET) generates images based on the detection of a desired molecular target of interest *in vivo*, and has been proposed to have potential as a highly sensitive and specific means of imaging inflammatory arthritis.

The major goal of the work documented in this thesis was to undertake a proof of principle pilot study to assess the ability of the purportedly macrophage-specific second generation translocator protein (TSPO) targeted PET tracer [^{11}C]PBR28, to detect and quantify synovitis in a small cohort of patients with inflammatory arthritis. Measures of tracer uptake were compared with clinical examination and ultrasound imaging, as standard means of assessment for evidence of synovitis. Additionally, the relationship between TSPO PET tracer signal and immunohistochemical staining for TSPO on synovial tissue samples was assessed. The positive correlation between TSPO tracer signal in the joint compartment and synovial tissue staining for TSPO, provided strong evidence that the tracer signal was the result of target expression, and not due to confounding factors.

In order to ascertain which cell groups in inflamed synovium were likely to be significant contributors to the TSPO PET signal observed in RA, an expression profiling of the tracer target (i.e. TSPO), in cell types comprising human pannus was conducted. Using immunofluorescence studies of human RA synovial tissue, *ex vivo* expression of TSPO on macrophages as well as fibroblast-like synoviocytes and CD4+ T cells was noted. By measurement of mRNA expression by real-time PCR, and TSPO protein quantification, using [^{3}H]PBR28 radioligand binding saturation assays, I have provided the first data comparing TSPO expression in major cellular components of human pannus. Collectively, data presented herein demonstrated that TSPO was not solely a macrophage specific marker in synovium. Rather, the most significant cellular contributors to TSPO PET signal were activated ‘M2 phenotype’ macrophages, and activated fibroblast-like synoviocytes. These findings establish the likely cellular correlates of the TSPO PET signal generated on imaging of inflamed joints in human RA.

Finally, this thesis also provided preliminary data regarding the expression of TSPO in macrophages of different phenotypes, and demonstrated a consistent downregulation of TSPO in macrophages polarised to the pro-inflammatory ‘M1’ end of a spectrum of macrophage phenotypes, whereas TSPO expression remained unchanged in macrophages of ‘M2 phenotype’. These novel findings suggest a role for TSPO in the negative regulation of inflammation, which we hypothesise is secondary to a function of TSPO in cholesterol transport within macrophages.

Acknowledgements

I am grateful to my supervisor Professor Peter Taylor for giving me the opportunity to undertake a DPhil, and for all his support and time. Likewise, I am indebted to my supervisor Professor Afsie Sabokbar, for her advice, feedback, and for her constant encouragement and support.

I am grateful to the staff in the Botnar Research Centre for their warmth, and kindness. Thank you to Drs Fiona McCann and Lynn Williams for imparting me with knowledge of how to process RA synovial tissue. I am grateful to Dr Stephanie Dakin, for teaching me immunohistochemistry and immunofluorescence. Thank you to Trish Green, Jenny Cole and Mike Goddard at the Kennedy Institute, in teaching me elutriation, and how to generate cryosections. Thanks to Drs Liye Chen and Tak Sekine, for teaching me flow cytometry, MACS, and for being a constant source of entertainment on long days in the lab. I am grateful to Dr Fernando Martinez and Graham Wells, for advising me on macrophage culture, and PCR.

I would also like to thank Dr Ronja Bahadori and Carol Cornelius, who helped me find my feet in the world of IRAS forms and REC applications. Thank you to Jo MacDonald, who despite her own busy schedule, made time to help me with my study visits. A huge thank you to Dr Francesco Carlucci, for all his support, and help with obtaining synovial tissue. Likewise, I am indebted to Dr James Teh for feedback with ultrasound, and for helping me learn synovial biopsy. Many thanks to Professor Hemant Pandit, for all his help with provision of healthy synovial tissue.

I owe a massive thank you to all the staff at Imanova; specifically, my study lead Dr Saleem Azeem, study nurse Rohini Akosa, and PET scientist Ryan Janisch. Likewise, I am indebted to Drs Lisa Wells and Erica Smyth for their generosity in having me in their lab, and teaching me radioligand binding work. I am much obliged to Dr David Owen at Imperial College, for all his kindness, advice, and for taking time to critique my work, showing me not only how to behave as a successful academic clinician, but also how to generate fruitful collaborations based on mutual respect and sharing of ideas. Thank you for believing in me.

I am indebted to Harpreet Mandhair, who has been a constant source of support, advice and fun, despite the challenges we have both faced in the past years. My time in research has been all the better for working alongside you. I am so lucky to call you my friend.

My path through research has not been a smooth one, for some reasons I expected, and many I did not. Thank you so, so much to my mum, dad and all my family whose unfailing support and faith I am eternally grateful for; thank you for showing me how to work hard, think laterally, and persevere when faced with adversity.

I would lastly, like to thank all the patients who participated in my study; it's been a privilege to be involved in your care over my time in Oxford. Without your kindness and generosity, this work would not have been possible.

Statement of originality

The data presented herein is my own work.

Statement of word count

The word count is approximately 50,000 words, not including references and appendix.

Table of Contents

Abstract 2

Acknowledgements 3

Statement of originality 4

Statement of word count 4

List of tables 10

List of Figures 11

Abbreviations 12

Structure of Thesis 15

CHAPTER 1 Introduction 16

1.1 Inflammatory Arthritis 17

1.2 Rheumatoid Arthritis 17

1.2.1 Diagnosis of RA 18

1.2.2 Treatment of RA 20

1.3. Imaging techniques for rheumatoid arthritis 22

1.3.1 Plain radiographs (X-rays) 23

1.3.2 Ultrasound (US) 24

1.3.2.1 Grey scale (or B-mode) ultrasound (GSUS) *25*

1.3.2.2 Power Doppler ultrasound (PDUS) *26*

1.3.2.3 Scoring systems for ultrasound *27*

1.3.3 Magnetic Resonance Imaging (MRI) 29

1.3.4 Computed Tomography (CT) 32

1.3.5 Nuclear Imaging 33

1.3.5.1 Planar scintigraphy and Single Photon Emission Computed Tomography (SPECT). *33*

1.3.5.2 Positron Emission Tomography (PET) *36*

1.4 The translocator protein (TSPO); distribution and potential functions 46

1.4.1 TSPO distribution 46

1.4.2 TSPO structure and functions in immune regulation 47

1.4.2.1 TSPO in cholesterol transport and steroidogenesis *49*

1.4.2.2 TSPO in apoptosis *51*

1.4.3 TSPO as an imaging target in PET 51

1. 5 Aims & objectives of DPhil thesis 53

CHAPTER 2 The utility of [^{11}C]PBR28 for the detection and quantification of synovitis; a proof of principle pilot study 54

2.1 Introduction 55

2.1.1 The evolution of Positron Emission Tomography Computed Tomography (PET-CT). 55

2.1.2 Development of tracers for PET 56

2.1.2.1 Choosing an appropriate ligand for PET *56*

2.1.3 The process of PET-CT image generation *in vivo* 57

2.1.3.1 The annihilation reaction and photon detection *57*

2.1.3.2 The scanning process *59*

2.1.4 PET tracer quantification 60
2.1.4.1 Visual assessment *62*
2.1.4.2 Standardised uptake value and Volume of distribution measures *62*
2.1.4.3 Volume of Distribution (V_T) *63*
2.1.5 The utility of TSPO targeted PET for the imaging of inflammatory arthritis 63
2.1.5.1 Second generation TSPO PET for the imaging of inflammatory arthritis *64*
2.1.5.2 rs6971 ..... *65*

2.2 Aims 66

2.3 Study design rationale 67
2.3.1 PET-CT 67
2.3.2 Rationale for inclusion of RA and PsA patients 68
2.3.3 Ultrasound and clinical examination 68
2.3.4 Synovial biopsy and immunohistochemistry 69
2.3.5 Genotyping study to assess study feasibility 70

2.4 Methodology 71
2.4.1 Recruitment for clinical study 71
2.4.2 Screening tests 72
2.4.3 DNA extraction 72
2.4.4 Genotyping assay for *rs6971* 73
2.4.5 Clinical examination and ultrasound 74
2.4.6 [^{11}C]PBR28 PET-CT procedure 74
2.4.6.1 Production of [^{11}C]PBR28 ..... *75*
2.4.6.2 Quality control checking of [^{11}C]PBR28 ..... *75*
2.4.6.3 PET-CT scanning patient preparation procedures *76*
2.4.6.4 [^{11}C]PBR28 PET scanning *76*
2.4.6.5 Analysis of PET data *76*
2.4.6.6 Arterial blood sampling *77*
2.4.6.7 Arterial blood processing *78*
2.4.7 Synovial biopsy 78
2.4.8 Immunohistochemistry 79
2.4.8.1 Optimisation of the primary antibody *81*
2.4.8.2 Quantification of staining *82*
2.4.9 Statistical analysis 83

2.5 Results 83
2.5.1 Analysis of patient specific potential confounding factors 85
2.5.2 Images of [^{11}C]PBR28 PET-CT 86
2.5.3 Volume of distribution (V_T) 86
2.5.4 Optimal time for [^{11}C]PBR28 SUV measurement 87
2.5.5 Comparison of [^{11}C]PBR28 uptake with ultrasound scores 89
2.5.6 Immunohistochemical analysis of synovium 90

2.6 Discussion 91

CHAPTER 3 An Investigation of TSPO expression in major cell groups of human RA pannus 96

3.1 Introduction 97
3.1.1 Human synovium in health and inflammation 98
3.1.1.1 The healthy synovium *98*
3.1.1.2 The synovium in inflammatory arthritis *99*
3.1.2 Main cell groups of RA synovium 101

3.1.2.1 Synovial macrophages ... *101*
3.1.2.2 Macrophage polarity in inflamed synovium ... *102*
3.1.2.3 Fibroblast like synoviocytes (FLS, synovial fibroblasts) ... *104*
3.1.2.4 T lymphocytes ... *105*
3.1.3 Cell markers in synovial tissue-distinguishing between fibroblasts and macrophages ... 107
3.1.3.1 Macrophage markers in synovium ... *107*
3.1.3.2 Fibroblast markers in synovium ... *108*
3.2 Aims: ... 109
3.3 Methodology ... 110
3.3.1 DNA extraction and genotyping ... 110
3.3.1.1 DNA extraction ... *110*
3.3.1.2 rs6971 genotyping ... *110*
3.3.2 Cell harvesting and culture ... 110
3.3.2.1 Isolation of FLS from synovial tissue ... *110*
3.3.2.2 Cell culture of FLS ... *111*
3.3.2.3 Isolation of healthy peripheral blood human monocytes for in vitro studies ... *111*
3.3.2.4 Purification of Lymphocytes ... *114*
3.3.2.5 Macrophage differentiation and stimulation ... *115*
3.3.2.6 Lymphocyte cell culture and stimulation ... *117*
3.3.3 Enzyme Linked Immunosorbent Assay (ELISA) ... 117
3.3.4 RNA extraction ... 118
3.3.5 cDNA synthesis ... 119
3.3.6 Real-time, quantitative Polymerase Chain Reaction (PCR) ... 119
3.3.7 Radioligand saturation binding ... 121
3.3.7.1 Preparation of protein lysates ... *122*
3.3.7.2 Radioligand concentrations ... *123*
3.3.7.3 Analysis of saturation binding data ... *124*
3.3.8 Autoradiography ... 125
3.3.8.1 Tissue acquisition ... *125*
3.3.8.2 Cryopreservation of tissue ... *125*
3.3.8.3 Preparation of gelatin-subbed slides for use in autoradiography ... *125*
3.3.8.4 Sectioning of tissue ... *126*
3.3.8.5 Autoradiography ... *127*
3.3.9 Immunohistochemistry and immunofluorescence ... 128
3.3.9.1 Tissue acquisition and generation of sections for staining ... *128*
3.3.9.2 Staining procedures ... *128*
3.3.9.3 Image acquisition and quantification of staining on immunohistochemistry ... *129*
3.3.9.4 Immunofluorescence (IF) staining ... *129*
3.3.9.5 Immunofluorescence imaging ... *131*
3.3.9.6 Isotype negative controls, and negative controls for staining ... *131*
3.3.10 Statistical analysis ... 133
3.4 Results ... 134
3.4.1 Tissue Autoradiography studies ... 134
3.4.1.1 [^{3}H]PBR28 signal is highest in those tissue samples with the most cellular infiltrate ... *134*
3.4.2 Immunohistochemistry studies ... 136
3.4.3 Immunofluorescence studies ... 138

3.4.4 *In vitro* mRNA and protein studies 140
3.4.4.1 PMA and ionomycin activated T Lymphocytes produce IFN-γ *140*
3.4.4.2 T Lymphocyte activation does not significantly alter TSPO expression *141*
3.4.4.3 TSPO mRNA and protein expression increases on differentiation of monocytes to macrophages *141*
3.4.4.4 TSPO expression in macrophages of different phenotype *142*
3.4.4.5 Activation of FLS with TNF-α or IL-1β for 24 hours induces IL-6 production *144*
3.4.4.6 TSPO mRNA and protein expression increases on activation of FLS *145*
3.4.4.7 Activated FLS and M2 macrophages possess the highest amount of TSPO in all cell groups and conditions analysed *146*

3.5 Discussion 149
3.5.1 Synovial tissue autoradiography 149
3.5.2 Immunofluorescence staining of synovial tissue 149
3.5.3 *In vitro* study of TSPO on main cell groups known to make up pannus 150

CHAPTER 4 A preliminary investigation of TSPO expression in macrophages of different phenotype 156

4.1 Introduction 157
4.1.1 Macrophages; origins and function in inflammatory disease 157
4.1.2 Macrophage activation and phenotypes 158
4.1.3 TSPO expression in macrophages 160
4.1.4 A potential role for TSPO in macrophage biology 162

4.2 Aims 163

4.3 Methodology 164
4.3.1 Isolation of healthy peripheral blood human monocytes for *in vitro* studies 164
4.3.2 THP-1 monocytes for *in vitro* studies 164
4.3.3 Isolation of synovial fluid monocytes from synovial fluid 164
4.3.3.1 Synovial fluid aspiration *164*
4.3.3.2 Preparation of synovial fluid *164*
4.3.3.3 Magnetic Activated Cell Sorting (MACS) *165*
4.3.4 Macrophage differentiation and stimulation 166
4.3.4.1 Differentiation of human monocytes to macrophages *166*
4.3.4.2 Activation of macrophages *166*
4.3.5 Cytospin slide generation 166
4.3.6 Immunofluorescence 167
4.3.7 RNA extraction, cDNA synthesis and Real-time, quantitative Polymerase Chain Reaction 167
4.3.8 Western Blots 169
4.3.8.1 Protein extraction *169*
4.3.8.2 Protein concentration assay *169*
4.3.8.3 Gel electrophoresis *170*
4.3.8.4 Transfer *171*
4.3.8.5 Immunodetection *171*
4.3.9 Radio-ligand saturation binding 172
4.3.10 Enzyme-linked immunosorbent assay (ELISA) of cell culture supernatants 173
4.3.11 Statistical Analysis 173

4.4 Results 174
4.4.1 TSPO expression on monocytes compared to macrophages 174

4.4.2 Activation of macrophages by M1 and M2 stimuli 175
4.4.3 TSPO expression in MDM treated with M1 or M2 stimuli 178
4.4.3.1 Immunofluorescence staining *178*
4.4.3.2 mRNA and protein expression studies *179*
4.4.4 Cholesterol efflux pathway components in macrophages treated with different stimuli 184

4.5 Discussion 186
4.5.1 Comparison of TSPO expression between monocytes and macrophages 186
4.5.2 Immunofluorescence staining of macrophages of different phenotype 187
4.5.3 In vitro mRNA and protein expression studies of MDM of different phenotype 188
4.5.4 A hypothesis for the role of TSPO in MDM signalling and functions 191

CHAPTER 5 Discussion and Concluding Remarks 195

5.1 The utility of [^{11}C]PBR28 for the detection and quantification of synovitis; a proof of principle pilot study 197
5.1.1 Study limitations 198
5.1.2 Further validation of [^{11}C]PBR28 as a means of measuring synovitis 200

5.2 An Investigation of TSPO expression in major cell groups of human RA pannus 202
5.2.1 Limitations and Further work 204

5.3 A preliminary investigation of TSPO expression in macrophages of different phenotype 206
5.3.1 Limitations and further work 209

5.4 Concluding remarks 211

5.5 Future studies 212
5.5.1 Clinical studies 212
5.5.2 Studies to further investigate the expression of TSPO in RA pannus 212
5.5.3 Studies to further investigate the role of TSPO in inflammation and macrophage function 212

References 214

APPENDIX 245
A1. Publications and Presentations 246
A2. Summary of study design and approval processes 247
A3. Real-time PCR 248
A4 Positive controls for staining 250
A5 Optimisation of autoradiography 251

List of tables

Table 1.1 The revised 1987 ACR classification criteria for RA……..*19*
Table 1.2 The 2010 ACR/EULAR classification criteria for RA……..*20*
Table 1.3 Advantages and disadvantages of plain radiographs as an imaging modality for inflammatory arthritis……..*24*
Table 1.4 Different ultrasound scoring systems for inflammatory arthritis……...*28*
Table 1.5 Advantages and disadvantages of ultrasound as an imaging modality for inflammatory arthritis……..*29*
Table 1.6 Advantages and disadvantages of MRI as an imaging modality for inflammatory arthritis……..*32*
Table 1.7 Summary of studies using scintigraphy/SPECT for imaging in RA patients……..*35*
Table 1.8 Summary of advantages and disadvantages of PET as an imaging modality for RA……*37*
Table 1.9 Summary of PET radioligands used thus far for the imaging of RA in humans……*39*
Table 1.10 Summary of main outcomes of studies of PET in RA aiming to detect and quantify synovitis, categorized according to tracer used……*41*
Table 1.11 Summary of main comparisons between PET and other imaging modalities, for the imaging of RA……*43*
Table 2.1 Summary of advantages and disadvantages of methods of measuring PET tracer uptake……..*61*
Table 2.2 Comparison of genotype frequency and patient demographics between arthritis patients and a similar population of healthy controls……...*71*
Table 2.3 Grey Scale and Power Doppler semi-quantitative scoring……*74*
Table 2.4 Summary of antibodies used for DAB immunohistochemistry (IHC)……..*80*
Table 2.5 Demographics of all participants……*84*
Table 2.6 Clinical details of all patients with inflammatory arthritis participating in the study……*85*
Table 2.7 V_T (Volume of Distribution) data for 6 arthritis study participants……*87*
Table 2.8 Summary of [^{11}C]PBR28 uptake measures ±SD (standard deviation), according to clinical synovitis severity score……*89*
Table 2.9 median SUVR of each joint compartment grouped according to ultrasound score……*90*
Table 3.1 Summary of most common cell groups present in RA synovium……..*100*
Table 3.2 Primer sequences used for *TSPO* mRNA expression studies……*120*
Table 3.3 Summary of fold changes of FLS stimulated with TNF-α or IL-1β after 24 hours stimulation……*121*
Table 3.4 Details of primary antibodies used in Immunofluorescence and Immunohistochemistry studies……*130*
Table 3.5 [^{3}H]PBR28 binding in fmol/mg in knee synovial tissue derived from six healthy controls and clinically mild to moderate inflamed knees of six patients with RA……..*135*
Table 3.6 summary of Pearson's correlates of number of immunopositive cells on immunohistochemical staining with [^{3}H]PBR28 specific binding, in RA synovial tissue……..*138*
Table 3.7 summary of *TSPO* mRNA fold change (relative to unstimulated T lymphocytes) and [^{3}H]PBR28 binding……..*148*
Table 4.1 Summary of macrophage functions……*157*
Table 4.2 Sequences of primers used for PCR……..*168*
Table 4.3 M1:M2 ratio of mean fold changes of M1 and M2 phenotype macrophage markers in healthy human peripheral blood MDM……..*176*
Table 4.4 Mean fold change *TSPO* mRNA expression in THP-1, healthy peripheral blood and RA synovial fluid MDM treated with LPS/IFN-ɣ, IL-4, dexamethasone or TGF-β1……..*181*

List of Figures

Figure 1.1 Representative example of MRI hand of a patient with rheumatoid arthritis……*31*
Figure 1.2 The 'transduceosome'……..*50*
Figure 2.1 The process of production of photons within human tissue from positron emitting radioisotopes……..*58*
Figure 2.2 Demonstration of two photons generated by the annihilation reaction leading to the recording of a coincidence event……*58*
Figure 2.3 Generation of light through a scintillation crystal and its subsequent passage through a photomultiplier tube to generate an electrical signal……*59*
Figure 2.4 Isotype control staining of RA synovial tissue……*82*
Figure 2.5 Representative example of CT, PET-CT images and SUV of tracer in 3 study participants……..*86*
Figure 2.6 example of SUV time activity curve for a study participant with RA……..*88*
Figure 2.7 Average tracer uptake for each joint imaged with [^{11}C]PBR28 PET, grouped according to clinical synovitis severity score……*89*
Figure 2.8 Serial sections of synovial biopsy tissue, depicting lining and sublining, each stained for H & E, TSPO, CD68 and CD163……*90*
Figure 2.9 Spearman's rank correlations between [^{11}C]PBR28 SUVR of biopsy compartment of arthritis patients and synovial tissue biopsy staining scores……..*91*
Figure 3.1 Haematoxylin and Eosin (H&E) stains of cryosections……*99*
Figure 3.2 H & E stained cryosection of knee synovial tissue from study participant with Rheumatoid Arthritis……..*99*
Figure 3.3 The main patterns of cellular infiltrate in RA synovial sublining……*101*
Figure 3.4 Representation of the expression of several markers on monocytes, macrophages and fibroblasts……..*107*
Figure 3.5 The set-up of the centrifugal elutriation apparatus……*113*
Figure 3.6 the three steps of separation of cells according to size and granularity by centrifugal elutriation……..*114*
Figure 3.7 A representative FACS of healthy monocytes, and healthy MDM after 7 days culture with 100ng/mL M-CSF……*116*
Figure 3.8 An example of a saturation binding curve……*122*
Figure 3.9 The Brandell Harvester……*124*
Figure 3.10 Example of order of sectioning of tissue on slides for use in autoradiography……*126*
Figure 3.11 Isotype control staining of RA synovial tissue……..*132*
Figure 3.12 Negative control staining of RA synovial tissue……*132*
Figure 3.13 Representative example of autoradiography study of RA synovial biopsy specimen……*134*
Figure 3.14 Representative autoradiography serial sections of a healthy control knee synovial biopsy specimen……..*135*
Figure 3.15 Specific binding of [^{3}H]PBR28 in fmol/mg in synovial tissue derived from six healthy controls and six RA patients……..*136*
Figure 3.16 Average number of immunopositive cells per section on DAB immunohistochemistry staining of synovial tissue……..*137*
Figure 3.17 representative images of total [^{3}H]PBR28 binding for RA and healthy synovium……*137*
Figure 3.18 Representative confocal immunofluorescence images of RA synovial tissue for macrophage markers……..*139*
Figure 3.19 Representative confocal immunofluorescence images of RA synovial tissue for PDPN and TSPO……..*139*
Figure 3.20 Representative confocal immunofluorescence images of RA synovial tissue for CD55, PDPN and TSPO……*139*
Figure 3.21 Representative confocal immunofluorescence images of RA synovial tissue for CD4, CD3 and TSPO……*140*
Figure 3.22 Evidence of IFN-ɣ release by unstimulated T cells versus T cells activated with PMA and ionomycin for 6 hours……..*140*

Figure 3.23 mRNA expression and radioligand saturation binding studies of unstimulated and treated CD4+ T lymphocytes……..*141*
Figure 3.24 Mean fold change mRNA expression of TSPO in unstimulated monocytes, and monocytes treated with 100ng/mL M-CSF for 7 days (M0 macrophages)……*142*
Figure 3.25 ELISA measurement of TNF-α (pg/mL) in supernatant of 'M1' macrophages (treated with LPS and IFN-ɣ) and 'M2' macrophages (treated with IL-4)……..*143*
Figure 3.26 Mean fold change mRNA expression of TSPO in unstimulated macrophages, and macrophages treated with 10ng/mL LPS plus 20ng/mL IFN-ɣ for 24 hours or 20ng/mL IL-4 for 24 hours……..*144*
Figure 3.27 Measurement of IL-6 in supernatant of cultured FLS……..*145*
Figure 3.28 mean fold change mRNA expression of TSPO and mean specific binding of [^{3}H]PBR28 to TSPO in FLS……*145*
Figure 3.29 summary of mRNA and [^{3}H]PBR28 binding data for all cell groups……..*147*
Figure 4.1 Diagrammatic representation of a proposal for new human macrophage nomenclature, to consist of M1, M2a, M2b and M2c phenotypes……*159*
Figure 4.2 functional subdivisions according to stimulation of human monocyte derived M-CSF macrophages within the existing M1-M2 spectrum concept……*160*
Figure 4.3 *TSPO* mRNA expression of monocytes compared to monocyte-derived macrophages……*174*
Figure 4.4 TSPO protein expression in monocytes and macrophages……*175*
Figure 4.5 Messenger RNA expression of M1 markers in healthy human peripheral blood MDM……..*177*
Figure 4.6 Messenger RNA expression of M2 markers in healthy human peripheral blood MDM……..*177*
Figure 4.7 The levels of TNF-α in supernatant of stimulated MDM……...*178*
Figure 4.8 Immunofluorescence staining of cytospin slides of healthy peripheral blood MDM……..*179*
Figure 4.9 *TSPO* mRNA expression of M-CSF differentiated MDM, treated with LPS/IFNγ, IL-4, dexamethasone or TGF-β1……*180*
Figure 4.10 *TSPO* mRNA expression of various MDM, treated with 10ng/mL LPS/IFN-γ, for 2,4,6 and 24 hours……*182*
Figure 4.11 Western blots assessing TSPO protein expression in MDM ± 10ng/mL LPS and 20ng/mL IFN-ɣ……*182*
Figure 4.12 Western blots assessing TSPO protein expression in untreated MDM, MDM with 24 hours of IL-4, dexamethasone or TGF-β1……*183*
Figure 4.13 [^{3}H]PBR28 tracer uptake expressed in fmol per 1x10^6 cells in healthy human peripheral blood MDM ± treatment with 10ng/mL LPS plus 20ng/mL IFNγ (LPS), or 20ng/mL IL-4……*183*
Figure 4.14 Relative *CYP27A1* mRNA expression of M-CSF treated healthy peripheral blood MDM……..*184*
Figure 4.15 Relative *ABCA1* mRNA expression of M-CSF treated healthy peripheral blood MDM……..*185*
Figure 4.16 Summary of Cholesterol trafficking pathway……*193*

Abbreviations

ABCA	ATP-binding cassette transporter
ACPA	Anti-Citrullinated Peptide Antibody
ACR	American College of Rheumatology
AS	Ankylosing Spondylitis
BCA	Bicinchoninic acid
BME	Bone Marrow Oedema
BSA	Bovine Serum Albumin
CD	Cluster of Differentiation
cDNA	complementary Deoxyribo-Nucleic Acid
CNS	Central Nervous System
CRP	C-Reactive Protein
CT	Computed Tomography
CYP27A1	Sterol-27-hydroxylase 1
DAB	Diaminobenzidine
DAS28CRP	Disease Activity Score 28-C-reactive protein
Dexa	Dexamethasone
ELISA	Enzyme Linked Immunosorbent Assay
ESR	Erythrocyte Sedimentation Rate
EULAR	European League Against Rheumatism
FACS	Fluroscence Activated Cell Sorting
FCS	Foetal Calf Serum
FLS	Fibroblast-like synoviocytes
GSUS	Grey Scale Ultrasound
H and E	Haematoxylin and Eosin
HRP	Horseradish peroxidase
HV	Healthy Volunteer
IA	Inflammatory Arthritis
IF	Immunofluorescence
IFN	Interferon
IHC	Immunohistochemistry
IL	Interleukin
kDa	kiloDalton
LPS	Lipopolysaccharide
MACS	Magnetic Activated Cell Sorting
M-CSF	Macrophage-colony stimulating factor

MCP	Metacarpophalangeal joint
MDM	Monocyte derived macrophage
MMP	Matrix metalloproteinase
MRC1	Mannose Receptor C type-1
MRI	Magnetic Resonance Imaging
mRNA	messenger Ribonucleic Acid
MTP	Metatarsophalangeal joint
OMERACT	Outcome Measures in Rheumatology
PBS	Phosphate Buffered Saline
PCR	Polymerase Chain Reaction
PDUS	Power Doppler Ultrasound
PET	Positron Emission Tomography
PIP	Proximal Interphalangeal Joint
PMA	phorbol 12-myristate 13-acetate
PsA	Psoriatic Arthritis
PTGS2	Prostaglandin endoperoxide synthase 2
RA	Rheumatoid Arthritis
RF	Rheumatoid Factor
RT-PCR	Real-time polymerase chain reaction
SJC	Swollen Joint Count
StAR	Steroidogenic Acute Regulatory Protein
SUV	Standardised Uptake Value
SUV_{max}	Maximal Standardised Uptake Value
SUVR	Standardised Uptake Value Ratio
TGF-β	Tumour Growth Factor beta
TGM2	Transglutaminase 2
TNF-α	Tumour Necrosis Factor alpha
TJC	Tender Joint Count
TNFα	Tumour Necrosis Factor alpha
TSPO	Translocator protein
US	Ultrasound
VA	Visual Assessment
VDAC	Voltage Dependent Anion Channel
V_T	Volume of Distribution
WCC	White Cell Count

Structure of Thesis

The following provides a summary outline of each chapter of this DPhil thesis:

Chapter 1 of this work introduces the main imaging techniques used in both clinical practice and research, for the imaging of rheumatoid arthritis. Here, evidence for the utility of PET for the imaging of rheumatoid arthritis (RA) is presented. The main functions of Translocator protein (TSPO), a purported molecular imaging target for RA synovitis, are also reviewed, as is its potential as a tool for PET imaging in RA.

Chapter 2 overviews the evolution of PET, as well as the different methodologies used to measure PET tracer uptake. This Chapter describes the design, methodology and results of a proof of principle pilot study, aiming to ascertain the ability of the second generation TSPO PET tracer [^{11}C]PBR28, to detect and quantify synovitis in a small cohort of patients with inflammatory arthritis, along with healthy control participants.

Chapter 3 provides the acquired data assessing the expression of TSPO in cells constituting pannus using human RA and healthy synovial tissue autoradiography and histology, in addition to mRNA (RT-PCR) and protein (radio-ligand binding) studies. These investigations were conducted using a number of *in vitro* cell cultures; lymphocytes, monocytes, macrophages and fibroblast-like synoviocytes, all in unstimulated and activated states.

Chapter 4 describes the TSPO expression in monocytes and macrophages of different phenotype. Such experiments utilised THP-1 monocytes, healthy human peripheral blood monocytes, and RA synovial fluid monocytes, employing RT-PCR, western blotting, and radioligand binding studies to assess TSPO expression.

Chapter 5 offers a detailed discussion of the overall findings and the proposed mechanistic role of TSPO in RA, its impact in potential treatment investigations into RA, the overall general conclusions, limitations of the investigations and plans for future studies.

CHAPTER 1

Introduction

1.1 Inflammatory Arthritis

Rheumatoid Arthritis (RA), along with Psoriatic Arthritis (PsA) and Ankylosing Spondylitis (AS) are the three most common forms of inflammatory arthritis(1). The estimated annual incidence of early arthritis ranges from 115-271 patients per 100,000 adults(2). The inflammatory arthritides are the result of autoimmune driven inflammation of the joints, likely triggered by interactions between multiple genetic and environmental factors, many of which are as yet, unclear(3, 4).

1.2 Rheumatoid Arthritis

RA is the most common inflammatory arthritis, affecting approximately 1% of the UK population (5), and continues to rank in the top 50 causes of disability worldwide (6). Women are more commonly affected than men. with a female: male ratio of 2:1 or 3:1 reported (7). RA can occur at all ages, but prevalence increases with age, reaching approximately 2% in adults aged over 60 (8).

Multiple factors are thought to be implicated in the aetiology of RA. Genetic factors have long been recognised to play a role in RA (as with other autoimmune diseases); certainly, there is a slight increase in RA prevalence in the first-degree relatives of patients with RA (9). Furthermore, identical twins share RA in about 12-15% of occasions, compared to a prevalence of 1% in the general population (10). The most strongly associated RA alleles code for Human Leukocyte Antigen (HLA) proteins which share a region of highly similar amino acid sequence, referred to as the ‘shared epitope’(11).

The relatively low concordance of RA in identical twins does suggest that non-genetic factors are also likely contributing to disease aetiology. Indeed, cigarette smoking is a well recognised environmental factor known to increase the risk of RA (12), especially in patients positive for anti-citrullinated C-peptide antibody (ACPA) (13, 14). Indeed, it is postulated that cigarette smoking in patients possessing the shared epitope may

promote the generation of ACPA, through the loss of tolerance to citrullinated autoantigens (15).

RA typically presents as a symmetrical polyarthritis of small joints of hands, with metacarpophalangeal (MCP), proximal interphalangeal (PIP) joints being involved. However, the metatarsophalangeal (MTP) joints, elbows, shoulders, ankles and knees are also commonly affected (16, 17).

1.2.1 Diagnosis of RA

The diagnosis of RA is largely clinical (18), aided by peripheral blood tests (both haematological, and biochemical), to provide supporting evidence of inflammation. Additionally, testing for the presence of autoantibodies is routinely performed, including testing for Rheumatoid Factor (RF) (IgM to Fc portion of IgG) (19) and anti-citrullinated C-peptide antibody (ACPA) (20). The presence of RF identifies those patients who are more likely to develop erosive arthritis, and who may have extra-articular manifestations (such as vasculitis and rheumatoid nodules) (19, 21). However, RF are not particularly specific for RA; RF are present in 5% of the healthy population, and in 10-20% of the ageing population (22). In contrast, ACPA have increased specificity for RA (21), and further can be present prior to clinical onset of joint inflammation (23).

Classification criteria for RA, such as the 1987 revised American College of Rheumatology (ACR) are a set of clinical and laboratory standards, initially established for use in epidemiology studies and clinical trials (24) (see **Table 1.1**). However, they are limited by poor sensitivity and specificity for the classification of patients with early inflammatory arthritis, as having RA. Therefore, in 2010, ACR and the European League Against Rheumatism (EULAR) devised new classification criteria for RA, including features of early RA (25).The 2010 ACR criterial assesses joint involvement, autoantibody status, acute phase response, and duration of symptoms (see **Table 1.2**).

The 1987 American College of Rheumatology classification criteria for Rheumatoid Arthritis*
1. morning stiffness (≥ 30 minutes) 2. arthritis of three or more joint areas 3. arthritis of hand joints (≥ 1 swollen joint) 4. symmetrical arthritis 5. rheumatoid nodules 6. serum Rheumatoid Factor (RF) 7. radiographic changes (erosions) *Four of these seven criteria must be present, and criteria 1-4 must be present for ≥ 6 weeks for a diagnosis of rheumatoid arthritis to be made.

Table 1.1 The revised 1987 ACR classification criteria for RA, adapted from *Arnett et al. 1988(24)*

The ACR/EULAR 2010 classification criteria for RA

1. Joint involvement (0-5)

1 medium/large joint (0)
2-10 medium/large joints (1)
1-3 small joints (large joints not counted) (2)
4-10 small joints (large joints not counted) (3)
more than 10 joints (at least 1 small joint) (5)

2. Serology (0-3)

negative RF and negative ACPA (0)
low positive RF or low positive APCA (2)
high positive RF or high positive ACPA (3)

3. acute phase reactants (0-1)

normal CRP and normal ESR (0)
abnormal CRP or abnormal ESR (1)

4. duration of symptoms (0-1)
< 6 weeks (0)
≥ 6 weeks (1)

Points are denoted in brackets.
Diagnosis of RA requires ≥6 points.

Patients can also be classified as having RA if they have:

i) typical erosions
ii) longstanding disease meeting the previous classification criteria

Table 1.2 The 2010 ACR/EULAR classification criteria for RA (25)

1.2.2 Treatment of RA

The treatment strategy for RA aims to achieve remission, or low disease activity, and prevent joint damage (26).

Corticosteroids are a long established treatment for RA, being capable of reducing synovitis, and improving signs and symptoms of arthritis, in the short term. They are capable of reducing joint damage, and can be used in combination with other

treatments in early disease (27). However, due to their side effects, corticosteroids are only recommended for short term use (26).
Synthetic Disease Modifying Anti-Rheumatic Drugs (DMARDs) still form the mainstay of first line treatment of RA in clinical practice (26). Synthetic DMARDs comprise a broad group of agents, including methotrexate, sulfasalazine, hydroxychloroquine, and leflunomide. The mechanism of action of these drugs still remains poorly understood (28). However, the efficacy of such agents has been established in placebo controlled drug trials (28, 29). Methotrexate is generally considered as a key first therapy initiated upon treatment of RA, either given alone, or in combination with other synthetic DMARDs (26).

For those patients failing to respond to synthetic DMARDs (after trialing two separate synthetic DMARDs, or a combination of DMARDs), the initiation of biologic DMARDs is recommended(26). Unlike synthetic DMARDs, the mechanism of action of biologic DMARDs is based on our knowledge of RA pathogenesis. The first such biologic therapy to be used successfully for the treatment of RA (30) are anti-TNF-α therapies, with TNF-α being described as a 'master regulator' in the complex cytokine network underlying the inflammatory processes in RA (31). Such agents comprise monoclonal antibodies directed to TNF-α (infliximab, adalimumab, certolizumab) or its receptor (etanercept).

However, it is well recognised that not all patients will respond to anti-TNF-α therapy. This has helped to drive the development of other biologic DMARDs ritixumab, tocilizumab and abatacept, all used in routine clinical practice today (26). Rituximab is a monoclonal antibody targeted to CD20, recognised to bring about amelioration of disease through B cell depletion (32). Tocilizumab (an IL-6 receptor antagonist) was first demonstrated to be efficacious at reducing disease activity in RA patients not responding completed to methotrexate (33), and now forms part of the armamentarium of biologics for RA in clinical practice. The fusion protein abatacept, blocks the costimulatory signal required for T cell activation, and was demonstrated to have efficacy in ameliorating disease in RA patients responding inadequately to anti-TNF-α therapy (34). The investigation of the efficacy of Janus kinase (JAK) inhibitors for the treatment of RA is currently underway, with the JAK inhibitor, baricitinib, being

demonstrated to be superior to both placebo and adalimumab in bringing about clinical improvement, in a recent phase III clinical trial (35).

1.3. Imaging techniques for rheumatoid arthritis

Early diagnosis of RA arthritis has long been established as essential to ensure prompt treatment, hence preventing permanent joint damage, comorbidity associated with chronic inflammation, and disability (36). The confirmation of the presence of synovitis is the main feature in the classification criteria of multiple inflammatory arthritides (25, 37), as well as for the scoring of disease activity (38). Likewise, accurate assessment of response to treatment is also dependent on the ability to detect synovitis. However, for the purposes of sensitive and specific detection of synovitis, clinical examination is increasingly recognized to be subjective; indeed, physical examination of joints for synovitis has been demonstrated to yield significant inter and intra-observer variability (39, 40).

Imaging is increasingly recognized as having an important role in providing objective, early evidence of synovitis to enable early diagnosis. Furthermore, imaging is increasingly used as an objective and sensitive means of assessing response to treatment early after treatment initiation. This not only has utility for individual patients; where the cost, and risk of adverse effects of new therapies are important considerations, but also for clinical trials of novel treatments, to help decide which experimental drugs are worth progressing to larger, later phase clinical trials.

Multiple imaging techniques have been used for the imaging of RA to enable diagnosis and monitor disease progression, with multiple modalities (such as X-rays, ultrasound and magnetic resonance imaging (MRI) demonstrating superior sensitivity to clinical examination (41, 42). Such imaging techniques rely on structural changes to detect inflammation(43). More recently, nuclear cellular imaging techniques, such as positron emission tomography (PET), have been investigated for their utility as a highly sensitive and specific means of detecting and quantifying synovitis.

1.3.1 Plain radiographs (X-rays)

The characteristic X-ray changes of established rheumatoid arthritis (RA) were first described in the 1940s (44). X-ray changes remained an important component in the diagnosis of RA for many years. This is reflected by the fact that erosions and peri-articular decalcification on hand and wrist X-ray were included in the 1987 ACR diagnostic criteria for RA (24). Common early plain X-ray changes in RA include non-specific tissue swelling and peri-articular osteopaenia (45), neither of which are pathognomonic for RA. The characteristic radiographic sign of marginal erosions is most often seen in the 5th MTP, likely as radiographic images of this area easily allow both anteroposterior and lateral views to be taken (45).

It is now acknowledged that X-rays of hands and feet are abnormal at first presentation in only 15-30% of patients (46, 47), a figure that is likely to continue to decrease as RA is diagnosed ever earlier in the course of the disease. Hence, radiographic changes now no longer form part of the diagnostic criteria for RA (25). Due to the association of erosions in RA with aggressive, damaging disease (48), the detection of erosions at diagnosis remains an important use of X-rays.

X-rays to monitor disease progression

For RA, X-ray changes in early disease have little correlation to functional outcome measures (49). However, damage seen on X- ray and functional status correlate significantly in those with established disease (arthritis of duration 5-8 years) (49). Multiple extensively-validated quantitative scoring systems for radiographs are available for the evaluation of RA. Such scoring systems evaluate different joints and bony features; the most widely used scoring methods are the Larsen and Sharp methods, along with further modifications (50-52). Although such scores may be feasible to undertake in the context of data analysis in clinical trials, the time and additional training for the employment of such scoring systems makes them impractical for use in routine clinical care (53).

Despite this, in the routine clinical monitoring of progression of joint damage over time, X-rays continue to be the gold standard imaging modality, aiming to determine the progression of erosions and joint space narrowing (54). This is due to its low cost, widespread availability, and ability to image multiple small joints speedily. Rather than utilizing quantitative scoring systems, in clinical practice, rheumatologists generally score radiographs qualitatively as to whether or not joint erosions and/or joint space narrowing are seen. **Table 1.3** summarises common advantages and disadvantages of the use of X-rays for the imaging of RA.

Advantages of plain X-rays
- cheap and widely available (55) - quantitative scoring systems widely validated for use in clinical trials (56) - can detect erosions, a characteristic sign of rheumatoid arthritis (57) - can reflect cumulative joint damage over time (46)
Disadvantages of plain X-rays
- low specificity of many radiographic changes (peri-articular osteopaenia and joint space narrowing are not specific to RA) (58) - low sensitivity in detecting early morphological changes associated with RA; ultrasound and MRI have been demonstrated to be superior in detection of soft tissue changes that tend to occur at early stages of RA (59, 60) - one dimensional images are generated, which can cause significant findings to be missed (55) - quantitative scoring is not practical for the clinical setting (53) - radiographs change slowly; at least 6 months is required to assess changes within a single patient (55)

Table 1.3 Advantages and disadvantages of plain radiographs as an imaging modality for inflammatory arthritis

1.3.2 Ultrasound (US)

The use of ultrasound as a medical diagnostic tool was first described in 1942, where Dussik attempted to use ultrasound to image brain lesions (61). Over a decade later, ultrasound was investigated for its ability to detect abdominal masses by Donald *et al*. (62).

Subsequently over the past two decades, both greyscale and power Doppler ultrasound have become valuable tools in the detection of early arthritis, and in assessing response to treatment in both clinical practice and research studies.

1.3.2.1 Grey scale (or B-mode) ultrasound (GSUS)

This technique relies upon the use of sonographic transducers to generate ultrasonic pulses, of frequency that is reflected by the tissues being imaged, in order to generate an image, in a monochromatic colour scale. Each soft tissue structure has different reflecting capabilities that affect its appearance on ultrasound (63). GSUS is utilized for visualization of anatomic structures, enabling visualization of synovial hypertrophy, effusion and bony erosions.

The first reported use of GSUS to demonstrate synovitis was in 1978, where ultrasound was used to delineate synovitis pre- and post- yttrium injection in knee joints (64). This was then rapidly followed by the use of ultrasound to guide a joint aspiration in a patient with RA (65), and subsequently to demonstrate effusion and synovitis in patients with active RA (66, 67).

Multiple studies have demonstrated the superiority of GSUS compared to clinical examination for the detection of synovitis (68-70). Furthermore, studies comparing ultrasound with MRI demonstrate the former has similar sensitivity in the detection of synovitis in the small joints of the hands. One study even demonstrated US to be superior to MRI, for the detection of effusion in PIP joints (71).

However, it is increasingly realized that a certain degree of grey scale change on ultrasound may not reflect inflammation in particular joints. Witt *et al*. in 2013 undertook a study of GSUS of MCPs, PIPs, MTPs and wrists in patients with RA, along with healthy controls, using a semiquantitative scoring system as described in Backhaus *et al.* (68) (see **Table 1.2**). The investigators found an average of 56.4% of all grey scale changes in RA patients, were a GSUS score of 1 (a small anechoic line beneath the joint capsule). However, 15% of all healthy control joints had a GSUS score of 1 too. Further, when the frequency of GSUS score of 1 in MCPs was

compared between patients with early RA, established RA, or healthy controls, no significant difference in frequency could be found (72). This suggests that low grade GSUS change may not be specific for synovitis.

1.3.2.2 Power Doppler ultrasound (PDUS)

This technique is based on the Doppler effect, relying on the change of frequency of a sound wave reflected back to the source when it encounters a moving object (73). Doppler technique detects the movement of red cells in blood vessels (74). Unlike simple colour Doppler, PDUS displays the total integrated Doppler power in colour, increasing the sensitivity to detect flow in small blood vessels, as well as low velocity blood flow (75). In 1994, the first study of PDUS was carried out by Rubin *et al*. indicating the superiority of PDUS to colour Doppler in demonstrating blood flow in the kidney, and the capability of PDUS to delineate hyperaemia (increased blood flow) in a torsive testicle compared to the contralateral normal testicle (76).

Not only is increased blood-flow a long-recognised feature of inflammation, but the formation of new blood vessels (angiogenesis) is essential for the expansion of inflamed synovial tissue in RA, with vessels further providing a portal of entry of circulating leukocytes into synovial sublining, potentiating inflammation (77). Therefore, PDUS may be a more objective and sensitive measure of inflammatory activity, particularly in early inflammatory arthritis, where structural changes of synovial thickening and effusion (best seen on GSUS) may not yet be fully apparent (78). Power Doppler may also be particularly useful in detecting active inflammation in those with longstanding inflammatory arthritis, where chronic synovial thickening may be present (78). The first description of the use of PDUS in musculoskeletal imaging was by Newman *et al.* who described hyperaemia detected by PDUS, in the joints of 23 patients with musculoskeletal pain (79).

The utility of PDUS is evidenced by the correlation of PDUS scores with histological signs of pannus (80), as well as with synovial enhancement on MRI (with PDUS being demonstrated to have a sensitivity of 88.8% and specificity of 97.9% compared to MRI (81)). Furthermore, PDUS has been demonstrated to have superior sensitivity to MRI

in the prediction of disease flare in RA patients with low disease activity, perhaps due to the fact that PDUS is detecting vascularity, a key component of active synovitis (82). The utility of PDUS for prediction of flare in psoriatic arthritis, has also been recently indicated by a 6-month longitudinal study of psoriatic arthritis patients in remission (83).

1.3.2.3 Scoring systems for ultrasound

In order to standardize ultrasound findings, the Outcome Measures in Rheumatology task force (OMERACT) endeavored to generate definitions of findings on ultrasound, such as tenosynovitis, synovial hypertrophy, synovial effusion and erosions (84).

Further employment of semi-quantitative ultrasound scoring systems aim to standardize the quantification of synovitis using grey scale and power Doppler ultrasound. Such scoring systems evaluate bony erosions, synovial hypertrophy, synovial effusion and vascularization. Currently, multiple scoring systems exist (detailed in **Table 1.4**), assessing different parameters in different groups of joints, and research is increasingly working towards a single internationally recognized scoring system.

Author	Parameters assessed by semi-quantitative scoring	Joints	No. of patients in first study
Wakefield *et al.* (85)	Bone erosion	Unilateral MCP II-IV	100
Szkudlarek *et al.* (86)	Joint effusion Synovial thickening Bone erosion PD activity	Unilateral MCP II, III, PIP II, MTP I, II	30
Scheel *et al*. (87)	Synovitis	Unilateral MCP II-IV, PIP II-V	46
Naredo *et al.* (88)	Joint effusion Synovial thickening PD activity	Sum of bilateral 60-,18-,16-, 12-, 10, 6-joint score	49
Backhaus *et al.* (68)	Synovitis Tenosynovitis/ paratendonitis PD activity Bone erosions	Unilateral wrist MCP II, III, PIP II,III, MTP II,V	120
Ellegaard *et al*. (89)	PD activity	Unilateral wrist	109
Dougados *et al.* (90)	Synovitis	Bilateral 28 joints vs 28 joints (28 + MTPs) vs 20 joints (20 MCPs + 20 MTPs)	76
Hammer *et al.* (91)	Synovitis Tenosynovitis PD activity Bursitis	Bilateral 78 vs 44, 28, 12, 7 joints	20

Table 1.4 Different ultrasound scoring systems for inflammatory arthritis. Adapted from Ohrndorf and Backhaus (84). PD=Power Doppler.

As ultrasound is increasingly used in the study of inflammatory of arthritis, its advantages and disadvantages are becoming increasingly apparent. **Table 1.5** summarises the advantages and disadvantages of ultrasound as a technique for imaging inflammatory arthritis.

Advantages of ultrasound:

- more accurate than clinical examination at detecting synovitis and effusion (68-70)
- relatively lower cost than other imaging modalities (59)
-no ionizing radiation exposure
- portable (ultrasound can be undertaken directly in outpatient clinics or at the patient's bedside, if needed)
- clinical examination can be performed at the same time as ultrasound, improving reliability of any correlations observed (59)

Disadvantages of ultrasound:

- thorough knowledge of anatomical structures is required from operators
- highly operator dependent (for example, selecting a probe of the incorrect frequency can lead to falsely negative or positive results, applying too much pressure can lead to suppression of Doppler signal), hence rigorous training is required to perform ultrasound accurately and reliably (74)
- interpretation of results (especially GSUS), can be subjective, and training is required to ensure the operator can interpret results according to desired standardized scoring practices (92)
- synovial hypertrophy on GSUS may not be specific to activity of inflammatory arthritis; indeed, a certain degree of grey scale change is acceptable in particular joints (for example weight-bearing joints, the first MTP) (93)
- numerous scoring systems currently being employed (59)
- time consuming to image multiple joints
- most commonly performed in 2 dimensions only, but 3-dimensional ultrasound increasingly being investigated for arthritis imaging (74)

Table 1.5 Advantages and disadvantages of ultrasound as an imaging modality for inflammatory arthritis.

1.3.3 Magnetic Resonance Imaging (MRI)

MRI relies on image generation through measuring the spatial distribution of specific nuclear spins (usually those of proteins) in the tissue being imaged (92). Electric signals from the spins are measured using processional motion of the proton spins after they are excited by radiofrequency pulses irradiated in a static magnetic field (43, 94). A radiofrequency coil, which generates an additional magnetic field perpendicular to the main field, acts as a receiver and transmitter. Such coils are of specific shape and size according to the body region being imaged. The part of the body being imaged is placed into the coil, and held immobile for the duration of the scan. The phenomenon in which the nuclear spins generate electric signals of a specific frequency in a static magnetic field is called nuclear magnetic resonance (92).

The evolution of MRI dates back to studies performed in 1938, where Rabi demonstrated that molecules in a magnetic field could be made to emit radio waves at specific frequencies (95). In 1971, Damadian used MRI to distinguish between normal and malignant tissue in rats (96). However, such data was one dimensional and lacked spatial information. In 1974, Lauterbur, and Mansfield described the use of magnetic field gradients for spatial localization of nuclear magnetic resonance signals(95), and by 1977, the first MRI image in humans was generated; a cross-section through a finger (95). The first study of MRI in RA was in 1988, describing a superiority of MRI to X-rays for the detection of carpal erosions (97). MRI allows assessment of both bony and soft tissue structures involved in inflammatory arthritis (43) and is also particularly useful for the detection of bone marrow oedema (BME), a likely herald of bone erosions (98). The ability to detect BME is a feature unique to MRI as an imaging technique (98, 99).

Several types of images can be generated in MRI for the imaging of joint structures. T1-weighted images take the least amount of time, and visualize the anatomy well, with fat appearing bright, and structures containing water appearing dark. For the imaging of synovium, pre- and post-gadolinium contrast obtained T1 images are often used, since the contrast will demonstrate hyperaemic synovium well, with the T1 images providing anatomical localization, to reduce any spatial resolution issues caused by diffusion of contrast into the surrounding fluid (43, 92). See **Figure 1.1A** for an example of T1-weighted images.

T2-weighted images depict water containing structures as bright, and fat containing structures as dark. T2 images are therefore useful for the detection of oedema in fatty tissue, and for imaging of arthritis, are particularly useful in detecting BME (43, 92). **Figure 1.1B** provides an example of T2-weighted images.

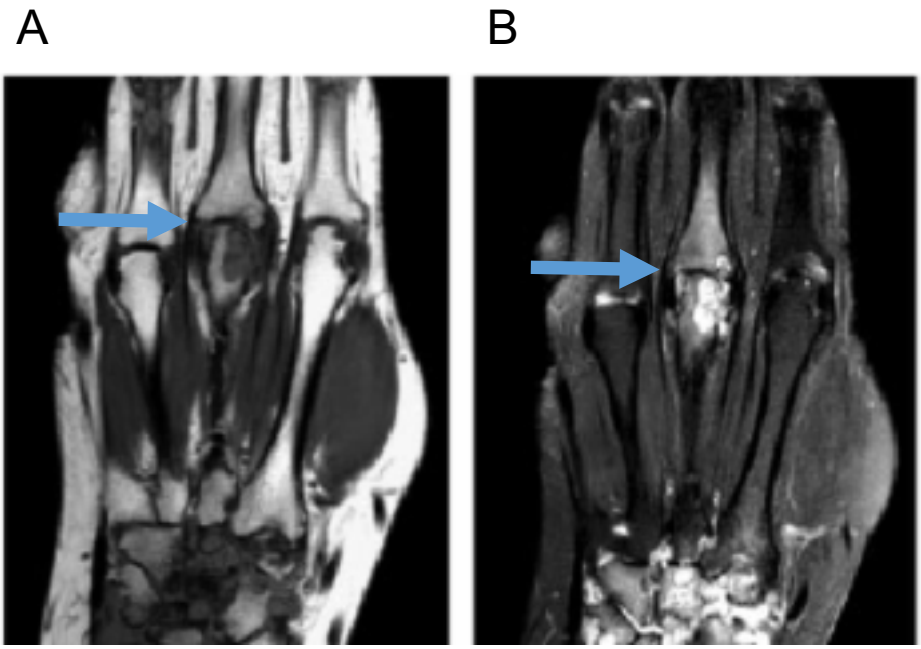

Figure 1.1 Representative example of MRI hand of a patient with rheumatoid arthritis **A** T1 weighted image, demonstrating synovitis in the 3rd metacarpophalangeal (MCP) joint (blue arrow) **B** T2 weighted image of the same hand demonstrating synovitis in the 3rd MCP joint, with bright area indicating likely BME (blue arrow).Image adapted from Sudol-Szopinska *et al.*(100)

Scoring of MRI pathology of RA (bone erosions, BME, synovitis) have been defined by OMERACT, leading to the generation of RA-MRI score (RAMRIS) (101, 102). Such a scoring system requires several different types of MRI images to build up an accurate picture of inflammatory arthritis. It is recommended imaging is taken in two planes (preferably coronal and axial), with T1- weighted imaging before and after the administration of a gadolinium based contrast material, and a fat saturated T2-weighted sequence, or a short inversion time inversion recovery sequence (STIR) (103).

MRI has been shown to be more sensitive for the detection of inflammation and destructive changes than clinical examination and X-rays by numerous studies (104-106). Indeed, in a 2-year longitudinal study of patients with RA, RAMRIS BME score was demonstrated to be superior to X-ray, DAS28 clinical disease activity scores and even anti-CCP antibody status in predicting bone erosion (107). Further, the measurement of synovitis by synovial thickness on MRI has been extensively validated by histological studies, demonstrating that synovial thickness on MRI correlates with macroscopic evidence of synovitis in knee joints and MCPs (108-111).

Multiple clinical studies have compared the effectiveness of MRI and ultrasound, as tools for the detection for synovitis, tenosynovitis and erosions. The majority of studies establish that MRI and ultrasound are at least comparable in their sensitivity of detection of changes, although multiple studies demonstrate MRI to be the more sensitive imaging technique, especially for bone erosions (60, 112, 113), although of course, ultrasound is unable to view BME, unlike MRI. **Table 1.6** summarises the main advantages and disadvantages of MRI for the imaging of RA.

Advantages of MRI:
- highly sensitive (114) - able to reliably calculate volumetric measurements of synovitis on MRI - 3-dimensional imaging possible (99) - can view both soft tissue inflammatory change and bony inflammatory change - uniquely able to detect BME, a feature of early inflammatory bone change (84) - no exposure to ionizing radiation (115) - able to view spinal inflammation
Disadvantages of MRI:
- long duration of scan, requiring immobilization of joints being imaged (115) - expensive compared to X-rays and ultrasound (59) - less widely available than plain radiographs or ultrasound (59) - can be uncomfortable for imaging of extremities due to use of coils (99) - contraindicated in patients with pacemakers, metallic implants (115) - administration of intravenous contrast can be invasive (115)

Table 1.6 Advantages and disadvantages of MRI as an imaging modality for inflammatory arthritis

1.3.4 Computed Tomography (CT)

CT is a tomographic imaging method that demonstrates calcified tissue with high resolution. It has long been considered the most sensitive modality for detecting bony erosions in RA (116), and indeed, has been used as a standard to validate the ability of MRI and ultrasound to detect bony erosion in RA (117), and its uses in rheumatology has been mainly directed towards spondyloarthritis, for the imaging of the spine to detect sacroileitis (118). However, in comparison with MRI and ultrasound, CT is poor at visualizing soft tissue changes in peripheral joints, which are an essential component of inflammatory arthritis, especially early in the course of disease.

Furthermore, for the imaging of inflammatory arthritis involving the spine, MRI continues to remain the investigation of choice, since it can visualize bone oedema (119), which can be a marker of future bone damage (120). CT also carries the disadvantage of ionizing radiation exposure, which makes repeated imaging of patients particularly undesirable.

1.3.5 Nuclear Imaging

Nuclear imaging encompasses imaging techniques employing radioactivity to visualize a molecular target or cellular process of interest(43).

The imaging techniques thus far, rely on morphological changes, to be useful tools for the imaging of rheumatoid arthritis. In contrast, nuclear imaging is able to provide functional information about disease activity *in vivo*(43).

By targeting inflammatory components of arthritis at a cellular level, nuclear imaging has the potential to be highly sensitive and specific to inflammation.

1.3.5.1 Planar scintigraphy and *Single Photon Emission Computed Tomography (SPECT).*

For both these imaging modalities, a gamma radiation emitting radioisotope is administered intravenously, followed by detection of the site of isotope accumulation using gamma cameras (92). All with all nuclear medical imaging techniques, development of these techniques started from early works where a Geiger counter was placed above the organ of interest in order to detect photons emitting from the administered radioisotope (121). With the development of scintillation cameras, it became possible to view an entire organ of interest at one time-point, greatly increasing the efficiency of detection of radiation emitting from the radioisotope (121). Planar scintigraphy detects photons (generated from gamma radiation) in a single plane, whereas SPECT (single photon emission computed tomography) detects photons from gamma radiation in multiple directions, through the use of an Anger

scintillation camera (as is the case with computed tomography) (122), but is more time consuming and costly than scintigraphy (121).

Over the years, multiple different gamma radiation emitting radioligands have been developed, targeted to specific components of inflammation, in order to image RA in humans using (see **Table 1.7** for a summary).

[^{99m}Tc]-HIG (polyclonal human IgG)
- demonstrated to accumulate in clinically inflamed joints in multiple studies of RA patients (123, 124)
- accumulated in joints of arthralgia patients with positive RF (pre-clinical RA), predictive of progression to clinical inflammation (125).

[^{99m}Tc]-RP128 (ligand for tuftsin receptors)
- aims to localise to sites of leukocyte recruitment through binding to tuftsin receptors on neutrophils and mononuclear phagocytes (126)
- able to visualize clinical synovitis in a study of 10 patients with RA (although lesser uptake also seen in joints of healthy controls) (127).

[^{99m}Tc]-HMPAO (hexamethylpropylene amine oxide)
- penetrates cell membranes and becomes trapped. Used to label patient's own neutrophils, which are then administered to detect areas of inflammation.
- correlation between [^{99m}Tc]-HMPAO labelled neutrophil accumulation in hands and feet of 21 RA patients, and number of clinically swollen joints

[^{99m}Tc]-anti E-selectin (targeted to the endothelial marker E-selectin)
- capable of delineating synovitis in RA, but high degree of background uptake in clinically inactive joints (128)

[^{111}In]-pentreotide (radioactive indium labelled form of octreotide)
- targeted to somatostatin receptors, known to be overexpressed in RA synovium (129, 130)
- uptake in inflamed synovium of 14 RA patients, with no uptake in healthy controls(129)

[^{99m}Tc]-OKT3 (Orthoclone OKT®3, an anti-CD3 antibody clone)
- in a study of 7 RA patients, uptake correlated with clinical findings, but did also accumulate in inactive joints (131)
- study complicated by adverse reaction of rigors and neck pain on isotope administration (131)

[^{99m}Tc]-MAX.16HS (an anti-CD4 antibody clone)
-Increased tracer uptake in arthritic joints in a study of 6 patients with active RA

[^{99m}Tc]-rituximab
- radiolabelled rituximab (monoclonal antibody to CD20) aims to visualize B cells. In a study of 20 patients with a variety of autoimmune diseases (including RA), uptake of the isotope was seen in most, but not all clinically inflamed joints in RA patients (132)

[^{99m}Tc]-adalimumab
-radiolabelled adalimumab was shown to accumulate in some, but not all clinically inflamed joints in a study of 10 RA patients (133).

Table 1.7 Summary of studies using scintigraphy/SPECT for imaging in RA patients.

Despite the fact that scintigraphy and SPECT can be targeted to molecular targets of interest, they are never likely to be able to compete with Positron Emission Tomography (PET) as a molecular targeted nuclear imaging technique (122). This is because the image quality generated by a PET scan currently far exceeds that of scintigraphy and SPECT, with superior spatial resolution for the same field of view, with PET additionally being up to ten times more sensitive than SPECT (122).
The radioisotope of choice for scintigraphy and SPECT is mainly [^{99m}Tc], due to its often lower radiation burden, and improved spatial resolution when used as a radioisotope to label ligands (43). However, due to a current global shortage in the manufacture of its precursor, molybdenum, there are concerns about the sustainability of [^{99m}Tc] based imaging (134).

1.3.5.2 Positron Emission Tomography (PET)

Positron emission tomography (PET) is a nuclear imaging modality utilising radiolabelled ligand ("radioligands"), to detect and measure cellular processes *in vivo* (135). Its history and principles are discussed in detail in **Chapter 2**. PET is performed in combination with a structural imaging modality (most commonly Computed Tomography (CT)), to provide detailed cross sectional anatomical images, on which the functional information can be superimposed (43), helping to provide far superior spatial resolution compared to the aforementioned nuclear imaging modalities of planar scintigraphy and SPECT (43). The main advantages and disadvantages of PET are outlined in **Table 1.8**.

Advantages of PET

- Highly sensitive detector of cellular markers of inflammation; may be useful for early assessment of response to treatment, and for early diagnosis of RA

- Can choose tracer depending on disease marker of interest (potential to tailor imaging according to pathogenic mechanisms within individual patients)

- Can image multiple joints rapidly; whole body [^{18}F]-FDG PET scanning takes about 30 minutes (136), whilst MRI assessment of all joints is impractical due to time constraints,.

Limitations of PET	*Current solutions*
Radiation exposure of subjects (from PET scan and from accompanying CT scan)	radiation exposure associated with PET/CT is in the same range as many CT scans used routinely in clinical practice (137). Through low resolution CT during the PET scan, radiation dose can be minimized. Hybrid PET/MRI instead of PET/CT will reduce radiation exposure (138, 139) ongoing developments resulting in increasingly sensitive PET scanners, will further reduce dose of PET tracer required to detect synovitis.
Poor spatial resolution of PET(140); may be problematic when imaging small joints of hands and feet	development of high resolution PET scanners for extremities (141) will further improve the anatomical localization of PET signal in small joints of RA patients Hybrid PET/MRI will further improve spatial resolution of images, as MRI visualizes early inflammatory changes in soft tissue and BME, which may further knowledge of what increased tracer uptake in an area reflects
Some PET tracers used in research have a short half-life (11-C has half-life of about 20 minutes (142)). These need to be used at the site of manufacture, which is not financially feasible for clinical use	^{18}F labelled ligands have a longer half-life (~110 mins) (143), therefore can be made in a central facility and transported for use on other sites.
Not all units have PET facilities	Development of ever smaller and cheaper cyclotrons may improve the availability of PET

Table 1.8 Summary of advantages and disadvantages of PET as an imaging modality for RA

Inflamed synovial tissue differs widely from healthy synovial tissue in cellular constituents, with hypertrophy of the lining layer, large quantities of infiltrating leukocytes, and new blood vessel formation (144-146). Because such cellular changes precede structural changes (43), the ability of PET to image inflammatory cellular components *in vivo,* makes it a potentially highly sensitive and specific means of assessing synovitis (43). Several studies have already shown PET may predict subsequent development of RA in patients without arthritis (147), predict development of joint destruction (148), and can be more sensitive and specific than MRI in detecting subclinical synovitis and predicting flare in those with known RA (149).

The most common PET tracer in clinical use is [^{18}F]-FDG , a radiolabeled glucose analogue (150). Through the ability of [^{18}F]-FDG to delineate inflammatory tissue surrounding tumours, the potential of [^{18}F]-FDG to assess inflammatory disease was recognized (151). Indeed, [^{18}F]-FDG is currently used in clinical practice to image vasculitis, such as giant cell arteritis (152, 153). As evidence grows to support the role of PET in imaging of inflammatory disease, it is increasingly recognized that [^{18}F]-FDG, as a marker of glucose metabolism, is not particularly specific to the process of inflammation. Hence, multiple further tracers have been developed targeted to more specific components of the inflammatory process in RA synovitis, including those targeted to macrophages (154), markers of bone metabolism (155), and angiogenesis (156). See **Table 1.9** for a summary of PET radioligands investigated thus far for use in the imaging of RA in humans.

Tracer	No. of studies	Target/mode of cellular uptake	Reason for tracer choice in imaging of inflammatory arthritis
[^{18}F]FDG	24	[^{18}F]FDG is taken up into cells by glucose cell surface transporters (151)	Reflects aerobic glycolysis, with increased uptake of [^{18}F]FDG in areas of inflammation (151)
[^{11}C]PK11195	4	Translocator protein (TSPO)	TSPO is a mitochondrial membrane protein, known to be highly expressed as a marker of macrophage activation (157). Since macrophages play a crucial role in pathogenesis of inflammatory arthritis (158), PET tracers targeted to TSPO have been proposed to be useful for imaging of inflammatory arthritis.
[^{18}F]-NaF	1	^{18}F ions exchange hydroxyl ions in bone crystals to form fluoroapatite (159)	[^{18}F]-NaF incorporates into bone by osteoclasts and osteoblasts, at sites of bone formation or remodeling(159). Pathological bone resorption by osteoclasts is a feature of RA (160), hence [^{18}F]-NaF may be useful for detecting active disease in RA.
[N-methyl-^{11}C]-D-deprenyl	1	As yet unknown binding site or exact mechanism of uptake in synovium	[^{11}C]-D-deprenyl is a ligand for monoamine oxidase B (MAOB) (161). Some evidence for accumulation in arthritic joints, but mechanism for this unknown. A blocking agent to MAOB administered to one patient failed to reduce tracer uptake in inflamed synovium, suggesting this may not be the binding site in such tissue for [^{11}C]-D-deprenyl (162).
[^{11}C]-Choline	1	Choline is taken up by dividing cells and phosphorylated by choline kinase to phosphorylcholine (163)	Proliferating cells have a higher demand for choline than resting cells (163). The importance of choline demand in inflammatory has been suggested by recent RA fibroblast and synovial fluid and tissue metabolomic studies demonstrating activation of choline metabolism in RA (164, 165). Therefore, may be a suitable imaging target for inflammatory arthritis.
[^{68}Ga]-PRGD2	1	targets $\alpha_V\beta_3$ integrin, a transmembrane heterodimeric receptor, a predominantly endothelial cell adhesion marker (166)	$\alpha_V\beta_3$-integrin has been identified as a key marker of angiogenesis in RA (166), with angiogenesis known to play a key role in inflammatory synovitis (77), hence tracers targeted to $\alpha_V\beta_3$-integrin may be suitable for the imaging of inflammatory arthritis.
[^{124}I]-rituximab	1	Rituximab is a monoclonal antibody to CD20 (32)	CD20 is a cell surface antigen highly and stably expressed on B cells, well recognized to have a pathogenic role in rheumatoid arthritis (32). The specificity of rituximab for its target may make it a suitable imaging marker for B cells in RA synovial tissue.

Table 1.9 Summary of PET radioligands used thus far for the imaging of RA in humans

Data has accumulated to demonstrate the utility of PET to assess RA; not only in detecting synovitis and assessing response to treatment, but also for the detection of subclinical diseases, and in early prediction of clinical disease course (see **Table 1.10** for a summary of outcomes of studies used to assess the ability of PET to detect synovitis in RA). Findings suggesting that PET may be a tool for early prediction of response to therapy in RA; indeed, Roivainen *et al.* demonstrated that [^{18}F]FDG PET was capable of detecting a response to treatment in peripheral joints as early as 2 weeks post initiation of triple therapy with disease modifying anti-rheumatic drugs in a cohort of RA patients (167). This highlights a potential utility of this imaging modality for early phase clinical trials, determining which experimental molecule is most likely to produce an amelioration of synovitis in RA.

Ability of PET to detect and quantify active RA

The majority of studies investigating the ability of PET to detect and quantify RA, utilized the tracer [^{18}F]FDG, with the next most frequently investigated tracer being [^{11}C]PK11195 (see **Table 1.9 and 1.10**). Clinical examination, disease activity scores, and other imaging modalities have all been utilized in such studies, to indicate presence or absence of inflammation (155, 167, 168). Several studies utilized histology from joints imaged to provide proof of tracer target expression in inflamed joints; in one study correlating this with tracer uptake (154, 156).

Tracer	No. of studies	Evidence for ability to assess active arthritis
[^{18}F]FDG	24	Increased [^{18}F]FDG uptake in clinically inflamed joints on visual assessment and semi-quantitative uptake scores (169-171). Multiple studies demonstrated significantly higher uptake of [^{18}F]FDG in patients with IA compared to healthy controls (172, 173).
[^{11}C]PK11195	4	[^{11}C]PK11195 uptake highest in clinically severely inflamed RA joints compared to non-inflamed (154). [^{11}C]PK11195 uptake in joints of patients with RA in remission was predictive of flare within 6 months (149). [^{11}C]PK11195 uptake in joints of ACPA positive patients with arthralgia was predictive of progression to clinical disease (147).
[^{18}F]-NaF	1	Uptake of [^{18}F]-NaF was significantly higher in erosive compared to non-erosive joints of RA patients ($p<0.001$) (44). Tracer uptake (measured as SUV_{max}) of [^{18}F]-NaF correlated with serum MMP-3, a known peripheral blood marker of joint damage (174).
[N-methyl-^{11}C]-D-deprenyl	1	In a 1997 study of PET/CT knees, all clinically inflamed joints demonstrated a regional high uptake of [N-methyl-^{11}C]-D-deprenyl compared to unaffected joints, within regions compatible with the anatomical location of synovium (162).
[^{11}C]-Choline	1	A Study of patients with IA (including RA and AS) underwent PET/CT of both knees with [^{11}C]-choline (175), with tracer accumulating to a greater extent in the synovium of clinically affected joints, compared with non-affected joints.
[^{68}Ga]-PRGD2	1	[^{68}Ga]-PRGD2 has been demonstrated to accumulate in clinically inflamed joints of a study of 20 RA patients, with less tracer uptake (on visual analysis) in OA controls (156).
[^{124}I]-rituximab	1	Uptake of [^{124}I]-rituximab was seen in 5/6 RA patients imaged, but not all clinically inflamed joints had uptake of tracer, and likewise, some clinically unaffected joints had high tracer accumulation on visual assessment (176).

Table 1.10 Summary of main outcomes of studies of PET in RA aiming to detect and quantify synovitis, categorized according to tracer used. SUV_{max}=standardized uptake value

Ability of PET to assess response to treatment of RA

Multiple studies have been conducted with the main objective of utilizing PET to assess treatment response in RA. Change in uptake of [^{18}F]FDG, as early as 2 weeks post treatment initiation for anti-TNF therapies (177, 178), methotrexate (139, 167), or combination of hydroxychloroquine, sulfasalazine, methotrexate and 10mg prednisolone daily (167), was noted to be capable of predicting response to treatment.

A study of [^{11}C]-D-deprenyl demonstrated a reduction in SUV of inflamed knees at 6-14 days post intra-articular steroid administration (162). Similarly, in clinical non-responders, PET corresponded to a lack of change in SUV or even an increase (155, 156, 179).

The fact that early changes in tracer uptake at 2 weeks after treatment correlated with later changes in more standard clinical measures of inflammation, such as change in DAS28 and CRP by 12 weeks of treatment (167), indicates that PET may be an early predictor of clinical response to therapy.

Comparison of PET with other imaging modalities

PET has been compared with multiple imaging modalities, in studies investigating PET as a tool for detecting synovitis, or for prediction of clinical course of disease (see **Table 1.11** for a summary of the main comparisons between X-rays, ultrasound and MRI and PET in studies of inflammatory arthritis). [^{18}F]FDG PET tracer uptake has been demonstrated to correlate with US measures of synovitis in studies of RA(172), with one study demonstrating highest correlation between PDUS and [^{18}F]FDG PET uptake measures(172, 177). Likewise, the uptake of both [^{18}F]FDG, and [^{11}C]Choline on PET also correlated with MRI measures of synovitis(175).

Imaging technique	Use of imaging techniques as comparators in PET studies
X–rays	**Detection of erosive disease**: Watanabe et al. demonstrated uptake of [^{18}F]NaF and [^{18}F]FDG were higher in RA joints with erosions on X-ray than non-erosive joints (155). **Detection of degenerative change:** to assess ability of PET to distinguish between degenerative disease and inflammation; Chaudhari *et al.* demonstrated [^{18}F]FDG uptake in the 1st CMC was associated with severity of OA grading on X-ray (141). **Prediction of joint damage:** [^{18}F]FDG SUV_{max} of large joints was higher in RA patients with progressive joint destruction on X-ray (180), with significant correlation between initial [^{18}F]FDG SUV of each joint and the progression of joint destruction 5 years later according to Larsen scores on X-ray ($r=0.47$, $p<0.01$) (181).
Ultrasound	**Detection of synovitis:** Synovial thickness on US was positively correlated with [^{18}F]FDG SUV (168, 172), with significantly higher [^{18}F]FDG SUV in power Doppler positive joints on US (172). Further work demonstrated good agreement between [^{18}F]FDG PET and US assessment of synovitis, with highest agreement between [^{18}F]FDG SUV and Power Doppler US ($\kappa=0.90$) (177). **Assessment of response to treatment:** change in [^{18}F]FDG SUV after anti-TNF therapy initiation did not correlate with change in synovial thickness on US (168). However, in the same study, change in US parameter after treatment initiation did not correlate with CRP or MMP-3, unlike change in [^{18}F]FDG SUV (168).
MRI	**Determination of anatomical site of soft tissue and synovial inflammation:** increased [^{18}F]FDG uptake at sites of synovitis and tenosynovitis as identified on MRI (139, 170), and a linear relationship between volume of enhancing pannus on MRI and [^{18}F]FDG tracer uptake (169). [^{11}C]choline uptake also correlated with synovial volume on MRI (175). **Determination of anatomical sites of inflammation related bone changes:** demonstration of co-localisation of [^{18}F]FDG with presence of oedema on MRI at sites of bony erosion in RA (156). **Assessment of response to treatment:** significant correlation between change in [^{18}F]FDG SUV at 4 weeks after anti-TNF initiation, and changes in MRI parameters (168). Although change in [^{18}F]FDG SUV correlated with CRP and MMP-3, MRI parameters did not (168). **Prediction of arthritis flare:** In a study of RA, Gent demonstrated that cumulative scores for [^{11}C]PK11195 PET differed significantly between patients who did and did not flare, whereas no significant difference was found for MRI scores (149).

Table 1.11 Summary of main comparisons between PET and other imaging modalities, for the imaging of arthritis. SUV_{max}=maximal Standardised Uptake Value, SUV= Standardised Uptake Value, CMC= carpometacarpal

Multiple studies of RA thus far have employed [^{18}F]FDG PET itself as a comparator for a novel PET tracer (155, 156, 175, 182). Comparing tracers in PET studies lends support to the fact that different tracers may reflect different components of the disease process, and thus may provide insight into disease pathogenesis (43). For example, in a study of RA patients by Watanabe. *et al.*, the wrist of one subject responded clinically to treatment. In this joint, [^{18}F]FDG uptake had decreased to an almost undetectable level (155). However, [^{18}F]NaF uptake in the same joint persisted. Furthermore, [^{18}F]NaF accumulated in more joints that were not clinically swollen than did [^{18}F]FDG (30% compared to 16%) (155). These observations may indicate that [^{18}F]NaF may be taken up in bony reparative processes as well as inflammation (155).

Ability of PET to distinguish between inflammatory and degenerative change in joints

In 2007, Elzinga *et al.* directly compared [^{18}F]FDG uptake between RA and osteoarthritis (OA) patients (183). Fibromyalgia patients were included as negative controls. [^{18}F]FDG uptake in RA and OA patients was significantly higher than in fibromyalgia patients ($p=0.01$ and $p=0.03$, respectively) (183). Although the number of PET positive joints in RA patients on visual analysis was significantly higher than those seen in OA patients ($p<0.001$), the degree of [^{18}F]FDG uptake in PET positive OA and RA joints were not significantly different [5.4 ± 1.2 in RA and 3.7 ± 1.7 in OA patients] (183). Two further studies have demonstrated increased [^{18}F]FDG uptake in joints known to have OA on X-ray (155, 171). These results indicate that [^{18}F]FDG PET of single joints or joint regions may not differentiate between RA and OA.

The tracer [^{18}F]-NaF has also been investigation in typical OA sites in patients with RA, being found to accumulate at some sites of typical OA lesions (such as osteophytes) in the hand (155), although as this was in RA patients, this could be attributed to subclinical RA.

With the development of further tracers, targeted to increasingly specific markers of disease pathogenesis in RA, it is possible in the future that PET could distinguish between RA and OA joints more accurately.

Detection of subclinical disease and prediction of clinical outcome by PET

The ability of PET to detect subclinical joint inflammation has been most thoroughly assessed using the tracer [^{11}C]PK11195 (147, 149). Uptake of [^{11}C]PK11195 in clinically non-inflamed joints of arthritis patients is significantly higher than in healthy controls, indicating that this tracer may be capable of detecting subclinical disease.

A further study of patients with known RA, in clinical remission, aimed to assess the ability of [^{11}C]PK11195 to detect subclinical synovitis. Here, 29 patients underwent PET/CT hands and wrists (along with MRI) and were then followed up for 3 years. Analysis revealed that 16 patients with RA in remission had at least one joint with high [^{11}C]PK11195 tracer uptake at baseline; 69% of these patients (11/16 with a joint with high tracer uptake at baseline) developed a flare during follow up. 46% (6/13) with a negative PET also developed a flare, but in 2 of these patients, the flare was localized outside the regions imaged by the PET scan. All 3 patients who developed a flare within 6 months had increased uptake of [^{11}C]PK11195 in between 6-24 joints at baseline. Those who had fewer joints demonstrating tracer accumulation at baseline, developed a flare after 6 months. No patients with a negative PET developed a flare within 6 months (184).

Several studies also demonstrate the ability of PET to predict joint destruction in RA. Suto *et al.* undertook a study of 23 patients with RA, who underwent [^{18}F]FDG PET of large joints, with X-rays at 6 months (181). SUV_{max} at baseline was positively associated with progression to joint destruction on X-rays at 2 years (OR 1.350, 95% CI=1.013-1.798). Additional support for the ability of [^{18}F]FDG PET to acts as an early predictor of destruction of large joints was provided by Yonemoto *et al.*; here 42 RA patients underwent [^{18}F]FDG PET and X-ray of large joints (148). X-rays were subsequently repeated 5 years later in 19 patients. After excluding joints with advanced destruction (Larsen grades 4 and 5) on X-ray at the time of the PET scan, a significant correlation was found between the initial SUV of each joint, and the progression of joint destruction 5 years later ($r=0.47$, $p<0.01$) (148). Significant correlations between SUV and progression of joint destruction were observed in both loadbearing and non-loadbearing joints ($r=0.52$, $p<0.01$ and $r=0.52$, $p<0.01$, respectively). Logistic regression demonstrated that higher SUV and lower

prednisolone dose were associated with greater risk of progression of joint destruction (148).

Watanabe *et al.* also demonstrated that uptake of the tracer [^{18}F]-NaF in joints of the hands and wrists of RA patients prior to biologic commencement or switching, was independently associated with radiographic progression on X-ray at 6 months, whereas physical examination and DAS scores were not (155). The sum of SUV_{max} for [^{18}F]NaF correlated with serum MMP-3 levels, already previously demonstrated to be capable of predicting joint destruction (174).

1.4 The translocator protein (TSPO); distribution and potential functions

Translocator Protein (TSPO) is an 18kDa cholesterol transporter, localised to the outer mitochondrial membrane (157). It was first identified in 1977 during the investigation of central benzodiazepine receptor (CBR) distribution in the brain (185). In this study another type of benzodiazepine receptor was identified using rat kidney tissue as a control during CBR studies, which also bound the benzodiazepine radioligand ^{3}H-diazepam, and was termed the Peripheral Benzodiazepine Receptor (PBR) (186) (185). Subsequent studies demonstrated PBR to be structurally and physiologically distinct from the CBR, with potential function as a transporter protein. Therefore, in 2006, PBR was renamed to Translocator protein (TSPO) (187). The identification of high expression of TSPO on infiltrating macrophages in areas of inflammation in both humans and animal models, predominantly in studies of the brain (188-193), has furthered interest in TSPO as an imaging marker for inflammatory disease.

1.4.1 TSPO distribution

The TSPO gene is found on the 22q13.31 chromosome in the human genome as a single copy (157). TSPO appears to be conserved throughout evolution, emphasizing the importance of its function.

TSPO itself is found in most tissues, but in normal conditions is thought to be expressed at the highest level in steroid synthesizing cells (187). Previous steady-state mRNA profiling demonstrated that *TSPO* mRNA is present in all tissues, and correlates with reported protein expression levels (157). Steady-state mRNA levels are high in adrenal tissue and other steroid synthesizing cells, kidney, spleen, skeletal muscle and lung, intermediate in heart and testicles and low in the liver and brain (157). TSPO has been long established to be highly expressed on macrophages (194, 195). Indeed, in a study of TSPO protein expression on healthy human PBMCs, expression of TSPO was highest on macrophages and monocytes; up to 1000 times more than expression on erythrocytes and platelets, and 7 times higher than on lymphocytes (195).

In disease states, TSPO has been demonstrated, in multiple studies, to be highly expressed on infiltrating macrophages at sites of inflammation (157, 187). High TSPO protein expression on macrophages has been found in human CNS inflammatory lesions in traumatic brain injury (196), in multiple sclerosis (197), and in Alzheimer's disease (198). Macrophages expressing high levels of TSPO have also been found in atheroma in carotid artery disease (199). In addition, TSPO protein has been found to be highly expressed in inflammatory tissues associated with tumours, being significantly upregulated in breast, prostate, colon and brain cancers, with higher TSPO expression being linked to tumour formation and cancer progression (157, 189).

More recently, uptake of the TSPO specific tracer [^{11}C]PK11195 in the knee joints of RA patients was found to correlate with synovial biopsy staining for the macrophage marker CD68 (154), indicating the potential utility of TSPO as a macrophage marker of synovitis.

1.4.2 TSPO structure and functions in immune regulation

Since TSPO is membrane bound, its structure has been difficult to study. However, electron cryomicroscopy and single-particle helical reconstruction have described TSPO to consist of a pair of TSPO monomers that form a highly associated dimer, with each monomer consisting of five transmembrane α-helices arranged to form a channel, thought to be implicated in cholesterol transport (200). It has also been suggested that ligand binding can induce changes in the organization of TSPO, and

TSPO polymerization, but the functional significance of this has not yet been confirmed (201).

The importance of TSPO remains the subject of intense debate. For decades, attempts to knock out TSPO were lethal during embryonic development, reinforcing the notion that TSPO was essential to steroidogenesis and mitochondrial function *in vivo* (157). More recently, however, *Banati* et al. developed a viable global murine TSPO knockout (202), followed 2 years later by *Wang* et al.(203), who did the same. Such TSPO knockouts survived to adulthood, with no apparent development defects or cholesterol metabolism disorders, although mitochondrial ATP production was reduced(202).

Multiple studies have provided indirect evidence for a role for TSPO in inflammation. For example, one *in vitro* study suggested TSPO promoted chemotaxis, with an increase in human monocyte recruitment generated by stimulating TSPO (204). In another study a rat model of inflammatory bowel disease, TSPO ligands were found to increase local expression of the chemoattractant cytokine, CINC-1 (Cytokine-induced neutrophil chemoattractant-1) (205).

Further, TSPO was implicated in the generation of a pro-inflammatory phenotype in a study of peritoneal mouse macrophages; here the authors observed that chlorodiazepam (a supposedly TSPO specific ligand) suppressed the production of TNF-α by macrophages in response to LPS (206). However, it must be noted that the TSPO ligand PK11195 had the opposite effect on the same macrophages (206), hence it is unclear from this study whether TSPO truly potentiates or negatively regulates the generation of a pro-inflammatory macrophage phenotype. Certainly, a later study by Torres *et al.* demonstrated that TSPO ligands PK11195 and Ro5-4864 (a chlorodiazepam based ligand) (207) inhibited the generation of carrageenan-induced mouse paw oedema (207). The same study went on to use a mouse model of carrageenan-induced pleurisy to demonstrate a reduction influx of neutrophils, and amount of pro-inflammatory cytokines IL-6 and IL-13, in pleural exudate, on treatment with the same TSPO ligands (207).

The most widely recognized function of TSPO is in the transport of cholesterol into mitochondria, postulated as being essential for endogenous steroid production(157, 192). Additional studies also support a role for TSPO in apoptosis(157, 192).

1.4.2.1 TSPO in cholesterol transport and steroidogenesis

The best-characterized function of TSPO is its role as a cholesterol transporter, regulating the passage of cholesterol through mitochondrial membranes, which is proposed as the rate-limiting step in steroid biosynthesis (157, 208). There is a large body of evidence to support the role of TSPO in steroidogenesis; indeed, in one study, disrupting *TSPO* gene expression in the rat Leydig cell line, inhibited steroidogenesis in these cells (209). Similarly, activation of TSPO using exogenous TSPO ligands has been demonstrated to stimulate steroidogenesis in steroid producing cell lines of animal models in multiple studies (210-213).

Cholesterol is the sole precursor of steroids. Steroid synthesis is initiated at the inner mitochondrial membrane (IMM), where the cytochrome P450 cholesterol side chain cleavage enzyme (CYP11A1) catalyzes the conversion of cholesterol to pregnenolone; which then enters the endoplasmic reticulum of the cell where further enzymatic reactions occur to produce the final steroid product. As transport of cholesterol from the outer mitochondrial membrane (OMM) to the IMM is the rate-limiting step in steroid production, the ability of cholesterol to move into mitochondria determines the efficiency of steroid production (214).

The protein-protein interactions involved in cholesterol transport are numerous and complex. The collection of hormone inducible steroidogenic proteins has been dubbed the ‘transduceosome’ (214) (see **Figure 1.2**). The binding of trophic hormones to G-protein coupled receptors in cell membranes leads to cyclic AMP formation (c-AMP). This then induces the activity of PKA (protein kinase), which then phosphorylates the proteins Star (steroidogenic acute regulatory protein) and PAP7 (peripheral benzodiazepine receptor-associated protein 7 (214, 215)). Star interacts with cholesterol to direct it to the OMM. At the OMM, Star interacts with TSPO, with TSPO having as yet unknown effects on this protein, to increase Star activation, thus further

increasing cholesterol transport to the mitochondria. The activated PAP7 interacts with TSPO, functioning as an A Kinase Anchoring Protein (AKAP). AKAPs aim to confine the activity of PKA enzyme, and PAP7 brings PKA to the OMM, in closer proximity to proteins mediating cholesterol transport, allowing PKA to regulate activity via phosphorylation more efficiently, reducing the amount of c-AMP needed to stimulate steroid production(214, 215).

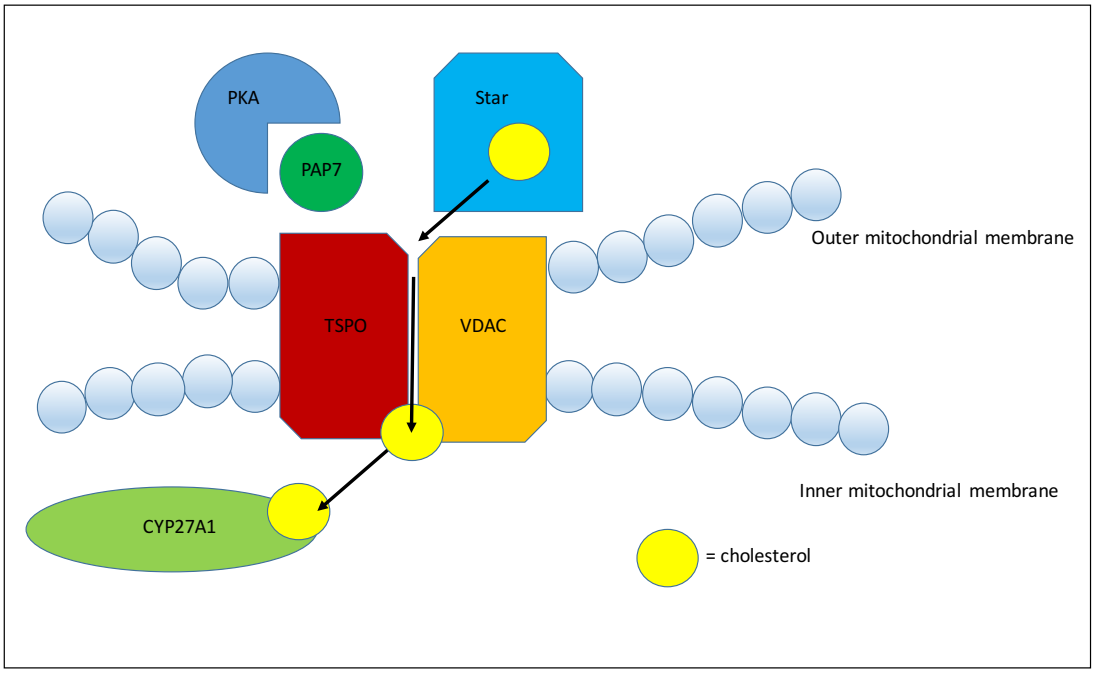

Figure 1.2 The 'transduceosome' –a collection of proteins responsible for the translocation of cholesterol across mitochondrial membranes (a rate-limiting step for the production of steroids in cells)-adapted from Rone *et al.* (214). PKA=protein kinase A, PAP7=peripheral benzodiazepine receptor-associated protein, Star= steroidogenic acute regulatory protein, VDAC= Voltage Dependent Anion Channel. CYP11A1=cytochrome P450 family 11 subfamily A member 1.

VDAC (Voltage Dependent Anion Channel) is an OMM channel forming protein that regulates the passage of ions and small molecules through the OMM. This function determines membrane potential, thus assisting in the regulation of apoptosis and cell metabolism. Through TSPO-VDAC interactions, cholesterol transport rates through the OMM, and therefore steroid production, may be affected (214).

Despite the body of evidence existing to support a role for TSPO in steroidogenesis, recent studies have contradicted this. In 2014, Morohaku *et al.* developed a mouse model where TSPO had been selectively knocked out in testicular cells(216). Such

knockout mice had no difference in baseline testosterone levels compared to non-knockout mice, and were fertile (216). Tu *et al.* developed a viable global TSPO knockout mouse, which likewise did not demonstrate any deficiency in ability to produce steroid(217). These studies challenge the idea that TSPO is essential for steroidogenesis.

Although the importance of TSPO in steroidogenesis may be debatable, evidence for the involvement of TSPO in mitochondrial cholesterol transport continues to accumulate. This is discussed in greater detail in **Chapter 4.**

1.4.2.2 TSPO in apoptosis

Multiple studies indicate a role for TSPO in apoptosis. In Drosophilia, *TSPO* gene inactivation inhibited wing disk apoptosis in response to radiation or hydrogen peroxide (218).

A body of evidence supports the idea that TSPO is part of the mitochondrial permeability transition pore (MPTP), giving a role for TSPO in apoptosis (157). TSPO is thought to be part of the functional subunit of MPTP to which extra-mitochondrial molecules bind (208, 219). Mitochondria have both a highly permeable outer membrane and an impermeable inner membrane(220). Opening of the MPTP causes a phenomenon known as 'mitochondrial permeability transition' where the inner membrane suddenly becomes permeable to small solutes, resulting in mitochondrial swelling and rupture of the outer membrane, causing release of reactive oxygen species, with resultant cell damage and apoptosis (221). The involvement of TSPO in apoptosis has been supported by human cell and malaria studies, which demonstrate that TSPO ligands are capable of inducing caspase production (222, 223), inducing the cytosolic release of cytochrome c, causing a release of reactive oxygen species (224) which activated p38 mitogen activated kinase, triggering opening of the MPTP (223).

1.4.3 TSPO as an imaging target in PET

Currently, the main PET tracer in clinical use is [^{18}F]FDG (150), which is a glucose analogue, therefore, tracer uptake corresponds with areas of increased metabolic

activity (150). However, the increased metabolic activity detected by [^{18}F]FDG is not specific to inflammation; a shift from oxidative phosphorylation to aerobic glycolysis for cellular energy production (known as the 'Warburg effect') is a well-established characteristic of malignant, as well as inflammatory cells (225). Indeed [^{18}F]FDG is widely used as a means of detecting and staging malignancy (150). Further, the high accumulation of [^{18}F]FDG in organs with high metabolic activity (such as the heart and brain), makes it difficult to detect inflammatory foci near such organs (226). Therefore, the more macrophage-specific TSPO ligand PET tracers may be a more sensitive and specific means of detecting inflammation (227). This idea is supported by a study that compared the uptake of TSPO ligand [^{18}F]-FEDAA1106 with [^{18}F]FDG, in a murine model of vascular inflammation (227). Here carotid artery inflammation was induced by the employment of a constrictive cuff. TSPO PET ligand accumulation was significantly higher than [^{18}F]FDG accumulation in the same inflamed area, suggesting TSPO PET may be a more sensitive detector of inflammation than [^{18}F]FDG. Furthermore, TSPO PET was able to more clearly distinguish between inflamed and non-inflamed areas, with ratio of TSPO ligand accumulation in inflamed: non-inflamed artery being greater than the ratio of [^{18}F]FDG accumulation, suggesting TSPO PET is a more specific marker for inflammation compared to [^{18}F]FDG (227).

The TSPO PET tracer [^{11}C]PK11195 is widely considered as the reference ligand for TSPO PET (228). After being utilised in a first study of imaging of the canine and human heart *in vivo* (229), PK11195 was then used to image TSPO in activated microglia in the central nervous system in a rat model *in vivo* (230). Since then, [^{11}C]PK11195 has been used to image neuro-inflammation related to stroke (231), multiple sclerosis (232) and a variety of neuro-degenerative diseases, including Alzeihmer's (233), and idiopathic Parkinson's disease (234) in human studies.

TSPO PET is being increasingly investigated as a tool to detect and quantify synovitis in RA (142, 147, 154), and the evidence to support its utility in detecting joint inflammation is accumulating. The use of TSPO PET in inflammatory arthritis will be discussed in more detail in **Chapter 2**.

1. 5 Aims & objectives of DPhil thesis

The main aims of this DPhil thesis are:

1. To undertake a proof of concept pilot study, to assess the ability of the second generation TSPO PET radioligand, [^{11}C]PBR28, to detect and quantify synovitis in a small cohort of patients with RA or PsA.

2. To profile the expression of TSPO in cellular constituents of human pannus, at mRNA and protein level, with supporting evidence from immunofluorescence of synovial tissue. This aims to give a more accurate understanding of the cellular contributions to TSPO PET signal when imaging inflamed joints, hence providing further data as to the utility of TSPO PET in assessing synovitis.

3. To investigate the *in vitro* expression of TSPO on different macrophages phenotypes, to obtain preliminary evidence of its potential role in macrophage biology.

CHAPTER 2

The utility of [^{11}C]PBR28 for the detection and quantification of synovitis; a proof of principle pilot study

2.1 Introduction

2.1.1 The evolution of Positron Emission Tomography Computed Tomography (PET-CT).

The first description of positron emitting radionuclides was by Curie and Joliot in the 1930s(235). They observed that bombarding elements with alpha particle radiation causes the target element to emit positrons long after the bombardment had stopped (235). This was quickly followed up by the development of the cyclotron by Ernest Lawrence (235). The cyclotron accelerates particles using magnetic force to generate the kinetic energy required to produce high energy protons and neutrons to overcome electrostatic repulsive forces of two positively charged nuclei (known as the Coulomb Barrier), enabling these particles to bombard elements, to create positron emitting radionuclides. This process led to the creation of the radioisotopes ^{11}C and ^{18}F, which are utilised in academic and clinical PET examinations today.

The use of positron emission in medical imaging was first described in 1951, where positron emitting phosphorus injected *in vivo* was proposed to aid in the diagnosis of intracranial tumours (236). Over the second half of the 20th century, positron emitting compounds were injected *in vivo*, to demonstrate blood flow (^{11}C-glucose, 0-15 water and N-13 ammonia), oxygen utilisation (O-15), and F-18 fluoride for bone scans (137). In 1979, PET was revolutionized by the use of ^{18}Fluoro-deoxyglucose in humans, to demonstrate cellular metabolism of glucose (237).

With the development of increasingly sophisticated tomography imaging over the next few decades, a prototype combined PET-CT scanner was proposed by Townsend, Nutt and co-workers in the 1990s (137). In 1998, such a prototype had become fully operational, with data processing including an algorithm to scale the CT images from X-ray radiation to PET annihilation photon energy, and generate the appropriate attenuation correction factors (238). Through the use of X-ray CT images to generate attenuation correction factors for the positron emission imaging, the duration of the PET imaging was dramatically reduced. Further, the co-registered anatomy provided by CT images localized functional abnormalities identified by the PET, and helped provide clarity in equivocal situations, thus improving the accuracy and confidence of the scan interpretation.

2.1.2 Development of tracers for PET

2.1.2.1 Choosing an appropriate ligand for PET

The tracer principle was founded by George de Hevesy, in which a radioactive, biologically active tracer substance, was chosen in such a way that its spatial and temporal distribution reflected a biological process *in vivo* (235). Due to the fact that radioisotopes give off tens of thousands of locatable decays (in the case of ^{11}C, 500,000) in one second, resulting in a uniquely sensitive imaging technique (able to image even nanomolar concentrations), the amount of administered radioactive substance is miniscule- in the order of femto mols- thus risk of ligand toxicity is extremely low (239). This allows new PET radioligands to be rapidly introduced for *in vivo* imaging.

Several considerations need to be taken into account when designing a radiotracer:

(a) The concentration of the tracer target

The concentration of the target (B_{max}) is an extremely important consideration in PET tracer development, with the lowest B_{max} of target protein successfully imaged by PET being around 1nM (10 femto mols/mg of protein) (240). Lower concentrations than this would result in a high amount of non-specific binding and a low PET tracer signal from areas of increase PET tracer target expression (240).

(b) The size of the region of interest

Small regions of interest (ROI) introduce problems of partial volume (here, the PET tracer signal from areas of high target concentration can 'spill' over into areas of low target concentration). With small ROI, motion correction is highly important, since small movements of the patient can have a big impact on the region of interest being analysed. The PET camera resolution must also be considered when looking at small ROI.

(c) the affinity of the tracer for its target

The affinity of the tracer needs to be high enough to minimise non-specific binding (to non-target structures such as cell membranes and other proteins), but not so high as to bind too fast to areas of low target concentration (241). Uptake from a tracer of too high affinity may reflect blood delivery to ROI (as the tracer adheres fast to any circulating target), rather than target in the ROI itself. High affinity tracers may also bind irreversibly to their targets, making quantification unreliable, as no equilibrium between tracer influx and efflux from an ROI is established.

The size of the ROI and B_{max} of the tracer target will also impact on the required affinity. For lower B_{max}, higher affinity tracers are beneficial to reduce non-specific binding, and increase signal from tracer binding to target. For higher $B_{max,}$ tracers do not have to be of such high affinity, since this may lead to more non-specific binding.

2.1.3 The process of PET-CT image generation *in vivo*

A PET study begins with the intravenous administration of a radiopharmaceutical (PET tracer), containing a proton rich isotope, to the subject being imaged. The PET tracer enters tissue via the circulation, and binds to its target, accumulating at sites of tracer target(242).

2.1.3.1 The annihilation reaction and photon detection

The proton rich isotope within the radiopharmaceutical decays via positron emission, in which a protein in the nucleus decays to a neutron, a positron and a neutrino. As positrons pass through the tissue of a subject, they collide with electrons, resulting in an ‘annihilation reaction’. This causes the mass of both positron and electron to be converted into energy, which is predominantly released as two 511 keV photons travelling in opposite directions (see **Figure 2.1**).

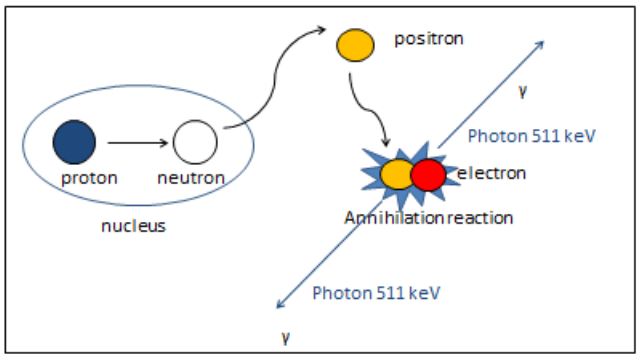

Figure 2.1: The process of production of photons within human tissue from positron emitting radioisotopes. Modified from: https://depts.washington.edu/nucmed/IRL/pet_intro/intro_src/section2.html (243).

The detectors within a PET camera pick up these photons simultaneously, and record this as a 'coincidence event' (i.e. two detectors positioned opposite from each other pick up a photon at the same time), gaining positional information from the detected radiation (see **Figure 2.2**). Through the collection of millions of these coincidence events from cameras surrounding the study subject, PET devices reconstruct images of the distribution of the PET tracer.

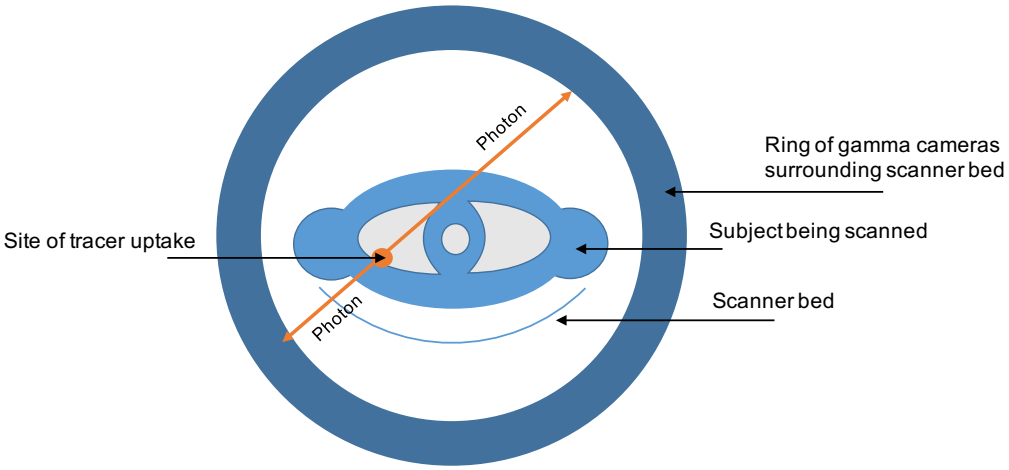

Figure 2.2: Demonstration of two photons generated by the annihilation reaction leading to the recording of a coincidence event by opposing PET cameras surrounding the subject. Adapted from Valk *et al.* (242)

The detectors within a PET camera detect photons by a process called scintillation, using a crystal of scintillating material (most commonly sodium iodide). Here, the high energy photons (emitted from the positron emitting PET tracer) are converted into visible light. A photon passes through the scintillating crystal, exciting an electron,

which then excites further electrons. As the excited electrons return to their baseline state, they emit the excess energy acquired as light. The light given off by the scintillator crystal then falls on a photomultiplier tube (PMT) which then generates an electrical signal. The PET scanner uses millions of these electrical signals to build up a 3D image of the distribution of tracer within the area being scanned (**Figure 2.3**).

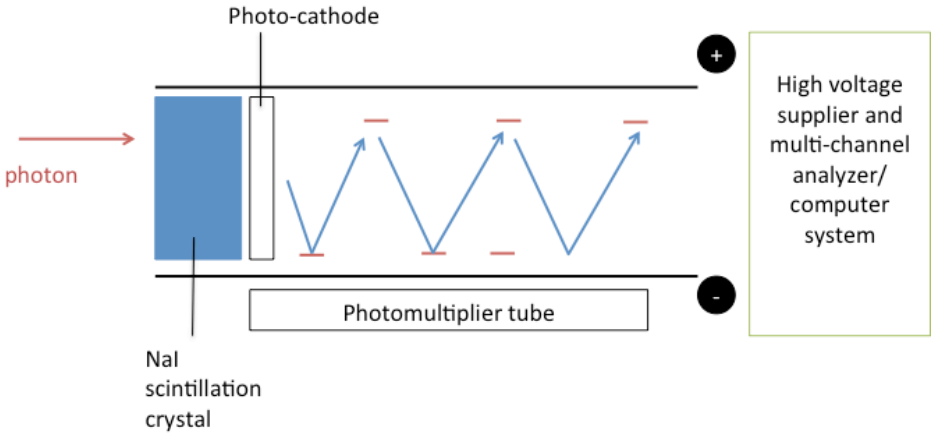

Figure 2.3: Generation of light through a scintillation crystal and its subsequent passage through a photomultiplier tube to generate an electrical signal. Modified from Valk *et al.* (242)

2.1.3.2 The scanning process

Correction for degradation factors

The images generated by PET can be degraded by attenuation. Attenuation refers to a decrease in the intensity of a photon signal as it passes through matter, either by absorption or scatter. Attenuation effects are directly proportional to the density and thickness of the various tissues through which photons travel; hence the thicker and denser a tissue, the more the photons attenuate (244). The phenomenon of absorption occurs if the matter, through which a photon is travelling, stops the photon completely. Scatter refers to the alteration in the direction of a photon's path due to its interaction with matter along that path.

Transmission scan

Attenuation can give rise to image reconstruction errors that can affect the accuracy of a PET scan. At the start of a PET-CT scan, a quick, low resolution CT scan of the area of interest is undertaken. This is referred to as a "transmission" scan. The main aims of this are to allow correction for degradation factors, undertake attenuation

correction, and to provide more detailed anatomical data, used to localise areas of increased PET tracer uptake. To correct for attenuation CT images are generated to create an 'attenuation map' of the patient. In this way, the PET computer system obtains data about the likely attenuation effects of each individual patient's body. The transmission image, together with the emission image, enables the PET scanner to create an attenuation corrected image of the patient (245, 246).

Emission scan

During this part of the scan, photons emitting from the patient are continuously detected by the PET cameras surrounding the patient in the scanner, to build up images of PET tracer distribution within tissues over time (245) .

2.1.4 PET tracer quantification

The majority of PET studies of arthritis to date utilise several different means of ascertaining PET tracer uptake in a ROI. The advantages and disadvantages of the various means of quantifying tracer binding are summarised in **Table 2.1**.

Measure of tracer uptake	Advantages	Disadvantage
Visual assessment	Can be done with static images, so short scan time Non invasive (no blood sampling required)	Mostly qualitative
Standardised Uptake Values (SUV)	Can be done with static images, so short scan time Semiquantitative (unlike qualitative visual measures) Non-invasive (no blood sampling required) Simple calculations required	Time dependent; hence to compare between scans, values must be taken at the same time point in all scans) (247-249) Dependent on body weight and habitus (247, 250) Affected by plasma clearance differences between subjects and study conditions (e.g. Liver and renal tracer metabolism variance) (249, 251) Affected by variability of tracer uptake by tissues other than the one of interest; e.g. Skeletal muscle uptake may be more in some patients than others (252)
Volume of Distribution (V_T)	Quantitative Less dependent on tracer uptake time Useful for the validation of novel tracers, where little is known about tracer kinetics *in vivo* (253)	Invasive; requiring blood sampling (often arterial) Requires dynamic scanning, hence a lengthy scan time Complex calculations required; for example, need to take into account existence of tracer metabolites when measuring radioactivity in plasma (254)

Table 2.1 Summary of advantages and disadvantages of methods of measuring PET tracer uptake

2.1.4.1 Visual assessment

One of the most commonly used measures of tracer uptake for inflammatory arthritis has been Visual Assessment. Here, two imaging specialists review PET images, and subjectively decide what is considered to be significant tracer accumulation in a ROI, with some works specifically mentioning the use of a reference region to determine what was deemed to be significant tracer uptake on visual analysis (255, 256). Other studies attempted to generate a semi-quantitative visual score, with the visual appearance of tracer uptake in a reference region scoring 0 (169, 172, 253).

2.1.4.2 Standardised uptake value and Volume of distribution measures

The movement of PET tracer from the circulation into the tissue of interest can be described using the compartmental model (246). Inside a compartment, it is assumed that the PET tracer is distributed uniformly. By convention, the first compartment is the concentration of tracer in the blood (or plasma). Other compartments represent the tissues in which tracer is taken up and contained. There is a constant flow of tracer between compartments, with k_1 representing the unidirectional transport of the tracer from the blood compartment to the first tissue compartment.

k_1 depends on perfusion, tissue permeability and surface area. The unidirectional transport of tracer from tissue back to blood is denoted by k_2, and defined in terms of k_1 and the volume of distribution of tracer within the first tissue compartment. The time at which equilibrium is reached between the rate of movement of tracer between blood and tissue, is considered the optimal time for measurement of PET tracer uptake.

In order to make the measured tissue concentration of the same PET tracer reproducible between scans, the tissue concentration of the tracer has to be normalised to a reference value. In clinical practice, where arterial blood measurement is not practicable, tissue tracer uptake values are normalised to the administered dose of the tracer in addition to patient weight (247). This generates a standardised uptake value (SUV).

2.1.4.3 Volume of Distribution (V_T)

By normalising tissue concentration to cumulative arterial concentration from injection time to measurement time, a volume of distribution (V_T) value is generated, which is widely considered the gold standard for PET tracer quantification in tissues (257), providing the most accurate reflection of PET tracer uptake within the tissues. Volume of distribution values are advantageous, in that they correct for variations between individuals e.g. in some individuals, there may be a higher uptake of tracer in skeletal muscle, leading to less tracer uptake and delivery to the synovium; this is obviated by measuring arterial tracer concentration over time, as the uptake in synovium can be corrected to the integral of the arterial curve.

2.1.5 The utility of TSPO targeted PET for the imaging of inflammatory arthritis

Tracers targeting cell proliferation or metabolism are obviously not specific to inflammation. A large body of evidence demonstrates a very high expression of TSPO on activated macrophages (142, 196-199). It is well recognised that macrophages play a central role in the pathogenesis of inflammatory arthritis (158) and macrophage staining in synovial tissue is known to correlate closely with disease activity and joint erosions in RA (258). PET tracers targeted to TSPO macrophages therefore have the potential to be a highly sensitive method for the imaging of synovitis.

TSPO PET is being increasingly investigated as a tool to detect and quantify inflammatory arthritis. The TSPO PET tracer, [^{11}C]PK11195, is widely considered as the reference ligand and has been used, mainly in neurological studies, for two decades (259). Several studies of [^{11}C]PK11195 PET in RA have been performed. A pilot study established that uptake of [^{11}C]PK11195 was higher in inflamed compared with unaffected knees in arthritis patients, with lowest uptake in knees of healthy controls (154). That [^{11}C]PK11195 may be capable of quantifying synovitis was suggested by significant differences in tracer uptake between knees with severe, moderate and no synovitis on clinical examination. Additionally, immunohistochemistry of synovial samples from knee joints demonstrated significantly more staining of tracer target in knees with severe synovitis compared to moderate synovitis, with knee synovial tissue from healthy controls having the least TSPO on

staining. Later work demonstrated that sites of highest [^{11}C]PK11195 uptake in joints correlated with the highest MRI synovitis and bone marrow oedema severity scores (147).

[^{11}C]PK11195 may also be of use in detecting very early RA. [^{11}C]PK11195 PET of hands and wrists were performed in 29 ACPA (Anti-Citrullinated C-Peptide Antibody) positive patients with arthralgia (147). 4/29 were found to have positive joints on PET imaging. At 2-year follow up, all 4 patients with positive hand or wrist PET findings had developed clinically apparent arthritis in those specific joints. The remaining patients (n=25) had no signs of arthritis on baseline imaging. Of these, only 2 of 25 developed clinically apparent hand or wrist arthritis at 2-year follow up. A further 3 patients developed arthritis at locations outside of the areas imaged.

The utility of TSPO PET in predicting flare in those with known RA, has been demonstrated by two studies of patients with clinically inactive or minimally active arthritis, both of which concluded that cumulative [^{11}C]PK11195 PET scores were significantly higher in patients who flared within at 1 year (149), and 3 years (184) after scan, compared to those who did not. In both studies, MRI scores did not distinguish between those who flared and those who did not.

In the most recent study, 25 patients underwent PET-CT of hands and wrists, MRI of the same joints, and were then followed up. By 1 year, 14 patients had experienced a flare, 11 had not. Of those who had a positive PET scan, 83% went on to have a flare. Of those who had a negative PET scan, 43% went on to flare. However, of the PET negative group that did flare, all but one of these patients had flares outside of the group of joints imaged by PET (149).

2.1.5.1 Second generation TSPO PET for the imaging of inflammatory arthritis

[^{11}C]PK11195 has technical limitations due to high non-specific background signal, which makes signal quantification difficult (259). Second generation TSPO ligands have been developed to overcome this complication, and their widespread use for other applications (mainly in the CNS) has produced encouraging results (188, 260). Indeed, [^{11}C]PBR28 has been demonstrated to have 300% increased affinity for TSPO

compared to [^{11}C]PK11195 (259).

So far in arthritis there is only preclinical published data at the time of writing for the use of second generation TSPO tracers in arthritis imaging. For example, in a rodent model of arthritis, the second generation TSPO ligands [^{11}C]DPA-713 and [^{18}F]DPA-714 showed much greater accumulation in arthritic knees than did [^{11}C]PK11195 (149). The TSPO ligand [^{11}C]PBR28 has been demonstrated to detect synovitis in a rat models of arthritis (261).

It should be noted that the binding affinity of these second generation tracers for their target (hence tracer uptake values), is affected by a Single Nucleotide Polymorphism (SNP) in TSPO (*rs6971*), and which needs to be considered when analyzing the PET data (262).

2.1.5.2 rs6971

In 2008, the then novel TSPO ligand [^{11}C]PBR28 was assessed for its ability to quantify TSPO in the human brain, in a study of 12 participants. The study found that 2 participants exhibited no tracer binding, but did not further investigate this (263).

Kreisl *et al.* assessed binding affinity across multiple different tissues; in a sample of 10 primates (5 exhibiting high binding of [^{11}C]PBR28, and 5 with low binding of [^{11}C]PBR28 in the brain), binding affinity was consistent across all tissues analysed (lung, heart, brain, kidney and spleen) (264).

In 2010, Owen *et al.* undertook studies of autoradiography of human brain tissue, to better elucidate the cause of lack of tracer binding, comparing binding of [^{3}H]PK11195 with the second generation tracer [^{3}H]PBR28 (265). Tissues from 22 post-mortem donors (20 with a diagnosis of multiple sclerosis, a known neuro-inflammatory disorder, and 2 control patients) was utilised in this study. Their results demonstrated that in 5 out of 22 donors, [^{3}H]PBR28 binding was negligible compared to [^{3}H]PK11195, whereas in the remaining donors, strong correlation between [^{3}H]PBR28 and [^{3}H]PK11195 binding was observed (265). Saturation studies (where tissue was incubated with a range of concentrations of [^{3}H]PBR28 or [^{3}H]PK11195), enabled the binding affinity for each tracer to be calculated for specific donor tissue. This confirmed that the 5 patients that exhibited no binding of [^{3}H]PBR28, had a 25-

fold reduction in binding affinity compared to the rest of the cohort. In contrast, binding affinity of [^{3}H]PK11195 was unchanged throughout the cohort. This gave support to the idea that some individuals possessed TSPO with a 'low affinity binding site' (hence were termed 'low affinity binders' or LABs), and others a 'high affinity binding site' for [^{3}H]PBR28 (and were thus termed 'high affinity binders' or HABs (262)). Saturation studies further identified a subgroup with intermediate binding affinity for [^{3}H]PBR28, and two binding sites for [^{3}H]PBR28; one high affinity and one low affinity, that were represented in equal proportion. Such donors were designated 'moderate affinity binders' (MABs (262)). From this work, it was proposed that genetic differences may be responsible for a conformational change in TSPO binding sites, to account for donors of different binding affinity for [^{3}H]PBR28.

In 2012, a study of TSPO polymorphisms, and [^{3}H]PBR28 binding affinity was undertaken in a cohort of 41 healthy volunteers (262). This demonstrated complete agreement between the SNP *rs6971* and PBR28 binding affinity phenotype ($p=3.1x10^{-13}$). The SNP *rs6971* encodes an amino acid substitution from alanine to threonine at position 147 (Ala147Thr) in the fifth transmembrane domain of the TSPO protein (262).

2.2 Aims

Through a proof of principle pilot study, I aim to assess:

1. The ability of [^{11}C]PBR28 to detect and quantify synovitis, using clinical examination, ultrasound and synovial histology as comparator variables.

2. The optimal measure(s) of tracer uptake for this particular tracer, out of standardised uptake values (SUV), or volume of distribution (V_T).

3. Whether or not [^{11}C]PBR28 uptake reflects TSPO expression in corresponding synovial biopsy tissue.

2.3 Study design rationale

2.3.1 PET-CT

The ideal joints to image for those with inflammatory arthritis would be the small joints of the hands and wrists, as these tend to be the most commonly affected (16), and any impact of weight-bearing on joint biomechanics, and hence potentially tracer signal, would not be an issue. However, a pair of joints of the lower limbs were chosen to image in this study, for several reasons.

Firstly, at the time of conducting this study, no previous data existed to describe the optimal time point to image synovium to accurately measure [^{11}C]PBR28 binding in synovial tissue. In a tissue compartment, a steady state between influx of radioligand in and radioligand out is eventually reached, when all ligand binding sites have been occupied. It is at this time, when equilibrium exists, when measurement of tracer signal is optimal, as bound tracer best reflects occupancy of all binding sites with tracer (266). In order to ascertain the optimal time at which to measure tracer signal, a dynamic PET-CT scan was performed, taking measures at serial time points, over a 90 minute scan. This meant that the whole body could not be imaged during the scan, since a dynamic scan is reliant on taking measures of tracer signal from the same area over time; hence only one area of the patient could be in the field of the ring of PET cameras surrounding the patient for the 90-minute scan duration.

Secondly, at the time of conducting this study, no previous data existed to describe the optimal mode of measuring [^{11}C]PBR28 tracer uptake in synovium. Therefore, it was decided to use all common methodologies of calculating tracer uptake, including the 'gold standard' V_T as well as SUV. To acquire V_T data, arterial blood samples through the radial artery were required at regular intervals throughout the scan. This would unavoidably generate some movement artefact in the small joints of the wrist and hands, impairing the reliability of data acquisition, and the accuracy of comparisons made between joint groups in each upper limb of the same patient. The ankles or knees of the lower limbs were chosen, as there was no chance of movement artefact due to repeated blood sampling, and the scan was more likely to be comfortable for the patient; they could be scanned either semi-recumbent, or recumbent. Furthermore, the lower limb joints are larger than those of the hands and

wrists, enabling ease of synovial biopsy, to obtain sufficient tissue for immunohistochemistry to correlate with PET tracer data, in this proof of principle pilot study.

2.3.2 Rationale for inclusion of RA and PsA patients

Although there may be fewer lining layer macrophages in PsA synovium compared to RA(267), macrophages still play a key role in the pathogenesis of PsA. Multiple studies demonstrate a correlation between clinical response to therapy in PsA, and a reduction in synovial macrophages(268-270).

Patients with either RA or PsA were included in this study, for a number of reasons. Firstly, it was decided joints of the lower limbs were to be imaged due to the proof of principle nature of this study, as described in **section 2.3.1**. RA is typically a symmetrical polyarthritis, often predominating in the small joints of the hands in both early and established disease(16, 17). Therefore, given the limited resources for this study, it would likely be impractical to recruit only eligible RA patients with knee synovitis. In contrast, monoarthritis, or oligoarthritis of large joints (such as the knee) is well-recognised in those with PsA(37), hence facilitating the completion of the study within the allotted time. Additionally, in order to demonstrate the tracer is indeed capable of quantifying synovitis, it is highly desirable to image a pair of joints in the same patient (to negate any impact on tracer uptake caused by patient specific factors), with one joint being clinically inflamed, and the other clinically non inflamed. Since RA is most frequently symmetrical and upper limb predominant(16), it would be difficult to find any RA patients with asymmetric synovitis in the lower limbs. Given that monoarthritis, and asymmetrical arthritis is well recognised in PsA(37), the inclusion of PsA patients also enabled us to acquire participants with a clinically inflamed, and corresponding non-inflamed joint, to compare tracer uptake within the same patient.

2.3.3 Ultrasound and clinical examination

The assessment of synovitis on clinical examination was used to provide some quantifiable evidence of the degree of synovitis in each joint imaged with PET-CT. However, it is well recognized that clinical examination of the knee lacks sensitivity for the detection of synovitis compared to ultrasound (70). Therefore, Grey Scale and Power Doppler ultrasound of each joint was undertaken at the same time as clinical

examination, to provide further quantitative evidence of synovitis present in joints to be imaged with PET-CT.

Semi-quantitative Grey Scale and Power Doppler ultrasound scoring was undertaken, as extensively described in the literature. A semi-quantitative ultrasound score was used for this study, since such scores are well established, have good inter-observer reliability (271), and are increasingly accepted as a means of quantifying synovitis using ultrasound (68, 89, 90).

2.3.4 Synovial biopsy and immunohistochemistry

Ultrasound guided synovial biopsy of one joint imaged was undertaken within 7 days of the PET-CT, to provide histological correlates for PET tracer data. Time interval between PET-CT and biopsy was short, so as to reduce the likelihood of change in cellular infiltrate in the synovium from time of the PET-CT, as much as practically possible.

Ultrasound guided biopsy was undertaken for arthritis patients, as this procedure is well established to be better tolerated than arthroscopic biopsy under local anaesthetic, which also carries increased risk of infection (272). Further, the degree of synovial inflammation may not be equal throughout each knee joint being imaged; therefore, by obtaining biopsy tissue from one compartment of the joint only, histological staining could be compared with tracer uptake in that specific compartment, improving accuracy of any correlation seen.

Each synovial biopsy was stained for the tracer target, TSPO, as well as for the presence of macrophages. CD68 is a widely recognized and long accepted macrophage marker(273). However, it is increasingly recognized that this may not be a specific macrophage marker in synovium, with accumulating literature suggesting other cells in synovium, such as fibroblasts, also express this surface marker (274, 275). CD163 is increasingly thought to be more specific to macrophages in synovium, and able to distinguish between macrophages and fibroblasts (274); therefore, synovial staining for both CD68 and CD163 was carried out, to investigate the relationships between the presence of macrophages, and tracer uptake.

2.3.5 Genotyping study to assess study feasibility

It is well recognized that low affinity binders (those homozygous rare for *rs6971* SNP), bind negligible [^{11}C]PBR28, thus do not produce a measurable specific PET signal (265). Therefore, low affinity binder arthritis patients would not be suitable for inclusion in a proof of principle pilot study of [^{11}C]PBR28 PET.

Genetic differences between the arthritic and healthy population are well recognized; indeed, genetic variance has long been established as an aetiological factor in inflammatory arthritis (276, 277). Therefore, an assessment of the frequency of *rs6971* in an inflammatory arthritis population was undertaken, to ensure that recruitment to the study (and further use of [^{11}C]PBR28 in arthritis imaging) was feasible.

A total of 45 patients with an established diagnosis of inflammatory arthritis (23 patients with rheumatoid arthritis, 16 patients with ankylosing spondylitis, and 6 patients with psoriatic arthritis) underwent genotyping (peripheral blood from this cohort kindly donated by Professor Peter Taylor, ethics reference number 09/H0707/80). Genotyping of this arthritis patient cohort demonstrates a highly similar frequency of all genotypes to the healthy population frequencies of 49% for homozygous high-affinity (G/G); 9% for homozygous low-affinity (A/A); and 42% for heterozygotes (A/G) (http://hapmap.ncbi.nlm.nih.gov/). To avoid discrepancies resulting from population ethnic origin, and population geography, the genotype frequencies of the arthritis patient cohort were further compared with those of a similarly ethnically diverse population of healthy volunteers from the same area in North West London (see **Table 2.2**).

Healthy volunteers (262)	**Patients with inflammatory arthritis**
Cohort size: 41	Cohort size: 45
Age at time of genotyping: 36.3 ± 1.4 yrs	Age at time of genotyping: 57.6 (range 27-72 yrs)
Population location: North-West London	Population location: North-West London
Ethnicity: 37/41 Caucasian 2/41 Asian 1/41 mixed Caucasian/Asian, 1/41 Hispanic.	Ethnicity: 34/45 Caucasian, 6/45 Asian 2/45 Far-East 1/45 mixed Caucasian/Asian 2 unspecified ethnicity
Genotype frequency: 29% heterozygotes (MAB) 9% homozygous (LAB)	Genotype frequency: 56% G/G (HAB) 32% A/G (MAB) 12% A/A (LAB)

Table 2.2 Comparison of genotype frequency and patient demographics with a similar population of healthy controls who underwent genotyping for *rs6971* in Owen *et al* (262).

2.4 Methodology

Ethical approval was obtained from the West London and GTAC research ethics committee (REC reference 15/LO/0013). The study was subsequently approved by Oxford University Hospitals NHS trust Research and Development department. For details of study design and approval processes please see **Appendix (section A2)**.

2.4.1 Recruitment for clinical study

Patients were recruited from the Nuffield Orthopaedic Centre rheumatology outpatients department. Healthy volunteers were recruited through advertisement using ethically approved posters set up in the Nuffield Orthopaedic Centre, the Botnar Research Centre and the Kennedy Institute, as well as an ethically approved online advert on the OUH trust website. Five patients with active RA (as per ACR criteria (25)) and 5 patients with psoriatic arthritis (as per CASPAR criteria (37)), ages 38-71, 5 female, 5 male. Four healthy volunteers were recruited; ages 41-65. Out of inflammatory arthritis participants, 7 patients were heterozygotes for *rs6971* SNP

(moderate affinity binders, MABs), 3 were wildtype genotype (high affinity binders, HABs). Of the 4 healthy volunteers, 3 were wildtype genotype for *rs6971*, and 1 was heterozygous for the SNP. All patients gave written informed consent.

2.4.2 Screening tests

At screening visit, patients underwent peripheral blood sampling, to extract whole blood into a 5 or 10ml EDTA bottle for DNA extraction, and also into a 5mL potassium citrate bottle for international normalized ratio (INR) to ensure the patient was not at risk of haemorrhage at the arterial line insertion site.

2.4.3 DNA extraction

DNA extraction from peripheral whole blood was undertaken using a QIAamp DNA blood mini kit (QIAGEN, Hilden), as per manufacturer's instructions. In brief, 200µL of whole blood was placed in a 1.5mL eppendorf. To this, 20µL of proteinase K (activity 600 mAU/ml, QIAGEN, Hilden) was added to the blood, along with 200µL of Buffer AL (containing guanidine salts). The samples were vortexed, and incubated in a waterbath at 50°C for 10 minutes in order to denature proteins. To the resulting mix, 200µL of 96% ethanol was added. The samples were again vortexed, and the mixture applied to spin columns. The spin columns were then placed in a centrifuge and spun at full speed for 30 seconds. The DNA adherent to the spin column filters were subsequently washed in AW1 buffer, and AW2 buffer (wash buffers), followed by a further spin in the centrifuge to remove any remaining AW2 buffer. 30µL of DNAse free water was added to the spin column, and the samples incubated at room temperature for 10 minutes, before a final centrifuge step to extract the water containing patient DNA. The quality and quantity of the DNA was then checked using the NanoDrop2000^{TM}, with Abs260/Abs280 ratio of above 1.7 was considered to indicate DNA of sufficient purity for use. The TaqMan ® SNP Genotyping Assay (Taqman® SNP Genotyping assay, Applied Biosystems) was utilized to undertake genotyping for the *rs6971* SNP on TSPO.

2.4.4 Genotyping assay for *rs6971*

This genotyping assay uses two allele-specific TaqMan® MGB probes (Thermo-Fischer Scientific) to allow discrimination between 2 alleles of a specific SNP. TaqMan probes consist of a fluorophore covalently attached to the 5'-end of the oligonucleotide probe and a quencher at the 3'-end. The quencher molecule quenches the fluorescence emitted by the fluorophore when excited by the cycler's light source. As long as the fluorophore and the quencher are in proximity, quenching inhibits any fluorescence signals (278). As the Taq polymerase extends the primer and synthesizes the nascent strand, the 5' to 3' exonuclease activity of the polymerase degrades the probe that has annealed to the template. Degradation of the probe releases the fluorophore from it and breaks the close proximity to the quencher. This relieves the quenching effect, allowing fluorescence of the fluorophore.

Patient DNA extracts, checked for quality using a NanoDrop2000^{TM} spectrophotometer (Eppendorf AG, Hamburg, Germany) were placed on ice. The master mix/genotyping assay/dH_20 mixture was pipetted into a 384 well PCR plate (Applied Biosystems, Life Technologies, Paisley, UK) and DNA added. Amounts for one reaction are outlined below:

Taqman Mastermix (x2)	*10μL*
Genotyping Assay (20x):	*0.4μL*
dH_2O:	*7.6μL*
DNA:	*2μL*

In every plate, samples of known genotype were run (wildtype, heterozygous and homozygous for SNP), to act as positive control samples. PCR plates were sealed with a plate cover, and briefly spun before placing into the PCR machine (ViiA^{TM} 7 Real-Time PCR System, Life Technologies, UK). The FAST Taqman genotyping programme was selected.

2.4.5 Clinical examination and ultrasound

Semi-quantitative scoring of synovitis on clinical examination was undertaken as adapted from Mandl *et al.* (279), with a score of 0 meaning "*definitely no synovitis on examination",* a score of 1 meaning "*no, but I am hesitating (possible presence of synovitis)",* a score of 2 meaning "*moderate synovitis"* and a score of 3 meaning "*severe synovitis".*

Both grey scale and power Doppler ultrasound examination were also undertaken of joints to be imaged using PET-CT. For knee ultrasound, 3 compartments of each joint were imaged (both lateral and transverse views); lateral, medial and suprapatellar compartments. For the ankle, 2 compartment was imaged (tibio-talar joint), in both lateral and transverse views. Semi-quantitative scoring of synovitis for each compartment imaged on ultrasound was undertaken according to the SOLAR criteria for large joints as described in Hartung *et al*.(280) (see **Table 2.3**).

Grey Scale Ultrasound (GSUS) score	**Power Doppler (PD) score**
0 = none	0 = no vascular signal
1=mild	1 = 3 single vascular signals/ 2 single signals plus 1 continuous signal
2=moderate	2 = vascular signals more than grade 1, but less than 50% of the intra-articular area
3=severe	3 = vascular signals over 50% of the intra-articular area

Table 2.3 Grey Scale and Power Doppler semi-quantitative scoring- Adapted from Hartung *et al.* (280)

2.4.6 [^{11}C]PBR28 PET-CT procedure

[^{11}C]PBR28 PET-CT was carried out in Imanova Centre for Academic Imaging Sciences, Hammersmith, London, UK. [^{11}C]PBR28 tracer synthesis and quality checks were performed as described in Owen *et al.* (281), and are outlined below.

2.4.6.1 Production of [^{11}C]PBR28

Cyclotron produced [^{11}C]CO_2 was converted to [^{11}C]methyl iodide using a GE Microlab system (GE, Uppsala, Sweden). The [^{11}C]methyl iodide was subsequently passed through a solution containing 1 mg of desmethyl-PBR28 in 350 µL DMF (dimethylformamide), and 0.5 M tetrabutyl ammonium hydroxide in methanol (4 µL) as base. The reaction mixture was heated to 120°C for 5 minutes, allowed to cool and diluted with high-performance liquid chromatography (HPLC) solvent (ammonium formate 10 mmol/L: acetonitrile 57/43 (v/v), 8 mL/minute) prior to injection onto an Agilent Eclipse XDB-C18 HPLC column (5 µm, 250 × 9.4 mm, Agilent, Santa Clara, CA, USA). The fraction containing [^{11}C]PBR28 was collected into a vessel containing 20 mL water for injection before trapping onto a solid-phase cartridge (C18 Classic SepPak, Waters, Milford, MA, USA). The cartridge was washed with water for injection and [^{11}C]PBR28 was eluted using ethanol (1 mL) followed by saline for injection (9 mL) through a 0.2 µm sterile filter (Pall Acrodisc, Sterile, 33 mm, 0.22 µm, Pall, Port Washington, NY, USA) into a sterile vial (Adelphi, Manchester, UK).

2.4.6.2 Quality control checking of [^{11}C]PBR28

The final product was tested using validated procedures in accordance with good manufacturing practices for the following:

- visual appearance clear, colourless and practically free from particles
- pH between 4.5 and 8.5, total endotoxins <175EU/dose
- PBR28 mass ≤10 µg per dose (3.43 ± 1.69 µg), desmethyl-PBR28 <1µg per dose, total unknown chemical impurities ≤12 µg per dose
- radiochemical purity >95%
- radiochemical identity co-elution with cold PBR28
- isotopic half-life within 10% of expected value
- filter integrity pass
- isotopic purity (no additional gamma peaks in a fully decayed sample),
- residual solvents within limits set by International Conference on Harmonization Q3C R4
- sterility confirmed

All batches used for this study successfully passed the specifications listed above.

2.4.6.3 PET-CT scanning patient preparation procedures

The patient was prepared for the PET scan by the insertion of an intravenous cannula. Weight, blood pressure and pulse were checked prior to entering the scan room. Allen's test was performed to ensure collateral ulnar blood supply to the hand in event of radial arterial cannulation, and an arterial cannula was inserted into the radial artery (here, 1mL of 2% lignocaine was infiltrated around the radial artery. An arterial cannula was then inserted into the radial artery, and a dressing applied, in addition to a splint, to ensure the line remained patent and did not become dislodged. The line was flushed with Heparin-Saline).

2.4.6.4 [^{11}C]PBR28 PET scanning

[^{11}C]PBR28 PET was carried out in Imanova Centre for Academic Imaging Sciences, Hammersmith, London, UK. For all participants, approximately 400MBq [^{11}C]PBR28 was injected as an intravenous bolus over approximately 20 seconds at the start of a 90-minute dynamic PET acquisition.

All arthritis patients underwent PET scanning using a Siemens Biograph 6 PET-CT scanner (SIEMENS, Knoxville, TN). Following a 30 second transmission CT scan (2 dimensional (2-D) acquisition mode) to correct for photon attenuation, a dynamic emission scan of the knees or ankles (of duration 90 minutes) was undertaken in 3-D acquisition mode. PET data were reconstructed using filtered back projection with corrections for attenuation and scatter.

For healthy controls undergoing imaging, a 30 second transmission CT scan was obtained, followed by a 20-minute static emission PET scan of the knees or ankles starting at 50 minutes post tracer administration.

2.4.6.5 Analysis of PET data

Positron emission tomography data were reconstructed using filtered back projection with corrections for attenuation and scatter (based on a low-dose CT acquisition). ROI were drawn manually using the Analyze® 12.0 software (AnalyzeDirect, USA), and defined by outlining anatomical location of synovium using CT as a guide (in the medial, lateral and suprapatellar compartments of each knee, and tibiotalar ankle joint

in the case of ankle imaging), in addition to a reference region in adjacent bone, as previously described (154) (lateral femoral condylar bone for those undergoing knee imaging, and distal tibia for those undergoing ankle imaging). ROI were drawn on consensus between a rheumatologist (NN) and a radiologist (AS). These ROI were applied to the [^{11}C]PBR28 data to generate mean voxel radioactivity for the full duration of the scan. Time activity curves for the full duration of the scan corrected for radioactive decay and normalized for injected radioactivity were generated. Semiquantitative SUV (249) and Standardised Uptake Value Ratios (SUVR, using bone as reference region) were calculated (154).

A two-tissue compartment model, utilizing the metabolite corrected plasma input function was applied to the dynamic PET data as previously described (263) to calculate V_T. For each ROI, the V_T tracer uptake was estimated from the rate constants as previously described (281).

2.4.6.6 Arterial blood sampling

In order to normalise [^{11}C]PBR28 uptake in the tissue for measurement of V_T, arterial blood sampling was undertaken. Discrete blood samples were manually withdrawn at 5, 10, 15, 20, 25, 30, 40, 50, 60, 70, 80, and 90 minutes after scan start to facilitate measurement of whole blood and plasma activity. Some of these samples (5, 10, 20, 30, 50, 70, and 90-minute time point samples) were also analyzed using HPLC (see **section 2.4.6.7**) to determine the fraction of parent radioactivity in arterial plasma. The procedure used to generate the metabolite corrected plasma input function has been described previously (282). In brief, the total plasma curve was generated by multiplying the whole blood curve by plasma-over-blood ratio, and the parent fraction data were fitted to a sigmoid model:

$$f = (\left(1 - \frac{t^3}{t^3 + 10^a}\right)^b + c)/(1 + c)$$

where *t* is time and *a, b*, and *c* are fitted parameters

The resulting fitted parent fraction profile was multiplied by the total plasma curve and then smoothed post peak using a tri-exponential fit to derive the required parent plasma input function. A time delay correction was performed for each scan to account

for any temporal delay between blood sample measurement and the tomographic measurements of the tissue data.

2.4.6.7 Arterial blood processing

[^{11}C]PBR28 parent fraction over the course of the PET scan was determined using the 'Hilton method' (283). Briefly, urea was added to the plasma samples to give an 8 mol/L concentration to break up plasma–protein binding. The sample was diluted 1:1 with 0.1 mol/L unbuffered Tris and filtered through a 0.45 μm polyvinylidene fluoride syringe filter (Waters Acrodisc LC 13 mm Minispike and 25 mm, Waters, USA) before injection onto the dual HPLC system. System 1 operated as trapping system where parent and non-polar metabolites were collected on a Biotrap 500 MS (ChromTech, Cedex, France) sample enriching column using 5% acetonitrile in 0.1 mol/L unbuffered Tris as solvent at a flow rate of 2 mL/minute. Following trapping, the Biotrap column was switched in line with HPLC system two. Parent and non-polar metabolites were eluted using a gradient method (0 to 4 minutes 5% acetonitrile: 95% unbuffered Tris, 4 to 10 minutes 5% acetonitrile → 95% acetonitrile) and separated using an Agilent Zorbax Eclipse XDB-C18 column (5 μm, 150 × 4.6 mm, Agilent). A total of 30 fractions were collected and activity measured in a Perkin Elmer 1470 10-well automated gamma counter (Perkin Elmer, Turku, Finland).

2.4.7 Synovial biopsy

Synovial biopsy of one joint imaged for each patient, was undertaken within 7 days of the PET-CT scan. Patients underwent synovial biopsy under ultrasound guidance. The GE Healthcare LoqiqE9 ultrasound machine was used to identify an appropriate location in the joint for biopsy. The area was disinfected with chlorhexidine, and sterile drapes applied. Using asepsis, 2% lignocaine (Hameln Pharmaceuticals Ltd) was infiltrated into the skin at the biopsy site. Following this, a larger needle was inserted into the joint, to create a tract for the biopsy needle, and also to infiltrate a mixture of lignocaine and sterile saline into the joint, for pain relief and also to help visualize thickened synovium.

A Terumo^{TM} needle of appropriate gauge and length (selected according to the size of the joint being biopsied) was used to obtain between 10-15 passes of tissue. A

dressing was then applied, and a power Doppler ultrasound was then performed, to ensure there was no bleeding. Post-injection advice was given, and the patient was followed up with a telephone call the next day to check for any complications. Samples were immediately transferred to sterile media. Samples were then embedded within cryomolds (TissueTek) containing OCT (Leica) and frozen in isopentane at -70ºC, before being stored at -80°C for serial sectioning at a thickness of 5µm within 2 weeks.

2.4.8 Immunohistochemistry

Immunohistochemistry utilises specific antigen-antibody interactions, which can be visualized by a marker or reporter such as fluorescent dye (immunofluorescence) or enzyme (immunoenzyme). Staining can be direct or indirect. The direct method of staining is a one-step staining procedure than involves a labeled primary antibody, reacting directly with the antigen of interest in tissue sections (284). However, this technique lacks sensitivity due to relatively little signal amplification when only one layer of antibody is applied (284). Indirect staining involves a layer of unlabeled primary antibody, which binds to the tissue antigen of interest, and a labeled secondary antibody that reacts with the primary antibody and amplifies the signal. The secondary antibody is raised against the IgG of the animal species in which the primary antibody has been raised. The secondary antibody can be labeled with an enzyme (such as horseradish peroxidase, HRP) or a fluorescent dye, such as Texas red. In this study, staining was undertaken in a Dako Auto-stainer (285), which includes automatic quenching, blocking and application of antibody stains.

a) Quenching of endogenous peroxidase activity

Endogenous peroxidase activity in erythrocytes, leucocytes and other cells could sometimes cause heavy background staining with HRP conjugated antibodies. This could lead to false positives or masking of true staining. This can be minimized by immersing sections in a 2% solution of 0.3% hydrogen peroxide (Dako®) for 30 minutes. The sections were then washed 3 times for 5 minutes each with PBS.

b) Blocking

Besides endogenous peroxidase activity which could be quenched by hydrogen peroxidase treatment, non-specific background staining could also be caused by non-

specific binding of antibodies to Fc receptors expressed on inflammatory cells, and also to other sites within the tissue sections. Such non-specific binding was reduced in this study by blocking these sites with 3% equine serum (Dako®).

c) Primary antibody

Following blocking, sections were treated with the primary antibody against the antigen of interest (**Table 2.4**) The primary antibody was diluted to the appropriate concentration in FLEX Antibody Diluent (Dako®). For isotype control slides, the sections were incubated with the same concentration of the same isotype as the primary antibody, but to a target not present in the human synovium.

Antibody target	**Clone**	**Isotype**	**Titre used**
CD68	KP-1	Mouse IgG1	1:4000
TSPO	EPR5834	Rabbit	1:10,000
CD163	3B4	Mouse IgG2a	1: 2000

Table 2.4 Summary of antibodies used for DAB immunohistochemistry (IHC)

d) Secondary antibody

Following incubation with primary antibody and washing, a polymer detection system was used in which the secondary antibody was polymerically conjugated with HRP or alkaline phosphatase by using a synthetic polymer carrier. This technique increased the number of available enzymes or ligands binding at the antigenic site, therefore increasing their reactivity to the reporting chromogen (284).

e) DAB staining

Following secondary antibody staining, the autostainer proceeded to the DAB (3,3'-diaminobenzidine) staining step. Here DAB is oxidized by HRP to produce a brown stain, before being washed off with water.

f) Counterstaining

Following colour development with DAB, the sections were washed, and counterstained with haematoxylin and eosin in the autostainer.

H & E stain consists of the basic component haematoxylin, which colours basophilic structures (such as nucleic acids within the nuclei) with blue-purple, and alcohol-based acidic eosin, which stains eosinophilic structures (such as the cytoplasm) pink(284). In this study, H & E stain was used to assess the structural quality of the tissue obtained (in order to confirm the presence of synovium), and confirm presence of histological changes consistent with synovitis.

g) Dehydration and clearing

Following counterstaining, the sections were washed gently in running tap water for 5-10 minutes to remove excess haematoxylin. The sections were then immersed in dH_20 for 5 minutes. Then, they were taken through a series of graded IMS (industrial methylated spirit) bath of increasing concentration (70%, 90% and twice absolute alcohol for 10-minute intervals each) to dehydrate the sections, and remove aqueous fixative and any tissue water content before the clearing process. Clearing was achieved by sequential transfer of the tissues into two xylene baths for 10-minute intervals.

h) Mounting

The sections were mounted with Pertex® (Leica), and coverslips laid gently over the mounting medium, with care taken to prevent the inclusion of air bubbles. The sections were left to dry for 30 minutes before storing at room temperature.

2.4.8.1 Optimisation of the primary antibody

The conditions required for immunostaining of each antibody were optimized with paraffin embedded tissue sections known to express antibodies in abundance. Five different dilutions of the primary antibody and PBS only were used during optimization, and the dilution with the least non-specific staining and clearest positive staining was then selected for subsequent immunostaining of synovial tissue sections.

A positive control slide was also stained in each run for TSPO, CD68 and CD163- this was cytospin slides containing *in vitro* differentiated macrophages. The positive slide helped to determine if that particular run of immunohistochemistry against the antibody of interest was successful.

A corresponding serial cross section slide of all tissues being staining, was stained against an isotype negative control antibody at the same time of each run of immunohistochemistry. The isotype negative control antibody used was of same immunoglobulin isotype raised from the same species as the antibody of interest in the same concentration, but was not directed to human antigen. The isotype negative control antibody stained slides were studies along with their corresponding sections stained with antibody of interest to identify areas of non-specific staining. **Figure 2.4** depicts isotype control staining for CD68 and CD163 (using a cocktail of monoclonal mouse isotype controls, Dako®), and for TSPO (using a rabbit monoclonal IgG isotype).

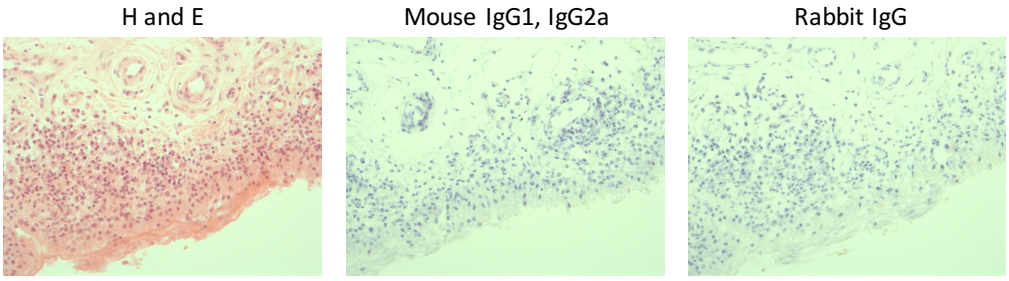

Figure 2.4 Isotype control staining of RA synovial tissue. Figures show representative images of synovial tissue of RA study participant (from a knee with severe synovitis clinically). Sections were stained with isotype control antibodies for mouse IgG1, IgG2a, and rabbit IgG fractions. Nuclear counterstain is haematoxylin. Magnification x200.

2.4.8.2 Quantification of staining

Images were acquired on an inverted microscope using Axiovision software (Zeiss) x400 magnification using immersion oil. Twelve images of synovial sublining on each slide were taken at random. Two independent investigators (NN and HM) then viewed each image, scoring the degree of staining on a scale from a scale of 0 to 3, as previously described in Revu *et al.* (286). An average was taken of the staining score over the 12 slides, to generate a semi-quantitative staining score for each stain, for each patient sample.

2.4.9 Statistical analysis

Multivariate regression analysis was undertaken to establish the impact of potential patient specific confounding factors on SUV and SUVR, including age, weight and serum creatinine. Spearman's rank correlates were used to assess correlations between two variables. Mann-Whitney U test was used to compare SUV or SUVR values between different groups. For histological staining scores, paired Wilcoxon rank test was undertaken to provide an indication of differences in staining scores for same biopsy tissue.

2.5 Results

All ten patients and four healthy controls completed the study. Twenty joints were imaged in total over the 10 arthritis patients; of these joints, clinical synovitis severity was severe in 4/10, moderate in 6/20, mild in 8/20 and absent in 2/20 joints. **Table 2.5** demonstrates demographics of all study participants. **Table 2.6** lists swollen and tender joint counts, WCC (white cell count) and CRP (C-reactive protein) of all arthritis patient participants.

Patient ID	RA/PsA	Age (years)	Gender	Race	rs6971 genotype (binding affinity)	Medications
Patients with inflammatory arthritis						
PET001	PsA	38	F	Caucasian	AG (MAB)	Nil
PET002	PsA	48	M	Caucasian	AG (MAB)	leflunomide 20mg od
PET004	RA	54	M	Caucasian	GG (HAB)	methotrexate 15mg o/w, hydroxychloroquine 200mg bd, folic acid 5mg o/w
PET006	PsA	45	M	Caucasian	AG (MAB)	leflunomide 20mg od
PET008	PsA	71	F	Caucasian	AG (MAB)	methotrexate 25mg o/w, folic acid 5mg o/w
PET010	RA	52	F	Caucasian	AG (HAB)	Infliximab 3mg/kg every 8/52 i.v, methotrexate 10mg s/c, prednisolone 5mg od, folic acid 5mg o/w, ketoprofen 200mg prn
PET011	PsA	53	F	Caucasian	GG (HAB)	methotrexate 20mg o/w, folic acid 5mg o/w
PET012	RA	37	M	Caucasian	AG (MAB)	methotrexate 15mg o/w, hydroxychloroquine 200mg bd folic acid 5mg o/w
PET013	RA	40	F	Caucasian	AG (MAB)	Abatacept 500mg once monthly i.v, azathioprine 200mg od, ibuprofen 400mg bd
PET014	RA	43	M	Caucasian	GG (HAB)	Hydroxychloroquine 200mg
Healthy volunteers						
HV01	none	38	M	Caucasian	GG (HAB)	None
HV02	none	52	F	Caucasian	AG (MAB)	None
HV03	none	65	M	Indian	GG (HAB)	Bisoprolol 1.25mg od
HV04	none	41	M	Caucasian	GG (HAB)	None

Table 2.5 Demographics of all participants. HAB=high affinity binder, MAB=moderate affinity binder, od=once daily, o/w=once weekly, bd=twice daily, prn=as needed. All drugs were administered through oral route, unless otherwise specified; s/c=subcutaneous, i.v=intravenous.

Study Participant	Swollen Joint Count§	Tender Joint Count§	White cell count	CRP
PET001	2	4	6.35	2.2
PET002	12	16	7.07	5.5
PET004	11	13	6.06	65.3
PET006	1	1	4.68	0.8
PET008	1	1	6.71	4
PET010	14	14	14.64	34.2
PET011	1	1	7.25	10.4
PET012	20	24	11.45	55.7
PET013	4	8	7.9	13.5
PET014	10	21	7.05	28.2

Table 2.6 Clinical details of all patients with inflammatory arthritis participating in the study. Swollen and tender joint count (§ out of score 44, as per Ritchie et al. (287)); White cell count in units of $x10^9$ cells/L (normal range 4.0-11.0). CRP= C-reactive protein (normal range <5mg/L)

2.5.1 Analysis of patient specific potential confounding factors

Multivariate analysis did not demonstrate any correlation between SUVR or SUV and participant age, weight, or creatinine. Although SUV did appear to correlate with binding affinity (r^2=0.590, p<0.001), the strength of this correlation was reduced when comparing SUVR with binding affinity (r^2=0.299 p=0.041). Therefore, for the purposes of this pilot study, for SUV data, both imaged joints of each participant of the same binding affinity were treated as independent joints in the analysis. For SUVR, each joint imaged was treated as an independent joint, regardless of binding affinity.

There was no significant difference in age, between healthy controls and participants with arthritis undergoing scanning (48 ± 6.39 years for healthy controls compared with 48.1 ± 3.2 years for participants with arthritis). Likewise, there was no significant

difference in age between volunteers donating control tissue and participants undergoing PET imaging (mean age of control tissue donors 46.8 ± 3.5 years).

2.5.2 Images of [^{11}C]PBR28 PET-CT

Uptake of tracer could be seen along the anatomical location of synovium, corresponding to the clinical site of synovitis in arthritis patients. In contrast, there appeared to be no tracer uptake in the synovium of healthy controls (**Figure 2.5**)

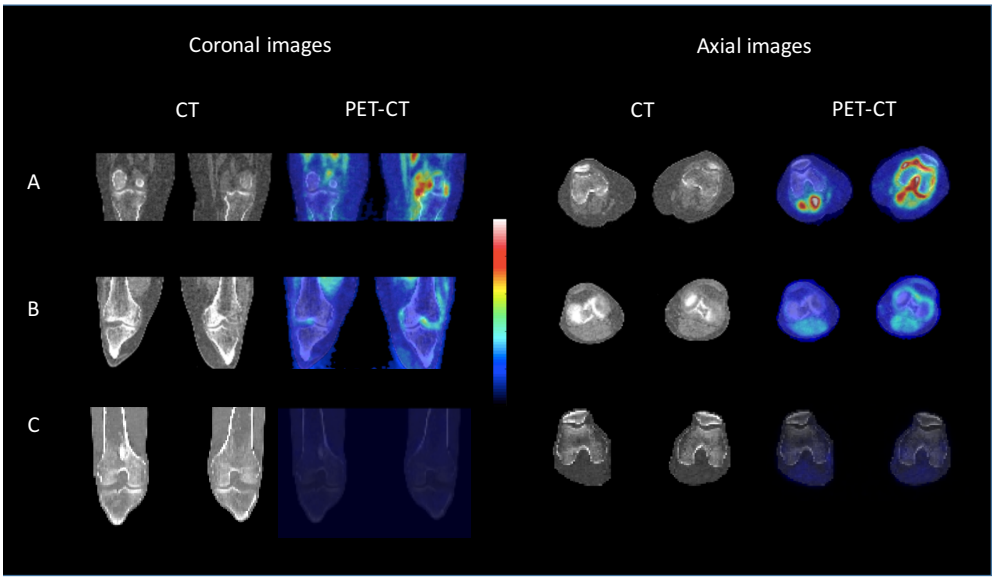

Figure 2.5 Representative example of CT, PET-CT images and SUV of tracer in 3 study participants**; A:** moderate affinity binder patient with clinically severe synovitis of left knee only. **B**: moderate affinity binder patient with clinically mild synovitis of left knee only **C:** moderate affinity binder healthy control. Colourimetric scale (centre) depicts red as high SUV, blue as low SUV.

Figure 2.5 also demonstrates that even on visual analysis of tracer signal, there appears to be more tracer signal in a knee with severe synovitis compared to mild synovitis (**Figures 2.5A & 2.5B**) in different patients of same binding affinity, as well as a significant difference between healthy control knees and those of participants with arthritis.

2.5.3 Volume of distribution (V_T)

Eight out of the ten arthritis patients undergoing PET imaging provided continuous arterial blood sampling during the PET scan to enable calculation of V_T data. The

remaining two arthritis patients did not have arterial sampling, due to technical difficulty in inserting a radial arterial line, due to presence of florid wrist synovitis.

Out of the 8 patients who provided V_T data, for 2 participants, it was not possible to generate results from the time activity curves generated, since no plateau of tracer uptake was reached over the 90 minute duration of the PET scan. Of the data obtained for the remaining 6 participants, for moderate affinity binders, the highest V_T values were seen in knees with most severe synovitis on clinical examination, and likewise, for high affinity binders, V_T was higher in a moderately inflamed knee on clinical examination, compared to a mildly inflamed knee (see **Table 2.7**).

Clinical synovitis severity score	**V_T (MAB) (8 joints) mean ± SD**	**V_T (HAB) (4 joints) mean ± SD**
0 (Control)	N/D*	N/D*
0 (arthritis patient)	N/D*	N/D*
1	3.70 ± 0.40 (4 joints)	N/D*
2	4.37 ± 0.22 (3 joints)	4.61 (1 joint)
3	6.38 (1 joint)	6.50 ± 0.70 (3 joints)

Table 2.7 V_T (Volume of Distribution data) for 6 arthritis study participants (4 MAB patients, 2 HAB patients), for whom V_T data was available, according to clinical synovitis score. MAB=moderate affinity binder, HAB=high affinity binder. N/D*=no data available

2.5.4 Optimal time for [^{11}C]PBR28 SUV measurement

Time activity curves for regions of interest for each study participant were plotted, using SUV against time, for the entire 90 minute duration of the PET scan. For all ROIs for all participants, a plateau of SUV was reached at approximately 50 minutes (**Figure 2.6**), indicating SUV values at 50 minutes post tracer injection are optimal for measurement of tracer uptake in synovium.

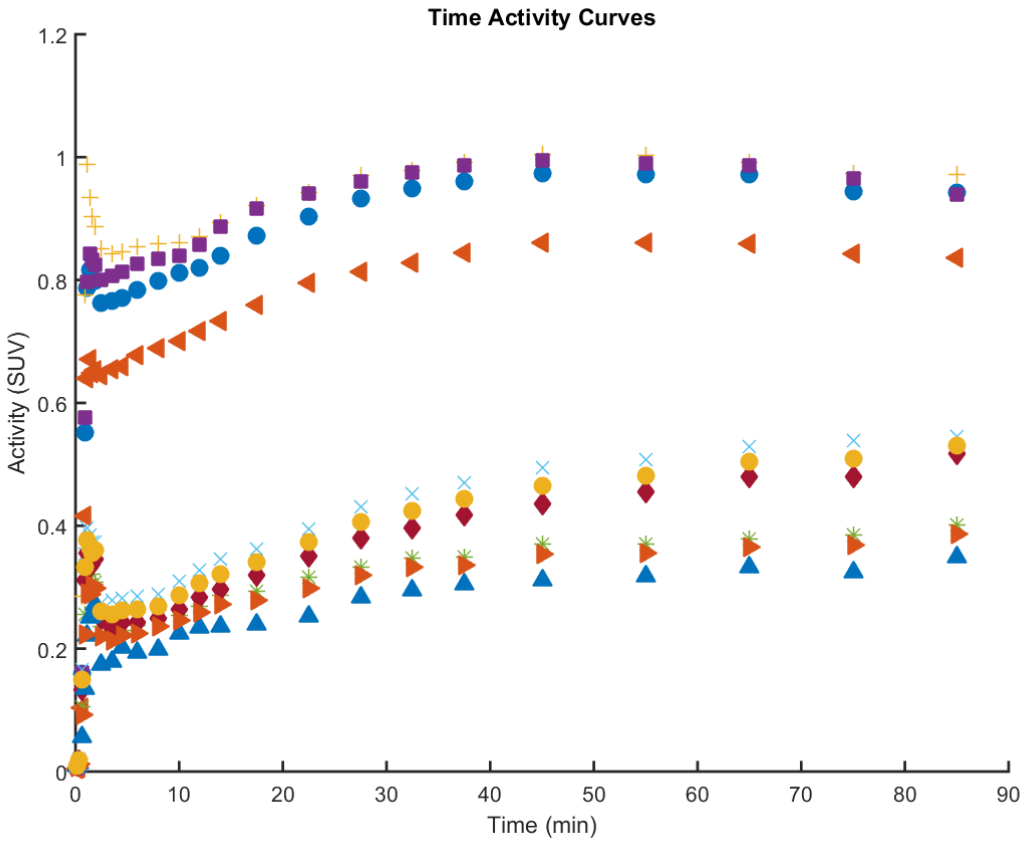

Figure 2.6 example of SUV time activity curve for a study participant with RA. Each line on the chart represents a single ROI.

There was a positive correlation between SUV and clinical synovitis severity score, regardless of binding affinity (r^2=0.940, p<0.01 for moderate affinity binders, r^2=0.916, p<0.01 for high affinity binders (**Figure 2.7** & **Table 2.8** for SUV according to clinical synovitis severity score). Likewise, a positive correlation was seen between SUVR and clinical synovitis severity score (r^2=0.953, p<0.01). Further, both SUVR and SUV were lower in control joints compared to clinically non-inflamed joints of patients with arthritis (**Table 2.8**); this was statistically significant for SUVR (p=0.05).

Clinical synovitis severity score	SUVR (28 joints) Mean ± SD	SUV (MAB) (16 joints) Mean ± SD	SUV (HAB) (12 joints) Mean ± SD
0 (Control)	0.93 ± 0.22	0.04 ± 0.001 (2 joints)	0.03 ± 0.001 (6 joints)
0 (arthritis patient)	1.33 ± 0.31	0.12 ± 0.02 (2 joints)	0.238 (1 joint)
1	1.67±0.11	0.34 ± 0.07 (6 joints)	N/D*
2	2.18 ± 0.34	0.51 ± 0.10 (5 joints)	0.81 (1 joint)
3	3.16 ± 0.60	0.79 (1 joint)	0.97 ± 0.05 (4 joints)

Table 2.8: Summary of [^{11}C]PBR28 uptake measures ±SD (standard deviation), according to clinical synovitis severity score. N/D* =no data available.

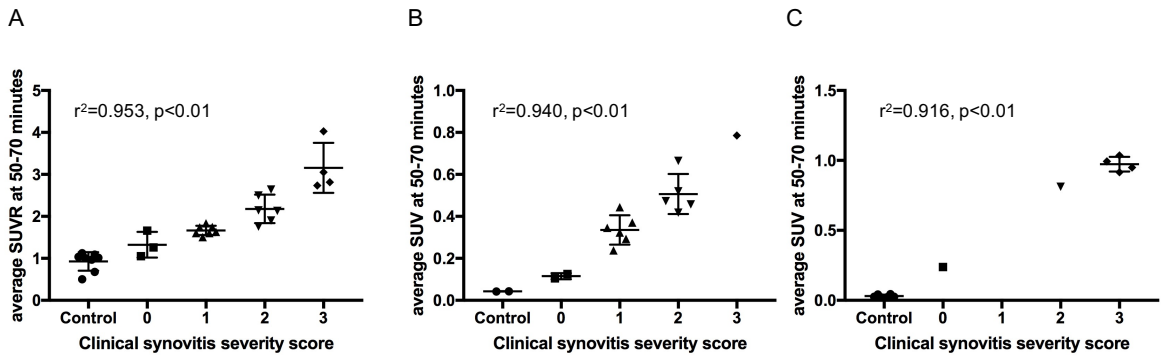

Figure 2.7 Average tracer uptake for each joint imaged with [^{11}C]PBR28 PET, grouped according to clinical synovitis severity score. Each point represents average SUVR or SUV for one joint. **A:** average SUVR for all participants **B:** average SUV for moderate affinity binder participants **C:** average SUV for high affinity binder participants.

2.5.5 Comparison of [^{11}C]PBR28 uptake with ultrasound scores

SUVR was highest in those joint compartments with highest GSUS or PD score (**Table 2.9**). Although GSUS score of 1 was seen in both controls (9/24 total joint compartments) and arthritis patients (12/52 total joint compartments), SUVR was significantly lower in healthy controls compared to arthritis patients, regardless of GSUS score ($p=0.05$ for GSUS score of 0, $p<0.001$ for GSUS score of 1).

	Healthy control		Arthritis patient			
GSUS score	0	1	0	1	2	3
Median SUVR (range)	0.97 (0.68-1.16)	0.95 (0.65-1.07)	1.16 (1.05-1.26)	1.61 (1.31-2.16)	1.97 (1.48-2.76)	2.99 (2.37-5.64)
PD score	0		0	1	2	3
Median SUVR (range)	0.97 (0.65-1.16)		1.64 (1.05-2.16)	2.21 (1.71-2.82)	2.97 (2.37-3.07)	3.06 (2.76-5.64)

Table 2.9 median SUVR of each joint compartment grouped according to ultrasound score. GSUS=Grey Scale Ultrasound, PD=Power Doppler. Data is expressed as mean (range).

2.5.6 Immunohistochemical analysis of synovium

Staining for TSPO, CD68 and CD163 demonstrated least staining in healthy controls, with semi-quantitative staining scores (mean ±SD) of 1.15 ± 0.15, 1.22 ± 0.19 and 0.83 ± 0.47, respectively. Most staining for all 3 markers in synovial tissue was seen in clinically severely inflamed knees, (staining scores of 3.06 ± 0.24 for TSPO, 2.96 ± 0.11 for CD68 and 2.81 ± 0.08 for CD163). See **Figure 2.8** for representative staining images.

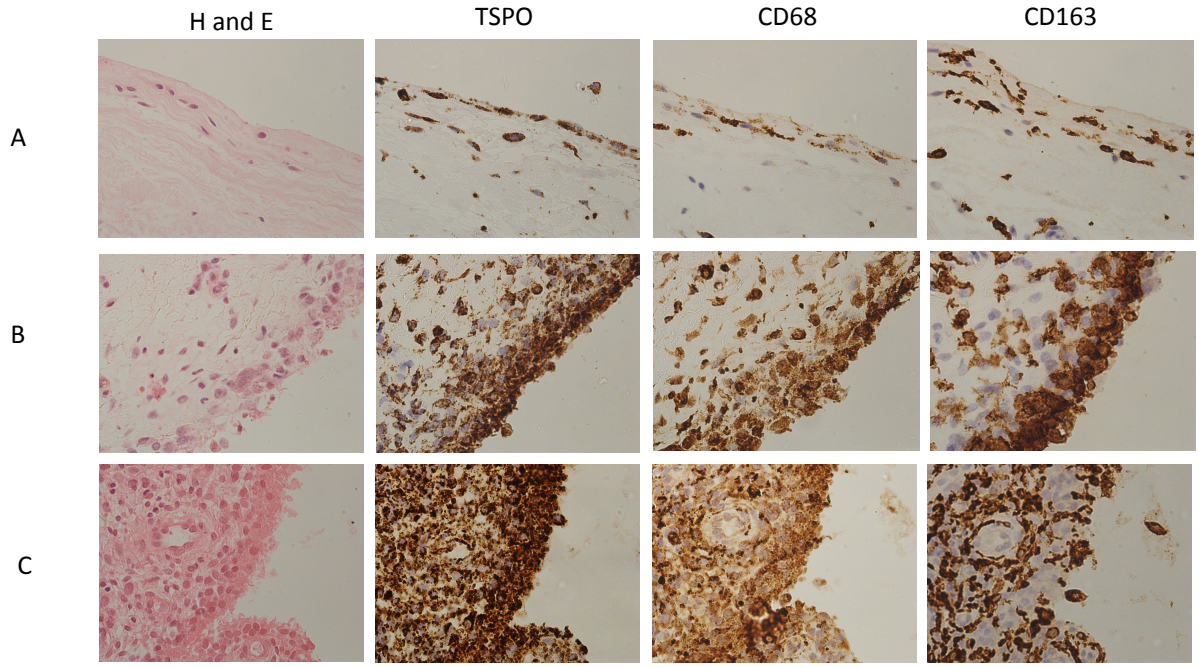

Figure 2.8 Serial sections of synovial biopsy tissue, depicting lining and sublining, each stained for H & E, TSPO, CD68 and CD163 (**A)** synovial tissue from healthy control knee; (**B)** synovial tissue from clinically moderately inflamed knee of RA patient; (**C):** synovial tissue from clinically severely inflamed knee of RA patient. x400 magnification.

To investigate whether [^{11}C]PBR28 uptake in the PET scan reflected synovial expression of TSPO, staining scores for TSPO of synovial biopsy from arthritis patients were compared with SUVR of the biopsy compartments, demonstrating a strong positive correlation of SUVR with TSPO staining (r^2=0.884, p=0.001).

To further ascertain whether [^{11}C]PBR28 uptake reflected macrophage infiltration, semi-quantitative synovitis scoring for the less specific, but widely accepted macrophage marker CD68 was undertaken, as well as the macrophage marker CD163, increasingly recognized to be more specific for synovial macrophages. Significant positive correlations between [^{11}C]PBR28 SUVR and staining scores for CD68 and CD163 were noted (r^2=0.833, p=0.003 and r^2=0.817, p=0.004, respectively, **Figure 2.9**).

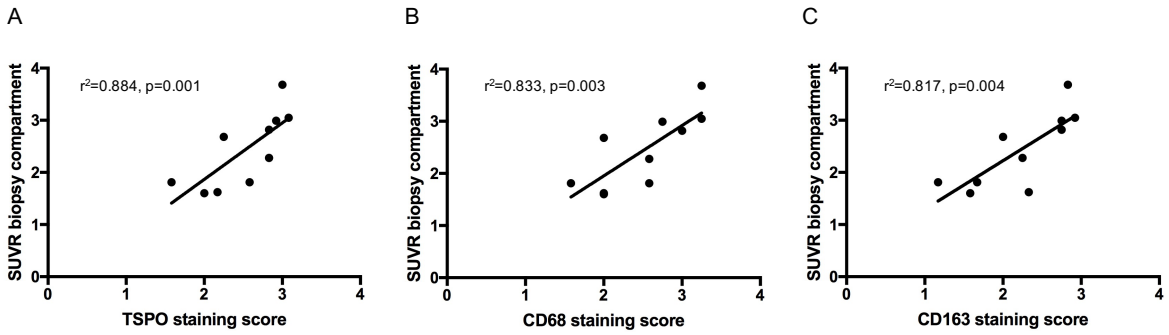

Figure 2.9 Spearman's rank correlations between [^{11}C]PBR28 SUVR of biopsy compartment of arthritis patients and synovial tissue biopsy staining scores for **A:** TSPO **B:** CD68 **C:** CD163

Paired Wilcoxon rank test did not demonstrate significant difference between TSPO and CD68 staining scores. However, CD163 staining scores were noted to be significantly lower (with median of difference at -0.21, p=0.01), compared to TSPO staining scores.

2.6 Discussion

The importance of macrophage infiltration in synovitis is long established, with histological staining for macrophages known to correlate with clinical disease activity (288, 289). As a protein purportedly highly upregulated on activated macrophages, TSPO, has potential as an imaging target for inflammatory arthritis, as evidenced by studies utilizing the first generation TSPO targeted tracer [^{11}C]PK11195. However, a

body of evidence suggests the second generation TSPO tracer [^{11}C]PBR28 is a technically superior tracer; with higher degree of specific binding, and hence, potential for a highly specific and sensitive tool for detection and quantification of synovitis.

This study demonstrated that even on PET images, [^{11}C]PBR28 PET appears capable of detecting synovitis, with [^{11}C]PBR28 outlining synovium in inflamed joints, with negligible uptake in control joints.

SUV time activity curves, for all 10 arthritis participants who underwent dynamic scanning, demonstrated a plateau of SUV at about 50 minutes from tracer injection; hence SUV and SUVR data were obtained for all participants. Semi-quantitative [^{11}C]PBR28 uptake data, in the form of SUV and SUVR were both capable of reflecting presence of synovitis, with least uptake of tracer in healthy controls compared to arthritis patients. SUVR correlated significantly with clinical synovitis severity score, as did SUV. Interestingly, both SUVR and SUV were lower in healthy control joints compared to clinically non inflamed joints in arthritis patients. This could indicate the potential of [^{11}C]PBR28 to detect subclinical synovitis.

V_T data from this study, as for SUVR and SUV measures, also demonstrated increased V_T with increased clinical synovitis severity. However, two tissue compartmental modelling was unable to provide V_T data for 2 out of 8 patients for whom arterial blood data was available, as a plateau of tracer uptake using V_T was not reached during the 90-minute scan duration. The reasons for this are uncertain, but it could be that the current tissue models to calculate [^{11}C]PBR28 V_T, previously almost exclusively used for brain tissue (239, 263), are not appropriate for synovial tissue. [^{11}C]PBR28 PET of a larger cohort of patients would lend clarity to this, but in practical terms, calculation of V_T data is highly invasive, requiring repeated, preferably arterial, blood sampling, hence is unlikely to be a routine measure of tracer uptake in large studies.

Much evidence exists to support the fact that ultrasound is a more accurate means of detecting synovitis compared to clinical examination (68-70). Ultrasound was therefore used as a measure of further assessing the ability of [^{11}C]PBR28 PET to detect and quantify synovitis. As with clinical examination, as GSUS and PD scores for synovitis increased, so did SUVR, providing further support for the hypothesis that [^{11}C]PBR28

can quantify synovitis. Further, a GSUS score of 1 was seen in joints of both healthy controls, and arthritis patients. This is in keeping with previous studies demonstrating that, a certain degree of GSUS change can be acceptable in healthy joints (72, 93), and operator judgement is required in deciding whether or not this GSUS change is reflective of inflammation. In contrast, [^{11}C]PBR28 uptake was significantly lower in healthy controls compared to arthritis patients of the same GSUS score, likely reflecting the increased specificity of [^{11}C]PBR28 for synovitis compared with GSUS.

Histological analysis of synovial biopsy lent further support for the ability of [^{11}C]PRB28 PET to reflect synovial tissue expression of its target, TSPO. SUVR of biopsy compartments positively correlated with synovial biopsy staining for TSPO (r^2=0.844, p=0.001), with TSPO synovial tissue staining scores being lowest in healthy control joints (1.15 ± 0.15 standard deviation), and augmenting with increasing clinical synovitis severity score (TSPO staining score of 2.05 ± 0.50 for joints with mild synovitis, 2.19 ± 0.34 for moderate synovitis clinically, and 3.06 ± 0.24 for tissue from joints with severe synovitis on clinical examination.

Likewise, [^{11}C]PBR28 uptake correlated positively with staining for the macrophage markers CD68 and CD163, providing indirect evidence that [^{11}C]PBR28 uptake likely reflects macrophage infiltration. Incidentally, no significant difference was noted between TSPO staining and CD68 staining on paired Wilcoxon rank test. In contrast, staining for the more specific macrophage marker CD163 was significantly lower than TSPO staining (median of differences 0.21 p=0.01).

Although the number of synovial biopsy samples used was small, and staining of serial sections was employed rather than all stains being used on the same section, this data raises the possibility that TSPO may not be a solely macrophage specific marker in synovium. CD68 is recognized to be expressed on both macrophages and synovial fibroblasts (274, 275), whereas CD163 is able to differentiate between these cell groups (274). Although TSPO is widely utilized as an imaging marker of macrophage infiltration in PET, its expression is in fact, fairly ubiquitous (157); therefore, it could be possible that, like CD68, TSPO is not macrophage specific in synovium.

As a proof of principle pilot study, the relatively low number of subjects included in this study limits the certainty of conclusions drawn. However, several variables, well

established as measures of synovitis or disease activity, all correlated with [^{11}C]PBR28 uptake measures, including clinical examination, ultrasound semi-quantitative scores, and synovial staining for macrophage markers. This study ascertained the optimal scan time to measure [^{11}C]PBR28 in synovial tissue, and determined that SUV and SUVR were likely suitable measures for tracer uptake, facilitating larger studies, where SUV or SUVR measures can be used to measure [^{11}C]PBR28 uptake. Further investigation of the expression profile of TSPO in human pannus would be useful, in providing an accurate idea of the major cellular contributors to [^{11}C]PBR28 PET signal in synovium. This would be particularly relevant if [^{11}C]PBR28 PET was to be used as a means of assessing response to novel targeted therapies, where the cellular origin of [^{11}C]PBR28 signal may give useful data as to the effectiveness of a particular treatment.

To more fully validate [^{11}C]PBR28 for use in the detection and quantification of synovitis, further investigation would be beneficial to provide conclusive proof that [^{11}C]PBR28 PET signal in synovium in vivo is reflective of synovial tissue expression of TSPO. This could be achieved by undertaking an *in vivo* blocking study, to assess the degree of non-specific binding of [^{11}C]PBR28. Non-specific binding can be estimated by using an unlabeled TSPO targeting agent, administered prior to [^{11}C]PBR28 PET imaging. This would block the binding of [^{11}C]PBR28 to TSPO, eliminating specific binding component of the PET signal, providing evidence of how much -if any- [^{11}C]PBR28 PET signal, is non-specific.

A previous *in vivo* blocking study of [^{11}C]PBR28 PET imaging of brains of healthy human volunteers used XBD173 (281) as a blocking agent. XBD173 (previously known as emapunil (290), and developed as a TSPO targeted anxiolytic), is a TSPO ligand, recognized to have no physiological effect in unpublished clinical trials (David R Owen, personal communication). XBD173 was used by Owen *et al*. in the first human *in vivo* study to block the specific component of [^{11}C]PBR28 PET signal in the imaging of brains of healthy volunteers(281). For a blocking study to investigate specificity of [^{11}C]PBR28 PET for detection of TSPO in inflamed synovium, subjects would undergo [^{11}C]PBR28 PET imaging of joints prior to, and after administration of a single oral dose of XBD173 at 90mg, as per the previous human blocking study by Owen *et al.* (281). The amount of tracer signal in synovium post XBD173

administration, would give an indication of how much of the [^{11}C]PBR28 PET signal in synovium is non-specific in origin (or 'background' uptake).

Through this work, we have provided the first preliminary *in vivo* data in humans to demonstrate that [^{11}C]PBR28 PET is capable of detecting and quantifying synovitis in those with RA and PsA, as measured by clinical examination and ultrasound. Furthermore, our pilot study data provides some initial evidence that [^{11}C]PBR28 PET could have potential to detect subclinical inflammation (with [^{11}C]PBR28 uptake being higher in clinically inactive joints of arthritis patients, compared to healthy controls). Additionally, we demonstrate that [^{11}C]PBR28 PET, is likely to be a more specific measure of synovitis than semiquantitative GSUS scoring, being able to distinguish between healthy and arthritis patients with the same GSUS score of 1 or 0. Through synovial tissue histology, this study provided some limited evidence that TSPO itself may not be solely expressed on macrophages in synovium, with synovial biopsy histology from the limited number of participants demonstrating a significantly lower staining score for the macrophage specific CD163 in synovial tissue, compared to TSPO staining scores. This provides some indication of the fact that TSPO may not, indeed, be a specific macrophage marker in synovium. In the next chapter, we investigate in further detail the expression of TSPO in human synovium in RA, to better understand the cellular contributions to TSPO PET signal, arising from *in vivo* imaging of inflamed synovium.

CHAPTER 3

An Investigation of TSPO expression in major cell groups of human RA pannus

3.1 Introduction

Despite the clinical use of TSPO as a means of imaging macrophages, TSPO is in fact ubiquitously expressed, although expression varies considerably according to region. Steady-state mRNA levels are high in adrenal tissue and other steroid synthesizing cells, kidney, spleen, skeletal muscle and lung, intermediate in heart and testicles and low in the liver and brain (157). Human tissues TSPO messenger RNA has being recognised to correlate with protein expression (157, 195); TSPO protein expression known to be abundantly expressed at the highest level in steroid-synthesizing cells(157). It has been long established that TSPO is highly expressed in human peripheral blood mononuclear cells. This was demonstrated in 1993, where an *in vitro* study of [^{3}H]PK11195 binding in cells from peripheral blood demonstrated the most binding of tracer- and hence TSPO protein expression- in monocytes and neutrophils followed by lymphocytes, with the least TSPO in platelets and erythrocytes (195).

Furthermore, TSPO has been demonstrated to be highly expressed on infiltrating macrophages in various human tissues in inflammatory disease states. Enhanced TSPO expression on macrophages has been found in human CNS inflammatory lesions in traumatic brain injury (196), in multiple sclerosis (197) and in Alzheimer's disease (198). Macrophages expressing high levels of TSPO have also been found in atheroma in carotid artery disease (199). Increased TSPO expression is also thought to be linked to tumour formation and cancer progression (157) with significant upregulation in inflammatory tissues associated in breast, prostate, colon and brain cancers.

Histological studies of inflamed synovium of RA patients indicated that TSPO staining positively correlate with CD68, a widely used macrophage marker (154). More recently, TSPO has been demonstrated to be highly expressed on infiltrating macrophages in the synovium of a rat model of inflammatory arthritis (142). Here, staining for TSPO by immunohistochemistry demonstrated an influx of TSPO positive cells (largely macrophages and neutrophils) in the synovium of knees with induced arthritis compared to the disease free knee.

Thus far, little work has been done to ascertain the expression profile of TSPO in cellular components of human pannus. Such work would provide a better

understanding of the exact source(s) of TSPO PET signal in inflamed synovium, enabling more accurate interpretation of TSPO PET signal for the imaging of inflamed joints. This would further help clarify the potential utility of TSPO PET as an imaging technique for assessing response to treatment in early clinical trials of novel therapies. Further, since the function of TSPO is as yet unknown, an assessment of TSPO expression in different cellular components in RA synovium and potential impact of activation of various cell types on TSPO expression, may lend further insight into any potential role for TSPO in RA inflammation.

3.1.1 Human synovium in health and inflammation

3.1.1.1 The healthy synovium

The healthy synovium lines the joint cavity and regulates the transport of molecules between the joint cavity and adjacent tissue. In the disease free state, synovium consists of an intimal layer few layers of fibroblast-like synoviocytes (FLS) and resident macrophage-like synoviocytes (291). The FLS secrete matrix metalloproteinases, hyaluronan and proteoglycans into synovial fluid (292). Beneath this intimal layer lies the subintima, consisting of a small number of blood vessels (see **Figure 3.1A**).

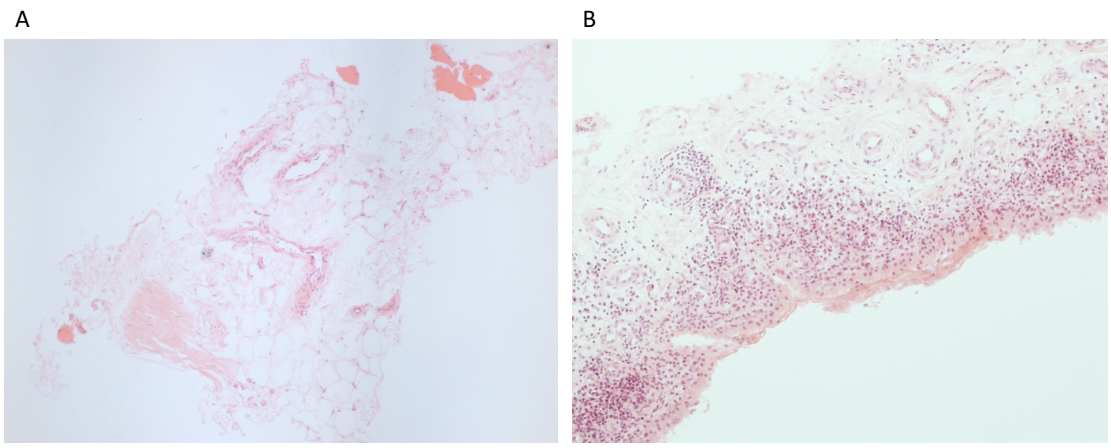

Figure 3.1 Haematoxylin and Eosin (H&E) stains of cryosections, from **(A)** example of healthy synovial tissue and **(B)** synovial tissue from biopsy of clinically inflamed RA patient (tissue provided from study participants from study described in Chapter 2), demonstrating a clear increase in cellularity in RA synovium, with hypertrophy of the lining layer visible. x100 magnification.

3.1.1.2 The synovium in inflammatory arthritis

In RA, synovium transforms from a relatively acellular structure, to a hyperplastic, invasive tissue containing multiple immune cells. Synovial tissue has two layers; the lining and sublining, both of which undergo major changes in inflammatory arthritis (293) (**Figure 3.1B and 3.2**).

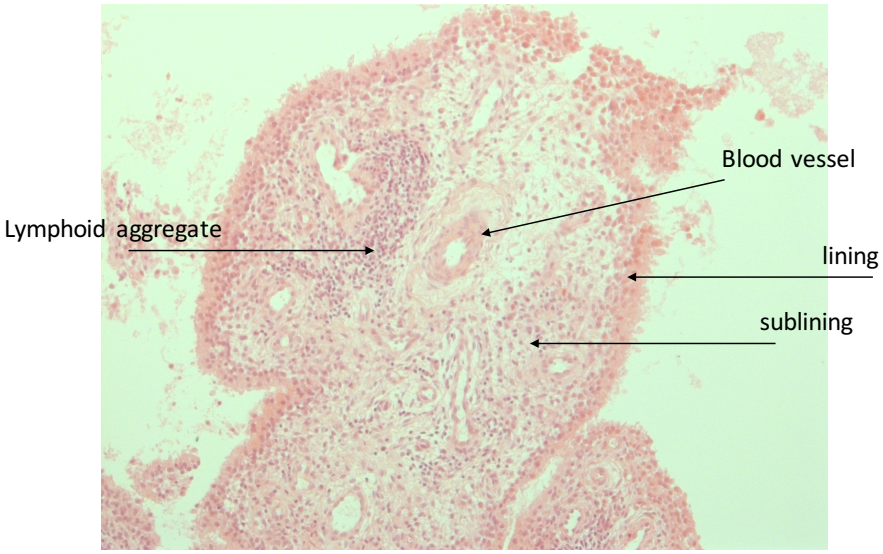

Figure 3.2 H & E stained cryosection of knee synovial tissue from study participant with Rheumatoid Arthritis (modified from study 'The Utility of [^{11}C]PBR28 in inflammatory arthritis', described in Chapter 2). x100 magnification

In RA, the lining becomes hyperplastic, and increases in cellularity, from 1-2 cells thick, to tens of cells in thickness. The hyperplasia is thought to be due to the presence of activated FLS, as well as infiltration by macrophages. Macrophages are thought to make up 30-40% of the inflamed synovium in rheumatoid arthritis (294).

The synovial sublining also changes in inflammatory arthritis. Increase in vascularity is noted (146)and the sublining contains an infiltrate of macrophages and lymphocytes, as well as other leukocytes such as osteoclasts (295). T cells (particularly CD4+ T cells) make up 30-50% of the sublining cellular component in RA (145, 293),(296). B cells are found in RA synovium, but in far lower numbers, making up about 5% of the cellular infiltrate in RA (293). **Table 3.1** depicts the most abundant, and less prevalent cell groups present in inflamed synovium in RA.

Cells abundant in rheumatoid synovium
Macrophages (30-40%)
Fibroblast like synoviocytes (FLS) T lymphocytes (estimated at 30-50%)
Less Abundant cells:
B cells Osteoclasts Mast Cells Endothelial cells Dendritic cells Plasma cells

Table 3.1 Summary of most common cell groups present in RA synovium. adapted from Tran *et al.* (297)

It is increasingly acknowledged that there are a variety of different appearances of inflamed synovium in individuals with inflammatory arthritis, with numerous different patterns of cellular infiltrate noted in RA in particular (298) (**Figure 3.3**).

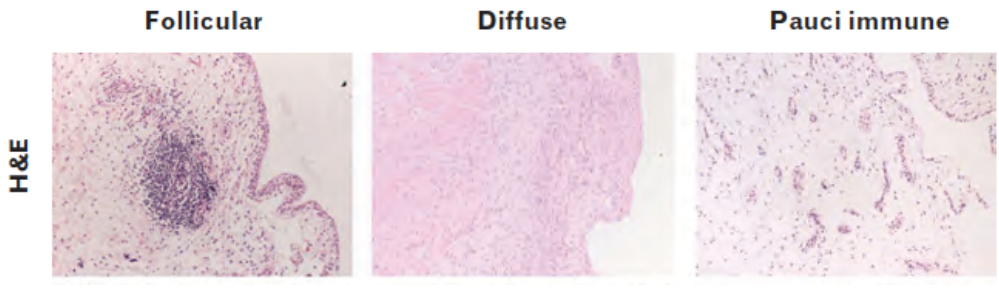

Figure 3.3 The main patterns of cellular infiltrate in RA synovial sublining. Adapted from Pitzalis *et al*. (298)

Here, immune cells can be found either randomly distributed within the synovial sublining (diffuse pattern) or spatially grouped into follicular structures (follicular pattern) (145, 298). Follicular and diffuse patterns are not necessarily mutually exclusive, and indeed, both patterns may exist in an individual's synovium, to different degrees (299). Additionally, Pitzalis *et al*. described a third pattern; Pauci-immune synovitis, with very little infiltrative leukocytes, despite clinically active disease or early untreated arthritis (298). More recent work by Dennis *et al*. further classified RA synovial histology as lymphoid, myeloid, low inflammatory or fibroid, each with a unique pattern of gene expression (300), with an indication of synovial phenotype being associated with response to anti-TNFα.

A highly sensitive cellular imaging tool, such as TSPO targeted PET, may have utility in the *in vivo* detection of even a small number of activated cells in synovium for the sensitive detection of synovitis, regardless of pattern of cell infiltrate. TSPO PET may further lend insight into those cell types that may predominate within the synovium of individual patients with inflammatory arthritis, hence potentially providing an idea of which targeted therapy would be most beneficial to an individual.

3.1.2 Main cell groups of RA synovium

3.1.2.1 Synovial macrophages

Macrophages are well known to play a central role in disease pathogenesis in inflammatory arthritis, as evidenced by, for example, the efficacy of anti-TNF therapies, treatments targeted to TNF-α, a cytokine predominantly produced by macrophages. Macrophage infiltration of synovial sublining has been demonstrated in

a variety of studies to correlate with disease activity (288, 289), as well as articular destruction (258, 301) in RA, further emphasizing the importance of macrophages in synovial inflammation.

Macrophages have multiple roles in inducing and potentiating inflammation in RA. Macrophages are potent producers of pro-inflammatory cytokines, including TNF-α, IL-6, IL-1 and MMPs, leading to promotion of angiogenesis, through release of VEGF (vascular endothelial growth factor) (77), release of acute phase proteins, and cartilage damage (302). Further, macrophages act as antigen presenting cells, presenting self to activate autoreactive T cells (303), potentiating inflammation, and cytokine release (such as IL-12, IL-15 or IL-18) produced by macrophages which can polarize T cells (302). Macrophages further produce chemokines, promoting the recruitment of leukocytes to synovial tissue (302). Additionally, the production of growth factors by macrophages -such as VEGF (304), TGF-β1 (305), and BAFF (306) (B-cell activating factor of the tumour-necrosis-factor family, also known as BLyS)- further propagating synovial inflammation, by promoting cell survival.

3.1.2.2 Macrophage polarity in inflamed synovium

Macrophages are known to exhibit considerable plasticity according to their milieu, lending support to the notion that macrophage polarity may depend on disease activity, with the proposal that M1 macrophages predominate in synovium during a flare, and M2 predominate in clinical remission or low disease activity (307). However, supporting evidence for this is lacking.

A dichotomy of macrophage phenotypes has been widely reported for decades (308). Here 'M1' or 'classically activated' macrophages are activated in the presence of M1 stimuli, such as LPS and IFN-**γ** (309). Such macrophages exhibit upregulation of antigen presenting receptors and toll like receptors (TLRs), produce TNF-α and reactive oxygen species, and are associated with Th-1 cell responses, potentiating inflammation (310).
In contrast, macrophages differentiated or activated in the presence of IL-4, glucocorticoid or TGF-β, are thought to differentiate into an anti-inflammatory or

‘alternatively activated’ ‘M2’ macrophage phenotype (309, 311). Such macrophages produce TGF-β and chemokines, such as CCL17, and are associated with Th-2 cell responses (311).

A number of studies have attempted to identify the predominant phenotype of macrophages present in inflamed synovium, but to date the data has not been conclusive. The following paragraphs summarise the current opinion about macrophage polarity in arthritic synovium.

Vandooren *et a*l. reported the prominence of M2 macrophages in PsA and other spondyloarthropathies (SpA), in contrast to M1 macrophages dominance in RA synovium (312). However, this study utilized healthy human peripheral blood derived monocytes, differentiated to macrophages using synovial fluid supernatant derived from PsA or RA patients. Although macrophages are known to be resident in synovial tissue, such a study did not take into account the fact that peripheral blood monocytes in arthritis patients (which enter synovium in arthritis) may be activated to a certain extent blood before infiltrating synovium and fully differentiating to macrophages (313, 314), and further may have a different phenotype to healthy peripheral blood monocytes, which could influence macrophage polarity in tissue. For example, some studies indicate that a subset of CD14+CD16+ monocytes is expanded in the peripheral blood of RA patients, and such a subset shares features of activated macrophages (315, 316). Hence, it may be that such pre-synovial activation, or expansion of a particular monocyte subset in peripheral blood could itself have an impact on macrophage polarity in arthritis patients, which is not taken into consideration when using healthy monocytes for studies of macrophage polarity in synovium.

Ambarus *et al.* provided further support for the notion that M1 macrophages predominate in RA compared to spondyloarthritis. Here, lining macrophages in synovium from those with SpA appear to express more of the M2 marker, CD163, compared to lining macrophages in RA synovium (317). However, there was no significant difference in expression of the IFN-ɣ induced marker (‘M1’), CD64, in any part of synovium between RA and spondyloarthritis synovium, and likewise, no significant difference in expression of the M2 markers, CD200R or CD32 (317-319),

thus it cannot be conclusively proven there is a true difference in macrophage polarity between RA and SpA, especially as it is increasingly recognized that a single marker alone is unlikely to be specific for a particular phenotype (320).

Further, it is well known that intima in RA is far more hyperplastic than in SpA (321). The study by Ambarus relied on using the marker, CD68, to confirm the presence of macrophages, and then further stained for more macrophage polarity specific markers. However, as CD68 is known to also be present on FLS (274), it could be possible, that since CD163 is macrophage specific, the lower CD163 staining of CD68 positive cells in RA synovium could be because more CD68+ cells were in fact FLS (and not macrophages), compared to SpA synovium.

3.1.2.3 Fibroblast like synoviocytes (FLS, synovial fibroblasts)

FLS are cells of mesenchymal origin, found in every tissue of the body (322), and known to be the largest group of stromal cells (323). Evidence suggests that the expansion of fibroblast populations in inflamed synovium (particularly in the lining) results from the inhibition of pro-apoptotic pathways, rather than proliferation (323).

The importance of FLS in the pathogenesis of RA was first indicated by Fassbender *et al*. who observed that aggressive resident synovial cells invaded and destroyed cartilage and bone in the joints of patients with RA (324). Animal model studies have provided further support for the importance of FLS in generation of synovitis; for example, mice deficient in cadherin-11 (an adhesion molecule selectively expressed on FLS (325)) had hypoplastic synovium, and displayed resistance to induction of inflammatory arthritis. A further animal model more directly demonstrated the importance of FLS, regardless of influence of leukocytes, in RA. Here, FLS from RA synovial fluid, when co-cultured with cartilage from a SCID (severe combined immunodeficiency) mouse (deficient in leukocytes), deeply invaded cartilage, unlike FLS from synovial fluid of OA patients (326). In humans, early evidence of the importance of FLS in RA was provided by a study of 36 patients, where the number of FLS (as well as T and B lymphocytes) was found to be related to the severity of joint damage on X ray (327).

FLS transform to an activated phenotype in RA (328), with several roles for activated FLS being identified in RA pathogenesis. Firstly, fibroblasts secrete damaging matrix metalloproteinases and cathespins (323), that break down cartilage and tissue, as well as secreting RANKL, which promotes differentiation of monocytes to osteoclasts, cells that further erode bone (329). Secondly, fibroblasts potentiate inflammation through recruiting, promoting the survival of, and retaining leukocytes in synovium. Activated fibroblasts express a range of inflammatory chemokines (such as IL-8), promoting leukocyte recruitment to synovium (330). Fibroblasts also promote survival of leukocytes within synovium through the inhibition of apoptosis, by secreting type 1 IFNs (promoting T cell survival (331)), IL-6 (promoting B cell survival (332)) and GM-CSF (promoting neutrophil survival (333)). Furthermore, through the upregulated expression of constitutive chemokines, activated fibroblasts may promote retention of leukocytes in synovial tissue, that would otherwise be removed to the lymphatics (334); hence further potentiating synovial inflammation. Interestingly, a SCID mouse model study demonstrated that RA-FLS are able to leave their primary place of implantation, enter the murine blood stream, and reinitiate destruction process at distant sites where human articular cartilage had been implanted without FLS. This suggests, that in addition to being locally destructive, RA FLS may also contribute to spread of disease from one joint to another (335).

3.1.2.4 T lymphocytes

T lymphocytes are recognized to have a central role in RA pathogenesis. Animal model work established that production of essential pro-inflammatory cytokines in RA, is likely to be T cell dependent. Here, SCID mice received grafts of RA synovial tissue. T cells were then depleted from the engrafted synovium using anti CD2 antibodies. This resulted in prompt cessation of tissue IFN-ɣ production, followed by decline in IL-1α, TNF-α, and MMP production. The exogenous administration of IFN-ɣ restored the production of these cytokines and MMPs, further indicating that T cell production of IFN-ɣ is critical to regulating RA synovitis (336).

Further indirect evidence for the importance of T cells in RA pathogenesis is provided by the long established fact that genetic predisposition to RA is associated with the

‘shared epitope’, an amino acid sequence within HLA-DRB1; present in 70% of Caucasians with RA, compared to about 30% of the healthy population (337). Since the main function of class II HLAs is to present antigen to T cells, it can therefore be theorized that T cells have a critical role in RA pathogenesis; indeed, it is postulated that presentation of citrullinated peptides by such HLAs to T cells, may contribute to a break in tolerance, through the generation of autoreactive T cells (338, 339).

Additional indirect evidence to support the fact that T cells are involved in RA pathogenesis, comes from the fact that the T cell surface molecule CD40L (essential for T cell interactions to activate other cell groups) is upregulated on CD4+ peripheral blood T cells in RA, compared to healthy controls, suggesting that inflammatory responses mediated by activated T cells are likely involved in RA pathogenesis (340). The success of abatacept (CTLA-4 Ig) therapy in treatment of RA also provides indirect evidence for the importance of T cells in the generation of inflammation in RA. Abatacept, a fusion protein, acts by blocking the T cell costimulatory signal generated by interaction of T cell expressed CD28 with CD80/ CD86 (expressed on antigen presenting cells, activated T cells and B cells), through binding CD80/CD86 (341).

The majority of T lymphocytes in inflamed synovium in RA are CD4 positive (342). However, a complex set of CD4 positive T cell subsets exist in inflamed synovium, with T helper cells, T regulatory cells, IL-17 producing Th17 T cells, each with their own contributions to disease pathogenesis.

T cells in RA provide B cells help, that can further increase B cell activation and antibody production, propagating inflammation in synovium (343). T cell production of IFN-ɣ and TNF-α activate macrophages and stromal cells in synovium (297). Additionally, T cell/monocyte CD40L-CD40 interactions promote the differentiation of monocytes to osteoclasts, which destroy bone (295).

Th17 cells produce IL-17, a strong effector inflammatory cytokine, inducing pro-inflammatory cytokine secretion (such as TNF-α, IL-1, IL-6) from stromal cells, neutrophils, macrophages and activating osteoclasts and chondrocytes, further contributing to synovial inflammation and bone and cartilage destruction (344). T regulatory cell functionality may be impaired in RA, leading to failure of suppression of

TNF-α and IFN-ɣ production by synovial CD4 T cells, promoting T cell induced inflammatory responses (345).

3.1.3 Cell markers in synovial tissue-distinguishing between fibroblasts and macrophages

It is well recognized that there is considerable overlap of cell markers between macrophages and fibroblasts present in synovium (158, 346), leading to difficulties in discriminating between these cell groups. Pilling *et al*. attempted to use multiple monoclonal antibodies to establish shared expression of multiple markers between macrophages and fibroblasts (see **Figure 3.4** for some examples of markers investigated) (346).

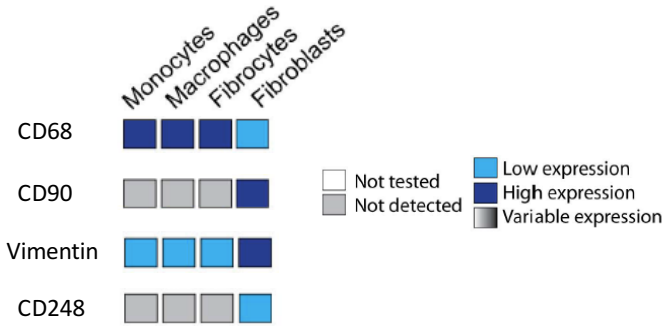

Figure 3.4 Representation of the expression of several markers on monocytes, macrophages and fibroblasts, adapted from Pilling *et al*. (346).

3.1.3.1 Macrophage markers in synovium

CD68, a scavenger receptor that binds to oxidized low-density lipoprotein, and has a postulated role in cell-cell interaction, is a widely accepted macrophage specific marker in both tissue and blood, being highly upregulated on macrophages compared to monocytes (347). CD68 has long been used as a macrophage marker in RA synovium, with synovial staining for CD68 being used as a means of correlating synovial macrophage infiltration with disease activity in multiple studies (258, 288).

However, in disease states, CD68 is also known to be expressed on intimal fibroblasts in synovium; certainly, Fonseca *et al*. demonstrated most intima (lining) cells of RA synovium (known to consist of both fibroblasts and macrophages) were CD68 positive

(274). The likelihood of CD68 being expressed on both macrophages and fibroblasts in synovium was further demonstrated by Kunisch *et al.* who demonstrated co-localisation of CD68 and the fibroblast markers CD90 and prolyl-4-hydroxylase in synovium (275). Therefore, CD68 is not macrophage specific for synovial tissue (274).

Although the predominant polarity of macrophages in inflamed synovium remains unknown, the M2 phenotype macrophage marker CD163 (a cell surface glycoprotein) is thought to be a more specific for macrophages than CD68 in synovial tissue, being demonstrated to be able to distinguish between synovial macrophages and fibroblasts (274).

3.1.3.2 Fibroblast markers in synovium

The appearance of FLS may be heterogeneous in synovial tissue; RA synovial FLS are thought to undergo phenotypic change, developing a rounded appearance, with pale nuclei, and prominent nucleoli, characterizing the activated FLS phenotype (348).

Multiple markers for synovial fibroblasts have been used to identify these cells. CD90 (Thy-1), a glycosylphosphatidylinositol (GPI)-linked cell surface glycoprotein, has long been recognized to be expressed highly on synovial fibroblasts, and is frequently used in studies as a fibroblast marker in synovial tissue (293, 346). Other well accepted markers include vimentin, the collagenase prolyl-4-hydroxylase, Decay Accelerating Factor (DAF, CD55), and cadherin-11 (293).

The phenotyping of synovial fibroblasts in inflammation is the subject of ongoing investigation, with the discovery of several fibroblast markers. The transmembrane glycoprotein CD248 (also known as endosialin) is increasingly recognized as a sublining marker of fibroblasts in inflamed synovium (323), and is thought to have roles in angiogenesis, adhesion and invasiveness (349). This marker is known to be upregulated in stroma inflammation and malignancy. CD248 positive synovial fibroblasts are increasingly thought to be phenotypically distinct from PDPN (or gp38) positive synovial fibroblasts, which are found in the synovial lining, but also in the

sublining (323). Like CD248, PDPN is not expressed in normal synovium compared to RA synovium (350, 351). PDPN staining has been demonstrated to correlate with the presence of lymphoid neogenesis, and also RF or ACPA positivity. Interestingly, activation of *in vitro* synovial fibroblasts with TNF-α further increased the expression of PDPN. In RA patients, anti-TNF-α therapy decreased synovial PDPN expression. *In vitro* studies demonstrated that PDPN silencing did not change the invasiveness of fibroblasts, but IL-6 production by these cells was reduced (351).

3.2 Aims:

1. To provide evidence that [^{3}H]PBR28 tracer uptake in synovium reflects tissue cellularity, using autoradiography of synovial tissue samples.

2. To provide *ex-vivo* evidence of TSPO staining of different cell types in human synovium.

3. To assess the expression of TSPO in the three main cell types known to make up pannus at both mRNA and protein level; T lymphocytes, monocytes/macrophages and fibroblasts.

3.3 Methodology

3.3.1 DNA extraction and genotyping

As described in Chapter 2, binding affinity of [^{3}H]PBR28 will be different in those of different rs6971 genotype, and hence affect comparability of results between donors in radioligand saturation binding and autoradiography work. Therefore, only donors wildtype for rs6971 (high affinity binders) were used for the work described in this chapter, to ensure comparisons made between groups are accurate.

3.3.1.1 DNA extraction

For cells acquired from healthy donor cones, 200 μL of donor cone blood was utilized for DNA extraction (as previously described in **Chapter 2 section 2.4.3**). Likewise, DNA was extracted from the peripheral blood of those patients and healthy controls donating synovial tissue (ethics references 15/LO/0013 and 07/H0706/81).

3.3.1.2 rs6971 genotyping

Genotyping for rs6971 was carried out as previously described in **Chapter 2 section 2.4.4**.

3.3.2 Cell harvesting and culture

3.3.2.1 Isolation of FLS from synovial tissue

Healthy synovial tissue was obtained from arthroscopic knee surgery of patients with ligamentous knee injury (ethics reference 15/LO/0013 and 07/H0706/81). For the generation of cytospin slides containing FLS, for staining optimisation, RA synovial tissue, isolated from the knee or hip joints of patients with established RA (as per ACR criteria), undergoing joint replacement surgery was obtained (ethics reference: 07/H0706/81). The tissue was placed into sterile RPMI at 4ºC, and transported to the

laboratory. The synovial tissue was digested as previously described in Brennan *et al.* (352) and Sivakumar *et al.* (353). The synovial tissue was disintegrated manually using scalpels (Leica Biosystems), and digested manually with 5mg/L collagenase A (Roche, Burgess Hill, UK) and a 0.15g/L DNase (Sigma-Aldrich, Poole, UK). After enzymatic incubation at 37ºC for approximately 1 hour, DMEM (Dulbecco's modified Eagle's medium, Biowhittaker™, Cambrex Bio Science, Belgium, supplemented with 10% endotoxin free Foetal Calf Serum, Sigma-Aldrich, and 1% penicillin and streptomycin, Sigma-Aldrich) was added to stop the digestion.

The cellular material was passed through a sterile nylon cell-strainer (Leica Biosystems) to obtain a single cell suspension, and spun down at 400g for 8 minutes. The pellets were resuspended in complete DMEM media, and cells counted using a Hawksley chamber (Neubauer, Lancing, Sussex UK), and plated at $1x10^6$ cells per $75cm^2$ flask (T-75). After incubation overnight, non-adherent cells were removed, leaving behind FLS, which were propagated further.

3.3.2.2 Cell culture of FLS

Cells were not grown past passage 6, in order to ensure that FLS remained as phenotypically unchanged as possible (354, 355). Fibroblasts were plated out at $8x10^5$ cells per $64cm^2$ tissue culture dish (Greiner Bio-One) and allowed to adhere for 48 hours. The day before the experiment, cells were starved for 24 hours in FCS free DMEM, to ensure that cell cycles were synchronized. The media was then removed, and cells were stimulated in complete DMEM with TNF-α 10ng/mL for 24 hours, or IL-1β 10ng/mL for 24 hours. For the unstimulated condition, complete DMEM alone was added. Following the stimulation period, overlying medial was removed, and the cells washed in PBS, scraped, and pelleted for further use.

3.3.2.3 Isolation of healthy peripheral blood human monocytes for *in vitro* studies

Peripheral blood monocytes and lymphocytes were isolated from blood cones of healthy donors purchased from the National Blood Service (Colindale, Edgware,

London, UK) using density gradient centrifugation, and centrifugal elutriation performed utilizing flow cytometry to isolate fractions of 90% purity monocytes, as well 90% purity lymphocytes.

3.3.2.3.1 Preparation of blood cones

The contents of a blood cone, containing buffy coat, was drained into a 50mL falcon, under asepsis in a sterile cell culture hood. The buffy coat was made up to 40mLs in Hanks Balanced Salt Solution (HBSS) (Gibco®, Life Technologies, Paisley, UK). Twenty mLs of the diluted buffy coat was layered onto 20mLs of Histopaque® (Sigma-Aldrich, St Louis, USA), in a 50mL falcon, and centrifuged at 2500rpm for 20 minutes, without the deceleration brake on the centrifuge, to yield an interphase layer of leucocyte rich cells.

The interphase layer was removed using a Pasteur pipette, and the pellets made up to 40mLs with HBSS, and centrifuged at 2000rpm for 10 minutes to undertake a first wash to remove residual Histopaque®. A second wash was performed on pooled pellets by resuspending to 40mLs in HBSS, and centrifuging at 1000rpm for 15 minutes. Finally, the resultant pellet was resuspended up to 40mLs in RPMI (Lonza, Biowhittaker®, Belgium) with 10% FBS.

3.3.2.3.2 Centrifugal elutriation

This is a well-established process for isolating cells of different size (356-358). It combines two separate processes: (a) centrifugation-the process of sedimentation under the influence of a centrifugal force; and (b) elutriation-the process of separation by washing.

Cells isolated from the blood cone underwent centrifugal elutriation in a Beckman JE6 Elutriator (Beckman Coulter, High Wycombe, UK) (**Figure 3.5**) at 2500rpm to obtained monocyte-rich fractions.

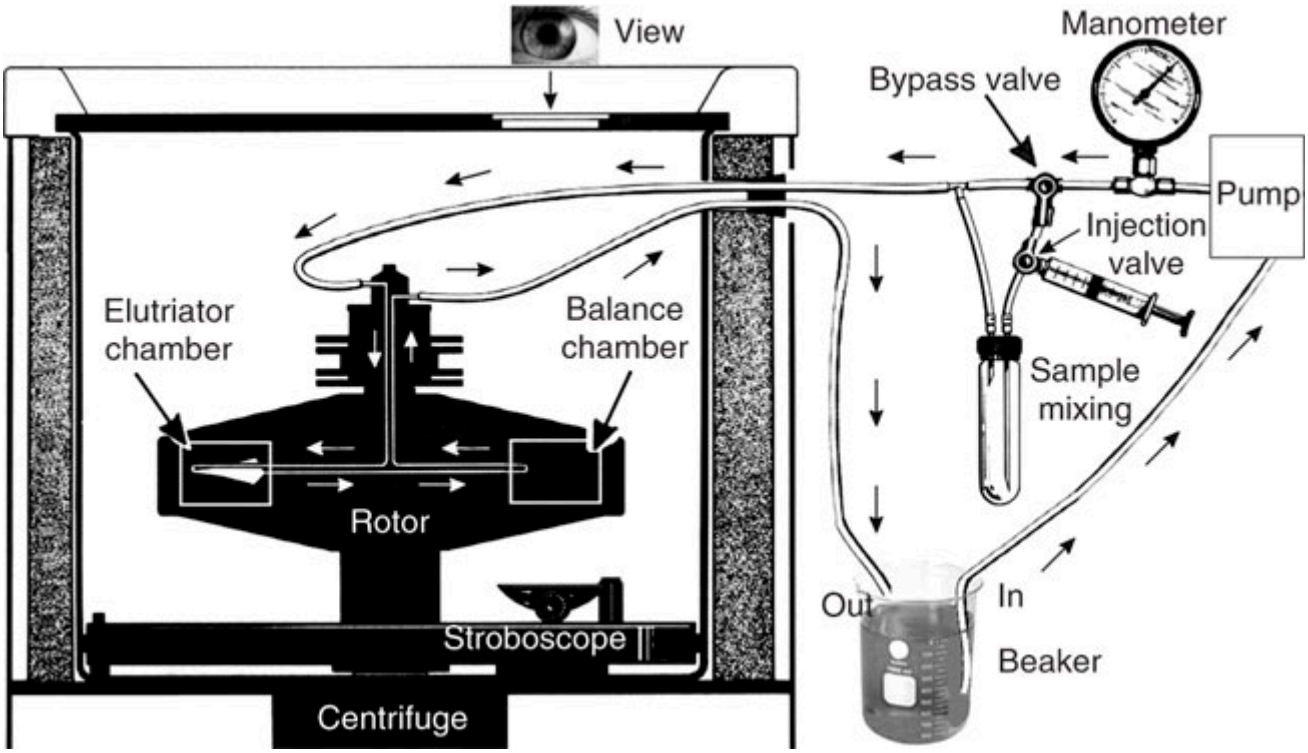

Figure 3.5 The set-up of the centrifugal elutriation apparatus; adapted from Banfalvi (359).

The centrifuge is run at room temperature and a constant speed of 2200rpm (as described in Banfalvi) (359). The pump was then turned on and the system cleaned with 70% ethanol, and then with 200mLs of phosphate buffered saline (Gibco®, Life Technologies, Paisley, UK). The physiological buffer was then replaced by freshly made elutriation fluid at an initial flow rate of 12mLs/minute used for the introduction of cells into the chamber. This serves to remove bubbles from the system (which can be left behind in the elutriation chamber, in the sample mixing chamber, tubing and the manometer). The sample mixer also serves as a bubble trap during elutriation.

Cells were loaded into the elutriation chamber at an increasing flow rate, and subjected to an opposing centrifugal force compared to the flow velocity (**Figure 3.6**). Since the centrifugal force is constant, separation of cells according to size and granularity occurs by altering the flow of the media into the centrifuge, done via a pump. Increasing the low rate in gradual steps yields successive fractions of increasingly large or dense cells being collected. Lymphocytes were ejected when the flow rate was at 12-15mLs/minute. Monocytes were ejected when the flow rate was increased

to 18-22mLs/minute. The percentage of monocytes or lymphocytes in the fraction being ejected was determined by concomitant analysis of cell size and granularity using flow cytometry. Only fractions containing more than 90% monocytes and less than 5% granulocytes were used for experimental purposes (360). As for monocytes, only fractions containing more than 90% lymphocytes were used for experimental purposes.

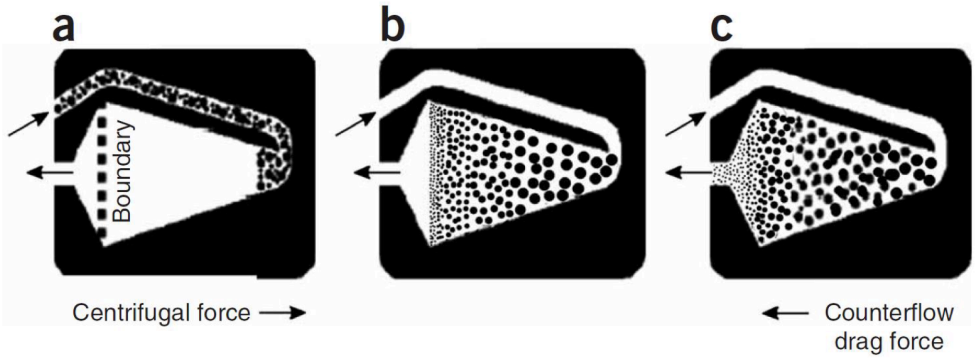

a Cells suspended in media enter the chamber at the centrifugal end
b Centrigual sedimentation of cells is balanced by flow velocity
c As the flow rate of cells is increased, smaller, slow sedimenting cells elutriate out of the chamber

Figure 3.6 a-c the three steps of separation of cells according to size and granularity by centrifugal elutriation; adapted from Banfalvi (359)

3.3.2.4 Purification of Lymphocytes

Lymphocytes extracted from elutriation were further separated into CD4+ positive T lymphocyte fraction, using the positive selection CD4+ T-cell Isolation kit (Miltenyi, Bisley, Surrey, UK). This uses magnetic activated cell sorting to isolate desired cells.

In brief, the lymphocyte cell suspension was counted, and centrifuged at 300g for 10 minutes. The supernatant was aspirated, and the cell pellet was resuspended in 80µL of MACS running buffer (containing PBS, BSA (bovine serum albumin) 0.05%, EDTA, and 0.09% azide) per 10^7 cells. 20µL of CD4 microbeads was added per 10^7 cells, and the resultant mixture was incubated for 15 minutes at 2-8°C. Cells were then washed by adding 1-2mLs of buffer per 10^7 cells and centrifuged at 300g for 10 min. The resultant pellet was re-suspended up to 10^8 cells in 500µL buffer. A MACS column

was placed in the MACS separator, and prepared by rinsing with 500 µL buffer. Cell suspension was then placed into the column, and allowed to run through under gravity. The flow-through was discarded. The column was removed from the separator, and placed over a 15mL falcon. One mL of MACS running buffer, was then placed into the column. The magnetically-labelled CD4-positive cells were then flushed through the column by firmly pushing the plunger into the column.

3.3.2.5 Macrophage differentiation and stimulation

Differentiation of monocytes to macrophages

Monocytes from healthy peripheral blood mononuclear fractions were counted, and resuspended to a density of $1x10^6$ cells/mL in complete RPMI (Lonza, Whittaker, with 10% endotoxin free FCS (Sigma-Aldrich), and 1% pencillin/streptomycin (Sigma-Aldrich)). Macrophages were differentiated from elutriated monocytes by culturing cells with 100ng/mL M-CSF (Peprotech Inc, Rocky hill, NJ, USA) at a concentration of $1x10^6$ cells/mL, for 7 days (320). For radioligand binding studies, macrophages were grown at a concentration of $1x10^6$ cells/mL in $20cm^2$ sterile petri dishes (Greiner Bio-One, UK). Monocytes were also pelleted by centrifugation at 400g for 10 minutes, washed twice in PBS, and then use for RNA studies, or radioligand binding work.

Flow cytometry (Fluorescence-activated Cell sorting, FACS) to confirm monocyte to macrophage differentiation

Flow cytometry was used to confirm that monocytes were differentiated to macrophages *in vitro* through culture with 100ng/mL M-CSF for 7 days. In brief, adherent cells were dissociated from the plate using EDTA solution (Sigma-Aldrich) and gentle scraping. Cells (monocytes or macrophages) were washed twice in PBS, before incubating at a count of 2 million cells/mL in 1.6% paraformaldehyde solution for 20 minutes. Cells were washed twice more, resuspended to a count of 1 million/mL before utilization for flow cytometry.

To confirm macrophage differentiation from monocytes, cells were incubated with

human anti-mouse CD68 antibody, conjugated to the fluorophore PE-Cy7 (Biolegend). Cells were also left unstained, and also with an isotype for CD14, or for CD68, respectively, to generated both unstained and isotype controls for FACS. **Figure 3.7** depicts increase in cell granularity and size (Figures 3.7A and 3.7B), and upregulation of the macrophage marker CD68 after culture with 7 days of M-CSF.

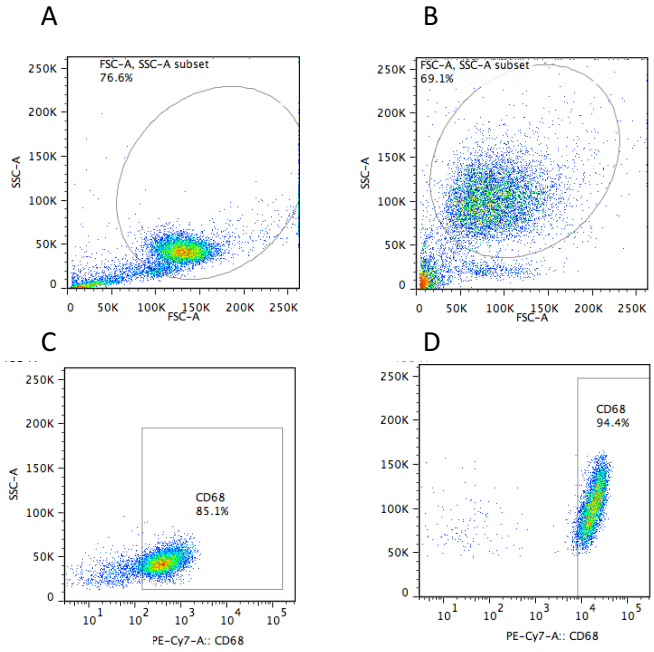

Figure 3.7 A representative FACS of healthy monocytes, and healthy MDM after 7 days culture with 100ng/mL M-CSF. **A**: SSC-A/FSC of harvested monocytes. **B**: SSC-A/FSC of unstimulated healthy human MDM, generated by the differentiated of monocytes for 7 days with M-CSF. **C:** SSC-A/PE-Cy7-A -CD68 staining of monocytes. **D**: SSC-A/PE-Cy7-A-CD68 staining of unstimulated healthy human MDM. MDM=monocyte derived macrophages, SSC-A=side scatter area (measure of cell granularity), FSC=forward scatter (measure of cell size).

Stimulation of macrophages

Monocyte derived macrophages (MDM) were then stimulated with 10ng/mL LPS (Peprotech) and 20ng/mL IFN-γ (Peprotech) or 20ng/mL IL-4 (Peprotech) for 24 hours. Cells were then scraped, pelleted by centrifugation at 400g for 10 minutes, washed twice in PBS, and then use for RNA studies, or radioligand binding work.

3.3.2.6 Lymphocyte cell culture and stimulation

The purity of lymphocytes used was checked using flow cytometry to ensure 85% purity of CD4 positive lymphocytes.

Lymphocytes were washed, and plated at $10x10^6$ cells per $64cm^2$ tissue (Greiner Bio-One, UK) in complete media. Cells were stimulated with 10ng/mL of phorbol 12-myristate 13-acetate (PMA, Sigma-Aldrich, Poole, UK) plus 1µg/mL ionomycin (Sigma-Aldrich, Poole, UK) for 6 hours as described (361), or left unstimulated. Cells were then pelleted by centrifugation at 400g for 10 minutes, washed twice in PBS, and then use for RNA studies, or radioligand binding work.

3.3.3 Enzyme Linked Immunosorbent Assay (ELISA)

In order to provide supporting evidence of cell activation, ELISA were performed using cell supernatant.

For macrophages, the concentrations of soluble human TNF-α in cell culture media were measured using commercially-available enzyme-linked immunosorbent assay (Quantikine human TNF-α ELISA Kits, R&D Systems Europe) according to the manufacturer's instructions. Each reaction was run in triplicate. The optical density measurements were carried out using ELISA plate reader (Multiskan Ascent Thermo Labsystems, Finland) at 450 nm wavelength. The lower and higher detection limits of the kits were 15.6pg/mL and 1000pg/mL, respectively.

For fibroblasts, the concentrations of soluble human IL-6 in cell culture media were measured using a Quantikine human IL-6 ELISA Kit (R&D Systems Europe) (detection range 0.2-10pg/mL), and similarly, for T cells, the concentrations of soluble human IFN-ɣ were measured using a Quantikine human IFN- ɣ ELISA Kit (R&D Systems Europe) (detection range 15.6-1000 pg/mL).

3.3.4 RNA extraction

For RNA isolation, cells were cultured in a 24 well plate at 1million cells/well. A total RNA kit E.Z.N.A^{TM} EaZy Nucleic Acid Isolation (VWR, Batavia, IL, USA) was used to extract RNA. Cells were put on ice, washed with PBS, and homogenized with 350µL of TRK lysis buffer with β-mercaptoethanol, and RNA was isolated following the kit protocol. Cells were scraped, mixed with lysis buffer by pipetting, and vortexed thoroughly with 350µL of 70% ethanol and spun using HiBind®RNA Spin Column at 10,000g for 1 minute. The extracted RNA on the spin column was then washed with RNA wash buffer I, followed by 2 washes of RNA wash buffer II. RNA was then eluted from the Spin Column with 30µL of nuclease free water (in which RNAses were inactivated using 0.1% DEPC (Diethyl pyrocarbonate) water.

RNA concentration was measured using a NanoDrop2000^{TM} spectrophotometer (Eppendorf AG, Hamburg, Germany).

The NanoDrop2000^{TM} software used the modified Beer-Lambert equation to calculate RNA concentration (362):

$$c = (A \times e)/b$$

where c = nucleic acid concentration (ng/µL)
A = absorbance in AU
e = wavelength dependent extinction coefficient (ng-cm/µL)
b = path length (cm)

Nucleotides, RNA, single-stranded DNA (ssDNA) and double-stranded DNA (dsDNA) absorb light at 260nm, hence nucleic acids were measured at this wavelength. However, protein and other contaminants absorb light strongly at around 280nm. The purity of the RNA was therefore evaluated by the ratio of the absorbance read at 260nm and 280nm (Abs 260/280). Abs260/Abs280 ratio of above 1.7 was considered to indicate RNA of sufficient purity for use (363).

3.3.5 cDNA synthesis

The mRNA of many genes of interest is usually expressed in very small amounts, and therefore needs to be amplified for analysis. RNA is relatively unstable, hence cannot be directly amplified using PCR. Therefore, converting RNA to dsDNA is necessary for the mRNA of the gene of interest to be analysed by quantitative PCR.

Reverse transcription is a process of creating a single stranded cDNA from an RNA template using reverse transcriptase, also known as RNA-dependent DNA polymerase. The enzyme helps the formation of a double stranded cDNA that can be used for PCR. Reverse transcription was performed using 500ng of purified RNA diluted in DEPC water to a total volume of 11µL. To this, 1µL of random primers (Invitrogen, Paisley UK) was added, followed by incubating the samples at 72°C in a Veriti^{TM} 96 well Thermal cycler (Applied Biosystems, Life Technologies, Paisley UK). A cocktail of random primers was preferred in order to produce cDNA from all mRNAs, and to increase the probability that 5'ends of the mRNA would be converted to cDNA. Following this, samples were then cooled to 4°C, and 8 µL of a mixture of PCR buffer, RNAisin, dNTPs (dATP, dGTP, dCTP, dTTP), DEPC water and Moloney Murine Leukaemia Virus (M-MLV) reverse transcriptase (all purchased from Promega, Southampton, UK) was added to each sample. Samples then underwent PCR in the Veriti^{TM} 96 well Thermal cycler.

The dilution of cDNA produced was based upon optimization experiments utilizing the ViiA^{TM} 7 Real-Time PCR System (Applied Biosystems, Paisley UK) at the Botnar Research Centre in order to obtain most sensitive expression of housekeeping genes, to ensure PCR values obtained were sensitive and meaningful.

3.3.6 Real-time, quantitative Polymerase Chain Reaction (PCR)

Real-time Polymerase Chain Reaction (RT-PCR) allows the sensitive, specific and reproducible quantitation of nucleic acids in real time. Here, copies of a DNA template (specified by primers used) are generated exponentially, resulting in a quantitative relationship between the amount of starting target sequence and amount of PCR

product accumulated at any particular cycle (364). The process of PCR is described in detail in Appendix section A3.

For each sample, 5 µL of SYBR Green® (Applied Biosystems) was added to 1 µL cDNA (500ng/mL). In a 384 well PCR plate (Applied Biosystems) 4 µL of forward and reverse primer were added (500nM, Invitrogen). Three replicates of each sample were incubated at 50°C for 2 minutes, followed by the initial denaturation step at 95°C for 5 minutes. 40 amplification cycles were carried out and the thermocycling conditions were: denaturation at 95°C for 10 seconds, annealing at 60°C for 15 seconds and extension at 72°C for 20 seconds. A single peak in the dissociation curve reflects the generation of only one product per sample, thus excluding the possibility of contamination.

Primer sequences used in this study are outlined in **Table 3.2.**

GENE	SENSE PRIMER	ANTI-SENSE PRIMER
18S ribosomal RNA (18S)	GTAACCCGTTGAACCCCA	CCATCCAATCGGTAGTAGCG
Translocator protein (TSPO)	GCGGCCTGGCTAACTCCTGC	AAAGCGGGAGCCCACGAAGC

Table 3.2 Primer sequences used for *TSPO* mRNA expression studies.

It is well recognized that housekeeping genes experience fluctuations according to tissues and treatments (365). For this work, *18s* ribosomal mRNA was used as a housekeeping (reference) gene, as it has been demonstrated to be reasonably stably expressed over monocytes, macrophages, T lymphocytes by previous work (366). However, there is less information on synovial fibroblasts. Therefore, validation of three housekeeping genes was undertaken, to ascertain whether *18s* would also be suitable for use in synovial fibroblast mRNA studies. Here, the fold change of *TSPO* mRNA using *18s*, β-actin and ATP-synthase, was calculated (see **Table 3.3**).

Condition	*18s*	*β-Actin*	*ATP-synthase*
TNF-α	2.413	2.468	2.584
IL-1β	3.024	3.024	2.901

Table 3.3 Summary of fold changes of FLS stimulated with TNF-α or IL-1β after 24 hours stimulation (compared with unstimulated FLS), using *18s*, β-actin and ATP-synthase as housekeeping proteins.

There appeared to be no significant different in fold changes using the three different housekeeping genes, therefore *18s* was used as housekeeping (reference) gene in subsequent work.

3.3.7 Radioligand saturation binding

The principles of radioligand binding assays have been long established, and are as follows; a preparation containing the receptor of interest (TSPO) is incubated with a suitable radioligand (in our case [^{3}H]PBR28), and then the radioactivity bound to the receptor is determined. A saturation curve is generated by holding the amount of receptor (TSPO) constant, and varying the concentration of radioligand, to provide an estimate of receptor density (B_{max}), which can be calculated when an equilibrium is reached between radio-ligand/receptor binding (at the point at which the saturation-binding curve plateaus (see **Figure 3.8**) (266, 367). In order to take into account any non-specific binding of radioligand (for example, to the assay plate), on the same assay plate, the assay was also run with the addition of 'cold' (non-radio-labelled) TSPO ligand to the TSPO-[^{3}H]PBR28 mix, in order to block all specific binding sites for [^{3}H]PBR28. This gives a non-specific binding value, which can then be subtracted from total [^{3}H]PBR28 binding, to give a specific binding value, hence ensuring accurate calculation of B_{max} (266). Since B_{max} is a reflection of receptor protein expression, radioligand binding is commonly used for quantification of radioligand binding sites (and hence the protein which expresses the binding site), and can be used to investigate changes in target protein expression, perhaps resulting from disease states (368).

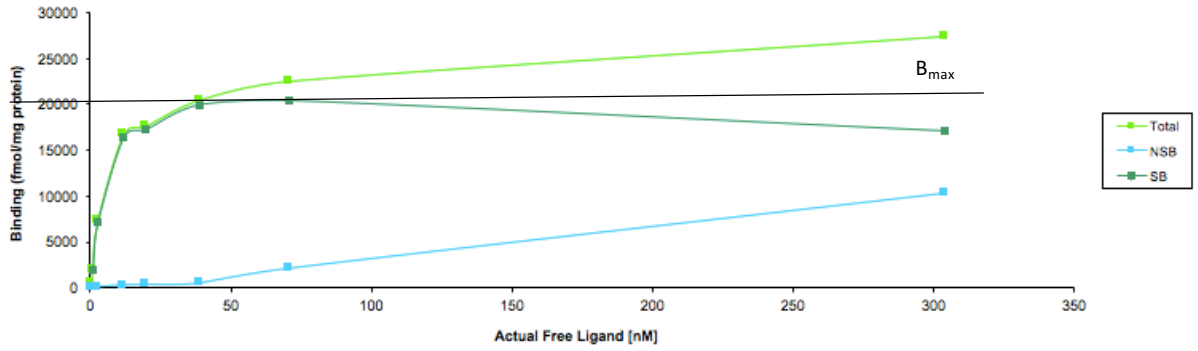

Figure 3.8 An example of a saturation binding curve generated from [^{3}H]PBR28 radioligand saturation binding using stimulated FLS. SB=specific binding, NSB=non-specific binding

PBR28 is well recognised to be a highly specific and high affinity ligand to TSPO (originally known as PBR, the peripheral benzodiazepine receptor) (259), and has been demonstrated in multiple *in vivo* studies to be reflective of PBR (TSPO) receptor expression (369, 370). Due to the high specificity of PBR28 for its target, in addition to the fact that PBR28 has been used as a radioligand for TSPO *in vivo* imaging in this thesis, PBR28 was chosen as the radioligand used in saturation binding studies for this work, to quantify TSPO protein expression. [^{3}H]PBR28 was chosen, as opposed to [^{11}C]PBR28 used for *in vivo* imaging, as tritium ([^{3}H]) has a far longer half-life (12 years compared to 20 minutes for [^{11}C] (142, 371)); hence is more stable for *in vitro* work, and further, did not need to be synthesized on a daily basis due to short half-life, unlike [^{11}C]PBR28. Further, unlike the ɣ-radiation emitting [^{11}C], tritium emits β-radiation(371), which is far less penetrating, making it safer for use for *in vitro* work.

3.3.7.1 Preparation of protein lysates

Due to the large volume of protein required to undertake saturation binding (minimum 2.4mg cytoplasmic protein per condition for each donor, based on our optimization work), only macrophages derived from healthy donor peripheral blood monocytes were used for radioligand saturation binding studies. Cells were washed twice in PBS, and centrifuged at 500g for 12 minutes to generate pellets. The cytoplasmic fraction of cell pellets was then extracted by sub-fractionation through homogenizing cell pellets in buffer 1 (0.32mM sucrose, 5mM Tris HCl, 1mM $MgCl_2$ at a pH of 7.4 at 4°C).

The resulting suspension was centrifuged at 1000g for 10 minutes at 4°C. The supernatant was then diluted 1:1 with buffer 2 (containing 50mM Tris HCl, 1mM $MgCl_2$ at a pH of 7.4 at 4°C). The total protein concentration was assayed using the Pierce® BCA Protein Assay Kit (Life Technologies, Lutterworth, Leicestershire UK).

3.3.7.2 Radioligand concentrations

No previous work of TSPO radioligand saturation binding studies, utilising healthy peripheral blood derived macrophages, lymphocytes, or synovial fibroblasts, have been performed to date. BV2 microglia are an immortalized form of murine microglia, widely accepted to be a model for primary microglia (372), resident macrophages in the brain (373). Such cells were utilized for optimization since they were readily available in large numbers required for an optimization protocol, are known to express TSPO (190, 374), and, as cells resembling macrophages, were assumed to at least give some indication of approximate concentrations of radioligand that would be suitable for radioligand saturation binding for macrophages.

From optimisation work done on BV2 microglia pellets (donated by David Owen, Imperial College London), eight different concentration of [^{3}H]PBR28 were decided upon to generate the saturation binding assay; 100mM, 30mM, 10mM, 5mM, 3mM, 1mM, 0.3mM and 0.1mM. 10μL of each concentration was added to 4mLs of scintillation fluid (Ultima Gold™), to generate standards. Each standard was made in triplicate.

The same stock of [^{3}H]PBR28 (ARC radiolabeled ligands, USA) was used for all saturation binding assays. Stock was diluted to the appropriate concentration using 'buffer 3' (comprising 50mM Tris Base, 140mM NaCl, 1.5mM $MgCl_2$, 5mM KCl, 1.5mM $CaCl_2$ at a pH of 7.4 at 37°C).

Cytoplasmic cell fraction was plated a 96 well plate (Thermo Fisher Scientific, Rochester, NY) in 6 wells for each radio-ligand concentration, with total binding, and non-specific binding of PBR28 being assessed in triplicate wells. 200μL of cell cytoplasmic fraction (with a total of 40μg of protein), 25μL of [^{3}H]PBR28 and 25μL

buffer 3, were placed in wells to assess total binding. 200μL of protein (with a total of 50μg of protein), 25μL of [^{3}H]PBR28 and 25μL of PK11195 (a non-radiolabelled ligand to TSPO) was placed in wells to assess non-specific binding). Plates were incubated for 1 hour at 37°C. The bound ligand was harvested onto GF/C filter paper (Brandel Inc. Gathersburg MD) using a Brandel Harvester (Brandel Inc. Gathersburg MD) (**Figure 3.9**) (265). Filter paper from each assay plate well were then punched out into a scintillation tube with 4 mLs of scintillation fluid (Ultima Gold^{TM}). A beta counter was used to measure the disintegrations per minute (DPM) (Tri-Carb 2900TR Liquid Scintillation Analyzer, PerkinElmer).

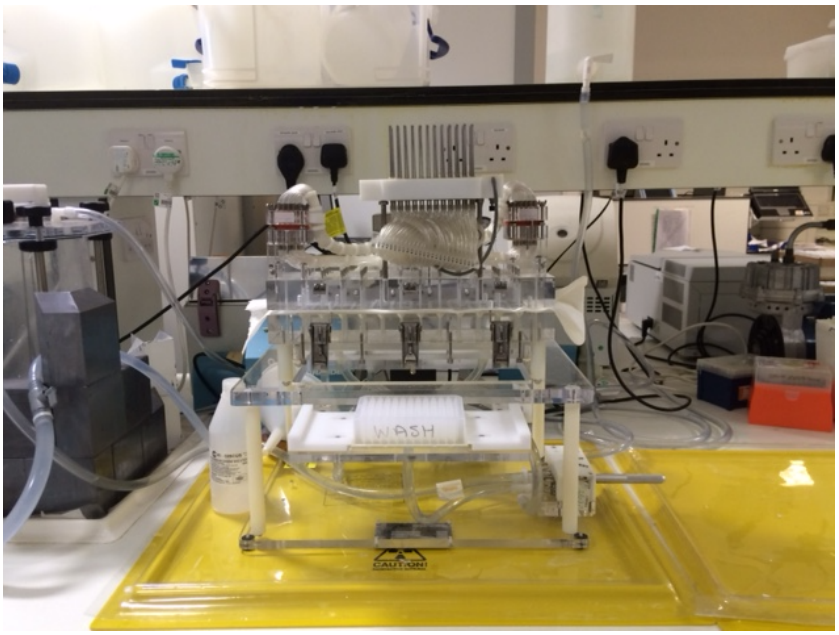

Figure 3.9 The Brandell Harvester.

3.3.7.3 Analysis of saturation binding data

An average was taken of DPMs for triplicate wells for total and non-specific binding at each radio-ligand concentration. Non-specific binding was subtracted from total binding to generate specific binding DPM. This was then plotted against radio-ligand concentration, and non-linear regression analysis generated to create a one site specific binding saturation curve, and a value of tracer required in fmol to bind to all TSPO in 1 mg of protein, known as B_{max}.

Since FLS and macrophages are inherently larger than monocytes and lymphocytes (375), with possible differing amounts of protein in each cell type, calculating tracer binding per cell (195) is a more accurate means of comparing tracer binding between cell groups than simply calculating tracer bound per mg of protein, and renders results more easily translatable back to TSPO signal from the pannus.

B_{max} value was therefore multiplied by the total amount of protein in each cell pellet used, and then divided by number of cells in each pellet, to generate a value of fmol of [^{3}H]PBR28 required to bind per 1x10^{6} cells (195), reflecting TSPO present in the cell pellet being assayed, rather than solely reflecting amount of tracer binding per mg of cell protein.

3.3.8 Autoradiography

3.3.8.1 Tissue acquisition

Acquisition of RA and healthy control was from participants undergoing synovial biopsy in 'The utility of [^{11}C]PBR28 PET-CT for the imaging of inflammatory arthritis' study described in **Chapter 2**, in addition to RA synovium provided from patients with established RA (as per ACR criteria(25)) undergoing knee replacement surgery. Only participants of high binding affinity were utilized for this study. Tissue was placed into sterile media for transport to the laboratory.

3.3.8.2 Cryopreservation of tissue

Tissue was rinsed in PBS, placed into TissueTek® cryomoulds, embedded in OCT (Leica®), before being frozen in isopentane cooled to -70ºC on dry ice. Tissue in OCT was wrapped in foil, and stored at -80ºC prior to sectioning.

3.3.8.3 Preparation of gelatin-subbed slides for use in autoradiography

Slides for use were purchased from Leica® (dimension of 25mm x 75mm, frosted at one end, and on one side). Slides were loaded into racks, and soaked in slide wash

(90% ethanol with hydrochloric acid at a concentration of 1:50) for 10 minutes. Slides were then dried in a cool airstream before fully submerging for 3 minutes in a cooled gelatin solution (1g of gelatin in 200mLs distilled water, with 0.1g chromic potassium sulphate (Chrom Alum). Slides were removed from the gelatin, and allowed to drain. Slides were left to dry overnight in a draft free area, before storage at -80ºC.

3.3.8.4 Sectioning of tissue

Tissue was then sectioned onto gelatin-submerged slides, at a thickness of 10 μm per section, using a cryostat microtome (Leica, Wetzlar, Germany; CM1900). Tissue was sectioned within 21 days of autoradiography. A minimum of 12 gelatin-submerged slides were generated per sample, with serial sections on all slides, with serial sections being placed adjacent along all slides (as described in **Figure 3.10**). A minimum of 3 sections were placed on each slide. This mode of serial sectioning aimed to ensure that comparisons made between consecutive slides were as accurate as possible, as tissue on these slides was from adjacent sections within the block of tissue. For every 3 sectioned gelatin subbed slides, one non gelatin subbed slide was obtained with sections (at a thickness of 5μm), to acquire stains for H&E or immunohistochemistry (see **Figure 3.10**).

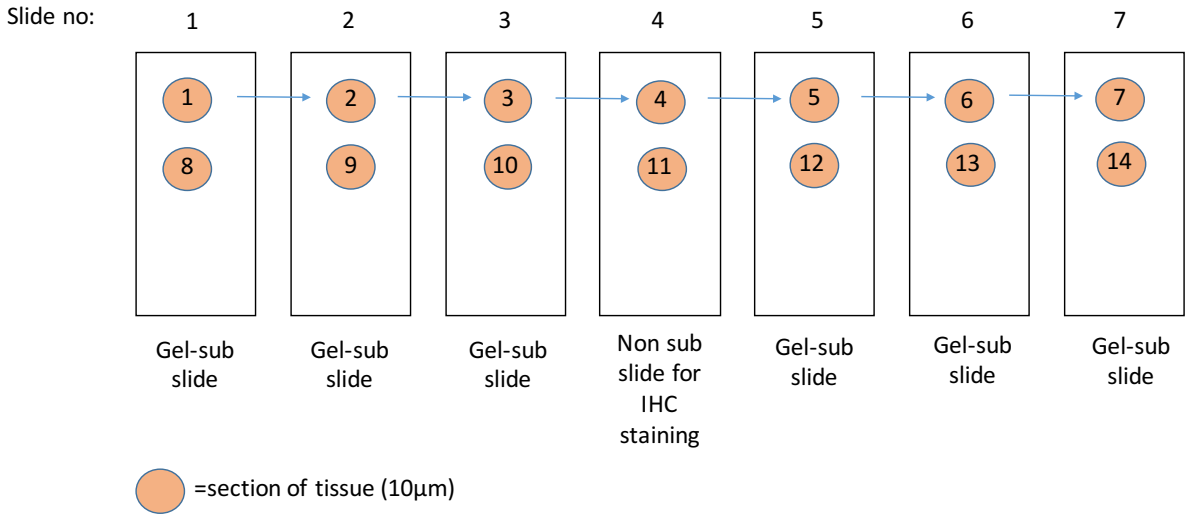

Figure 3.10 Example of order of sectioning of tissue on slides for use in autoradiography.

3.3.8.5 Autoradiography

From radioligand binding saturation work done for this study, using healthy monocytes, macrophages, fibroblasts and lymphocytes cultured *in vitro*, the binding affinity constant (Ki) of [^{3}H]PBR28 could already be estimated (at about 15nM, see Appendix section A5), to give a best estimate of the optimum radioligand concentration to maximize the ratio of specific to non-specific binding. Therefore, an optimization run of autoradiography was performed, using concentration at 5nM, 15nM and 25nM of [^{3}H]PBR28 on slides for 3 study participants. 15nM was deemed to be the optimal concentration to give maximal specific to non-specific binding ratio.

Autoradiography was carried out as described in Owen *et al*. (265). In brief, sections from each donor were brought to room temperature, and washed for 15 minutes in assay buffer (50 mmol/L Tris Base, 140 mmol/L NaCl, 1.5 mmol/L $MgCl_2$, 5 mmol/L KCl, 1.5 mmol/L $CaCl_2$, pH 7.4). Sections were incubated in buffer containing [^{3}H]PBR28 (5 nmol/L) for 2 hours. The nonspecific binding component was determined on adjacent sections in the presence of unlabelled PK11195 (10 μmol/L). After incubation, slides were washed twice in ice-cold wash buffer (50 mmol/L Tris Base, 1.4 mmol/L $MgCl_2$, pH 7.4, 4°C; 60 seconds) followed by a final wash in ice-cold distilled water (4°C; 60 seconds). Slides were dried in a cool airstream before exposure to tritium-sensitive film (Kodak Biomax MS film, Hemel Hempstead, UK) with [^{3}H]microscale standards (GE Healthcare, Amersham, UK) in X-ray cassettes at room temperature (6 weeks). After development of the radiograms, the films were quantified using microcomputer imaging device analysis software (Microcomputer Imaging Device Core 7.0; Interfocus Imaging Ltd, Linton, UK). Regions of interest (ROIs) were generated for each tissue section on each slide (entire tissue section was considered an ROI) using MCID Core™ Digital Imaging Software. Values were converted to fmol [^{3}H]ligand/mg wet tissue equivalent using the calibrated [^{3}H]microscale standards. An average for ligand binding was calculated for total and non-specific binding for each sample. The average non-specific binding was then subtracted from the total binding for each sample, to generate an average value of specific binding of [^{3}H]PR28 for each sample.

3.3.9 Immunohistochemistry and immunofluorescence

3.3.9.1 Tissue acquisition and generation of sections for staining

Tissue was acquired as previously mentioned above, and sectioned to a thickness of 5µm into serial sections onto Leica® Xtra adhesive slides.

Optimisation of staining was carried out using synovial tissue acquired from surgical synovectomy of the knee of a patient with RA, in addition to cytospin slides generated from cells cultured *in vitro* as described in **section 3.3.2.** Examples of positive control staining are depicted in **Appendix section A4**. In brief, for cytospin slide generation, macrophages were lifted using EDTA (Sigma-Aldrich), followed by gentle scraping. Fibroblasts were similarly lifted using Trypsin (Sigma-Aldrich). Cells were washed in PBS, counted and incubated at 1 million cells/mL in 1.6% Paraformaldehyde solution (Thermo-Fischer) at 4°C for 20 minutes. Using a cyto-centrifuge (Cytospin, Shandon Southern Products, Runcorn, UK), cells were spun onto slides, fixed for 15 min in ice cold acetone, and stored at -20°C until required. On cytospin slides for macrophage staining, 100,000 macrophages were centrifuged onto each slide. On cytospin slides for fibroblast staining, 20,000 fibroblasts were centrifuged onto each slide.

3.3.9.2 Staining procedures

Cryosections were brought to room temperature. For both DAB immunohistochemistry, and immunofluorescence studies, synovial tissue was acquired as above (**sections 3.3.81** and **3.3.8.2**), and sectioned to a thickness of 5µm into serial sections onto Leica® Xtra adhesive slides (3 sections per slide), and stored at -80ºC until use.

For immunohistochemistry, sections were stained with TSPO, CD68, CD163, PDPN, and CD4, according to protocols in (285), described in detail in **Chapter 2**. See **Table 3.8** for list of antibodies.

3.3.9.3 Image acquisition and quantification of staining on immunohistochemistry

Images were acquired on an inverted microscope using Axiovision software (Zeiss). 12 images were acquired in a systematic manner at x400 magnification with oil immersion. Image analysis was performed using ImageJ (NIH) as described previously (376). For every sample, immunopositive staining was normalized to number of haematoxylin-counterstained nuclei within the field of view. Statistical analysis was undertaken using GraphPad Prism 7 (GraphPad Software Inc., San Diego, CA). Normality was tested using a Kolmogorov-Smirnov test. Mann-Whitney U test was undertaken to assess comparisons of staining quantification between healthy and RA groups.

3.3.9.4 Immunofluorescence (IF) staining

For multiple antibody immunofluorescence staining and image acquisition, protocols were adapted from Dakin *et al.* (285). **Table 3.8** lists the details of the primary and secondary antibodies used.

Initially, an ImmEdge hydrophobic barrier pen (Thermo-Fisher) was used to outline synovial tissue on each slide. Slides were incubated in 5% normal goat serum (Sigma-Aldrich) diluted in PBS (Sigma-Aldrich) for 1 hour at room temperature, in a humidified chamber. Following this, 200µL of a primary antibody cocktail (made in 5% goat serum) was then added, and slides were incubated for 2 hours, followed by 3 washes using PBST for 5 minutes. A cocktail of 200µL secondary antibodies conjugated to fluorophores (made according to the primary antibody isotypes used), diluted in 5% equine serum (Sigma), was then applied to each slide (all secondary antibodies at a dilution of 1:200), and slides incubated for a further 2 hours in a darkened humidified chamber. Secondary antibodies were purchased from Life Technologies (goat anti-mouse IgG2a, IgG2b, or goat anti-rabbit IgG) or Southern Biotech (goat anti-mouse IgG1).

Slides were washed again 3 times in PBST, followed by incubation with POPO-1 nuclear stain in 0.05% saponin for 20 minutes. After 3 washes of slides with PBST, 0.1% Sudan black B (Applichem) in 70% ethanol was applied to each slide for 1.5 minutes, followed by washing, and mounting with VectaShield™ mounting medium. Coverslips were sealed with clear nail varnish, and slides were stored in the dark at -4ºC ready for imaging.

Antibody	**Clone**	**Isotype**	**Species**	**Dilution for IF (for DAB IHC)**
TSPO Abcam ab109497	EPR5384	IgG	Rabbit	1:1000 (1:10,000)
CD68 Dako M0814	KP-1	IgG1	Mouse	1:400 (1:4000)
CD163 LSBIO LS-C174770	34B	IgG2a	Mouse	1:2000 (1:2000)
PDPN (gp38) GeneTex GTX585772	5E2	IgG2b	Mouse	1:1000 (1:1000)
CD55 LSBIO LS-C134498	Mab67	IgG1	Mouse	1:2000 (1:2000)
CD3 Abcam ab699	PS1	IgG2a	Mouse	1:50 (1:50)
CD4 LSBIO LS-C336492	IG10	IgG1	Mouse	1:400 (1:400)

Table 3.4 Details of primary antibodies used in Immunofluorescence and Immunohistochemistry studies

3.3.9.5 Immunofluorescence imaging

Immunofluorescence images were acquired on a Zeiss LSM 710 confocal microscope as described in Dakin *et al.* (285) using x40 oil immersion objective. The fluorophores of POPO-1, Alexa Fluor 488, Alexa Fluor 568, and Alexa Fluor 633 were excited using the 405nm, 488nm, 561nm, and 633nm laser lines, respectively. To minimize bleed-through, all channels were acquired sequentially. Averaging was set to 2 and the pinhole was set to approximately 1 Airy unit. Two-dimensional image reconstructions were created using ZEN 2009 (Zeiss).

3.3.9.6 Isotype negative controls, and negative controls for staining

For isotype negative control staining, the primary antibody of interest was substituted for an antibody of the same immunoglobulin isotype raised from the same species as the antibody of interest in the same concentration. However, the isotype negative control antibody did not react with human antigen. Isotype negative controls were used on each run of immunohistochemistry, to identify areas of non-specific staining (see **Figure 3.11**).

Additionally, to provide further evidence that the secondary antibodies were not binding non-specifically to the tissue being used, a negative control staining was performed, to establish any background staining attributable to non-specific binding of secondary antibodies (see **Figure 3.12**).

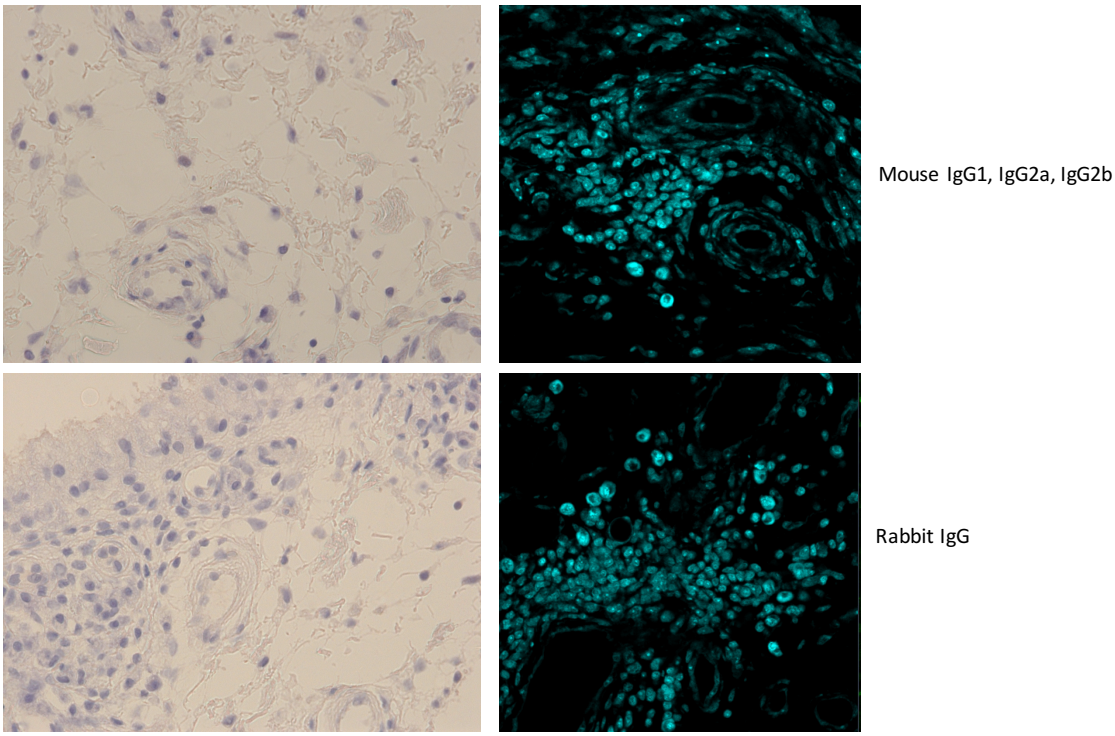

Figure 3.11 Isotype control staining of RA synovial tissue PET11 for all antibodies used in this study (x400 magnification for both immunohistochemistry and immunofluorescence). Isotype controls for DAB IHC on the left, isotype controls for immunofluorescence on the right.

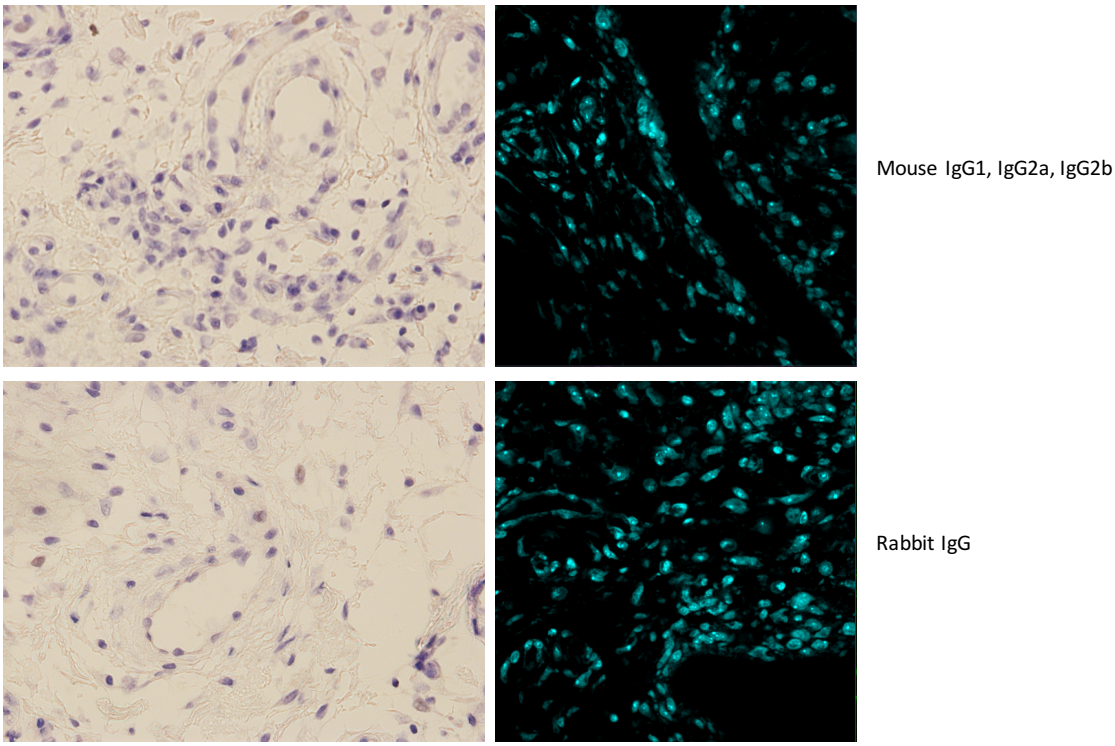

Figure 3.12 Negative control staining of RA synovial tissue PET 10 for all antibodies used in this study x400 magnification. Negative controls for DAB IHC on the left, negative controls for immunofluorescence on the right.

3.3.10 Statistical analysis

For autoradiography studies, data were analysed independently and expressed as mean ± Standard Deviation (SD). Mann-Whitney U test was used to determine statistical significance using GraphPad Prism 7 (GraphPad Software Inc., San Diego, CA). For immunohistochemistry staining quantification, mRNA quantification, and radioligand saturation binding studies, statistical analysis was undertaken using GraphPad Prism 7. Normality was tested using a Kolmogorov-Smirnov test. Mann-Whitney U test was undertaken to assess comparisons of staining quantification between healthy and RA groups, with Pearsons' correlates used to assess correlation between [^{3}H]PBR28 binding in synovial tissue, and staining for TSPO, and other cell markers. For mRNA and radioligand binding data, analysis of variance (ANOVA), followed by a Bonferroni's Multiple Comparison Test was used if there were more than two groups to compare, or Student *t*-test if two groups were analysed. *P* values less than 0.05 were considered significant (*p<0.05, **p <0.01, ***p≤0.001).

3.4 Results

3.4.1 Tissue Autoradiography studies

3.4.1.1 [^{3}H]PBR28 signal is highest in those tissue samples with the most cellular infiltrate

Tissue autoradiography was undertaken, using synovial tissue sections (knee tissue) from 6 RA patients, and 6 healthy controls. Using PK11195 cold radioligand to block TSPO binding sites, non-specific binding of the tracer [^{3}H]PBR28 to synovial sections of one donor was assessed on a single slide, along with total binding, by incubating an adjacent slide with [^{3}H][BR28 alone. Specific binding of [^{3}H]PBR28 was then calculated. A typical representation of the images generated, for RA tissue, and healthy control synovium, is depicted in **Figures 3.13** and **3.14** showing clearly increased [^{3}H]PBR28 total binding in RA tissue compared to healthy control.

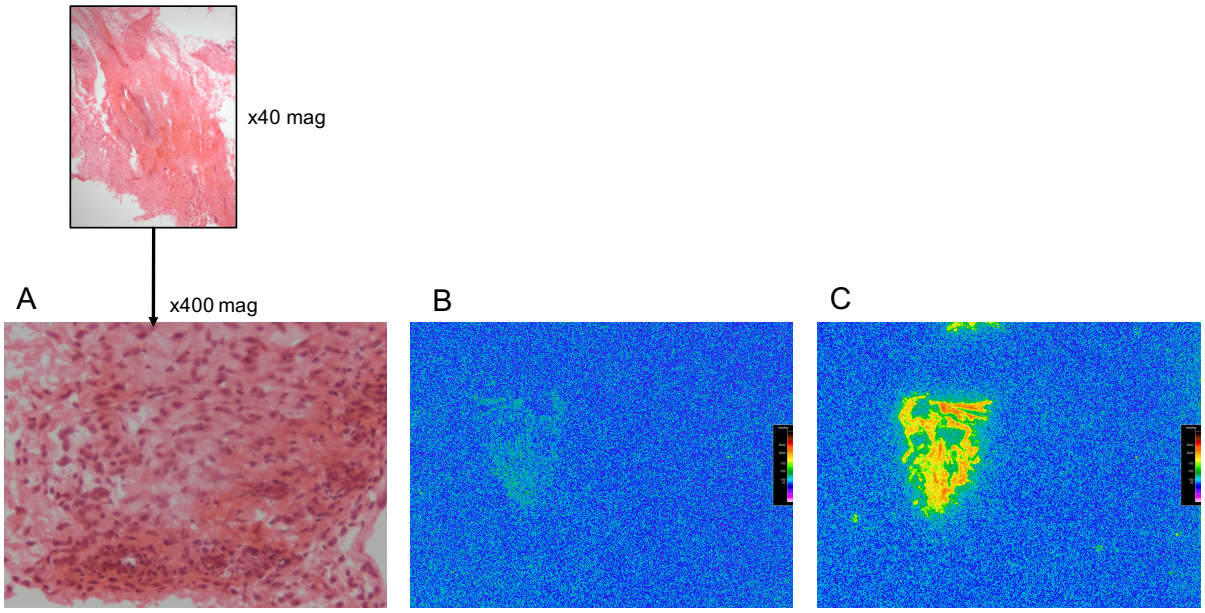

Figure 3.13 Representative example of autoradiography study of RA synovial biopsy specimen (clinically moderately inflamed knee). **A**: H & E staining of synovial biopsy x400 magnification**, B**: representative autoradiography film of one section for non-specific binding of [^{3}H]PBR28 and **C** for total binding of [^{3}H]PBR28. All sections used were serial sections from the same RA synovial specimen, cut to 10 μm thickness. Colour scale bar for autoradiography samples represents fmol/mg [^{3}H]PBR28 binding from 6500 fmol/mg (red) to 45 fmol/mg (light blue) x20 magnification.

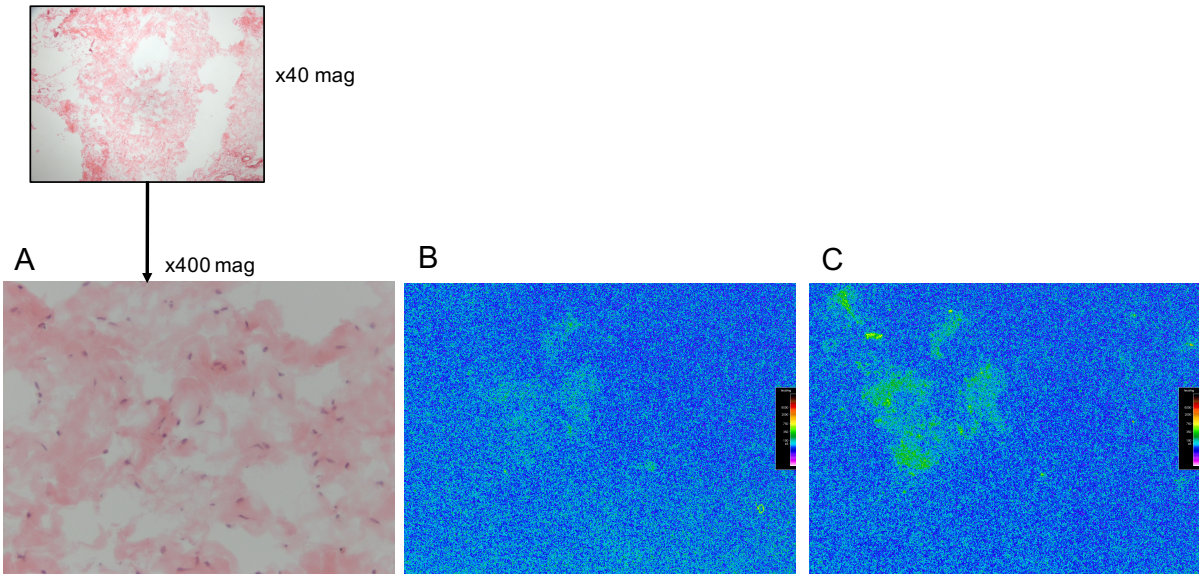

Figure 3.14 Representative autoradiography serial sections of a healthy control knee synovial biopsy specimen **A**: H & E staining of synovial biopsy x400 magnification**, B**: representative autoradiography film of one section for non-specific binding of [^{3}H]PBR28 and **C** for total binding of [^{3}H]PBR28. All sections used were serial sections from the same healthy synovial specimen, cut to 10 μm thickness. Colour scale bar for autoradiography samples represents fmol/mg [^{3}H]PBR28 binding from 6500 fmol/mg (red) to 45 fmol/mg (light blue) x20 magnification.

Mean specific binding of [^{3}H]PBR28 in the synovial tissue of 6 patients with RA was 1264 fmol/mg, compared to 122.8 fmol/mg for the synovial tissue of 6 healthy volunteers. Using student t-test, there was a significant increase in specific binding of [^{3}H]PBR28 in RA tissue, compared to healthy controls (see **Table 3.9** and **Figure 3.15**).

Synovium	**Specific binding of [^{3}H]PBR28 (fmol/mg)** Mean ± SD
Healthy control	122.8 ± 55.2
Rheumatoid Arthritis	1264 ± 144.2

Table 3.5 [^{3}H]PBR28 binding in fmol/mg in knee synovial tissue derived from six healthy controls and clinically mild to moderately inflamed knees of six patients with RA.

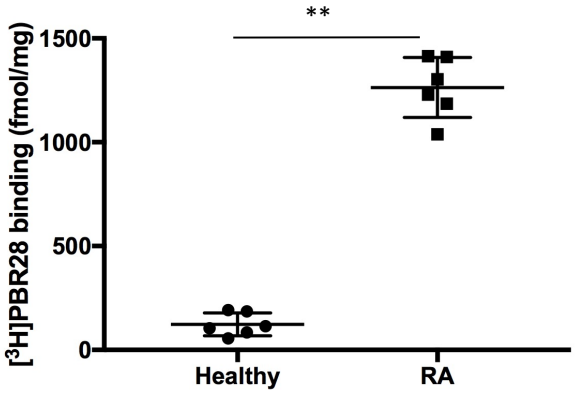

Figure 3.15 Specific binding of [^{3}H]PBR28 in fmol/mg in synovial tissue derived from six healthy controls and six RA patients. All tissue donors were of same binding affinity for [^{3}H]PBR28 (high affinity binders, see section 3.3.1). ***p<0.01 as determined by Mann-Whitney U test

3.4.2 Immunohistochemistry studies

In addition to TSPO, expression of the macrophage markers CD68, CD163 were significantly increased in RA tissue compared to healthy. Likewise, expression of the RA fibroblast activation marker, PDPN, was markedly enhanced in RA synovial tissue. Expression of the T lymphocyte marker, CD4, was significantly higher in RA tissues (see **Figure 3.16 and 3.17** for examples of staining in RA and healthy synovial tissues).

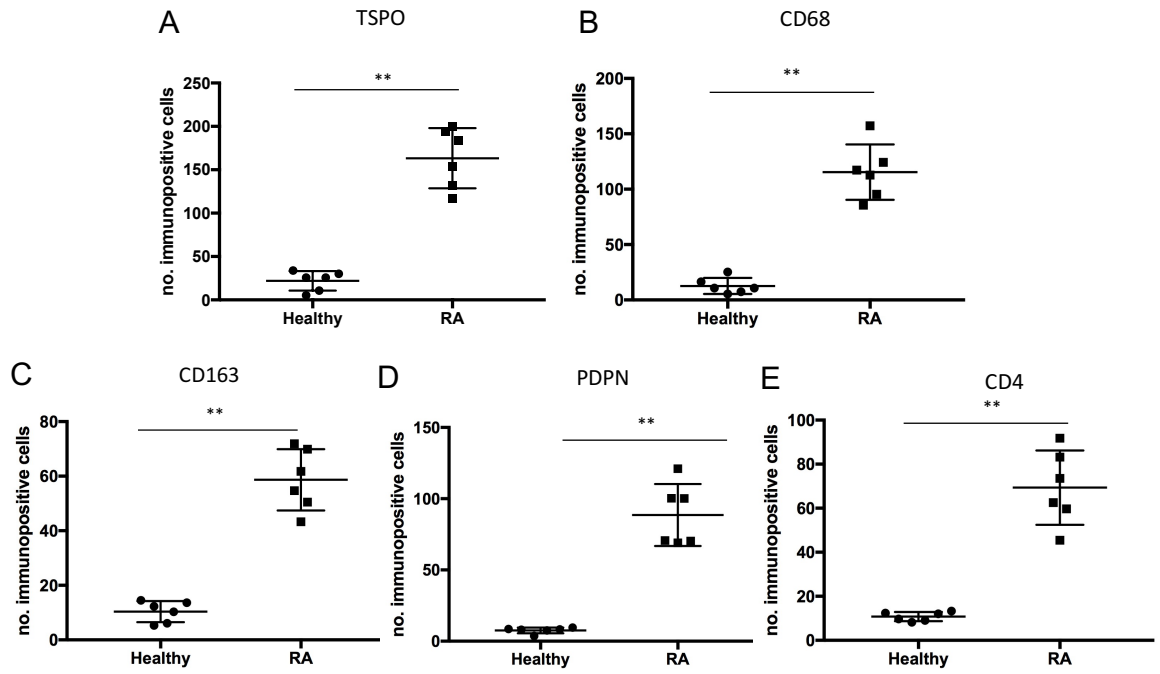

Figure 3.16 Average number of immunopositive cells per section on DAB immunohistochemistry staining of serial sections of same healthy control and RA synovial tissue for (**A)** TSPO, target for [^{3}H]PBR28, (**B)** CD68 non-specific macrophage marker, (**C)** CD163, marker specific for synovial macrophages, (**D)** PDPN, a fibroblast marker in RA synovium and (**E)** CD4, a marker for synovial T cells. **p<0.01 (as per Mann-Whitney U test) n=6 each group.

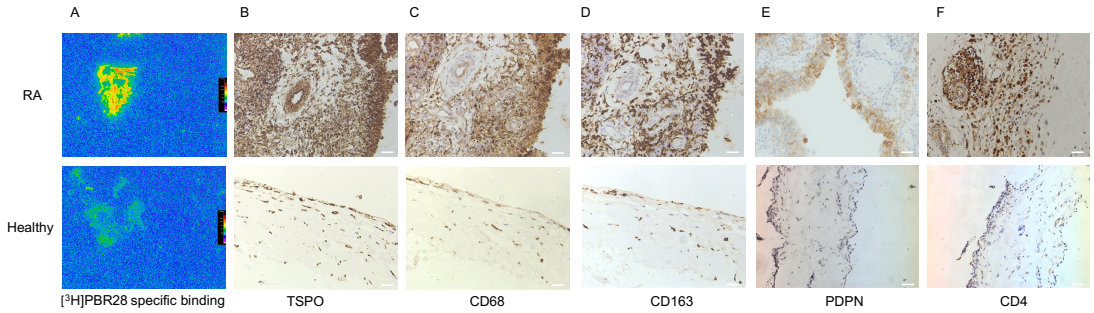

Figure 3.17 A: representative images of total [^{3}H]PBR28 binding for RA and healthy synovium x4 magnification, colorimetric scale indicates red as maximal [^{3}H]PBR28 binding, blue minimal [^{3}H]PBR28 binding. **B-F:** representative images of synovial DAB immunohistochemistry staining for TSPO, as well as macrophage, fibroblast, and T lymphocyte cell markers, in RA and healthy synovial tissue. x200 magnification, scale bar=50μm.

In the cohort of 6 RA synovial tissues, Pearson's correlates demonstrated a positive correlation between [^{3}H]PBR28 specific binding, and staining for TSPO, and all cell markers (see **Table 3.10**).

Immunohistochemical stain	Correlation of stain with [^{3}H]PBR28 specific binding (Pearson's correlation)
TSPO	r^2=0.94, p<0.001
CD68	r^2=0.79, p=0.02
CD163	r^2=0.98, p<0.001
PDPN	r^2=0.75, p=0.03
CD4	r^2=0.96, p<0.001

Table 3.6 summary of Pearson's correlates of number of immunopositive cells on immunohistochemical staining with [^{3}H]PBR28 specific binding, in RA synovial tissue, n=6.

3.4.3 Immunofluorescence studies

TSPO is present on macrophages, T lymphocytes and FLS in ex-vivo synovial tissue samples

Immunofluorescence staining was performed, to assess for co-staining of the widely accepted macrophage marker CD68, more specific macrophage marker CD163, and TSPO, providing evidence that in synovial tissue itself, TSPO is indeed, expressed on macrophages (**Figure 3.18**).

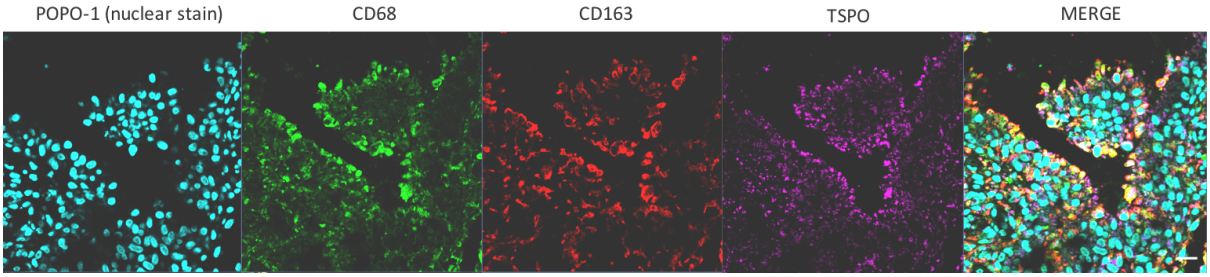

Figure 3.18 Representative confocal immunofluorescence images of RA synovial tissue demonstrating co-staining of macrophage markers CD68 (green), CD163 (red) with TSPO (purple). POPO-1 is nuclear stain (cyan). X400 magnification, scale bar=20μm.

Co-staining of TSPO and the FLS marker PDPN, a known FLS marker staining for RA lining as well as some sublining FLS (323), indicates that TSPO is likely to be present on FLS in RA synovial tissue (**Figure 3.19**).

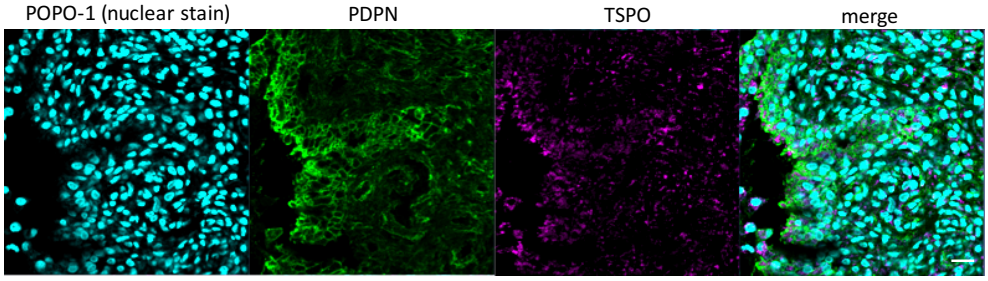

Figure 3.19 Representative confocal immunofluorescence images of RA synovial tissue demonstrating co-staining of the fibroblast marker PDPN (green), TSPO (purple). POPO-1 is nuclear stain (cyan). x400 magnification, scale bar=20μm.

Although PDPN is a highly sensitive marker for detection of RA FLS, there is a possibility that macrophages too, can express PDPN (although evidence for PDPN expression on synovial macrophages is lacking). Therefore, TSPO co-staining with the fibroblast lining specific CD55 and PDPN was also assessed (**Figure 3.20**).

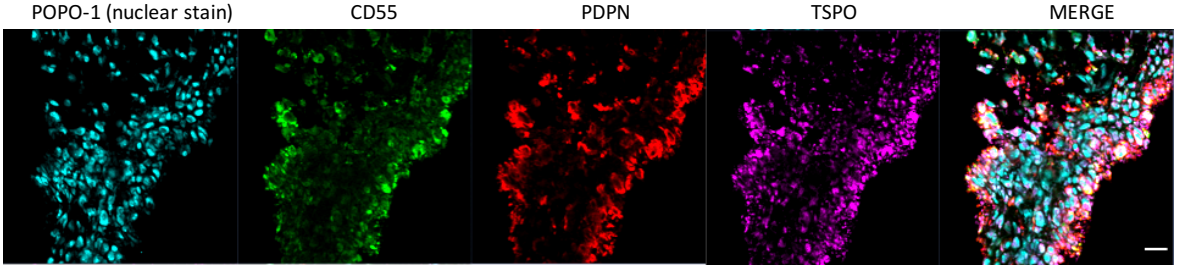

Figure 3.20 Representative confocal immunofluorescence images of RA synovial tissue demonstrating co-staining of the fibroblast marker CD55 (green), PDPN (red), TSPO (purple). POPO-1 is nuclear stain (cyan). x400 magnification, scale bar=20μm.

Immunofluorescence work further demonstrated co-staining of TSPO on CD3+CD4+cells, indicating that CD4 T cells express TSPO (**Figure 3.21**).

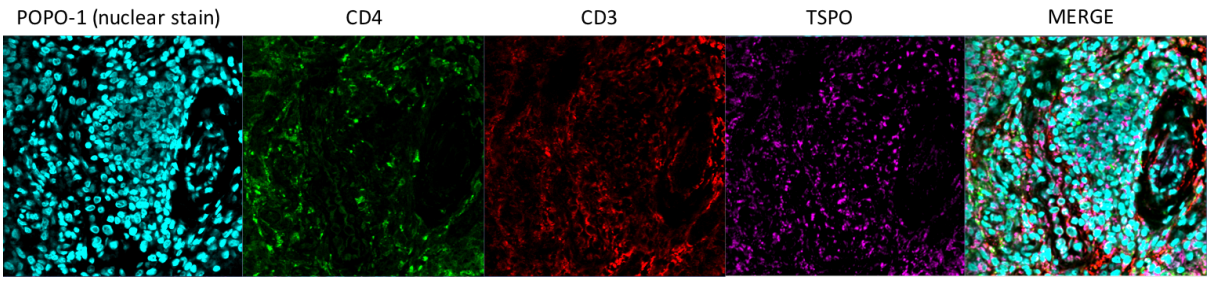

Figure 3.21 Representative confocal immunofluorescence images of RA synovial tissue demonstrating co-staining of T lymphocyte markers CD4 (green), CD3 (red) and TSPO (purple). x400 magnification.

3.4.4 *In vitro* mRNA and protein studies

3.4.4.1 PMA and ionomycin activated T Lymphocytes produce IFN-ɣ

ELISA for IFN-ɣ, a cytokine well recognised to be produced in increased amounts in activated T cells, was undertaken using the supernatant of cultured unstimulated and stimulated T lymphocytes, to provide evidence of T cell activation by PMA and ionomycin (**Figure 3.22**).

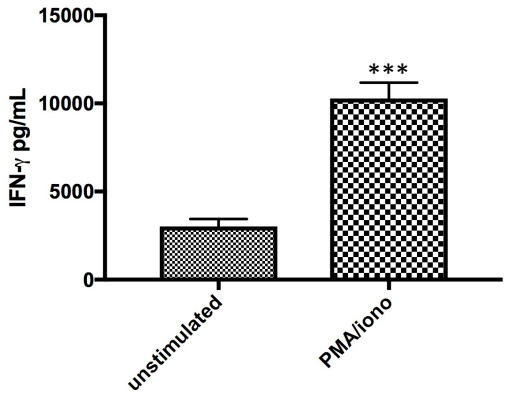

Figure 3.22 Evidence of IFN-ɣ release by unstimulated T cells versus T cells activated with PMA and ionomycin for 6 hours. Results demonstrated are mean±SEM from the supernatants of unstimulated and stimulated cells for 4 donors (same donors as from whom mRNA and radioligand binding data was acquired). ***p<0.001, as determined by Student t-test.

3.4.4.2 T Lymphocyte activation does not significantly alter TSPO expression

In order to provide some idea of the impact of T cell activation on TSPO expression, T cells were stimulated with PMA and ionomycin for 6 hours, before harvesting, and extracting RNA for PCR, and cell pellets for protein quantification of TSPO using [^{3}H]PBR28 radioligand binding. No significant difference in the expression of TSPO in unstimulated versus stimulated T cells was detected, using PMA and ionomycin as a means of activating T cells (**Figure 3.23**).

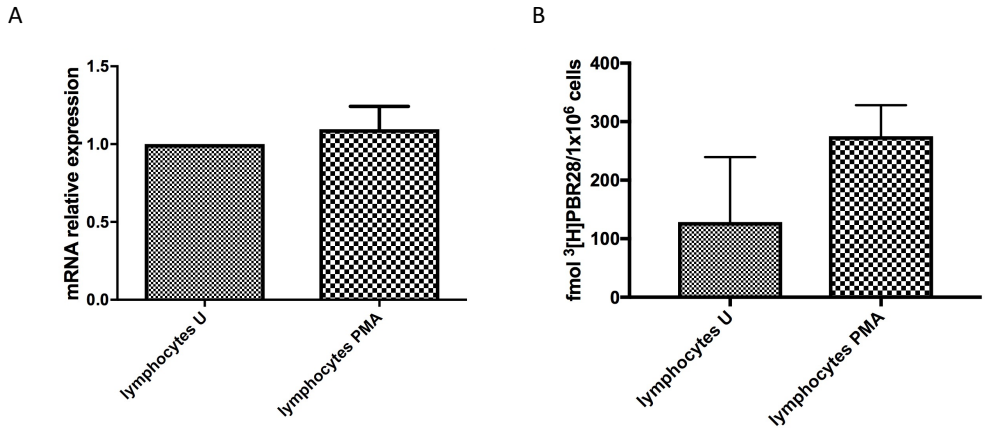

Figure 3.23 mRNA expression and radioligand saturation binding studies of unstimulated and treated CD4+ T lymphocytes (**A**) mean fold change mRNA expression of TSPO in unstimulated T lymphocytes, and T lymphocytes treated with 6 hours of PMA and ionomycin, with fold change of stimulated T cells normalised to that of unstimulated T cells. Results are for cells cultures from 4 donors. (**B**) specific binding of [^{3}H]PBR28 to TSPO protein in unstimulated T lymphocytes, and T lymphocytes treated with PMA and ionomycin for 6 hours. Data is expressed as mean ± SEM. Results are for cell cultures from 4 donors. (same cultures as for mRNA work).

3.4.4.3 TSPO mRNA and protein expression increases on differentiation of monocytes to macrophages

To provide evidence that TSPO is indeed upregulated on macrophages compared to monocytes, peripheral blood monocytes were differentiated to macrophages with 7 days of M-CSF, before cells were harvested for mRNA and radioligand binding studies. A significant upregulation of TSPO was noted on macrophage differentiation, at both mRNA and protein level (**Figure 3.24**).

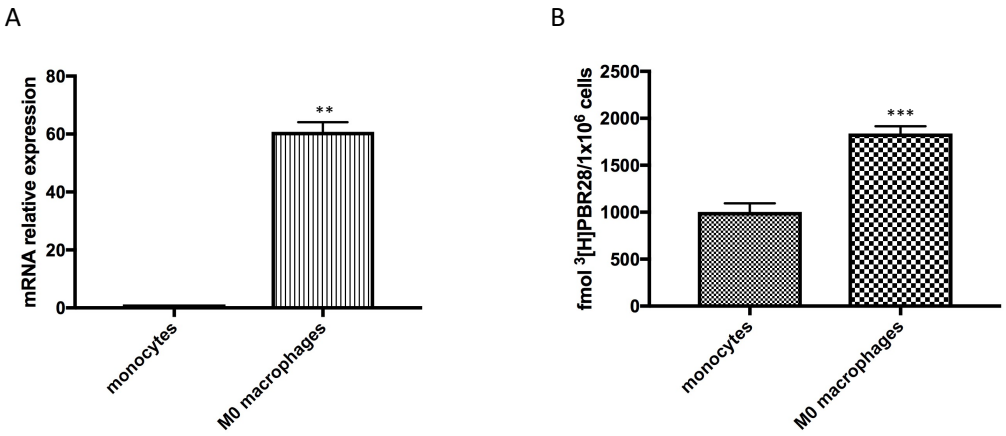

Figure 3.24 (A) Mean fold change mRNA expression of TSPO in unstimulated monocytes, and monocytes treated with 100ng/mL M-CSF for 7 days (M0 macrophages). Results are for cells cultures from 4 donors. (**B**) Specific binding of [^{3}H]PBR28 to TSPO protein in healthy unstimulated monocytes, and monocytes treated with 100ng/mL M-CSF for 7 days (macrophages). Results are expressed as mean ± SEM from 4 healthy donors (same cultures as for mRNA work).

3.4.4.4 TSPO expression in macrophages of different phenotype

Since the phenotypes of macrophages present in inflamed RA synovium remains under debate, the expression of TSPO on both M1 and M2 phenotype macrophages was assessed. For this study, 'M1' type macrophages were generated by stimulating macrophages (differentiated from healthy human monocytes with M-CSF for 7 days), with 24 hours of LPS 10ng/mL plus IFN-ɣ 20ng/mL. 'M2' macrophages were generated by stimulating macrophages with IL-4 20ng/mL for 24 hours.

ELISA was used to provide supporting evidence for generation of expected macrophage phenotypes, with higher TNF-α in the supernatant from cultures of macrophages treated with LPS and IFN-ɣ compared to macrophages treated with IL-4 (**Figure 3.25**).

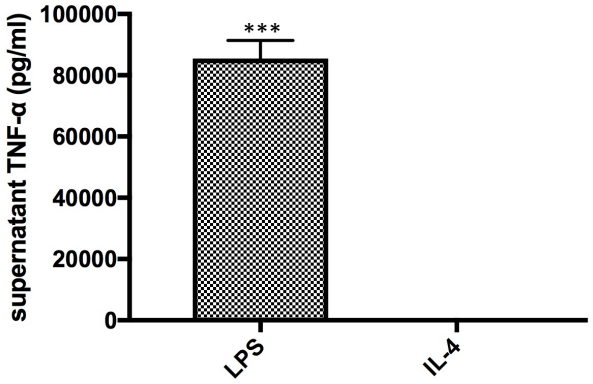

Figure 3.25 ELISA measurement of TNF-α (pg/mL) in supernatant of 'M1' macrophages (treated with LPS and IFN-ɣ) and 'M2' macrophages (treated with IL-4). Results are expressed as mean ± SEM for 4 donors (same donors as from whom mRNA and radioligand binding data was acquired), ***p<0.001 Student t-test.

TSPO mRNA and protein expression is significantly decreased in macrophages stimulated with LPS

The expression of TSPO at mRNA (**Figure 3.26 A**) and protein (**Figure 3.26 B**) level was compared in untreated macrophages, those treated with LPS plus IFN-ɣ ('M1' macrophages), and those treated with IL-4 ('M2' macrophages). The data demonstrating a statistically significant downregulation of TSPO in M1 macrophages compared to M2 at both protein and mRNA level, and also untreated macrophages. In contrast, although TSPO expression significantly increased at mRNA level in M2 macrophages compared to untreated macrophages, there was no significant change in TSPO expression at protein level in M2 compared to untreated macrophages.

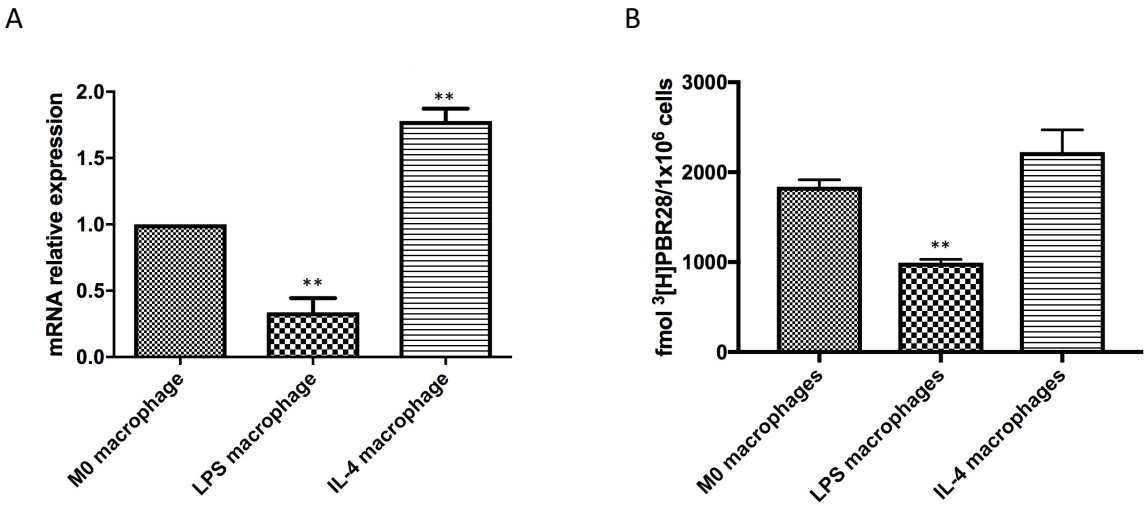

Figure 3.26 (A) Mean fold change mRNA expression of TSPO in unstimulated macrophages, and macrophages treated with 10ng/mL LPS plus 20ng/mL IFN-ɣ for 24 hours or 20ng/mL IL-4 for 24 hours. Results are mean±SEM for cells cultures from 4 donors, normalised to fold change in unstimulated macrophages. (**B)** Specific binding of [^{3}H]PBR28 to TSPO protein in unstimulated macrophages, and macrophages treated with LPS 10ng/mL plus 20ng/mL IFN-ɣ for 24 hours or IL-4 20ng/mL for 24 hours. Results are mean ± SEM for cell cultures from 4 donors (same cultures as for mRNA work). **p<0.01

3.4.4.5 Activation of FLS with TNF-α or IL-1β for 24 hours induces IL-6 production

In order to provide supporting evidence of FLS activation by TNF-α or IL-1β, supernatants from FLS cell cultures were collected and IL-6 levels were measured using a commercially-available ELISA assay. Data indicated a significant increase in IL-6 release in the supernatant of FLS stimulated with TNF-α or IL-1β compared to untreated FLS, consistent with FLS activation (**Figure 3.27**).

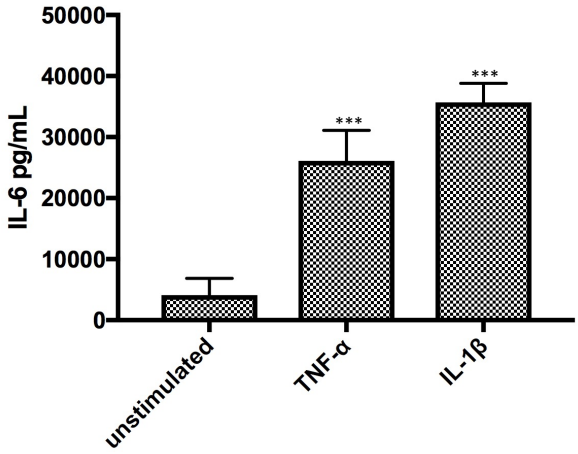

Figure 3.27 Measurement of IL-6 in supernatant of cultured FLS- IL-6 is significantly increased in FLS treated with TNF-α or IL-1β for 24 hours compared to unstimulated cells; ***p≤0.001 as determined by one way ANOVA, comparing IL-6 in supernatant of stimulated cells to unstimulated cells. Data is expressed as mean ± SEM from 4 different donors (same donors as from whom mRNA and radioligand binding data was acquired).

3.4.4.6 TSPO mRNA and protein expression increases on activation of FLS

Since the pro-inflammatory cytokines TNF-α and IL-1β are able to activate synovial FLS(377), the impact of these cytokines on TSPO expression in FLS was assessed. This demonstrated a significant increase in TSPO expression in FLS activated by both TNF-α or IL-1β, compared to unstimulated FLS, at both mRNA and protein level (**Figure 3.28**).

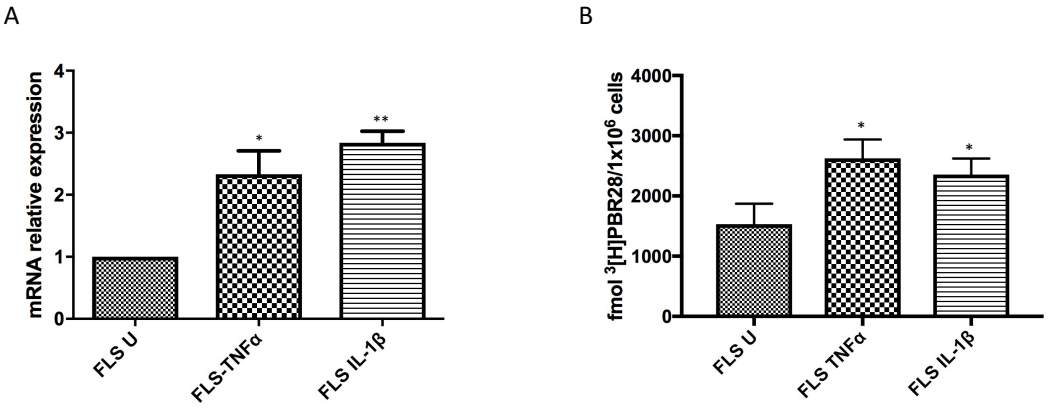

Figure 3.28 (**A)** mean fold change mRNA expression of TSPO in unstimulated FLS, FLS treated with TNF-α for 24 hours or IL-1β for 24 hours. Fold change normalised to that of unstimulated FLS. Results are for cells cultures from 4 donors. (**B**) specific binding of [^{3}H]PBR28 to TSPO protein in unstimulated FLS, FLS treated with TNF-α for 24 hours or IL-1β for 24 hours. Results are mean ± SEM, for cells cultures from 4 donors (same donors for mRNA, radioligand binding, and ELISA data). *p<0.05, **p<0.01, as per one way ANOVA analysis, comparing data to that of unstimulated cells.

3.4.4.7 Activated FLS and M2 macrophages possess the highest amount of TSPO in all cell groups and conditions analysed

For mRNA studies, the relative fold change mRNA expression of each cell group was calculated relative to the fold change mRNA of unstimulated T lymphocytes. Radioligand binding studies using [^{3}H]PBR28 are a quantitative means of assessing TSPO expression, hence direct comparisons between binding in fmol/1x10^6 cells could be made. At both mRNA and protein level, TSPO expression was highest in activated M2 macrophages and activated FLS (**Figure 3.29 and Table 3.11**).

In contrast, TSPO expression was dramatically upregulated on monocyte to macrophage differentiation (average mRNA fold change increase of 32.13, and average increase in [^{3}H]PBR28 binding of 834 fmol/1x10^6 cells). M2 polarization of macrophages with IL-4 increased TSPO expression further (average mRNA fold change increase of 14.65, and average increase in [^{3}H]PBR28 binding of 385 fmol/1x10^6 cells). However, M1 polarisation downregulates TSPO expression at both mRNA and protein level to levels similar to that expressed on unstimulated monocytes (see **Figure 3.29B**). This finding challenges the previous accepted dogma that activated macrophages upregulate TSPO expression, suggesting that M1 stimuli selectively activate macrophages to downregulate TSPO. Given the lack of certainty of macrophage phenotype in RA, and other inflammatory arthritides (see section 3.1.2.1.1), TSPO PET may itself lend further insight into macrophage phenotype in inflamed synovium.

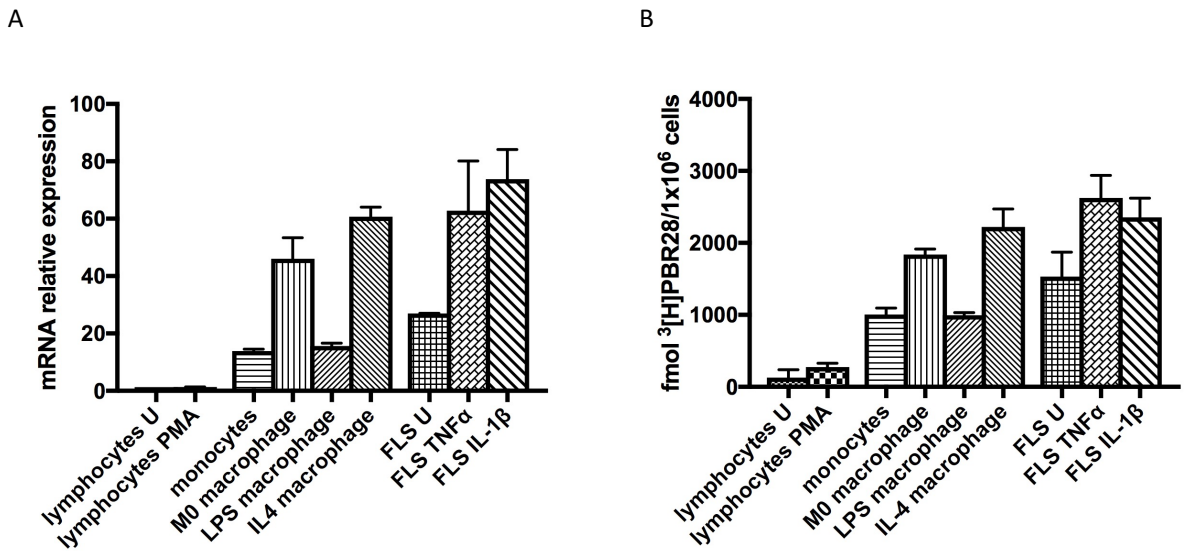

Figure 3.29 summary of mRNA and [^{3}H]PBR28 binding data for all cell groups **(A**) mean fold change mRNA expression of TSPO in unstimulated lymphocytes, lymphocytes stimulated with PMA and ionomycin, unstimulated monocytes, M0 macrophages, M1 (macrophages stimulated with 24 hours of LPS and IFN-ɣ) and M2 macrophage (stimulated with IL-4 for 24 hours), unstimulated FLS, FLS treated with TNF-α for 24 hours and IL-1β for 24 hours. Results are for cells cultures from 4 donors for each condition, fold change all relative to that of unstimulated lymphocytes. (**B)** specific binding of [^{3}H]PBR28 to TSPO protein in different cell groups.

	Mean fold change relative to unstimulated lymphocytes ±SEM	**Mean Specific binding of [^{3}H]PBR28 fmol/1x10^6 cells ±SEM**
Unstimulated T lymphocytes	1.00 (used for normalisation)	128.6 ±64.08
Stimulated T lymphocytes	1.096 ±0.15	275.2 ±30.07
Unstimulated monocytes	13.91±0.35	1004 ± 52.61
M0 macrophages	46.04 ± 5.19	1838 ± 45.37
Macrophages stimulated with LPS and IFN-ɣ	15.59 ± 0.74	994.3 ± 21.93
Macrophages stimulated with IL-4	60.69 ± 2.38	2223 ±143.6
Unstimulated FLS	26.92 ± 0.09	1532 ± 196
FLS stimulated with TNF-α	62.75 ± 10.03	2627 ± 180.4
FLS stimulated with IL-1β	73.82 ±7.31	2355 ± 113.4

Table 3.7 summary of TSPO mRNA fold change (relative to unstimulated T lymphocytes) and [^{3}H]PBR28 binding to TSPO in the three main cell groups known to make up pannus.

3.5 Discussion

3.5.1 Synovial tissue autoradiography

This work provides the first data to demonstrate that the TSPO tracer [^{3}H]PBR28 binds specifically to synovial tissue, and indeed, uptake is significantly increased in inflamed synovial tissue compared to healthy controls. This observation lends further credence to the assumption that [^{11}C]PBR28 signal seen in the anatomical location of synovium on *in vivo* imaging, is likely indeed, to be coming from inflamed synovial tissue itself, rather than as a result of artefact.

Further, utilising synovial tissue of both RA and healthy controls, this work provides support for the idea that [^{3}H]PBR28 is likely reflecting the expression of its target, TSPO, with staining for TSPO in RA tissue positively correlating with binding of [^{3}H]PBR28. Likewise, the significant positive correlation of [^{3}H]PBR28 signal with markers for multiple major synovial cell groups (macrophages, fibroblasts, lymphocytes), supports the notion that [^{3}H]PBR28 binding is a reflection of synovial cellularity.

Autoradiography of larger cohorts of patients, with a variety of stages of RA, ranging from pre-clinical stages, to early RA, to those with established RA, as well as those in clinical remission, would provide additional insight into how [^{3}H]PBR28 binding may reflect changes in synovium according to disease stage.

3.5.2 Immunofluorescence staining of synovial tissue

Despite the fact that TSPO is predominantly utilised in the field of PET imaging as a marker of macrophage infiltration, and hence inflammation, it is also well known that the expression of TSPO is fairly ubiquitous (157, 187). Although TSPO distribution has been extensively profiled in the tissue of rodents using autoradiography (378-380), tissue autoradiography or histological studies in humans are lacking; the majority of human tissue data examining the expression of TSPO within brain tumours (189, 381).

Therefore, from the current histology and autoradiography data available in the literature, it cannot be assumed that TSPO is solely a macrophage marker in synovium. Previous synovial histology work of TSPO expression in human synovium used CD68 alone as a macrophage marker (154), correlating TSPO and CD68 staining of serial sections, with clinical synovitis severity, leading to the assumption that using TSPO could be used for macrophage targeted imaging of those with RA (154). However, CD68 is increasingly recognised as having poor specificity for macrophages, with synovial fibroblasts also expressing this marker (275, 346). Therefore, for this work we utilised the more macrophage specific marker CD163, to provide some means of distinguishing macrophages from other CD68 positive cells. Further, the previous histology work failed to conclusively demonstrate TSPO staining on the same cells expressing macrophage markers, since separate serial sections were stained for TSPO and CD68, rather than assessing for co-staining of TSPO with cell markers (154). The immunofluorescence data in this work is the first demonstration that TSPO likely co-stains on RA synovial tissue cells expressing macrophage markers (CD68, CD163), synovial FLS markers (CD55, PDPN), and also CD4+ T lymphocytes.

It must be recognised that the immunofluorescence of tissue sections performed in this study is limited in its ability to phenotype cells, as only a limited number of markers can be utilised. An increasing body of evidence supports the notion of complex subsets of lymphocytes (382), macrophages (383) and more recently, synovial fibroblasts (323, 384), in inflamed synovium, all of which may express specific combinations of markers.

3.5.3 *In vitro* study of TSPO on main cell groups known to make up pannus

Like autoradiography tissue studies, the majority of studies assessing TSPO mRNA or protein expression (mostly using radioligand binding with TSPO specific ligands) has been undertaken in rodent models (378, 385). Such studies, however, frequently aimed to assess TSPO expression in whole tissue lysates, rather than specific cell types, concluding that TSPO expression is present in highest amounts in steroid

synthesizing cells (such as Leydig cells of the testes), with intermediate levels in renal and myocardial tissues, and lower levels in brain and liver, and inferring that the same is likely for humans, since TSPO mRNA distribution in humans is similar to rodents (157, 187, 386). Other studies aimed to differentiate TSPO expression in different parts of tissue, with one study of the adrenal glands demonstrating TSPO expression was confined to the adrenal cortex (387), and another study demonstrating that TSPO expression in the kidneys was maximal in the convoluted tubule and ascending Loop of Henle (388).

In humans, cellular data regarding TSPO expression at protein and mRNA level, is far more scarce. Canat *et al.*, however, used the TSPO specific radioligand [^{3}H]PK11195 and PCR, to analyse TSPO expression in human peripheral blood cells, demonstrating most TSPO expression in neutrophils and monocytes, with less TSPO in NK cells, and T lymphocytes (195).

Given the sensitivity of TSPO PET for its target, a knowledge of TSPO expression on cell types known to make up inflamed synovial tissue is highly desirable to better interpret TSPO PET signal coming from RA pannus. Hence, I undertook an analysis of TSPO mRNA and protein expression using RT-PCR and radioligand binding, respectively. This study provides the first evidence of TSPO quantification at mRNA and protein level (using RT-PCR, and radioligand binding with the TSPO ligand [^{3}H]PBR28), in the main individual cell types present in human RA pannus.

Our findings adhere to previous observations that mRNA and protein expression of TSPO mirror one another in multiple studies (in human and rodents) (157, 389), and are consistent with Canat's observation that TSPO expression is lower in lymphocytes compared to monocytes (195). Moreover, this Chapter gives the first evidence that TSPO expression is higher in M2 macrophages, compared to M1 macrophages, and that expression of TSPO in activated fibroblasts is as high as that noted in M2 macrophages. This indicates that in synovium, the major cellular contributors to TSPO PET signal, are likely to be activated M2 macrophages and fibroblasts.

Understanding that all major cell groups in RA synovium express TSPO, is helpful in comprehending the potential for TSPO to be a sensitive tool for the early detection of

synovitis. Although our knowledge of synovial histology in pre-clinical RA is lacking, data so far suggests that synovial tissue, from those in pre-clinical stages of RA, has an increased number of T lymphocytes compared to healthy controls (390). Another histological study of pre-clinical RA synovium suggested that there is a lack of 'inflammatory cells' in the synovium of those with pre-clinical RA (391). Since this study defined such inflammatory cells by staining for markers of T cells, macrophages, activated endothelial cells, and not markers more specific for FLS, it is feasible that activated FLS may be a very early feature of synovitis. The fact that TSPO targeted PET would be able to detect all potential major cell groups involved in RA, would support its use for the imaging of early arthritis; indeed, studies of [^{11}C]PK11195- a TSPO PET tracer- have already demonstrated its ability to detect pre-clinical synovitis in participants with ACPA positive arthralgia (147).

The knowledge that activated FLS make a comparable contribution to TSPO PET signal compared to macrophages, is also useful in ascertaining the utility of TSPO PET to assess response to treatment; certainly, the suggested potential drug targets for FLS-focussed therapy, are on activated FLS themselves (such as cadherin-11) (323); hence, TSPO PET could be a sensitive indicator of depletion of activated FLS in response to novel targeted therapies.

In vitro mRNA and radioligand binding studies in this work comparing the impact of cell activation by inflammatory stimuli, on TSPO expression, may also give insight into the potential role of TSPO in inflammation. TSPO expression was significantly higher in activated fibroblasts compared to unstimulated fibroblasts. The reasons for this observation remain unclear, given the ambiguity in TSPO's function, but lend support to the notion that TSPO may have a role in inflammation potentiated by activated FLS.

In contrast, TSPO expression did not change significantly between unstimulated T lymphocytes, and T lymphocytes activated with PMA and ionomycin. The addition of PMA and ionomycin for 4-6 hours to T cells *in vitro* is a long-established means of activating T lymphocytes *in vitro;* PMA is thought to activate protein kinase C whilst ionomycin, a calcium ionophore, induces an increase in cytosolic-free calcium concentrations, activating T lymphocytes to proliferate (392). So it is plausible to suggest that the reason no difference in TSPO expression was seen on T cell

activation, using PMA and ionomycin, was because TSPO is upstream of the signalling pathways being activated by PMA and ionomycin, or may not be involved in those specific pathways at all. Activating T cells by direct stimulation of the T-cell receptor/co-stimulatory receptor using CD3/CD28 antibodies (393), or through co-culturing with antigen presenting cells, may produce a more physiological activation of T cells to more accurately assess for change in TSPO expression on activation of CD4+ T cells.

TSPO expression at both mRNA and protein level, increased on differentiation of monocytes to macrophages, in keeping with the notion in the literature that TSPO is highly expressed on macrophages (194, 195). TSPO protein expression on macrophages did not significantly change upon addition of IL-4, a cytokine that polarises macrophages towards a 'reparative' 'M2' phenotype(311). In contrast, TSPO expression was significantly downregulated in macrophages treated with the pro-inflammatory 'M1' phenotype inducing LPS and IFN-ɣ, a finding not previously reported in the literature. However, such findings require further investigation, perhaps by employing a time course of stimulation with reagents, to ensure no increase in expression occurs earlier than the 24 hour timepoint of cell stimulation used for these experiments. Additionally, our data could have been attributed to the monocyte source, with the use of healthy human monocytes in this study; therefore, testing the impact of M1 or M2 stimuli on macrophages derived from other monocyte sources, may lend further credence to these findings.

Caution must be employed in translating the findings of this *in vitro* work to synovial cells *in vivo.* Due to the complex milieu in which cells find themselves in synovial tissue, the exact phenotypes of macrophages or fibroblasts created in these *in vitro* experiments, are unlikely to exist *in vivo*. Further, the cells used in these experiments were derived from healthy humans, rather than RA patients, hence did not take into account phenotypic differences that may exist in cells from RA patients compared to healthy, which may affect TSPO expression. A more accurate means of examining TSPO expression at a cellular level *in vivo* would be to employ flow cytometry, or mass cytometry (CyTOF). CyTOF is a technique which employs metal conjugated fluorophores to identify a multitude of cell markers on a single cell (394). This would enable accurate phenotyping of cells extracted directly from RA synovial tissue, along

with an analysis of TSPO expression. Such work could also be combined with mRNA expression profiling, to build up a more accurate quantitative assessment of TSPO expression in different synovial tissue cell subsets *in vivo*. Examination of RA synovial cells in this way would further enable easier assessment of smaller cell groups in synovium, such as endothelial cells (difficult to culture *in vitro*) and osteoclasts, which are also known to play a major role in RA & other inflammatory arthritides (146, 295).

For the radioligand binding work for this study, only high affinity binders for PBR28 were chosen, to ensure accuracy of all radioligand data obtained. High affinity binders are wildtype (representing the majority of the population), lacking a mutation in the TSPO binding site for PBR28 (262). It has been postulated that this binding site may have a role in TSPO function, with one study demonstrating that cells from those possessing the rs6971 SNP, being less capable of steroidogenesis, than wildtypes (395). Therefore, it is conceivable, that the absence of the SNP, could be affecting the TSPO expression patterns seen in this work. Our previous work in **Chapter 2** demonstrated that there was no significant difference in SNP frequency between those with inflammatory arthritis, and healthy controls, making it seem unlikely the SNP has a significant role in the generation of inflammatory arthritis, at least.

It must also be recognised, that although PBR28 is a highly specific TSPO radioligand, there is no data to date that indicates whether or not the conformation of the ligand binding site on TSPO changes through stimulation of cells. Previous data suggested that TSPO may form dimers, to act as a mitochondrial transporter (187); there is no data to date, to indicate whether or not such dimer formation may affect the binding site for PBR28, and hence, potentially affect binding of PBR28. Any impact of cell stimulation on affecting binding sites in this way is unlikely in this study, since mRNA expression of TSPO mirrored that of PBR28 specific binding.

Our findings challenge the pre-existing literature that suggests that TSPO is a likely imaging marker of macrophage infiltration in synovium (154). Certainly, our findings suggest that TSPO PET signal is as likely to represent the presence of activated stroma as it is macrophages.

The study of mRNA and [^{3}H]PBR28 radioligand binding in this work demonstrated the unexpected finding that activation of macrophages with pro-inflammatory stimuli, downregulates TSPO. Such a finding is out of keeping with the existing literature, where it is established that TSPO is upregulated on activated macrophages, and warrants further investigation, since this finding may impact on the utility of TSPO PET as a macrophage targeted imaging tool, as well as providing insight into the potential role of TSPO in the generation of macrophage phenotype. In the next Chapter, a preliminary assessment of TSPO expression in macrophages of different phenotype is undertaken, to lend clarity as to whether TSPO expression differs in macrophages at opposite ends of the phenotype spectrum.

CHAPTER 4

A preliminary investigation of TSPO expression in macrophages of different phenotype

4.1 Introduction

4.1.1 Macrophages; origins and function in inflammatory disease

Macrophages are mononuclear phagocytic cells with functions in both innate and adaptive immunity (396). In adults, they are widely thought to originate from circulating monocytes, which are recruited from the bone marrow into the circulation, migrate to tissues, and differentiate into macrophages, of a phenotype dependent on the milieu in which they find themselves (397). However, it is increasingly thought that some tissue macrophages may also arise from primitive haematopoietic progenitors during embryonic development (398). **Table 4.1** summarises some of the innate and adaptive immune functions of macrophages.

Innate Immune functions of macrophages
Phagocytosis of pathogens (399) Opsonin recognition (399) Production of pro-inflammatory and anti-inflammatory cytokines (400) Release of G-CSF and GM-CSF(401) Release of toxic species (nitric oxide, superoxide, matrix metalloproteinases) (402)
Adaptive Immune functions of macrophages
Antigen processing and presentation (403) Induction of Th1 cell differentiation (404) Controlling effector T-cell homeostasis & promoting T-cell priming (405)

Table 4.1 Summary of macrophage functions - Adapted from Navegantes *et al.* (396).

Macrophages have been implicated as key players in disease pathogenesis of multiple inflammatory diseases, including RA (267, 397). In inflammatory disease, macrophages are a major source of many of the critical inflammatory cytokines driving the inflammatory process, including IL-12, IL-23 and TNF-α (406).

The complexity of macrophage phenotypes is increasingly recognized; not only may macrophages be responsible for propagating inflammation, but also in tissue repair in those with chronic inflammatory disease.

4.1.2 Macrophage activation and phenotypes

The term macrophage activation was introduced in the 1960s, by Mackaness *et al.* (407), to describe the enhanced antigen-dependent microbicidal activity of macrophages in response to BCG (bacillus Calmette-Guerin) and Listeria upon secondary exposure to pathogens. This enhanced activity was then associated with Th1 responses through IFN-γ stimulation of macrophages (408, 409), which was also found to enhance the cytotoxic and anti-tumoural properties of these macrophages.

Subsequently, Mills *et al.* (410) demonstrated that macrophages derived from mice with Th2 predominant lymphocytes (and hence provided an IL-4 and IL-10 predominant environment for macrophages), were less easily activated by IFN-γ or LPS stimulation to produce NOS (nitric oxygen species), compared to macrophages derived from mice where lymphocytes were Th1 predominant (and hence an IFN-γ predominant environment). Further, such Th2 lymphocyte influence macrophages demonstrated increased ornithine production in response to IFN-γ or LPS, in contrast to increase arginine production in Th1 lymphocyte influenced macrophages. The increased ornithine production enhances cell replication, in contrast to the arginine induced production of NO (nitric oxide), which inhibits cells replication. The authors therefore concluded that two metabolically different phenotypes of macrophages existed, according to cytokines produced by Th1 and Th2 lymphocytes, giving rise to the nomenclature M1 and M2.

Further work changed the macrophage phenotype nomenclature again, adding M2 subsets (see **Figure 4.1** and legend), according to particular stimuli (411).

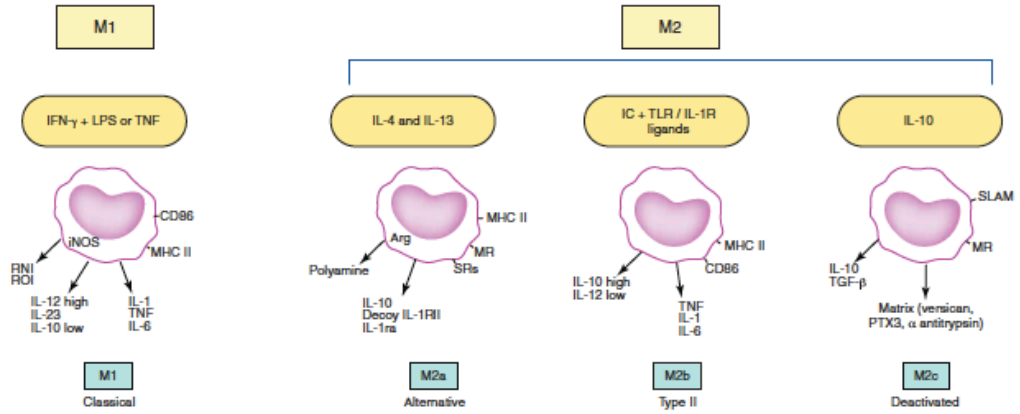

Figure 4.1 Diagrammatic representation of a proposal for new human macrophage nomenclature, to consist of M1, M2a, M2b and M2c phenotypes. As with pre-existing literature, Mantovani *et al* (17) defined M1 macrophages as those producing large amounts of NO and ROI (reactive oxygen intermediates), with a high capacity to present antigens, with high IL-12 production. This M1 macrophage phenotype was again induced by IFN- γ with or without LPS. Phenotypically distinct M2 macrophages activated by IL-4 or IL-13 were designated M2a, those activated by immune complexes (IC) or Toll-like Receptor (TLR) ligands were designated as M2b, and macrophages activated by IL-10 or glucocorticoids were designated as M2c. Modified after Mantovani *et al* (411).

Later, another macrophage model was supported by Fleetwood *et al*. (412) and Joshi *et al*. (413), who investigated differences between macrophages differentiated using Granulocyte Macrophage Colony Stimulating Factor (GM-CSF), and those differentiated using Macrophage Colony Stimulating Factor (M-CSF). Here, GM-CSF macrophages demonstrated a more robust activation of pathways involving NF-κB (nuclear factor kappa-light-chain-enhancer of activated B cells) and AP-1 transcription factor (414) following LPS-stimulation, with previous work suggesting GM-CSF macrophages should be termed MΦ1 macrophages, and M-CSF macrophages MΦ2. However, it is increasingly recognized that caution is needed in terming a GM-CSF differentiated macrophage as an M1 macrophage; indeed, GM-CSF macrophage cultures have been demonstrated to contain high amounts of CD11c positive cells (311), that may represent a dendritic cell phenotype, hence the gene expression profile of this subset of cells must be accounted for in comparing GM-CSF and M-CSF macrophages.

More recently, Murray *et al.* (311) consolidated the literature on agreement with several laboratories, to generate a continuum of macrophage phenotypes, to represent an initial consensus of macrophage phenotypes within the spectrum of M1-M2 macrophage polarities (see **Figure 4.2**).

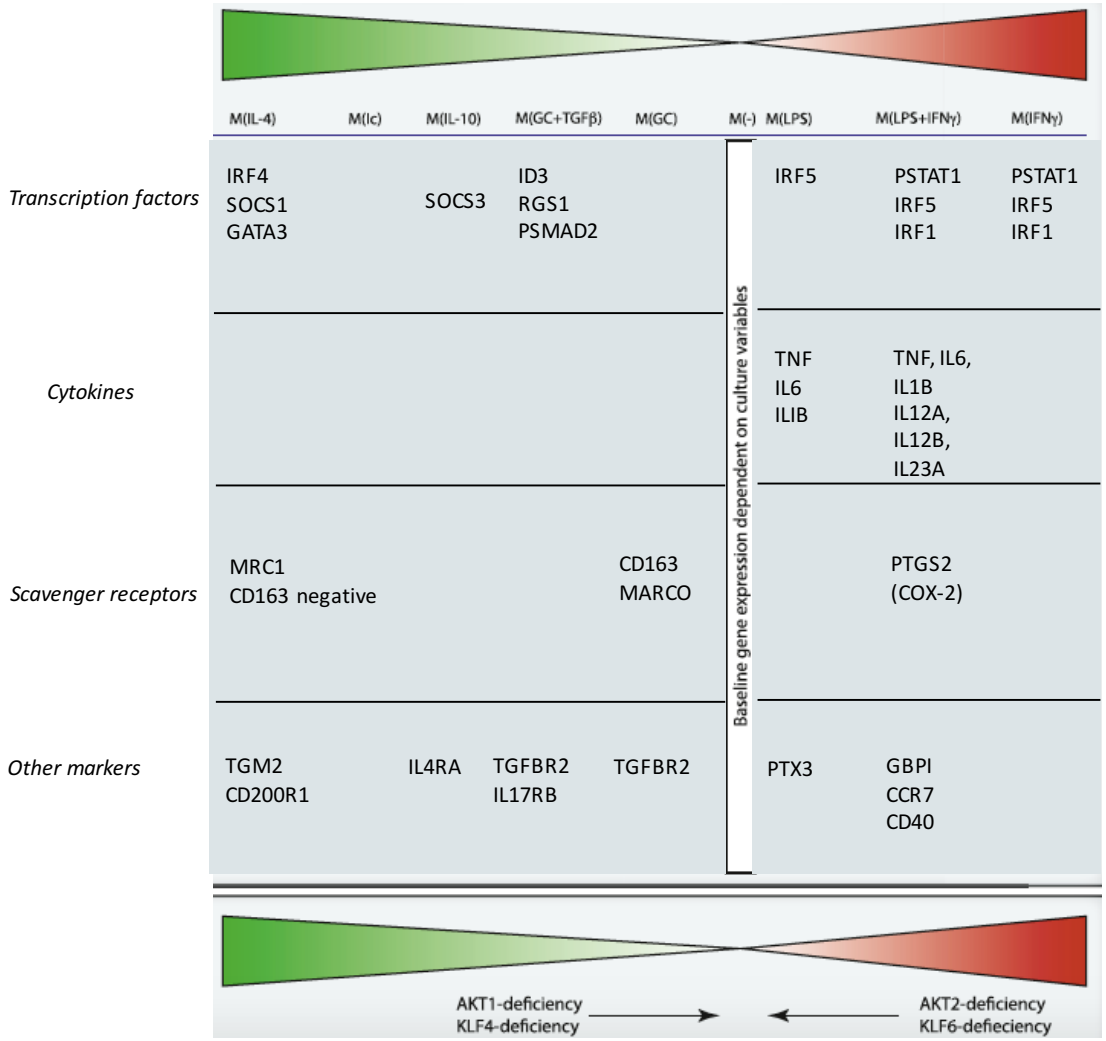

Figure 4.2 Modified from Murray *et al.* (311), depicting functional subdivisions according to stimulation of human monocyte derived M-CSF macrophages within the existing M1-M2 spectrum concept, according to stimuli applied to cells- as described in Martinez *et al* (308), Mosser and Edwards (415), Stout and Suttles (416)- with stimulation conditions being IL-4, immune complexes (Ic), IL-10, glucocorticoids (GC) with transforming growth factor-beta (TGF-β), glucocorticoids alone, LPS, LPS and IFN-ɣ, and IFN-ɣ alone. Marker data were taken from a range of publications; Edwards *et al*. (417), Fleetwood *et al.* (412), Gratchev *et al.* (418), Gundra *et al.* (419), Krausgruber *et al.* (360), Lang *et al.* (420), Shirey *et al.* (421), Shirey *et al.* (422), Shirey *et al.* (423), Xue *et al.* (424).

4.1.3 TSPO expression in macrophages

It has long been established that TSPO is highly expressed on macrophages (194, 195). In disease states, TSPO has been demonstrated, in multiple studies, to be highly expressed on infiltrating macrophages at sites of inflammation, such as CNS lesions in multiple sclerosis (197) and Alzheimer's disease (198), as well as in malignancies, such as brain tumours(381). More recently, a study of a rat model of inflammatory

arthritis demonstrated TSPO is highly expressed on infiltrating macrophages in the inflamed synovium (142). Staining for TSPO by immunohistochemistry demonstrated an influx of TSPO positive cells (largely macrophages and neutrophils) in the synovium of knees with induced arthritis compared to the disease free knee, implying that TSPO expression may also be abundant in human inflamed synovium due to similarities of expression patterns in rats and humans (157, 425, 426). This has been largely confirmed by a subsequent human study demonstrating uptake of TSPO targeted radioligand [^{11}C]PK11195 in an inflamed knee, correlated with staining for the macrophage marker CD68, in synovial tissue derived from the same knee (154).

Although evidence exists to confirm that TSPO is highly expressed on activated macrophages, data regarding whether macrophage phenotype affects TSPO expression, is lacking. A histological study of microglia, a cell group accepted as macrophage cell type in brain tissue (427-429), did not demonstrate a significant difference in TSPO expression on microglia expressing the M1 marker, CD16/32(430), and those expressing the M2 marker, CD206 (430), in brain tissue sections from a mouse model of intracerebral haemorrhage (190). However, this is unsurprising, given the fact that TSPO is largely ubiquitously expressed, regardless of species (208, 431, 432). Further, proof of M1 or M2 phenotype was designated by the use of only a single M1 or M2 marker, which may not provide conclusive proof of phenotype of microglia stained.

In vitro data of the murine macrophage cell line, RAW 264.7, demonstrates that TSPO protein levels were significantly up-regulated at 24 hours with addition of LPS, in a dose-dependent manner (261) as determined by an increase in the binding of the TSPO radio-ligand [^{11}C]PBR28, at various doses of LPS. In terms of human studies supporting the idea that LPS upregulates TSPO expression on macrophages, Sandiego *et al*. administered *Escherichia coli* LPS to eight patients (433). Patients had positron emission tomography (PET) brain imaging with the TSPO radio-ligand [^{11}C]PBR28 prior to, and 2 hours after, LPS administration. The PET imaging demonstrated a significantly increased binding of [^{11}C]PBR28 2 hours post LPS administration (by about 39-50% on average), reflecting increased TSPO expression. However, caution is needed in drawing conclusions that these findings means that LPS is activating microglia to upregulate TSPO. Firstly, since LPS was administered

peripherally, it cannot be definitively proven that TSPO on microglia is being directly upregulated by LPS. Furthermore, given a systemic inflammatory response to LPS, may have caused the upregulation of TSPO on microglia; indeed, it is well recognized that LPS disrupts the blood brain barrier in multiple ways (434), which could all lead to microglia activation. The idea that LPS does not directly activate microglia *in vivo* is supported by the fact that neurotransmitters (such as ATP) have a large role in the activation of these cells (435). Secondly, since TSPO is ubiquitously expressed, and multiple other cells exist in the brain other than microglia (such as neurons, astrocytes and oligodendrocytes) (436), as well as possible infiltrating leukocytes (due to increased trafficking of leukocytes through the blood brain barrier by LPS), it cannot be assumed that the increased TSPO uptake is solely attributable to microglia.

There is some evidence to indicate that TSPO may not always be upregulated on macrophages at sites of inflammation. Indeed, macrophages obtained from broncho-alveolar lavage in a study of patients with interstitial lung disease, demonstrated a reduction in TSPO expression compared to those from healthy volunteers (437). Another study of microglia demonstrated a lack of TSPO expression in the microglia of anaplastic astrocytomas (438).

4.1.4 A potential role for TSPO in macrophage biology

The function of TSPO is as yet, uncertain, with the recent development of a viable global TSPO knockout model apparently refuting any critical role for TSPO, except possibly in mitochondrial ATP synthesis (202). However, certainly, at an *in vitro* level, multiple recent overexpression studies of TSPO have indicated a potential role for TSPO in cholesterol efflux, with overexpression of TSPO promoting cellular cholesterol efflux from macrophages (439), hence preventing the generation of a pro-inflammatory macrophage phenotype. In this Chapter, we aim to build upon this study, and provide some preliminary data to generate a hypothesis regarding involvement of TSPO in the generation of macrophage phenotype, through a potential role in cholesterol efflux.

4.2 Aims

I chose to use three different monocyte sources in this Chapter, since TSPO is well recognized to be upregulated in malignancy and inflammatory disease. Therefore, by using the malignant monocyte cell line THP-1, RA synovial fluid monocytes, as well as healthy monocytes, I hope to provide evidence that changes in TSPO expression seen are as a result of polarization of macrophages to a particular phenotype using stimuli applied *in vitro*, rather than as a result of the source of monocytes. In this work, I aim to:

1. Ascertain any difference in TSPO expression between monocytes and MDM at mRNA and protein level.

2. Determine any difference in TSPO expression between macrophages of various phenotype, differentiated according to the spectrum of macrophage phenotypes as described by Murray *et al.* (311).

3. Provide preliminary data to suggest whether TSPO may have a role in the generation of macrophage phenotype, through a role in cholesterol efflux.

4.3 Methodology

4.3.1 Isolation of healthy peripheral blood human monocytes for *in vitro* studies

Peripheral blood monocytes were isolated from blood cones of healthy donors purchased from the National Blood Service (Colindale, Edgware, London UK) using density gradient centrifugation (357, 358), and centrifugal elutriation performed utilizing flow cytometry during centrifugal elutriation to isolate fractions of 85% purity monocytes, as described in **Chapter 3 section 3.3.2.5.**

4.3.2 THP-1 monocytes for *in vitro* studies

Human monocytic THP-1 cells, (originally derived from the peripheral blood of a Japanese paediatric patient with acute monocytic leukaemia) (440) were purchased from the American Type Culture Collection (ATCC, Maryland, USA) and were cultivated in 75cm^2 flasks, in culture media (stated above). THP-1 cells were passaged every 4 days at a ratio of between 1:2 and 1:3, to ensure cell density was not more than 0.8-1.2x10^6 cells/mL. Cells were used from passage numbers 4-6.

4.3.3 Isolation of synovial fluid monocytes from synovial fluid

4.3.3.1 Synovial fluid aspiration

Five patients with rheumatoid arthritis (meeting ACR/EULAR 2010 classification criteria(25), median duration of disease since diagnosis 2.5 years, age range 35-52, 3 female, 2 male, all on methotrexate, hydroxychloroquine and sulfasalazine), gave written informed consent to have knee aspiration (ethics reference: 07/H0706/81). Under aseptic technique, between 30-150mLs of synovial fluid was aspirated per patient and placed into 10mL lithium heparin tubes.

4.3.3.2 Preparation of synovial fluid

If synovial fluid volume was less than 40 mLs, the aspirate was made up to 40mLs in HBSS (Gibco®, Life Technologies, Paisley, UK). Twenty mLs of the synovial fluid was layered onto 20mLs of Histopaque® (Sigma-Aldrich, St Louis, USA), to isolate a pellet of mononuclear cell rich cellular fraction as described in **Chapter 3**.

4.3.3.3 Magnetic Activated Cell Sorting (MACS)

This technique is able to isolate desired cells through the use of magnetic microbeads, conjugated to an antibody known to be selectively expressed on the desired or non-desired cells. For this approach, we employed positive selection, where CD14 antibody conjugated beads were used to bind to CD14 positive cells. A suspension of cells with the microbeads were run through a column, placed in the magnetic field of a MACS separator. As a result, CD14 positive cells adhere to the column, and the run through contains CD14 negative cells, which can be discarded. The column is then removed from the magnetic field, and the CD14 positive cells can be eluted from the column. A Miltenyi Kit (Miltenyi Biotec, Germany) was used to isolate CD14 positive cells from synovial fluid, and used according to the manufacturer's protocol.

In brief, the cell suspension was counted, and centrifuged at 300g for 10 minutes. The supernatant was aspirated, and the cell pellet was resuspended in 80µL of buffer (containing PBS, BSA (bovine serum albumin) 0.05%, EDTA, and 0.09% azide) per 10^7 cells. 20µL of CD14 microbeads was added per 10^7 cells, and the resultant mixture was incubated for 15 minutes at 2-8°C. Cells were then washed by adding 1-2mLs of MACS running buffer (containing BSA, EDTA and 0.09% azide) per 10^7 cells and centrifuged at 300g for 10 min. The resultant pellet was re-suspended up to 10^8 cells in 500µL buffer. A MACS column was placed in the MACS separator, and prepared by rinsing with 500 µL buffer. Cell suspension was then placed into the column, and allowed to run through under gravity. The flow-through was discarded. The column was removed from the separator, and placed over a 15mL falcon. One mL of MACS running buffer was then placed into the column. The magnetically-labelled CD14-positive cells were then flushed through the column by firmly pushing the plunger into the column.

4.3.4 Macrophage differentiation and stimulation

4.3.4.1 Differentiation of human monocytes to macrophages

Monocytes from healthy peripheral blood and synovial fluid mononuclear fractions were counted, and resuspended to a density of $1x10^6$ cells/mL in RPMI (Lonza, Whittaker). Macrophages were differentiated from elutriated monocytes, and synovial fluid derived monocytes, by culturing cells with 100ng/mL of recombinant human M-CSF (Peprotech Inc, UK) at a concentration of $1x10^6$ cells/mL, for 7 days (320).

To differentiate THP-1 monocyte derived macrophages, THP-1 cells were plated at a density of $0.5x10^6/cm^2$ (CELLSTAR®, Greiner Bio-One, UK), and treated with 10ng/mL of phorbol 12-myristate 13-acetate (PMA, Sigma-Aldrich, Poole, UK), for 72 hours to generate a macrophage phenotype as previously described (441).

Flow cytometry was used to confirm macrophage differentiation from monocytes (see **Chapter 3**, **section 3.3.2.5** for details).

4.3.4.2 Activation of macrophages

Monocyte derived macrophages (MDM) from both healthy peripheral blood monocytes, and synovial monocytes, were stimulated with 10ng/mL LPS (Peprotech) and 20ng/mL IFN-γ (Peprotech), 20ng/mL IL-4 (Peprotech), 500nM dexamethasone (Sigma-Aldrich) or 3ng/mL TGF-β1 (Peprotech), as described previously (320, 360, 441, 442). Cells were stimulated with 10ng/mL LPS for 2,4,6 and 24 hours, and with other cytokines for 24 hours.

4.3.5 Cytospin slide generation

MDM were lifted from the cell culture plate using EDTA cell dissociation solution (Sigma-Aldrich), by incubating for 5 minutes, followed by gentle scraping. Cells were then washed twice in PBS, counted and incubated at 1 million cells/mL in 1.6% Paraformaldehyde solution (Thermo-Fischer) at 4°C for 20 minutes. Using a cytocentrifuge (Cytospin, Shandon Southern Products, Runcorn, UK), cells were

centrifuged onto slides (100,000 macrophages per slide in a total volume of 200µL PBS), and fixed for 15 min in ice cold acetone. Slides were stored at -80°C.

4.3.6 Immunofluorescence

Cytospin slides were blocked in 5% normal goat serum (Sigma) in PBS for 60 minutes in a humid chamber at room temperature. After removal of blocking solution, slides were incubated with the primary antibody cocktail diluted in 5% normal goat serum in PBS for 2 hours at room temperature. After incubation with the primary antibody (either TSPO, rabbit IgG, dilution of 1:1000, or CD68, mouse IgG1 1:400 (detailed in Chapter 3, section 3.3.10.4). Slides were washed 3 times with PBST for 5 minutes and subsequently incubated with the secondary antibody cocktail, each diluted 1:200 in 5% normal equine serum (Sigma) in PBS for 2 hours and shielded from light. Secondary antibodies were purchased from Alexa Fluor (goat anti-mouse IgG2a, IgG2b or goat anti-rabbit IgG, Life Technologies).

After washing with PBST, sections were incubated in 2µM POPO-1 nuclear counterstain (Life Technologies) diluted in PBS containing 0.05% Saponin (Sigma) for 20 minutes. Tissue auto fluorescence was quenched with a solution of 0.1% Sudan Black B (Applichem) in 70% ethanol for 10 minutes. After washing, slides were mounted using fluorescent mounting medium (VectaShield), sealed and stored at 4°C until image acquisition.

4.3.7 RNA extraction, cDNA synthesis and Real-time, quantitative Polymerase Chain Reaction

RNA extraction and cDNA synthesis were performed as described in **Chapter 3**, sections 3.3.4 and 3.3.5. Primer sequences used for RT-PCR in this study are outlined in **Table 4.2**.

GENE	SENSE PRIMER	ANTI-SENSE PRIMER
ABCA1 ATP binding cassette transporter	TTCCCGCATTATCTGGAAAGC	CAAGGTCCATTTCTTGGCTGT
CD200R1 (CD200 Receptor 1)	GACCAGAGAGGGTCTCACCA	TTGAAGCGGCCACTAAGAAG
CYP27A1 (Sterol-27-hydroxylase)	ACTGCACCAGTTACAGGTGCTTTACA	CCATGTCGTTCCGTACTGGGTACT
IL-10 (Interleukin 10)	TACGGCGCTGTCATCGATT	GGCTTTGTAGATGCCTTTCTCTTG
IL-12 β (Interleukin-12 beta)	GGACATCATCAAACCTGACC	GAACCTCGCCTCCTTTGTGAC
MRC1 (Mannose receptor C type-1)	AAGGCGGTGACCTCACAAG	AAAGTCCAATTCCTCGATGGTG
PTGS2 (Prostaglandin endoperoxide synthase 2)	ATGCTGACTATGGCTACAAAAGC	TCGGGCAATCATCAGGCAC
TGM2 (Transglutaminase 2)	GCCACTTCATTTTGCTCTTCAA	TCCTCTTCCGAGTCCAGGTACA
TNF-α (Tumour Necrosis Factor-α)	GGCCAAGCCCTGGTATGAG	TAGTCGGGCCGATTGATCTC
TSPO (Translocator protein)	GCGGCCTGGCTAACTCCTGC	AAAGCGGGAGCCCACGAAGC
18s (18S ribosomal RNA)	GTAACCCGTTGAACCCCA	CCATCCAATCGGTAGTAGCG

Table 4.2 Sequences of primers used for PCR

Real time, quantitative PCR acquires data throughout the process for the direct detection of PCR product, therefore combining amplification and detection in one convenient step. The detection process is carried out using a variety of fluorescent chemistries that correlate PCR product concentration to fluorescence intensity (443). See **Appendix section A3** for a detailed description of the amplification of mRNA fragments in real-time PCR reactions.

The detailed protocol for carrying out PCR is described in **Chapter 3**, **section 3.3.6.**

4.3.8 Western Blots

Identification of protein expression using Western blots is a well-recognized tool for separating proteins based on their molecular weight (444) by gel electrophoresis. Below is the brief account of a lightly-modified approach to the standard technique.

4.3.8.1 Protein extraction

Cells were harvested from the various cell plates used, by scraping, and washed as outlined in RNA extraction, and kept on ice. Samples were lysed in a denaturing buffer consisting of 8M urea, 1% sodium dodecyl sulphate, 10% glycerol and 10mM Tris (pH 6.8), 0.5mM protease inhibitor cocktail and 1 mM dithiothreitol (DTT) (all purchased from Sigma-Aldrich, Poole, UK). Samples were pipetted up and down vigorously, until the mixture became thick and viscous, and samples were sonicated and stored at -20°C.

4.3.8.2 Protein concentration assay

The total protein concentration of the extracted protein was assayed using the Pierce® BCA Protein Assay Kit (Life Technologies, Lutterworth, Leicestershire UK). This assay combines reduction of copper ion (Cu^{2+}) to cuprous ions (Cu^{1+}) by bicinchoninic acid (BCA) (445). The first step is the biuret reaction, where peptides, containing three or more amino acid residues, form a coloured chelate complex (light blue) with cupric ions in an alkaline environment containing sodium potassium tartrate. The second step involves BCA reacting with Cu^{1+} formed in the first step. The chelation of two molecules of BCA with one Cu^{1+} produces an intense purple product. The water soluble BCA/copper complex has a strong linear absorbance at 562nm with increasing protein concentrations, with detection of the purple product being 100 times more sensitive than the light blue product formed in the biuret reaction.

Protein concentration was determined using a serially diluted standard of known concentrations and a blank standard to generate a standard curve. Serially diluted

BSA (PAA Laboratories, Pasching, Austria), starting at 2% with urea/SDS lysis buffer was used as a standard. The blank standard used contained urea/SDS lysis buffer only.

First, protein lysates were broken down using a Sonicade for 15 seconds per sample. The Pierce® BCA Protein Assay Kit (Thermo Scientific, USA) was carried out according to the manufacturer's protocol. In brief, 200µL of BCA working reagent (50 parts of BCA™ Reagent A mixed with 1 part of BCA™ Reagent B) was added to 5µL of protein extract which was diluted 1:5 volume with urea/SDS lysis buffer, standards and blanks in a Costar® 96 well EIA/RIA plate (Corning Incorporated, Corning, NY, USA). Each sample, standard and blank was assayed in duplicates. The plate was then covered, gently mixed on a plate shaker (Orbit 300, Labnet International Incorporation) for 30 seconds followed by incubation in the dark at 37°C for 30 minutes. Once the plate was cooled to room temperature, the absorbance was read at 550nm on a plate reader (Multiskan Ascent model 354, Thermo Labsystem, Finland). The standard curve and protein concentration of each unknown sample was determined based on the standard curve automatically plotted using the Ascent Software Version 2.6 for Multiskan Ascent photometric microplate reader.

4.3.8.3 Gel electrophoresis

Gel electrophoresis uses electrical current to separate native or denatured proteins according to their molecular mass (444). Negatively charged SDS-coated proteins migrate in polyacrylamide gels towards the positive electrode. The gel consists of a separation gel (which acts to separate proteins) and a stacking gel (which concentrates the applied sample). Proteins with lower molecular mass migrate faster than those with higher molecular mass.

Equal amounts of protein from each sample were mixed with loading buffer. The samples were incubated at 95°C for 5 minutes in a water bath, in order to denature proteins. Samples were then centrifuged for a couple of seconds at $13.2x10^3$ rpm and placed on ice, before loading onto 4-12% Bis-Tris NuPage Ready Gels (Novex®, Paisley, UK). One well on each gel was loaded with 9µL Rainbow Ladder (Amersham, GE Healthcare, UK). Gels were immersed in 1 x MOPS (3-N-morpholino propane sulfonic acid)/SDS running buffer (NuPage Invitrogen, Paisley, UK), and run at 130V

for 190 minutes. The gel electrophoresis was carried out in an Xcell SureLock™ Electrophoresis Cell (Invitrogen, USA).

4.3.8.4 Transfer

The transfer process involves transfer of proteins resolved by gel electrophoresis to a polyvinylidene fluoride (PVDF) membrane. Proteins bound to the surface of the PVDF membrane are then accessible for analysis by immuno-detection. The transfer process involves applying an electric current across the gel and PVDF membrane, so that the negatively charged proteins migrate from the gel to the PVDF membrane.

Transfer of proteins was performed using the Transblot® Turbo™ Transfer system (Bio-Rad). PVDF transfer membranes (Bio-Rad, USA). Membranes were prepared by immersing in methanol for 2-3 seconds, followed by equilibrating in Transblot® Turbo™ Transfer Buffer (25nM Tris, 192mM glycine) for 30 seconds. Two stacks of filter paper ((Transblot® Turbo™ Transfer Stacks, Bio-Rad, USA) were likewise soaked in Transblot® Turbo™ Transfer Buffer.

One stack of soaked filter paper was placed in a Transfer System cassette, the prepared PVDF membrane was placed on top, and a further stack of soaked filter paper on top of this. This was then gently rolled to remove any creases, and the cassette was shut and locked. The cassette was run in the Transfer System as per manufacturer's protocol for 7 minutes (Bio-rad, USA http://www.bio-rad.com/webroot/web/pdf/lsr/literature/10016505D.pdf).

4.3.8.5 Immunodetection

Immunodetection involves targeting, probing and visualizing any protein of interest. A specific monoclonal or polyclonal primary antibody was used to target and probe the protein of interest on the membrane. The secondary antibody was directed against an epitope on the primary antibody. The secondary antibody was conjugated with a reporter fluorescence or enzyme such as horse radish peroxidase (HRP) and alkaline phosphatase, which would produce a colourimetric reaction, and emit light or fluorescence when exposed to an appropriate substrate.

Following transfer, membranes were then incubated for 1 hour at room temperature

with blocking buffer (PBS-T plus 5% milk and 1% BSA) on a rocking platform (Gyrotwister, Labnet, International Incorporation) to reduce non-specific binding of primary antibody. The protein of interest was then detected by incubating overnight (at 4°C on a rocking platform at 50rpm) in a solution of blocking buffer and appropriate concentration of antibody; in the case of TSPO, 1:10,000 concentration of monoclonal goat IgG anti human antibody (GeneTex, Irvine, USA) was found to be optimal. For β-actin, 1:20,000 concentration of monoclonal β-actin antibody (Sigma-Aldrich) was used (mouse, IgG2).

Membranes were washed with PBS-T for 10 minutes 3 times on a rocking platform at 100rpm. Membranes were then incubated at room temperature in a solution of PBS-T and 5% milk, and secondary antibody for 1 hour on a tipping platform at 50rpm. Secondary antibody for TSPO was rabbit polyclonal anti-goat antibody (Dako, Glostrup, Denmark) at a concentration of 1:3000. Secondary antibody for β-actin was rabbit monoclonal anti-mouse antibody (Dako, Glostrup, Denmark), at a concentration of 1:5000. Membranes were then washed 4 times for 10 minutes on a tipping platform at 100rpm.

Binding of the antibodies was visualized using enhanced chemiluminescence system, Pierce® ECL 2 Western Blotting Substrate (Thermo Scientific, Rockford, USA). This consisted of a lumigen PS 3 acridan substrate, which was converted to an acridinium ester intermediate when catalyzed by HRP. The ester intermediate reacted with hydrogen peroxide (H_20_2) in alkaline conditions and emitted light. The light emission could be detected by exposing the PVDF membrane to a photography film (Fuji Medical X-ray Film 100NIF, Fujifilm Corporation, Tokyo, Japan), which was then developed by a film processor (AGFA Curix 60).
http://www.bio-rad.com/webroot/web/pdf/lsr/literature/10016505D.pdf

4.3.9 Radio-ligand saturation binding

The process for radio-ligand saturation binding is described in section 3.3.7. Due to the high protein requirement for this technique, only macrophages derived from healthy control monocytes were utilized, in one of three phenotypes; unstimulated macrophages, macrophages treated with 24 hours of LPS plus IFN-ɣ, or macrophages

treated with IL-4 for 24 hours.

4.3.10 Enzyme-linked immunosorbent assay (ELISA) of cell culture supernatants

In order to provide supporting evidence of macrophage differentiation to an M1 or M2 phenotype, concentrations of soluble human TNF-α in cell culture media were measured using commercially-available enzyme-linked immunosorbent assay (Quantikine human TNF-α ELISA Kits, R&D Systems Europe) as described in **Chapter 3,** section 3.3.3.

4.3.11 Statistical Analysis

All experiments for RNA and Western blot were carried out in five replicates. Experiments for radio-ligand saturation binding were carried out in triplicate. Results are expressed as mean ± standard error of the mean (SEM). Graph Pad Prism 5.02 software package (Graph Pad Software, La Jolla, CA, USA) was used in the analyses of the data. To evaluate the effects of the stimuli (M-CSF, LPS, IFN-γ, IL-4, TGF-β, dexamethasone) analysis of variance (ANOVA), followed by a Bonferroni's Multiple Comparison Test was used if there were more than two groups to compare, or Student *t*-test was applied if two groups were analysed. Where appropriate *p* values less than 0.05 were considered significant (*$p<0.05$, **$p<0.01$, ***$p\leq0.001$).

4.4 Results

4.4.1 TSPO expression on monocytes compared to macrophages

Here, we provide evidence that TSPO is upregulated on MDM compared to monocytes, even without further addition of stimuli to generate an activated macrophage phenotype. We demonstrate upregulation of TSPO at both mRNA (see **Figure 4.3**) and protein level (see **Figure 4.4**), in MDM derived from monocytes of three different sources; THP-1, healthy human peripheral blood monocytes, and RA synovial fluid monocytes.

The increase in fold change mRNA TSPO expression on differentiation from monocytes to MDM was greatest in RA synovial fluid derived MDM (mean fold change of 207.7 ± 80.9, compared to 66.4 ± 29.24 for healthy MDM, and 5.27±1.55 for THP-1 MDM).

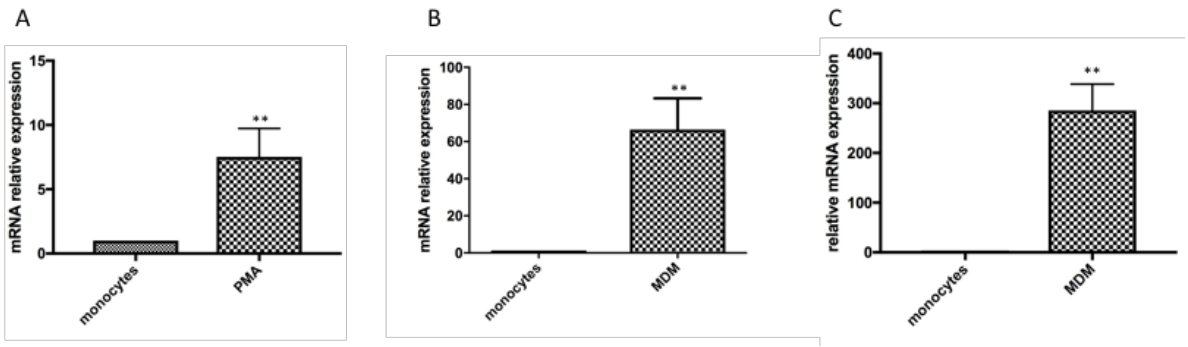

Figure 4.3 *TSPO* mRNA expression of monocytes compared to monocyte-derived macrophages (MDM). **A:** THP-1 monocytes compared to THP-1 monocytes treated with 10ng/mL PMA for 72 hours, **B:** healthy human peripheral blood monocytes, compared to healthy human peripheral blood MDM **C**: synovial fluid monocytes, compared to synovial fluid MDM. Results expressed as fold change mRNA expression (compared to *18s*), each graph representing n=5, with error bars representing SEM, **p<0.01 as per Student t-test.

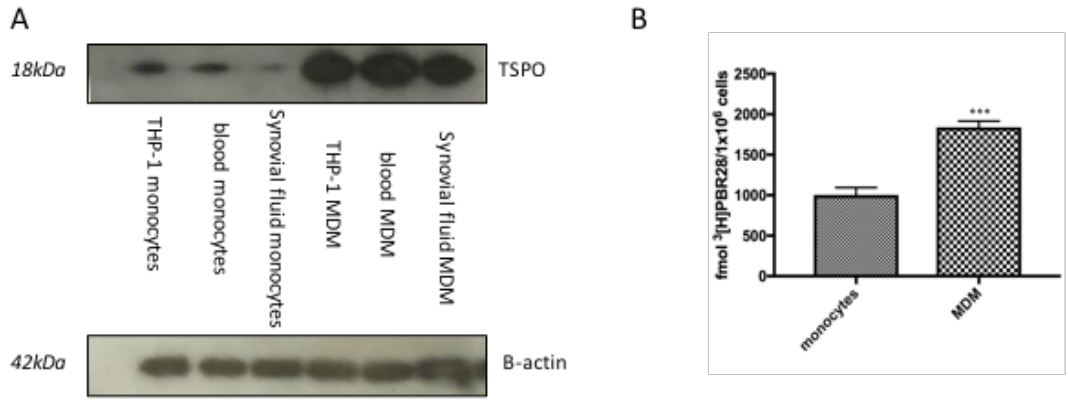

Figure 4.4 TSPO protein expression in monocytes and macrophages. (**A)** Representative TSPO protein expression (18kDa) as assessed by Western blots with β-actin as loading control. Results shown are for THP-1 monocytes, healthy human peripheral blood monocytes, synovial fluid monocytes, and MDM from each of these monocyte groups. Optical densitometry calculations for n=5 independent western blot experiments are published in Narayan *et al.* 2017(446) (**B)** Tracer binding as expressed in fmol of [^{3}H]PBR28 tracer uptake per 1x10^6 cells in healthy human peripheral blood monocytes and healthy human peripheral blood MDM, each graph representing n=5. Experiments were repeated at least three times. Data in (**B**) are expressed as mean ± SEM. *** $p<0.001$ as determined using Student t-test.

4.4.2 Activation of macrophages by M1 and M2 stimuli

In order to provide evidence that MDM stimulated with particular agents were indeed activated to an M1 or M2 phenotype, mRNA studies were performed to evaluate the expression of a selection of markers known to be differentially expressed on M1 and M2 phenotype macrophages (see **Figures 4.5**, **4.6** and **Table 4.3** for summary of marker expression in macrophages of different phenotype).

M1 markers	M1:M2 ratio
Tumour necrosis factor alpha (TNF-α)	18.12
Interleukin-12B (IL-12β)	9.66
prostaglandin-endoperoxide synthase 2 (PTGS2, also known as Cox2)	13.40
M2 markers	**M1: M2 ratio**
Interleukin-10 (IL-10)	0.16
CD200R	0.41
C-type mannose receptor 1 (MRC-1, also known as CD206)	0.04
Transglutaminase 2 (TGM-2)	0.34

Table 4.3 M1:M2 =ratio of mean fold changes in healthy human peripheral blood MDM treated with 10ng/mL LPS plus 20ng/mL IFN γ for 24 hours (M1) to mean fold change in healthy human peripheral blood MDM treated with 20ng/mL IL-4 for 24 hours (M2). Values expressed to nearest 2 decimal places.

Messenger RNA data provides evidence that, as expected, those MDM stimulated with 10ng/mL LPS and 20ng/mL IFNγ for 24 hours, have a higher expression of M1 markers (TNF-α, IL-12β and PTGS2, see **Figure 4.5**) compared to M2 markers (IL-10, CD200R1, MRC1, TGM2), and those MDM stimulated with IL-4 for 24 hours have a consistently higher expression of accepted M2 markers compared to M1 markers (see **Figure 4.6)**.

Figure 4.5 demonstrates expression of M1 markers TNF-α, IL-12β and PTGS2 were highest in macrophages stimulated with LPS and IFN-ɣ.

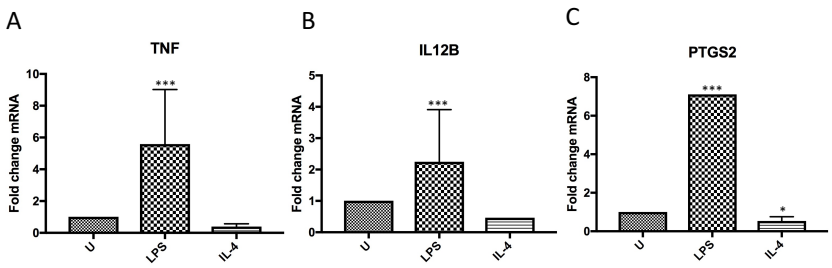

Figure 4.5 Messenger RNA expression of M1 markers [TNF-α (**A**), IL-12β (**B**) and PTGS2 (**C**)] in healthy human peripheral blood MDM that were either untreated (U), treated with 10ng/mL LPS and 20ng/mL IFN-γ for 24 hours (LPS), or treated with 20ng/mL IL-4 for 24 hours (IL-4). Data were normalised to that of unstimulated macrophages and expressed as mean ± SEM of five independent experiments. *** p<0.001 as determined by one way ANOVA.

Expression of M2 markers IL-10, CD200R, MRC1 and TGM2 were highest in macrophages stimulated with IL-4 as illustrated in **Figure 4.6**.

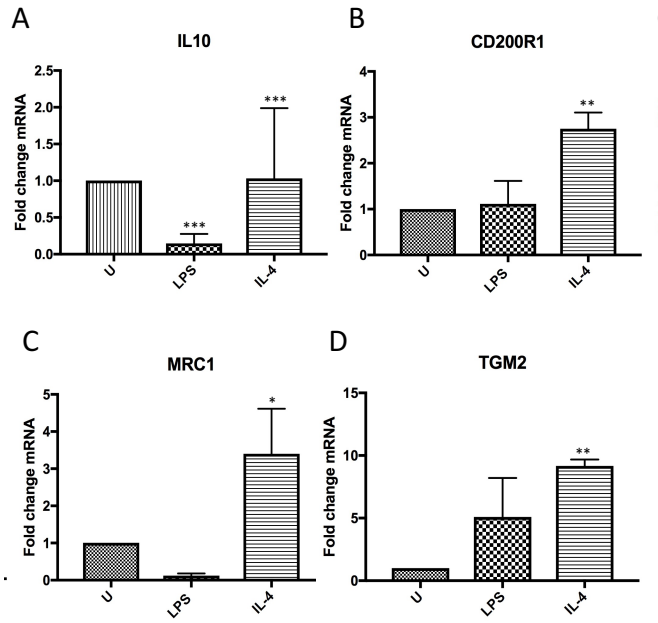

Figure 4.6 Messenger RNA expression of M2 markers in healthy human peripheral blood MDM that are untreated, treated with LPS 10ng/mL IFN-γ 20ng/mL for 24 hours, or treated with IL-4 20ng/mL for 24 hours. (**A**) Messenger RNA expression of IL-10, (**B)** mRNA expression of CD200R1, (**C)** mRNA expression of MRC-1, (**D)** mRNA expression of TGM2. Data were normalised to that of unstimulated macrophages and expressed as mean ± SEM of five independent experiments. *p<0.05, **p<0.01, *** p<0.001 as determined by one way ANOVA.

Further, enzyme-linked immunosorbent assay (ELISA) of cell supernatant was also used to assess TNF-α production, a cytokine well known to be produced to a greater extent by M1 compared to M2 MDM (see **Figure 4.7**).

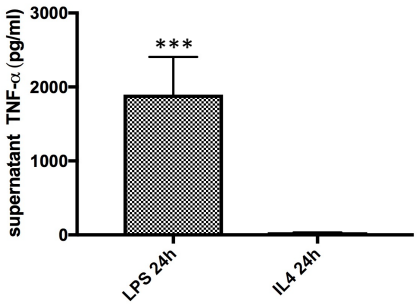

Figure 4.7 The levels of TNF-α in supernatant of stimulated MDM. Cells were activated for 24 hours with 10ng/mL LPS plus 20ng/mL IFNγ (LPS) or 20ng/mL IL-4, and TNF-α release was measured using an ELISA. Data is expressed as mean ± SEM of five independent experiments. Student t-test demonstrated significant difference in TNF-α in supernatant between MDM treated with LPS plus IFNγ, and those treated with IL-4, ***p<0.001.

4.4.3 TSPO expression in MDM treated with M1 or M2 stimuli

In order to compare TSPO expression between MDM treated with M1 or M2 stimuli, immunofluorescence of cytology of *in vitro* cultured and stimulated macrophages were undertaken. mRNA studies were also performed, in addition to semiquantitative assessment of TSPO protein expression (using Western Blotting), and quantitative assessment of TSPO protein (using [^{3}H]PBR28 radioligand saturation binding assays).

4.4.3.1 Immunofluorescence staining

Immunofluorescence staining was undertaken using healthy peripheral blood MDM, stimulated with LPS and IFN-ɣ, or IL-4 for 24 hours. Such cells were fixed in paraformaldehyde, before being centrifuged onto cytospin slides (as described in section 4.3.5). Immunofluorescence staining confirmed that healthy MDM viewed were macrophages (in that all were CD68 positive), and likewise, both M1 and M2 macrophages positively stained for TSPO (see **Figure 4.8**).

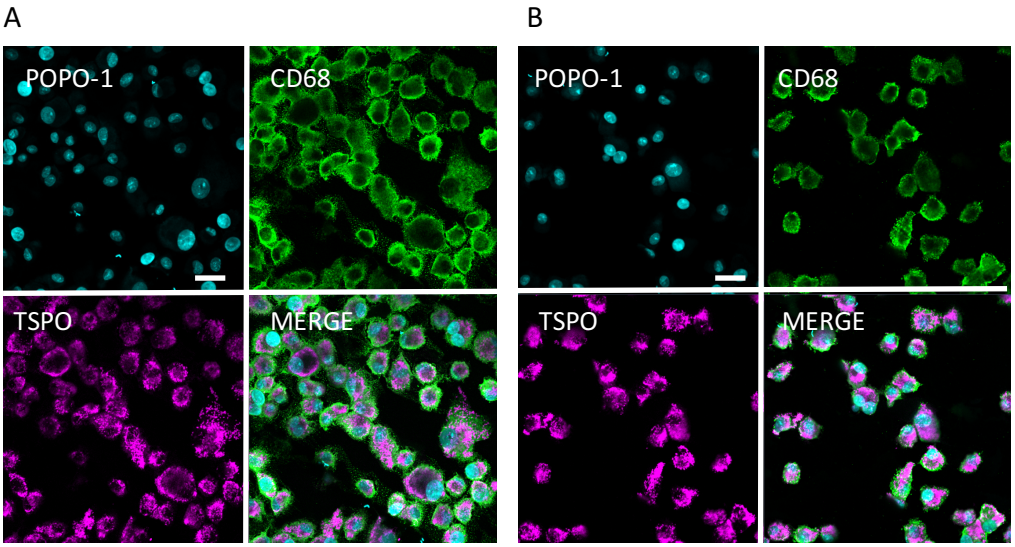

Figure 4.8 Immunofluorescence staining of cytospin slides of healthy peripheral blood MDM with the nuclear stain POPO-1 (to confirm presence of cells), TSPO, the macrophage marker CD68 and merging of the three stains. **(A)** staining of MDM stimulated with LPS plus IFN-γ for 24 hours (M1 macrophages); **(B)** staining of MDM stimulated with IL-4 for 24 hours (M2 macrophages). x400 magnification. Scale bar=20 μm.

4.4.3.2 mRNA and protein expression studies

For THP-1 MDM, there was a significant downregulation of *TSPO* mRNA expression in LPS/IFNγ treated MDM compared to unstimulated ($p<0.001$; **Figure 4.9A**). In contrast, *TSPO* mRNA expression was significantly increased in IL-4, TGF-β1 and dexamethasone treated THP-1 MDM compared to unstimulated ($p<0.001$ as determined by one way ANOVA, see **Table 4.4** for fold change data**)**, with no significant difference in fold change *TSPO* mRNA expression between THP-1 MDM treated with IL-4, TGF-β1, or dexamethasone.

For healthy human peripheral blood MDM, there was a significant downregulation in *TSPO* mRNA expression between unstimulated and LPS/IFN-γ treated MDM ($p<0.01$). There was, however, no significant difference in *TSPO* mRNA expression between unstimulated and IL-4, dexamethasone and TGF-β1 treated MDM (see **Table 4.4**). Importantly, there was significantly lower *TSPO* mRNA expression in LPS/IFN-γ treated MDM, compared to those treated with IL-4, dexamethasone and TGF-β1 ($p<0.001$) (**Figure 4.9B, Table 4.4**).

In the case of synovial fluid MDM cells, as with MDM of other sources, *TSPO* mRNA expression was significantly lower in LPS/IFNγ treated MDM ($p<0.01$) compared to

unstimulated (p<0.01). There was no significant difference in *TSPO* mRNA expression between unstimulated and IL-4, dexamethasone and TGF-β1 treated MDM. Furthermore there was no significant difference in mRNA expression between IL-4, dexamethasone and TGF-β1 treated synovial fluid MDM. As with MDM of all other sources, there was likewise significantly lower *TSPO* mRNA expression in LPS/IFNγ treated MDM, compared to those treated with IL-4, dexamethasone and TGF-β1(p<0.01) (**Figure 4.9C, Table 4.4**).

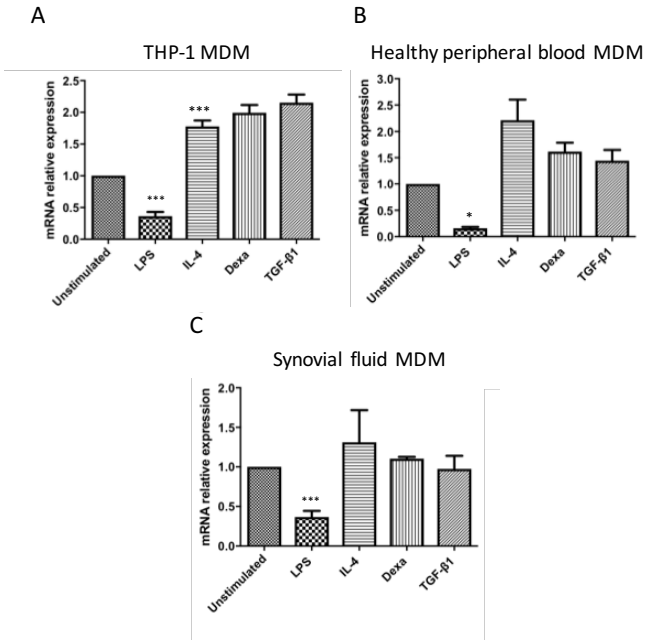

Figure 4.9 *TSPO* mRNA expression of M-CSF differentiated MDM, in response to 24hr treatment with 10ng/mL LPS plus 20ng/mL IFNγ or 20ng/mL IL-4 or 500nM dexamethasone or 3ng/mL TGF-β1, normalised to unstimulated (control) MDM cells. (A): THP-1 MDM; (B): healthy human peripheral blood MDM and (C): synovial fluid MDM. Results are expressed as fold change mRNA expression (using 18s as the reference gene). Data were normalised to that of unstimulated macrophages and expressed as mean ± SEM of five independent experiments. *p<0.05, *** p<0.001 as determined by one way ANOVA.

	Mean fold change *TSPO* mRNA expression ± SEM 24 hours post stimulation				
MDM	**Unstim**	**LPS plus IFN-ɣ**	**IL-4**	**Dexamethasone**	**TGF-β1**
THP-1	1	0.36 ± 0.07	1.78 ± 0.09	1.99 ± 0.12	2.15 ± 0.13
Healthy peripheral blood	1	0.16 ± 0.02	2.21 ± 0.39	1.62 ± 0.17	1.44 ± 0.20
RA synovial fluid	1	0.37 ± 0.08	1.31 ± 0.41	1.10 ± 0.02	0.98 ± 0.17

Table 4.4 Mean fold change *TSPO* mRNA expression in THP-1, healthy peripheral blood and RA synovial fluid MDM, stimulated with LPS plus IFN-ɣ, IL-4, TGF-β1, or dexamethasone for 24 hours. Data were normalised to that of unstimulated macrophages and expressed as mean ± SEM of five independent experiments. *p<0.05, *** p<0.001 as determined by one way ANOVA.

Next, a series of time course stimulation of the various MDM with LPS plus IFNγ was undertaken, to have a better understanding of any potential transient/early upregulation of TSPO expression (**Figure 4.10**). Regardless MDM source employed, there appeared to be a consistent downregulation of *TSPO* mRNA expression throughout the time courses, which was statistically significant as early as 2 hours in healthy human peripheral blood MDM (**Figure 4.10B**).

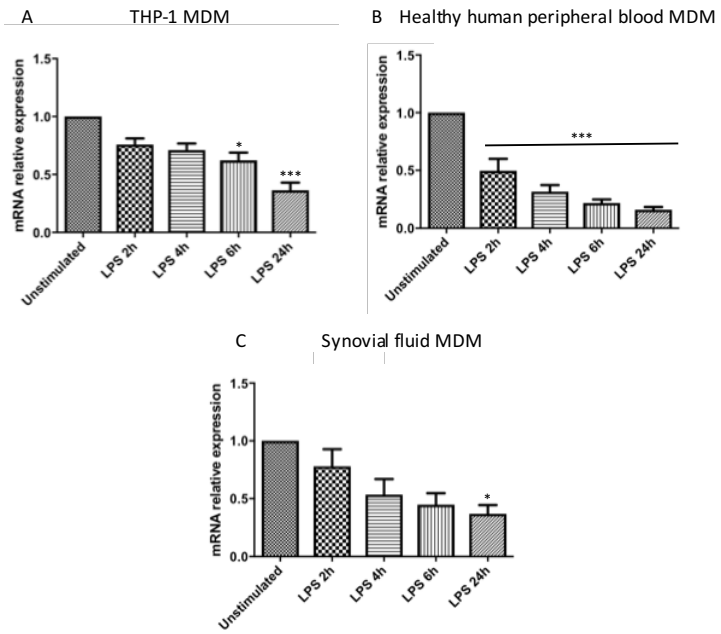

Figure 4.10 *TSPO* mRNA expression of various MDM, treated with 10ng/mL LPS plus 20ng/mL IFN-γ, for 2,4,6 and 24 hours, compared and normalised to unstimulated MD. A=THP-1 MDM, B=healthy human peripheral blood MDM, MDM C= synovial fluid MDM. Results expressed as fold change mRNA expression (compared to 18s). Data were normalised to that of unstimulated macrophages and expressed as mean ± SEM of five independent experiments. *p<0.05, ***p<0.001 as determined by one way ANOVA.

On semiquantitative analysis at protein level using western blot, there appeared to be a clear downregulation in TSPO expression by 24 hours in response to LPS/IFN-γ treatment (**Figure 4.11**). In contrast, TSPO protein expression was unaffected when treated with IL-4, dexamethasone or TGF-β1 (**Figure 4.12**).

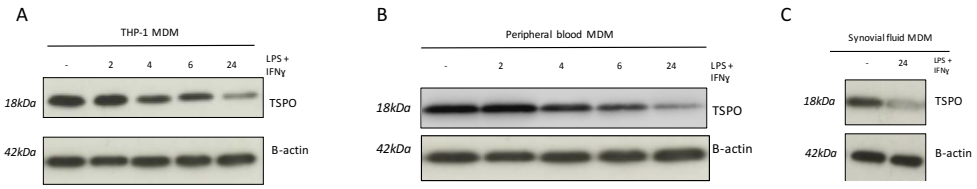

Figure 4.11 TSPO protein expression in MDM ± 10ng/mL LPS and 20ng/mL IFNγ in: **(A)** THP-1 treated for 2,4,6 and 24 hours; **(B)** Healthy human peripheral blood MDM treated for 2,4,6 and 24 hours and **(C)** synovial fluid MDM treated for 24 hours. TSPO protein (18kDa) was assessed by Western blot with β-actin as the loading control (42kDa). Optical densitometry calculations for n=5 independent western blot experiments are published in Narayan *et al*. 2017(446).

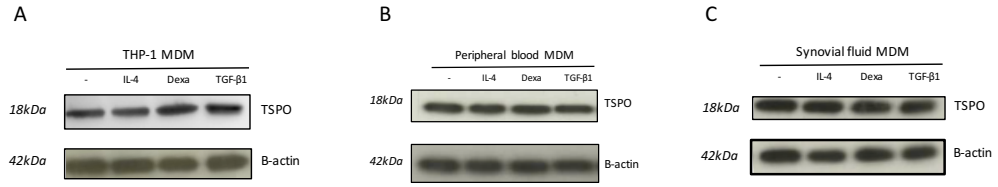

Figure 4.12 TSPO protein expression in untreated MDM, and MDM stimulated with 24 hours of IL-4 20ng/mL, dexamethasone 500nM, or TGF-β1 3ng/mL. **A:** THP-1 MDM **B**: healthy human peripheral blood MDM. **C:** synovial fluid MDM. TSPO protein was assessed by western blot with β-actin as loading control. Optical densitometry calculations for n=5 independent western blot experiments are published in Narayan *et al.* 2017(446).

Radioligand binding data provided quantitative protein data to support western blot findings, using the TSPO specific radioligand [^{3}H]PBR28 as a measure of TSPO protein expression. Radioligand binding demonstrated a significant downregulation of TSPO protein expression on MDM treated with 24 hours of LPS plus IFN-γ, compared to unstimulated MDM, and also compared to MDM treated with IL-4. The magnitude of this downregulation is realised by the fact that there was no significant difference in binding of [^{3}H]PBR28 in healthy human monocytes compared to MDM stimulated with LPS plus IFN-γ (1004 ± 52.4 fmol [^{3}H]PBR28 per 1x10^6 monocytes compared to 994.3 ± 21.93 fmol [^{3}H]PBR28 per 1x10^6 MDM stimulated with LPS plus IFN-γ).

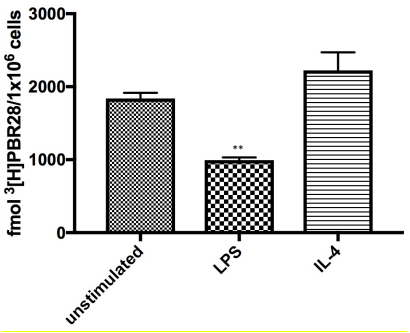

Figure 4.13 [^{3}H]PBR28 tracer uptake expressed in fmol per 1x10^6 cells in healthy human peripheral blood MDM ± treatment with 10ng/mL LPS plus 20ng/mL IFNγ (LPS), or 20ng/mL IL-4 for 24 hours. Data are presented as mean ± SEM of three independent experiments. ANOVA demonstrated no significant difference between untreated macrophages, and those treated with IL-4, but **p<0.01 between untreated macrophages, and those treated with LPS plus IFNγ, and ***p<0.001 between macrophages treated with LPS plus IFNγ and those treated with IL-4.

4.4.4 Cholesterol efflux pathway components in macrophages treated with different stimuli

Messenger RNA expression studies of two key components of the cholesterol efflux pathway were undertaken to ascertain any differences in expression of these components in macrophages of different phenotype.

CYP27A1

CYP27A1 is responsible for converting oxidised LDL to oxysterol, which acts as a ligand for LXRα. Activation of nuclear liver X receptors (such as LXRα) orchestrates the upregulation of genes encoding proteins involved in the cholesterol efflux pathway, such as those encoding ABCA1(439).

Statistical data analyses revealed a significant reduction in relative *CYP27A1* mRNA expression for all cells treated with LPS compared to unstimulated control (**Figure 4.14A**). However, there were no significant changes in *CYP27A1* expression in cells treated with M2 type stimuli, except for those treated with dexamethasone, where there was a statistically significant increase in *CYP27A1* mRNA expression compared to control (**Figure 4.14B**).

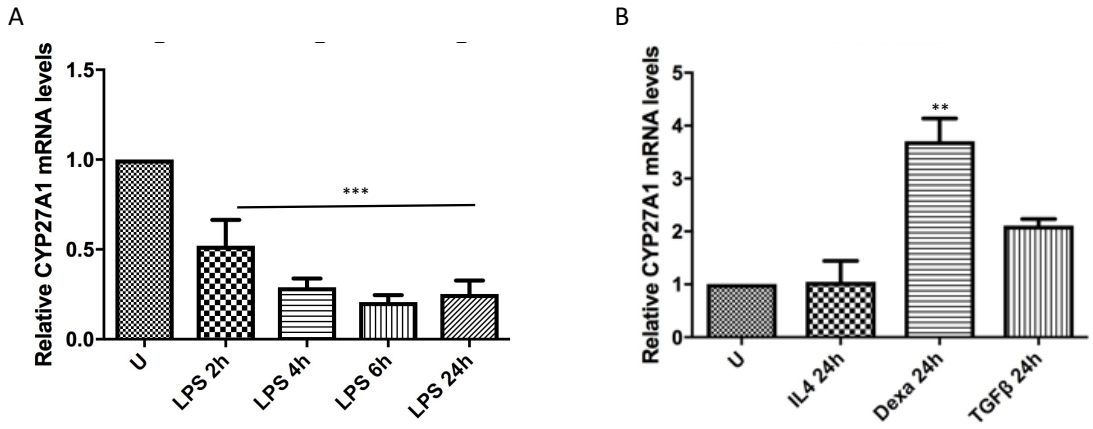

Figure 4.14 Relative *CYP27A1* mRNA expression of M-CSF treated healthy peripheral blood MDM in: (**A)** unstimulated cells normalised and compared to those treated with 10ng/mL LPS plus 20ng/mL IFNγ for 2,4,6 and 24 hours, and (**B)** unstimulated normalised and compared to cells treated with 20ng/mL IL-4, 500nM dexamethasone & 3ng/mL TGF-β1 for 24 hours. Results are expressed as fold change mRNA expression (compared to *18s*). Data were normalised to that of unstimulated macrophages and expressed as mean ± SEM of five independent experiments. **p<0.01, *** p<0.001 as determined by one way ANOVA.

ABCA1

Removal of excess cholesterol from macrophages can be achieved by the interaction of ATP binding cassette (ABC) transporters, such as ABCA1 with lipid-poor apolipoproteins and high density lipoproteins (HDL). ABCA1 promotes efflux of phospholipids and cholesterol to apolipoprotein (apo) A-I, apoE and other apolipoproteins (439).

When comparing relative *ABCA1* mRNA expression in cell cultures treated with LPS, a highly significant reduction was noted when compared its expression was compared to unstimulated control cell cultures (**Figure 4.15A**). However, there was no significant difference in *ABCA1* mRNA expression in MDM cell cultures treated with IL-4, dexamethasone and TGF (M2 type stimuli; **Figure 4.15B**).

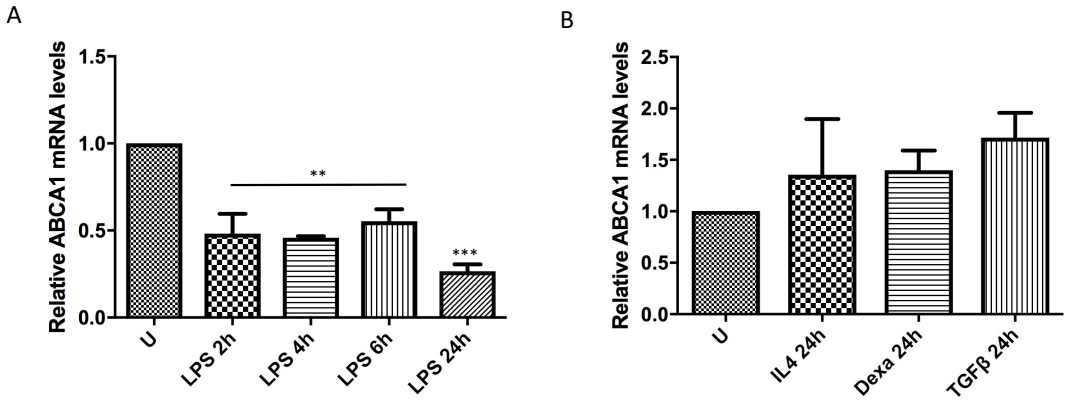

Figure 4.15 Relative *ABCA1* mRNA expression of M-CSF treated healthy peripheral blood MDM **A:** unstimulated compared to treated with LPS 10ng/mL plus IFNγ 20ng/mL for 2,4,6 and 24 hours. **B**: unstimulated compared to treated with IL-4 20ng/ml, dexamethasone 500nM, TGF-β1 3ng/mL for 24 hours. Results expressed as fold change mRNA expression (compared to *18s*). Data were normalised to that of unstimulated macrophages and expressed as mean ± SEM of five independent experiments. **p<0.01, *** p<0.001 as determined by one way ANOVA.

4.5 Discussion

This study aimed to ascertain the expression of TSPO in macrophages of different phenotype, in order to permit more accurate interpretation of TSPO PET signal in the future, as well as to provide further data that could implicate TSPO in the pathogenesis of macrophage driven inflammation.

Since TSPO is recognized to be expressed in macrophages in malignancy and inflammatory disease (157), I used three different sources of monocytes to investigate the expression of TSPO in macrophages. THP-1 monocytes, a widely accepted monocyte model, is an immortalized monocyte cell line, derived from peripheral blood of a Japanese paediatric patient with acute monocytic leukaemia, were utilized to represent a malignant disease monocyte/macrophage model. RA synovial fluid derived monocytes were used to represent an inflammatory disease monocyte/macrophage model. Healthy peripheral blood monocytes and MDM were used as a control group.

4.5.1 Comparison of TSPO expression between monocytes and macrophages

Although much data exists to support the idea that TSPO is highly expressed on activated macrophages (157, 197, 198), and even that monocytes express more TSPO than lymphocytes (195), data investigating the difference in TSPO expression between monocytes and macrophages is lacking. Herein we provided the first conclusive data to demonstrate that TSPO is upregulated significantly at mRNA and protein level in unstimulated human-derived MDM compared to monocytes, regardless of monocyte source (THP-1, healthy peripheral blood, and RA synovial fluid).

Interestingly, the fold change increase of TSPO mRNA on differentiation of RA synovial fluid monocytes to MDM was, on average, approximately 3-fold larger than upregulation seen on differentiation of healthy peripheral blood monocytes to MDM (fold change of 207.7 compared to 66.4, respectively). This could be secondary to the fact that fold change mRNA expression of TSPO in MDM are normalized to those of monocytes of the same source. Therefore, it could be that RA monocytes inherently

had a far lower expression of TSPO than healthy monocytes, hence, the differentiation of RA monocytes with M-CSF appeared to increase TSPO expression by a greater fold change than was the case for healthy MDM.

This hypothesis is supported by the fact that on Western blot, there was less TSPO in RA synovial fluid-derived monocytes compared to healthy monocytes. An exact quantification of TSPO protein expression in synovial MDM or monocytes was not possible, due to the amount of protein required for an accurate radioligand binding assay.

A difference in TSPO expression between RA synovial fluid monocytes and healthy monocytes would fit with a large body of evidence suggesting that monocytes in RA (both in peripheral blood, and synovial fluid) may differ phenotypically from healthy monocytes (314, 316, 447). The idea that TSPO may be downregulated on monocytes of patients with autoimmune disease is suggested by a study of patients with multiple sclerosis (MS). Here, peripheral blood mononuclear cells of MS patients expressed less TSPO protein than healthy volunteers (448), as determined by [^{3}H]PBR28 radioligand saturation binding assay.

Given the critical importance of monocytes and macrophages in RA (158, 258), further investigation into differential TSPO mRNA and protein expressions in monocytes and MDM from healthy and RA patients is necessary, to clearly elucidate any potential significance that TSPO may have in RA pathogenesis, and perhaps in autoimmune diseases in general.

4.5.2 Immunofluorescence staining of macrophages of different phenotype

There has been some previous work investigating the expression of TSPO in macrophages of different phenotype. Such studies frequently focussed on *in vivo* TSPO imaging, tissue immunofluorescence work. For example, Sandiego *et al.* undertook *in vivo* [^{11}C]PBR28 PET brain imaging pre-and post-administration of LPS in the peripheral blood of human participants; demonstrating an increase in TSPO PET signal in the brain post LPS administration. The authors concluded that the increase in TSPO PET signal demonstrated microglial activation by LPS, despite the fact that

the increase in signal could be due to infiltrating leukocytes from peripheral blood, as well as activation of non-microglial cells in the brain. Bonsack *et al.* used immunofluorescence of brain tissue taken from a rat model of intracerebral haemorrhage, to demonstrate no difference in TSPO expression on microglia expressing the 'M1' marker CD16/32 (430) compared to those expressing the 'M2' marker CD206 (188). However, such an observation is limited by the fact that TSPO is ubiquitously expressed in rodents (and humans) (157), and the fact that it is difficult to be certain of microglia phenotype on histology using a single marker (430).

In this study, we used immunofluorescence work of *in vitro* healthy human peripheral blood MDM, of known phenotype (as determined by multiple mRNA markers and ELISA), to look at any differences in TSPO expression between *in vitro* cultured M1 and M2 type healthy MDM. This failed to demonstrate any obvious difference in TSPO staining between M1 and M2 MDM. This is unsurprising, given that TSPO is largely ubiquitous (157), and could suggest that immunostaining may not be a sufficiently sensitive method to quantify TSPO staining in macrophages, in keeping with the rodent study of microglia by Bonsack *et al.* mentioned above (190).

4.5.3 In vitro mRNA and protein expression studies of MDM of different phenotype

In contrast to the large number of tissue studies of TSPO expression in macrophages, few studies of TSPO mRNA or protein expression in macrophages *in vitro*, have been performed to date. Shao *et al.* used the murine macrophage cell line, RAW 264.7, to demonstrate that TSPO protein levels were significantly up-regulated at 24 hours with addition of LPS, in a dose-dependent manner (261) as determined by an increase in the binding of the TSPO radio-ligand [^{11}C]PBR28, at various doses of LPS. However, RAW 264.7 is a murine macrophage cell line transformed by the Abelson leukemia virus. TSPO expression is well known to be aberrantly expressed in malignant cells (157); hence it cannot be assumed that the TSPO expression pattern seen in RAW 264.7 reflects that seen in non-immortalized cells.

Other studies have used whole tissue protein lysate to assess the impact of LPS administration on TSPO expression. For example, Hatori *et al.* used whole tissue

protein lysate, derived from a LPS induced model of acute lung injury in rats, to demonstrate that as the time interval post LPS administration increased, TSPO expression in the injured lung tissue also increased on Western blot. Since whole tissue lysate was used, it cannot therefore be assumed that the increase in TSPO expression is attributable to macrophages alone, or that simply an increase in infiltrating cells is contributing to the increase in TSPO seen.

More recently, TSPO mRNA over-expression and gene knock-down studies have been undertaken in microglia, using the immortalized murine microglia cell line BV2 (372). Bae *et al.* demonstrated that overexpression of TSPO appeared to decrease production of pro-inflammatory cytokines on LPS treatment of BV2 cells, with increased expression of 'M2' murine macrophage markers IL-10 and MRC1, compared to microglia that did not over express TSPO (374). However, no such study has been performed to assess the impact of 'M1', pro-inflammatory stimuli (such as LPS or IFN-ɣ) on TSPO expression in non-genetically altered macrophages, or the impact of M2 stimuli (such as IL-4, TGF-β or glucocorticoid).

In this study, we used both mRNA study (using RT-PCR), and western blotting, to provide semi-quantitative data regarding TSPO expression in MDM from three different human monocyte sources; THP-1, healthy human peripheral blood, and RA synovial fluid. Absolute quantification of TSPO protein expression was provided by radioligand saturation binding with the TSPO specific ligand [^{3}H]PBR28, in the first study of TSPO quantification in human macrophages *in vitro.*

This study presents the first data demonstrating a consistent downregulation of TSPO expression, at both mRNA and protein level in MDM stimulated with LPS plus IFN-ɣ, with no change in TSPO expression at protein level in those MDM treated with 'M2' type stimuli IL-4, TGF-β1 or dexamethasone. The magnitude of the downregulation was evidenced by radioligand saturation binding; implying that the significant upregulation of TSPO on differentiation from a monocyte state to a macrophage phenotype, is lost, upon stimulation of macrophages with LPS plus IFN-ɣ. Indeed, on radioligand saturation binding study of healthy monocytes and MDM, no significant difference in [^{3}H]PBR28 binding was noted between monocytes and MDM treated with LPS/IFN-ɣ.

Some caveats to this work must be noted. Firstly, the number of donors for healthy peripheral blood monocytes, and synovial fluid monocytes, was small.
Further, due to limited resources and finite cell numbers from RA synovial fluid and healthy peripheral blood monocytes provided sufficient quantities for any subsequent radioligand saturation binding studies.

An increasing body of research further has demonstrated that 'multiple' subtypes of monocytes exist in humans (447, 449). For example, it is increasingly thought that like macrophages, a spectrum of monocyte phenotypes exist in humans; with the subset $CD14^{++}CD16^{-}$ ('classical monocytes') are thought to make up the majority of human monocytes, with $CD14^{+}CD16^{++}$ ('non-classical') monocytes representing the opposite end of the monocyte phenotype spectrum (450). It is proposed that monocytes of different phenotype may have different roles in disease; with multiple studies demonstrating an expansion of CD16+ monocytes in both peripheral blood and synovium of RA patients (315, 451). However, in this study, I defined a monocyte as a CD14 positive mononuclear cell (according to flow cytometry), but did not undertake further sub-typing of monocytes utilised. Therefore, it is likely multiple monocyte subtypes were included in the current experiments. Conversely this argument may be of little relevance as we used monocytes from three different sources (THP-1, healthy peripheral blood, and synovial fluid monocytes), and still observed similar results. However, future work is needed to establish any differences in TSPO expression between monocytes of different subtypes, and any MDMs arising from each subtype, which would be particularly important for the investigation of TSPO in monocytes derived from RA patients, where expansion of certain subsets compared to the healthy population, is increasingly recognised (316).

One must be cautious in extrapolating significant conclusion from the *in vitro* findings to *in vivo* macrophages. Indeed, the M1 and M2 stimuli applied in this study do not exist in isolation *in vivo*; and hence a combination of stimuli may be acting upon monocytes and macrophages at any one time within any specific tissue (308, 452), thus macrophage phenotypes *in vivo* may be more complex than descried *in vitro*. For instance Martinez *et al.* recently theorized that it could be conceivable, that *in vivo*, M1 and M2 gene expression patterns may not necessarily exclude each other, and may

co-exist as one macrophage, with the resulting mixed phenotype depending on the tissue environment (308). Evidence to support this theory is currently scant, however, and further study of *in vivo* human MDM harvested from different tissues, and disease states, may help further clarify macrophage phenotypes *in vivo*.

The findings of this chapter may have implications for the field of PET imaging, where TSPO-specific radioligands are increasingly being used in a wide range of disease states as an imaging tool of macrophage infiltration (147, 453-455). With the increasing sensitivity and specificity of newer generation TSPO specific radioligands, such as [^{11}C]PBR28 and [^{18}F]PBR111 (142, 259, 455), it may be important to consider differences in TSPO expression in macrophages of M1 polarity compared to M2 when interpreting TSPO PET images.

The finding that TSPO is downregulated in MDM stimulated with pro-inflammatory 'M1' type stimuli (LPS/IFN-ɣ), compared to unstimulated MDM, and MDM treated with 'M2' type stimuli (IL-4, dexamethasone, TGF-β1), may also suggest a role for TSPO in the polarisation of macrophage phenotype; with our data suggesting TSPO may help negatively regulate inflammation, through promoting an M2 macrophage phenotype. Certainly, our findings are in keeping with the study of murine BV2 microglia by Bae *et al.*(374) where over-expression of TSPO, led to a reduction in microglia production of pro-inflammatory cytokines upon LPS stimulation, with upregulated expression of M2 type markers IL-10 and MRC1. We went on to provide some preliminary data to suggest how TSPO might be functioning to polarise MDM towards an M2 phenotype.

4.5.4 A hypothesis for the role of TSPO in MDM signalling and functions

Since it was out of the scope of this project to conclusively elicit a role for TSPO in macrophage phenotype polarization, we undertook a preliminary investigation to establish a hypothesis for how the differential expression of TSPO in macrophages could contribute to the generation of a particular phenotype.

Numerous functions for TSPO have been proposed over the past 4 decades since its discovery, ranging from roles in the respiratory burst (456), to steroidogenesis (209),

to apoptosis (219). Over recent years, there has been accumulating evidence to support the theory that TSPO acts a cholesterol transporter in the mitochondrial membrane in macrophages. Taylor *et al.* transfected THP-1 macrophages to over-express TSPO, and incubated these cells in media containing [^{3}H]cholesterol, to provide a means of measuring cholesterol efflux. THP-1 macrophages overexpressing TSPO exhibited a significant increase in efflux of cholesterol compared to non-transfected cells, whereas gene knockdown of TSPO in THP-1 macrophages had the opposite effect (457).

It has been proposed that, TSPO acts as a cholesterol transporter, regulating the passage of cholesterol through the mitochondrial membranes, a rate limiting step in cholesterol conversion by mitochondrial enzymes to oxysterol (439). Oxysterols then activate LXRα/β nuclear receptors, which subsequently generate a transcriptional upregulation in mRNAs involved in promoting cholesterol efflux from cells, such as *ABCA1*.

The importance of intra-cellular cholesterol in the generation of inflammation is demonstrated by both human and animal studies (458), with cholesterol accumulation within cells thought to potentiate inflammation through multiple mechanisms. Excessive free cholesterol may promote cholesterol crystal formation, resulting in complement-mediated activation of the inflammasome, with subsequent activation of caspase-1 and release of IL-1 β (459). Further, cholesterol accumulation can promote the formation of lipid rafts. Lipid rafts are cholesterol enriched microdomains within the plasma membrane, which are postulated to be involved in the response to pro-inflammatory stimuli (460), through localizing components of signaling pathways to them. For example, one study of RAW 264.7 macrophages demonstrated that lipid rafts contained increased amounts of proteins (such as CD14, and MAP-Kinase) necessary for Toll-Like Receptor 4 signaling, essential for the generation of a pro-inflammatory response to LPS (461).

Cholesterol efflux is thought to reduce the cholesterol enrichment of lipid rafts, hence having an inhibitory effect on signaling pathways mediated through lipid raft associated receptors. This is demonstrated by studies of murine macrophages

deficient in ABCA1 or ABCG1, cholesterol transporters that are well-recognized essential components of the cholesterol efflux pathway (462). These cholesterol transporter-deficient macrophages displayed a far reduced expression of inflammatory markers in response to LPS compared to wild type macrophages (463), with elimination of lipid efflux, increased intracellular free cholesterol and accumulation of lipid rafts in plasma membranes (464, 465). The acquisition and movement of cholesterol within cells is diagrammatically summarized in **Figure 4.16**.

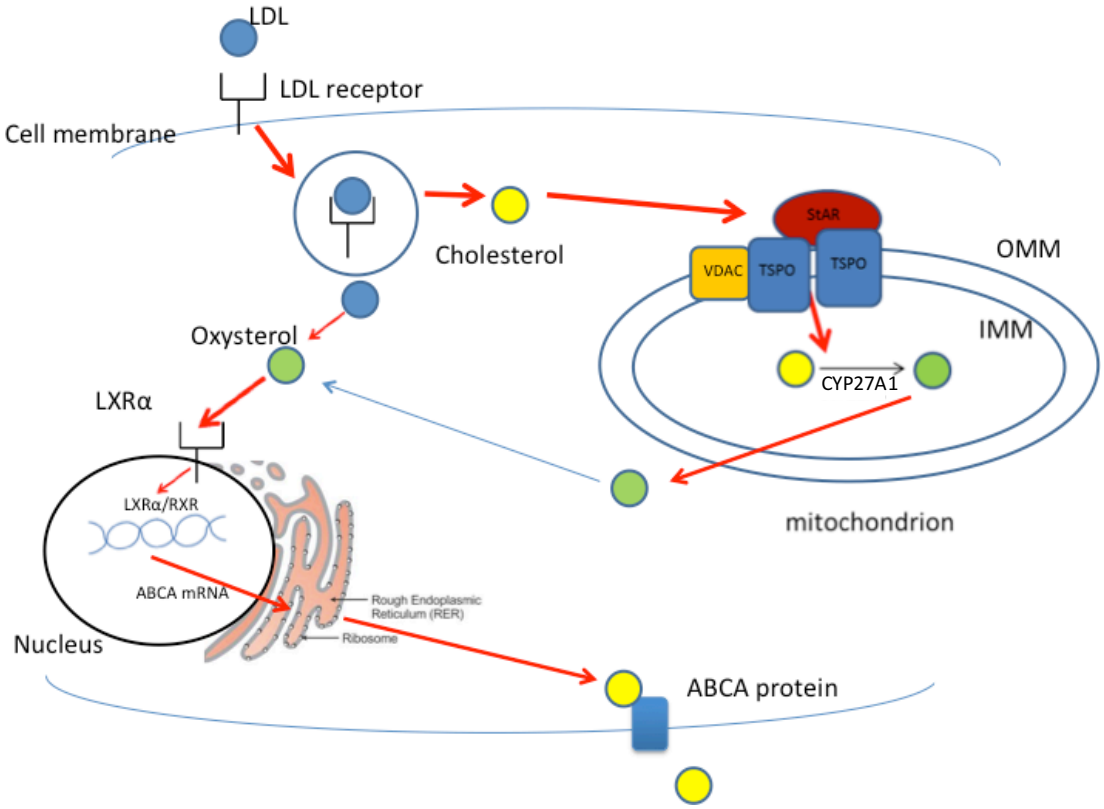

Figure 4.16 Summary of Cholesterol trafficking pathway: cholesterol enters the cell in the form of LDL, which binds to membrane LDL receptors. The LDL receptor complex is internalized in lysosomes, and cholesterol is released into the cell. Cholesterol is then transported into mitochondria by the TSPO/VDAC/StAR transduceosome complex, and converted to oxysterol by CYP27A1. Oxysterol then binds to LXRα, which forms a complex with RXR, inducing transcription of genes for the ABCA cholesterol transporters, upregulating protein production of ABCA, promoting cholesterol efflux from the cell membrane (adapted from *Graham et al.* (439) and Venkateswaran *et al* (466). LDL=low-density lipoprotein, VDAC=voltage-dependent anion channel, StAR=steroidogenic acute regulatory protein, LXR=liver X receptor alpha, RXR=retinoic acid receptor, ABCA=ATP binding cassette transporter.

Although the complex of proteins involved in mitochondrial cholesterol trafficking remains the subject of debate (439, 467), it is postulated that TSPO forms part of this complex (457). The importance of TSPO in cholesterol efflux is indicated by the fact

that THP-1 derived macrophages transfected to overexpress TSPO, exhibit an increase in cholesterol efflux (457) whilst ligation of TSPO increased cholesterol efflux further in macrophages.

We propose that TSPO down-regulation in response to LPS may further reduce cholesterol efflux from cells, through reducing cholesterol transport to the inner mitochondria for conversion to oxysterol by CYP27A1 (a rate limiting step in cholesterol efflux (439)). This would further promote intracellular lipid accumulation, potentiating pro-inflammatory signaling. We therefore hypothesized that the difference in TSPO expression in M1 and M2 macrophages is due to the role of TSPO in cholesterol efflux, with a down-regulation of TSPO in M1 type macrophages favouring less cholesterol efflux than M2 macrophages.

The present investigation has generated preliminary evidence that mRNA expression of key components of the cholesterol efflux pathway, CYP27A1 and ABCA1, are significantly down-regulated in LPS stimulated macrophages, whereas mRNA expression is increased or unchanged in macrophages treated with M2 stimuli, lending support to the idea that cholesterol efflux may be suppressed in M1 compared to M2 MDM. This could, in turn, lend support to the hypothesis that TSPO downregulation is important for the accumulation of cholesterol in M1 phenotype MDM.

In order to more definitively establish any role for TSPO in MDM cholesterol efflux, such observations require confirmation at protein level (using western blotting), along with silencing studies of TSPO in MDM combined with direct measurement of cellular cholesterol efflux, an approach which was outside the remit and timeline of the current thesis.

CHAPTER 5

Discussion and Concluding Remarks

TSPO has been used as target for the imaging of inflammatory disease for decades, all based on the assumption that TSPO is a marker of activated tissue macrophages (142, 431, 468). Recent research has demonstrated its potential utility as a target for PET imaging of synovitis in RA, with the TSPO tracer [^{11}C]PK11195 being capable of detecting and quantifying not only clinically apparent synovitis, as determined by clinical examination (154), but also subclinical inflammation (149), and synovitis at pre-clinical stages in ACPA positive patients (147).

Further study of TSPO PET tracers other than [^{11}C]PK11195 has been driven by the fact that imaging with [^{11}C]PK11195 is technically limited by high non-specific binding (259), which could lead to false positive interpretation of tracer accumulation on PET imaging *in vivo*. Therefore, 'second generation' TSPO ligands were developed, such as [^{11}C]PBR28 or [^{18}F]PBR111, with a far higher specificity (as well as sensitivity) for TSPO (259, 262, 282).

Data provided herein is the first human data to demonstrate that the second generation TSPO PET tracer [^{11}C]PBR28 is capable of detecting and quantifying synovitis *in vivo,* in patients with RA or PsA.

Since little work has been done previously to ascertain TSPO expression in major cell types of inflamed synovium, in this thesis, I provided the first data assessing TSPO expression in major cell groups of synovium on histological staining, as well providing more detailed quantification of TSPO expression, through mRNA and protein expression studies. These findings challenge the pre-existing literature that suggests TSPO PET is likely to be a means of imaging macrophages *in vivo* synovium(154), and rather, that TSPO PET signal is likely to reflect the presence of activated M2 phenotype macrophages, activated FLS, and also the presence of T lymphocytes.

The data in this work also demonstrated that TSPO appeared to be downregulated in macrophages activated with pro-inflammatory stimuli LPS and IFN-ɣ, with no significant change on activation of macrophages with 'M2' type stimuli, such as IL-4, TGF-β, and glucocorticoid. Such a finding was unexpected, and could lend insight into the role of TSPO in macrophage phenotype generation, in response to external stimuli, and hence indicate the role of TSPO in the pathogenesis of inflammatory disease.

5.1 The utility of [^{11}C]PBR28 for the detection and quantification of synovitis; a proof of principle pilot study

Through a proof of principle pilot study, the ability of the second generation TSPO PET tracer, [^{11}C]PBR28, to detect synovitis was assessed using clinical examination, ultrasound scanning and synovial histology as comparative variables.

This study provided technical data, to enable a reliable and accurate [^{11}C]PBR28 PET scan to be carried out in future clinical [^{11}C]PBR28 PET studies imaging synovitis. Indeed, through dynamic scanning, the time-point at which [^{11}C]PBR28 radioligand occupied all its binding sites in synovium (as measured by SUV), was determined at 50 minutes post tracer administration. This time-point represents the optimal time for tracer uptake to reflect target expression in synovium, and hence the optimal time to start a static [^{11}C]PBR28 PET scan to image synovitis. This now enables all future patients to be imaged in a static manner, allowing imaging of all joints in a single 20 minute static PET-CT scan.

Although the number of participants in this study was small, [^{11}C]PBR28 PET tracer uptake, measured as SUVR, SUV and V_T, all increased with synovitis severity score as determined by clinical examination. Furthermore, as both GSUS and PDUS scores of synovitis severity increased, so did [^{11}C]PBR28 SUV, further lending credence to the ability of [^{11}C]PBR28 to detect and quantify synovitis.

Histology of synovial tissue acquired from one joint of each arthritis participant imaged, aimed to investigate whether [^{11}C]PBR28 in the biopsy compartment correlated with TSPO expression, and macrophage infiltration (by staining for CD68 and CD163). The findings provide evidence that firstly, [^{11}C]PBR28 tracer uptake is indeed a reflection of tracer target expression in synovium, rather than representing non-specific binding of tracer, or other confounding factors, such as blood flow to the tissue. Secondly, by evaluating the relationships between [^{11}C]PBR28 tracer uptake and synovial staining for CD68 and CD163, I also provided indirect evidence in support of the hypothesis that [^{11}C]PBR28 tracer uptake likely reflects the presence of CD68+ and CD163+ cells. Histological investigations demonstrated a significant correlation between [^{11}C]PBR28 SUV in the biopsy compartment, and staining for TSPO, CD68 and CD163 in tissue

acquired from the same region, providing preliminary data to suggest that [^{11}C]PBR28 uptake is likely a true reflection of TSPO expression, and that the tracer uptake also correlates with the presence of CD68+ cells, as well as CD163+ cells.

Although only a small number of participants were involved in the present study, the paired Wilcoxon rank test did not demonstrate significant differences between mean TSPO and CD68 staining scores across all samples. However, CD163 staining scores were noted to be significantly lower on average for all samples than TSPO staining scores (with median of difference at -0.21, p=0.01). Since it is increasingly accepted that CD163 is a more specific synovial macrophage marker than CD68 (274), our data provides some supporting evidence that TSPO may be expressed on cells other than CD163+ macrophages. Given the existing evidence in the literature that CD68 is expressed on FLS as well as macrophages (275), it is therefore conceivable that TSPO is expressed on both FLS and macrophages.

Through better understanding the contribution of different cell types to TSPO signal, TSPO PET may be able to give insight into different stages of disease; indeed, there is accumulating data in the investigation of brain tissue malignancy, to suggest that cellular study of TSPO expression may enable the use of TSPO PET signal to indicate tumour grade *in vivo (381)*. For example; in the study of gliomas, it is well recognized that the higher the TSPO protein expression in the tumour site, the higher grade the glioma (469), with a drop in TSPO expression being associated with anaplastic transformation (438), providing evidence for altering any treatment strategy. In a similar way, further study of TSPO expression on human RA synovial cell types, would enable more accurate interpretation of TSPO PET tracer signal in RA synovium, and through this, could also provide *in vivo* data to further elicit cellular contributions in the pathogenesis of RA, which could provide predictive data for the clinical course of the disease, or aid in the selection of an appropriate target therapy for individual patients, depending on changes in TSPO PET signal in synovium.

5.1.1 Study limitations

Given that that this work was a proof of principle pilot study, with a small number of participants, care needs to be taken in inferring definitive conclusions from the data

obtained. That said, the collective data on clinical observations, ultrasound scanning and histological examinations, does suggest the ability of [^{11}C]PBR28 to detecting and quantify RA synovitis *in vivo*.

For the cohort imaged, calculating SUVR as opposed to SUV appeared to negate the impact of binding affinity on tracer uptake. However, this effect could merely be due to the small cohort size. A larger study is required to ascertain if SUVR can truly be used to allow comparisons of [^{11}C]PBR28 uptake between patients of moderate and high binding affinity.

In the cohort imaged, it was not possible to calculate V_T data for 2 out of the 6 arthritis patients, for whom arterial blood data was available. For these 2 patients, for the duration of the 90 minute scan, no plateau of V_T was reached, the reasons for which were unclear; certainly, to date, in humans, [^{11}C]PBR28 has not been used to image tissues outside the brain, where this has not been an issue (470). Positron emission from all known [^{11}C]PBR28 metabolites was taken into account in this study, to ensure accurate calculation of V_T value. The two tissue compartment model, used to calculate V_T, fits well to brain [^{11}C]PBR28 data (239, 263), but may not have been appropriate in synovial tissue where [^{11}C]PBR28 metabolites, which might not access the brain because of the blood brain barrier, may have added noise. Another potential confounder to the calculation of V_T in synovium, could be related to the fact that TSPO is well recognised to be expressed on circulating leukocytes; therefore, it is possible that variations in circulating leukocytes in blood could reduce the levels of free tracer and metabolites in the plasma that were measured to calculate V_T in this study. However, such a hypothesis is purely speculative. Further tissue compartment modelling studies of a larger patient cohort would be required to better ascertain reasons for anomalies in V_T data, perhaps also assessing any variance in plasma levels of [^{11}C]PBR28 and its metabolites according to circulating white cell count.

Although V_T is regarded as the gold standard for measurement of PET tracer uptake, the fact that SUV in this study correlated with clinical and ultrasound scoring for synovitis, as well as histology staining scores for TSPO, implies that V_T is a less optimal measure of tracer uptake in synovium compared to SUV, rather than [^{11}C]PBR28 being unable to detect and quantify synovitis. Further, since V_T requires

invasive blood sampling during scanning, such a measure of tracer uptake is hardly practical for larger studies, when comparing with non-invasive SUV measures.

5.1.2 Further validation of [^{11}C]PBR28 as a means of measuring synovitis

In order to further investigate the ability of [^{11}C]PBR28 to detect synovitis, a subsequent, larger cohort study would be ideal. Such a study would include participants of all binding affinity genotypes, and utilise a static scan method, in order to provide images of all joints in the body for all patients. Our pilot study has already provided sufficient data for reliable static scanning using [^{11}C]PBR28 . Any future study of this nature would not only better ascertain the real impact of binding affinity on tracer uptake in synovium, but also enable meaningful comparison of tracer uptake with DAS28-CRP scores, reliant on swollen and tender joint count of 28 joints throughout the body, as well as enabling more meaningful correlation of tracer uptake with peripheral blood markers of systemic inflammatory response. For example, a sum of [^{11}C]PBR28 SUV in all joints could be calculated as previously described in Zhu *et al.* (156), and such values could then be compared with composite disease activity scores that are inclusive of defined joint sets, and routine peripheral blood tests, such as CRP, WCC and ESR, in addition to more investigational peripheral blood markers of inflammatory disease, such as circulating MMP.

Additionally, an assessment of the ability of [^{11}C]PBR28 to detect subclinical disease, or pre-clinical synovitis, would be desirable, as further proof of the sensitivity of this modality to detect synovitis. This would require the participation of a cohort with established diagnosis of RA (or PsA) in remission, to assess ability to detect subclinical disease, or those with ACPA positive arthralgia (or those with skin psoriasis and arthralgia) to assess the ability of [^{11}C]PBR28 to detect synovitis at a pre-clinical stage. MRI would be ideal to use as a comparator, especially since the advent of PET-MRI (471), would mean both PET and MRI scans can be performed simultaneously, and superimposed on one another, enabling accurate temporal and anatomical comparisons.

Head to head comparison of [^{11}C]PBR28 with MRI, [^{18}F]FDG and [^{11}C]PK11195

The ability of PET-MRI to superimpose [^{11}C]PBR28 PET images over MRI images, will also provide highly accurate anatomical localization of [^{11}C]PBR28, further assessing the ability of [^{11}C]PBR28 to detect soft tissue inflammation, such as tenosynovitis, a recognized early feature of inflammation in arthritis, as well as bony inflammation (60, 105). Further, PET-MRI will provide simultaneous correlation of [^{11}C]PBR28 SUV measures with MRI scores of inflammation, providing further evidence for the ability of [^{11}C]PBR28 to detect inflammatory change in arthritis.

The most commonly used PET tracer in clinical practice is [^{18}F]FDG, used for the detection, and staging of malignancy, as well as to diagnose and assess the extent of inflammatory diseases, such as large vessel vasculitis (151). To support the hypothesis that TSPO targeted PET using [^{11}C]PBR28, is superior to [^{18}F]FDG (the most common PET tracer in use in clinical practice (472)) for the imaging of synovitis, a head-to-head comparison is desirable, with the imaging of patients with both tracers on the same day.

Although several human and non-human primate studies have demonstrated the superior specificity and binding affinity of [^{11}C]PBR28 compared to [^{11}C]PK11195, such studies are confined to brain imaging (259). Given the limitation to use of [^{11}C]PBR28 conferred by the impact of *rs6971* on binding affinity, it will also be desirable to compare [^{11}C]PBR28 PET with [^{11}C]PK11195 for the imaging of synovitis; PET-MRI would be an ideal means to compare the two tracers, with MRI providing measures of synovitis, soft tissue inflammation and bony inflammatory change, to compare with tracer uptake.

Ability of [^{11}C]PBR28 to assess response to treatment

We have established from this work that about 12% of the arthritis population, will be *rs6971* homozygous (in keeping with the frequency of this genotype for the healthy population (262)). Such low affinity binders will not produce a measurable signal with [^{11}C]PBR28 (265), hence perhaps rendering the tracer impractical for use in clinical

practice, since a genotyping test is required to decide if a patient is appropriate for [^{11}C]PBR28 imaging, and also possibly, to interpret tracer uptake. However, [^{11}C]PBR28 can still have utility in clinical trials, where low affinity binders can be routinely excluded from participation as part of screening tests.

In order to establish the ability of [^{11}C]PBR28 PET to detect response to treatment, [^{11}C]PBR28 PET pre- and post initiation of treatment with a proven history of efficacy (such as anti-TNF-α therapy), would be required. The use of an imaging time-point, as early as 2 weeks post treatment initiation, would permit assessment of the ability of [^{11}C]PBR28 to predict the outcome of the therapy at later dates. Furthermore, employing PET-MRI would add further validity to observations, and demonstrate whether or not [^{11}C]PBR28 is superior to MRI as an imaging modality for detection of response to treatment. Such a study would then permit progression to use of [^{11}C]PBR28 to assess treatment response in novel therapies.

Assessment of the utility of [^{11}C]PBR28 in ankylosing spondylitis (AS)

Although we have provided preliminary evidence of the ability of [^{11}C]PBR28 to detect and quantify peripheral synovitis in patients with known RA or PsA, there is no data assessing the ability of [^{11}C]PBR28 to detect spinal inflammation. A previous study by Bruijnen *et a*l. demonstrated that the TSPO PET tracer [^{11}C]PK11195 was unable to detect spinal inflammation in AS (as determined by MRI), unlike the tracers [^{18}F]FDG and [^{18}F]NaF (182). Although the number of participants in this study was small (12 patients), the inability of [^{11}C]PK11195 could be due to the high background uptake of [^{11}C]PK11195 in bone (154, 281), rendering [^{11}C]PK11195 unsuitable for the imaging of bony inflammation. Due to the far higher specificity of [^{11}C]PBR28, it could be possible this tracer may be a useful imaging tool for bony inflammation in AS.

5.2 An Investigation of TSPO expression in major cell groups of human RA pannus

Little previous data exists to evaluate TSPO expression on cellular constituents of RA pannus. Previous work by Van der Laken *et al.* demonstrated a significant

correlation between TSPO and CD68 staining on serial sections of RA synovial tissue (154), leading to the assumption that TSPO targeted PET is macrophage specific in synovium. Previous work has evaluated TSPO expression on peripheral blood leukocytes in whole blood, demonstrating more TSPO expression at protein and mRNA level in neutrophils, compared to NK cells and lymphocytes (195). However, to date, no data exists to profile the expression of TSPO in cell types present in synovium.

In this study, I demonstrated that [^{3}H]PBR28 uptake was significantly increased in RA synovial tissue compared to healthy control tissue. Further, there was greater staining for the tracer target, TSPO, higher expression of macrophage markers CD68, CD163, FLS activation marker PDPN, and CD4 in the same RA synovial tissues compared to healthy tissues. In RA patients, immunohistochemical staining for TSPO, CD68, CD163, PDPN and CD4 all significantly positively correlated with [^{3}H]PBR28 uptake, providing preliminary data to suggest that TSPO PET reflects synovial cellularity.

No previous immunofluorescence staining for TSPO has been undertaken using synovial tissue. The majority of histology work in TSPO has been undertaken in studies of brain tissue. One immunofluorescence study of a rat model of cerebral infarction used immunofluorescence to demonstrate that microglia, brain resident macrophages, upregulate TSPO expression when they are activated as part of the inflammatory response to cerebral infarction (191). Here, rat brain tissue was harvested at time intervals post induction of cerebral infarction. Tissue, harvested at rats culled at varying times post cerebral infarction, was stained for the rodent monocyte marker CD11b, along with TSPO. On day 1 post cerebral infarction, only a small fraction of CD11b positive cells at the site of infarct were TSPO positive. However, by day 4, CD11b+TSPO+ cells at the infarct site had significantly increased according to semiquantitative staining scores, providing evidence that activated microglia upregulate TSPO expression. However, such a study was limited by the fact that CD11b, is not specific for microglia or monocytes; indeed, CD11b is expressed on neutrophils, and blood borne macrophages (191, 473); hence it could be possible that rather than upregulation of TSPO on microglia at sites of inflammation, the increased number of CD11b positive cells may result from infiltration with peripheral blood derived leukocytes.

Unlike most previous studies, immunofluorescence in this thesis, was utilised as a means of confirming RA synovial tissue co-staining of TSPO on cells expressing the macrophage markers CD68 and CD163, the FLS activation marker PDPN, and the T lymphocyte marker, CD4. Such data implied that TSPO was present on synovial macrophages, FLS and T cells, with no inferences regarding the expression of TSPO on activated versus non-activated cells in synovium made.

mRNA and radioligand binding studies of cell types known to be present in RA synovium, aimed to provide more detailed quantitative data regarding TSPO expression, as well as investigating the impact of cell activation on TSPO expression. By using *in vitro* cellular work to investigate the impact of cell activation on TSPO expression, unlike the majority of previous studies of *ex vivo* tissue in the literature, any upregulation of TSPO expression would likely be the direct effects of cell activation with the stimuli used, rather than the result of interaction with other cells present in tissue, or due to infiltration of cells into the tissue being examined.

Although mRNA and radioligand bindings studies to assess TSPO and protein have evaluated peripheral blood leukocytes, demonstrating a clear increase in TSPO expression in lymphocytes compared to monocytes (195), no previous studies exist to conclusively demonstrate TSPO upregulation on monocytes compared to macrophages, and certainly, no previous comparison at mRNA or protein level has been made between lymphocytes, monocytes, macrophages, and FLS, in both activated and non-activated states. In this study, I provided the first data to indicate, that, at mRNA and protein level, most TSPO expression is in activated FLS, as well as unstimulated and activated ‘M2’ phenotype macrophages.

5.2.1 Limitations and Further work

Assessment of TSPO expression in cellular constituents of RA synovium aimed to improve interpretation of the TSPO PET signal from the RA joint. However, this work only assessed the expression of TSPO in broadly defined, major cellular components of RA pannus. Immunofluorescence work was limited by the number of antibody combinations that were feasible for study on a single section, confining cell defining

markers to a maximum of one or two. Further, mRNA and protein expression studies (using radioligand binding assays) were undertaken on unstimulated and stimulated healthy donor derived cells which only served as a model for TSPO expression in similar cell groups in RA synovium *in vivo*.

In order to provide a more accurate assessment of TSPO expression on major cell groups in inflamed RA synovium, mass cytometry of mixed synovial cells, obtained from digestion of RA synovial tissue, could be employed. Mass cytometry (CyTOF) uses antibodies conjugated to metals to phenotype cells (394), permitting multiple markers to be assessed on a single cell. CyTOF has been employed in several studies of human peripheral blood mononuclear cells (474, 475), using the identification of multiple cell subset markers on a single cell, to accurately phenotype multiple cell subsets, with only a small number of cells.

This process would be useful to provide accurate phenotyping of cell subsets, directly extracted from synovial biopsy of RA patients, where cell yield is small due to size of the biopsy. The lower tissue-yield procedure of synovial biopsy would be preferable to using tissue from RA joint replacement surgery, as often, at the time of joint replacement, significant degenerative change is also likely to be present, hence cells found could be attributable to osteoarthritis, or end-stage RA. Using CyTOF analysis of cells from RA synovial biopsy would enable a more accurate assessment of TSPO expression on different cell groups present in RA synovium enabling identification of TSPO expression on not only abundant cell groups in synovium, but rarer cells, such as osteoclasts, T regulatory cells, and even endothelial cells.

The fact that activation of macrophages with pro-inflammatory stimuli including LPS and IFN-γ downregulated TSPO, whereas IL-4 activation did not, may indicate TSPO is involved in signalling pathways that promote an M2 macrophage phenotype. The phenotype of macrophages in RA synovium remains uncertain, with some reports of an M1 predominance, yet other reports of predominant expression of M2 markers such as CD163 in RA synovial macrophages (312, 317). Hence extrapolation of this observation to the *in vivo* setting has to be cautiously considered. However, since the function of TSPO is as yet undefined, our finding of TSPO downregulation with pro-

inflammatory stimuli LPS and IFN-γ warrants further investigation using *in vitro* studies, to ascertain the function of TSPO in macrophage activation and behaviour.

5.3 A preliminary investigation of TSPO expression in macrophages of different phenotype

The idea that TSPO is upregulated on activated macrophages, is long accepted, and has driven support for the notion that TSPO can be used as a PET imaging target for macrophages *in vivo* (154). The notion that TSPO is upregulated on activated macrophages has been supported by multiple studies that demonstrate increased TSPO expression at the sites of active inflammation, with TSPO being expressed on macrophage type cells in multiple sclerosis (197), Alzheimer's disease (198), and RA (154). However, such work often concludes that TSPO is upregulated on activated macrophages based on whole tissue studies (using histology, or whole tissue lysates for protein work (190, 191, 476)), which fail to take into account that a significant contribution to increase in TSPO expression could be from influx of leukocytes (known to express high amounts of TSPO (195)) from peripheral blood into site of inflammation in tissue. Certainly, one study in fact, acknowledged that infiltrating neutrophils, were a significant contribution to increase in TSPO staining and TSPO PET signal in a model of acute lung injury (476), with a clear influx of neutrophils being demonstrated on immunofluorescence staining, after lung injury induction. Additionally, studies of TSPO using whole tissue, fail to take into account the possibility that tissue stromal cells, may also express TSPO in inflammatory states; a novel fact we have demonstrated from our work in **Chapter 3** of this thesis.

In this work, we used *in vitro* cultured monocytes and macrophages to investigate TSPO expression on differentiation of monocytes to macrophages, and on activation of macrophages with 'M1' type 'pro-inflammatory' stimuli LPS and IFN-ɣ, or 'M2' type 'reparative' stimuli IL-4, TGF-β or glucocorticoid. This aimed to provide clarity as to whether TSPO was upregulated on macrophage activation, and to better elicit whether activated macrophages at both ends of the spectrum of phenotypes were likely to upregulate TSPO.

There has been some previous work investigating the expression of TSPO in macrophages of different phenotype; however, again, the majority of such investigations focussed on *in vivo* TSPO imaging, tissue immunofluorescence work, or whole tissue lysates for protein analysis. For example, *Sandiego* et al. undertook *in* vivo [^{11}C]PBR28 PET brain imaging pre-and post-administration of LPS in the peripheral blood of human participants; demonstrating an increase in TSPO PET signal in the brain post LPS administration. The authors concluded that the increase in TSPO PET signal demonstrated microglial activation by LPS, despite the fact that the increase in signal could be due to infiltrating leukocytes from peripheral blood, as well as activation of non-microglial cells in the brain. *Bonsack* et al. used immunofluorescence of brain tissue taken from a rat model of intracerebral haemorrhage, to demonstrate no difference in TSPO expression on microglia expressing the 'M1' marker CD16/32 (430) compared to those expressing the 'M2' marker CD206 (188). However, such an observation is limited by the fact that TSPO is ubiquitously expressed, and the fact that it is difficult to be certain of microglia phenotype on histology using a single marker. Other studies have used whole tissue lysate to assess the impact of LPS administration on TSPO expression; *Hatori* et al. used whole tissue protein lysate, derived from a LPS induced model of acute lung injury in rats, to demonstrate that as the time interval post LPS administration increased, TSPO expression in the injured lung tissue also increased. Immunofluorescence was used to confirm that TSPO expression was present on macrophages, and neutrophils, at the site of lung injury; hence it cannot be concluded that the increase in TSPO expression is solely from macrophages in this study.

In contrast to the large number of tissue studies of TSPO expression in macrophages, few *in vitro* studies of TSPO expression in macrophages, have been performed. *Shao* et al. the murine macrophage cell line, RAW 264.7, to demonstrate that TSPO protein levels were significantly up-regulated at 24 hours with addition of LPS, in a dose-dependent manner (261) as determined by an increase in the binding of the TSPO radio-ligand [^{11}C]PBR28, at various doses of LPS. However RAW 264.7 is a murine macrophage cell line transformed by the Abelson leukemia virus. TSPO expression is well known to be aberrantly expressed in malignant cells (157); hence it cannot be assumed that the TSPO expression pattern seen in RAW 264.7 reflects that seen in non-immortalized cells.

More recently, TSPO mRNA over-expression and gene knock-down studies have been undertaken in microglia, using the immortalized murine microglia cell line BV2 (372). Bae *et al.* demonstrated that overexpression of TSPO appeared to decrease production of pro-inflammatory cytokines on LPS treatment of BV2 cells, with increased expression of 'M2' murine macrophage markers IL-10 and MRC1, compared to microglia that did not over express TSPO (374). However, no such study has been performed to assess the impact of 'M1', pro-inflammatory stimuli (such as LPS or IFN-ɣ) on TSPO expression in non-genetically altered macrophages, or the impact of M2 stimuli (such as IL-4, TGF-β or glucocorticoid).

Here, I undertook a first assessment of TSPO expression in macrophages activated to opposite ends of the spectrum of macrophage phenotype polarity, in accordance with phenotypes described by Murray *et al*. (311). This aimed to further clarify the difference in TSPO expression in macrophages at opposite end of the polarisation spectrum, by deriving monocytes from multiple sources, and activating macrophages with stimuli for increasing time intervals. Since the upregulation of TSPO expression on macrophages has been reported in both malignancy and inflammatory disease (157), the immortalised monocyte line THP-1, and monocytes derived from patients with active RA, in addition to monocytes from healthy volunteers were used. Regardless of monocyte source, our results demonstrated a statistically significant downregulation of TSPO in MDM stimulated with pro-inflammatory stimuli, but no significant change in TSPO expression was noted when 'M2' type stimuli were employed. The reasons for this are unclear, but could give insight into the function of TSPO.

Numerous functions for TSPO have been proposed over the past 4 decades since its discovery, ranging from roles in the respiratory burst (456), to steroidogenesis (209), to apoptosis (219). Over recent years, there has been accumulating evidence to support the theory that TSPO acts a cholesterol transporter in the mitochondrial membrane in macrophages. Taylor *et al.* transfected THP-1 macrophages to over-express TSPO, and incubated these cells in media containing [^{3}H]cholesterol, to provide a means of measuring cholesterol efflux. THP-1 macrophages overexpressing TSPO exhibited a significant increase in efflux of cholesterol compared to non-

transfected cells, whereas gene knockdown of TSPO in THP-1 macrophages had the opposite effect (457).

In this study, we provided some preliminary evidence to suggest that increased TSPO expression in 'M2' macrophages (macrophages stimulated with IL-4, TGF-β or glucocorticoid), was associated with an increase in mRNA expression of CYP27A1 and ABCA1, key components of the cholesterol efflux pathway (439), compared to unstimulated macrophages. Conversely, 'M1' macrophages (stimulated with LPS and IFN-ɣ) exhibited a reduction in expression of these cholesterol efflux related mRNAs. This is consistent with the existing study by Taylor, where increased expression of TSPO (induced by transfection) was associated with increased mRNA expression of ABCA1 and CYP27A1, and gene knockdown of TSPO had the converse effect.

5.3.1 Limitations and further work

This study only focussed on macrophages differentiated *in vitro*, activated by one, or a combination of two, stimuli at most. The phenotypes of macrophages present *in vivo* are likely to be far more complex, with many different factors influencing the phenotype of activated macrophages(473). Therefore, the implications of downregulation of TSPO in LPS/IFN-γ macrophages, on TSPO PET signal *in vivo*, still remains unclear. Further investigation into macrophage phenotypes *in vivo,* in different disease states, would lend further clarity to the impact of the observations of this study on TSPO PET imaging of inflammation. Such work is currently underway, using mRNA expression profiling of multiple markers (383, 473).

TSPO is recognised as having several potential roles in cell function, the most well reported of which are in steroidogenesis and cholesterol transport, through its purported function as an outer mitochondrial membrane cholesterol transporter. It is increasingly recognised that cholesterol loading in macrophages can alter cell phenotype; with a reduction in cholesterol efflux contributing to inflammatory activation of macrophages, and the generation of a pro-inflammatory M1 phenotype (477).

In this work, we also provide further confirmation that CYP27A1 and ABCA1 expression, recognised markers of the cholesterol efflux pathway (466), are

downregulated at mRNA level in macrophages activated by the pro-inflammatory stimuli, LPS and IFN-γ, but like TSPO, expression remains unchanged at mRNA level in macrophages activated by M2 type stimuli. This provides preliminary data on the role of TSPO in the cholesterol efflux pathway, which may in turn affect macrophage phenotype. Protein data for CYP27A1 and ABCA1 would be useful to confirm mRNA findings from our work; this could be acquired through western blotting, as we did for TSPO expression. To further validate these findings the use of lipidomics on cell supernatant would definitively indicate a difference in cholesterol efflux in macrophages of different phenotype.

To further establish a role for TSPO in cholesterol transport in macrophages, the use of silencing studies of TSPO would be valuable; by employing small interfering RNA (siRNA), to silence TSPO in macrophages (73), before they are activated to a particular phenotype. A detailed assessment of cholesterol efflux could then be undertaken by measuring the expression of known components of the cholesterol pathway, at both protein and mRNA level, as well as measuring the amount of intra- and extra-cellular cholesterol, as previously described in Taylor *et al.* and Borthwick *et al.* (457, 478).

The role of TSPO remains the subject of intense debate, and ongoing research, with conflicting evidence as to it function, especially regarding the role of this protein in steroidogenesis (479). Despite the provision of only preliminary data to suggest a role of TSPO in cholesterol efflux, we provided conclusive data to demonstrate the differential expression of TSPO in M1 and M2 macrophages *in vitro*. This may suggest TSPO negatively regulates pro-inflammatory responses in macrophages. Certainly, this notion is supported by the pre-existing investigation by Bae *et al.* where overexpression of TSPO in BV2 microglia was associated with a reduction in pro-inflammatory cytokine production on stimulation of cells with LPS. Indeed, TSPO over-expression was associated with upregulation of M2 markers, IL-10 and MRC1, in this work (374), and furthermore, was associated with an attenuation of NF-κB activation, a key transcription factor related to macrophage M1 phenotype generation (480).

The idea that TSPO negatively regulates pro-inflammatory responses has been supported by the use of TSPO ligands; here, TSPO ligands PK11195 and Ro5-4864 likewise promoted the expression of M2 markers in microglia, as well as being associated with a reduction in pro-inflammatory cytokine production in response to LPS stimulation (374). Whether or not TSPO could be used as a therapeutic target for the management of inflammatory disease, remains to be ascertained; certainly, in one study of a rat model of inflammatory bowel disease, the TSPO ligand PK11195 increased the rate of damaging colonic ulceration, but also tissue regeneration, whereas the TSPO drug ligand flunitrazepam partly prevented ulceration only (205). Further investigation of how TSPO may negatively regulate inflammation is needed to establish more clearly if this protein is suitable as a therapeutic target for inflammatory disease.

5.4 Concluding remarks

Data in this thesis provided convincing evidence for:

- The utility of the highly specific TSPO PET tracer, [^{11}C]PBR28, to detect and quantify synovitis in patients with both RA and PsA, demonstrating further that [^{11}C]PBR28 PET may have a potential use in detecting subclinical synovitis.
- [^{11}C]PBR28 PET could be more specific for inflammation than GSUS.
- [^{11}C]PBR28 PET *in vivo* is indeed, likely reflective of TSPO expression in the inflamed synovium.
- Majority of TSPO PET signal is likely to be from activated M2 macrophages and activated stromal cells. As our knowledge of cell subsets present in RA develops, TSPO may help provide *in vivo* imaging evidence of the importance of such subsets.
- A significant downregulation of TSPO in pro-inflammatory ‘M1’ macrophages, which may implicate TSPO in the negative regulation of inflammation, perhaps through its role in the cholesterol efflux pathway.

5.5 Future studies

5.5.1 Clinical studies

Further clinical studies would include:

- An investigation of the ability of [^{11}C]PBR28 PET to detect and quantify RA and PsA synovitis in comparison with [^{18}F]FDG PET and MRI (using PET-MRI to enable accurate comparison between PET and MRI). Such a study would be of sufficient power to establish whether SUVR could truly be used as a means of standardising [^{11}C]PBR28 SUV in participants of different genotype.
- A study to assess the ability of [^{11}C]PBR28 PET to detect pre-clinical synovitis; using a cohort of ACPA positive patients with arthralgia (representing pre-clinical RA), or patients with skin psoriasis and arthralgia (representing pre-clinical PsA). Here, patients would undergo [^{11}C]PBR28 PET, and be followed up for a specified period, with the relationship between [^{11}C]PBR28 SUV in particular joints, and the occurrence of clinical flare in those joints, being assessed.
- A pilot study to assess the ability of [^{11}C]PBR28 PET to detect bony inflammation in a cohort of patients with established, clinically active AS, using MRI as gold-standard.

5.5.2 Studies to further investigate the expression of TSPO in RA pannus

More detailed expression profiling of TSPO in RA pannus would be provided by:

- The use of CyTOF and mRNA studies to investigate the expression of TSPO in cell subsets from RA synovial tissue, in a variety of stages of disease.

5.5.3 Studies to further investigate the role of TSPO in inflammation and macrophage function

- An investigation of the impact of gene silencing of TSPO; here macrophages transfected with siRNAs to silence TSPO expression, would be treated with a

variety of macrophage stimuli, to confirm whether TSPO is involved in the polarisation of macrophages to a particular phenotype.

- Cholesterol efflux studies would likewise be utilised to demonstrate whether or not TSPO silencing affects this process in macrophages.
- An assessment of TSPO expression in monocyte subsets of RA and healthy control patients, to determine whether differences in TSPO expression in RA compared to healthy, could be contributing to the pathogenesis of inflammation in RA.

References

1. Arthritis Research UK. The inflammatory arthritis pathway: Arthritis Research UK; 2017 (accessed on 30th June 2017) Available from: http://www.arthritisresearchuk.org/arthritis-information/inflammatory-arthritis-pathway.aspx.
2. Hazes JM, Luime JJ. The epidemiology of early inflammatory arthritis. Nat Reviews Rheumatology. 2011;7(7):381-90.
3. Vojdani A. A Potential Link between Environmental Triggers and Autoimmunity. Autoimmune diseases. 2014;2014:437231.
4. Edwards CJ, Cooper C. Early environmental factors and rheumatoid arthritis. Clinical and experimental immunology. 2006;143(1):1-5.
5. Symmons D, Turner G, Webb R, Asten P, Barrett E, Lunt M, et al. The prevalence of rheumatoid arthritis in the United Kingdom: new estimates for a new century. Rheumatology. 2002;41(7):793-800.
6. Cross M, Smith E, Hoy D, Carmona L, Wolfe F, Vos T, et al. The global burden of rheumatoid arthritis: estimates from the global burden of disease 2010 study. Annals of the Rheumatic Diseases. 2014;73(7):1316-22.
7. Alamanos Y, Drosos AA. Epidemiology of adult rheumatoid arthritis. Autoimmunity reviews. 2005;4(3):130-6.
8. Rasch EK, Hirsch R, Paulose-Ram R, Hochberg MC. Prevalence of rheumatoid arthritis in persons 60 years of age and older in the United States: effect of different methods of case classification. Arthritis and rheumatism. 2003;48(4):917-26.
9. Hemminki K, Li X, Sundquist J, Sundquist K. Familial associations of rheumatoid arthritis with autoimmune diseases and related conditions. Arthritis and rheumatism. 2009;60(3):661-8.
10. Silman AJ, MacGregor AJ, Thomson W, Holligan S, Carthy D, Farhan A, et al. Twin concordance rates for rheumatoid arthritis: results from a nationwide study. Rheumatology. 1993;32(10):903-7.
11. Gregersen PK, Silver J, Winchester RJ. The shared epitope hypothesis. An approach to understanding the molecular genetics of susceptibility to rheumatoid arthritis. Arthritis and rheumatism. 1987;30(11):1205-13.
12. Heliovaara M, Aho K, Aromaa A, Knekt P, Reunanen A. Smoking and risk of rheumatoid arthritis. The Journal of rheumatology. 1993;20(11):1830-5.
13. Stolt P, Bengtsson C, Nordmark B, Lindblad S, Lundberg I, Klareskog L, et al. Quantification of the influence of cigarette smoking on rheumatoid arthritis: results from a population based case-control study, using incident cases. Annals of the Rheumatic Diseases. 2003;62(9):835-41.
14. Klareskog L, Stolt P, Lundberg K, Kallberg H, Bengtsson C, Grunewald J, et al. A new model for an etiology of rheumatoid arthritis: smoking may trigger HLA-DR (shared epitope)-restricted immune reactions to autoantigens modified by citrullination. Arthritis and rheumatism. 2006;54(1):38-46.
15. Wegner N, Lundberg K, Kinloch A, Fisher B, Malmstrom V, Feldmann M, et al. Autoimmunity to specific citrullinated proteins gives the first clues to the etiology of rheumatoid arthritis. Immunological reviews. 2010;233(1):34-54.
16. Fleming A, Crown JM, Corbett M. Early rheumatoid disease. I. Onset. Annals of the Rheumatic Diseases. 1976;35(4):357-60.

17. Jacoby RK, Jayson MI, Cosh JA. Onset, early stages, and prognosis of rheumatoid arthritis: a clinical study of 100 patients with 11-year follow-up. British medical journal. 1973;2(5858):96-100.
18. Mahtani KR, Miller A, Rivero-Arias O, Heneghan C, Price CP, Thompson M, et al. Autoimmune markers for the diagnosis of rheumatoid arthritis in primary care: primary care diagnostic technology update. The British Journal of General Practice. 2013;63(615):553-4.
19. Shmerling RH, Delbanco TL. The rheumatoid factor: an analysis of clinical utility. The American journal of medicine. 1991;91(5):528-34.
20. Aggarwal R, Liao K, Nair R, Ringold S, Costenbader KH. Anti-Citrullinated Peptide Antibody (ACPA) Assays and their Role in the Diagnosis of Rheumatoid Arthritis. Arthritis and rheumatism. 2009;61(11):1472-83.
21. De Rycke L, Peene I, Hoffman I, Kruithof E, Union A, Meheus L, et al. Rheumatoid factor and anticitrullinated protein antibodies in rheumatoid arthritis: diagnostic value, associations with radiological progression rate, and extra-articular manifestations. Annals of the Rheumatic Diseases. 2004;63(12):1587-93.
22. Cope A. Rheumatoid Arthritis. In: Robert RR TA, Williams TS, Harry WS, Anthony JC, Cornelia MW, editor. Clinical Immunology (Third Edition). Edinburgh: Mosby; 2008. p. 767-87.
23. Nielen MM, van Schaardenburg D, Reesink HW, van de Stadt RJ, van der Horst-Bruinsma IE, de Koning MH, et al. Specific autoantibodies precede the symptoms of rheumatoid arthritis: a study of serial measurements in blood donors. Arthritis and rheumatism. 2004;50(2):380-6.
24. Arnett FC, Edworthy SM, Bloch DA, McShane DJ, Fries JF, Cooper NS, et al. The American Rheumatism Association 1987 revised criteria for the classification of rheumatoid arthritis. Arthritis and rheumatism. 1988;31(3):315-24.
25. Aletaha D, Neogi T, Silman AJ, Funovits J, Felson DT, Bingham CO, 3rd, et al. 2010 rheumatoid arthritis classification criteria: an American College of Rheumatology/European League Against Rheumatism collaborative initiative. Annals of the Rheumatic Diseases. 2010;69(9):1580-8.
26. Smolen JS, Landewe R, Breedveld FC, Buch M, Burmester G, Dougados M, et al. EULAR recommendations for the management of rheumatoid arthritis with synthetic and biological disease-modifying antirheumatic drugs: 2013 update. Annals of the Rheumatic Diseases. 2014;73(3):492-509.
27. Scott DL, Wolfe F, Huizinga TW. Rheumatoid arthritis. Lancet. 2010;376(9746):1094-108.
28. Donahue KE, Gartlehner G, Jonas DE, Lux LJ, Thieda P, Jonas BL, et al. Systematic review: comparative effectiveness and harms of disease-modifying medications for rheumatoid arthritis. Annals of internal medicine. 2008;148(2):124-34.
29. Tugwell P, Welch V, Suarez-Almazor M, Shea B, Wells G. Efficacy and toxicity of old and new disease modifying antirheumatic drugs. Annals of the Rheumatic Diseases. 2000;59 Suppl 1:i32-5.
30. Maini RN, Breedveld FC, Kalden JR, Smolen JS, Davis D, Macfarlane JD, et al. Therapeutic efficacy of multiple intravenous infusions of anti-tumor necrosis factor alpha monoclonal antibody combined with low-dose weekly methotrexate in rheumatoid arthritis. Arthritis and rheumatism. 1998;41(9):1552-63.
31. Feldmann M, Maini RN. Lasker Clinical Medical Research Award. TNF defined as a therapeutic target for rheumatoid arthritis and other autoimmune diseases. Nature medicine. 2003;9(10):1245-50.

32. Cohen SB, Emery P, Greenwald MW, Dougados M, Furie RA, Genovese MC, et al. Rituximab for rheumatoid arthritis refractory to anti-tumor necrosis factor therapy: Results of a multicenter, randomized, double-blind, placebo-controlled, phase III trial evaluating primary efficacy and safety at twenty-four weeks. Arthritis and rheumatism. 2006;54(9):2793-806.
33. Maini RN, Taylor PC, Szechinski J, Pavelka K, Broll J, Balint G, et al. Double-blind randomized controlled clinical trial of the interleukin-6 receptor antagonist, tocilizumab, in European patients with rheumatoid arthritis who had an incomplete response to methotrexate. Arthritis and rheumatism. 2006;54(9):2817-29.
34. Genovese MC, Becker JC, Schiff M, Luggen M, Sherrer Y, Kremer J, et al. Abatacept for rheumatoid arthritis refractory to tumor necrosis factor alpha inhibition. The New England journal of medicine. 2005;353(11):1114-23.
35. Taylor PC, Keystone EC, van der Heijde D, Weinblatt ME, Del Carmen Morales L, Reyes Gonzaga J, et al. Baricitinib versus Placebo or Adalimumab in Rheumatoid Arthritis. The New England journal of medicine. 2017;376(7):652-62.
36. Emery P. The Roche Rheumatology Prize Lecture. The optimal management of early rheumatoid disease: the key to preventing disability. Rheumatology. 1994;33(8):765-8.
37. Taylor W, Gladman D, Helliwell P, Marchesoni A, Mease P, Mielants H. Classification criteria for psoriatic arthritis: development of new criteria from a large international study. Arthritis and rheumatism. 2006;54(8):2665-73.
38. Aletaha D, Smolen JS. The Simplified Disease Activity Index and Clinical Disease Activity Index to monitor patients in standard clinical care. Rheumatic diseases clinics of North America. 2009;35(4):759-72, viii.
39. Grunke M, Witt MN, Ronneberger M, Schnez A, Laubender RP, Engelbrecht M, et al. Use of the 28-joint count yields significantly higher concordance between different examiners than the 66/68-joint count. The Journal of rheumatology. 2012;39(7):1334-40.
40. Sokka T, Pincus T. Joint counts to assess rheumatoid arthritis for clinical research and usual clinical care: advantages and limitations. Rheumatic diseases clinics of North America. 2009;35(4):713-22, v-vi.
41. Naredo E, Bonilla G, Gamero F, Uson J, Carmona L, Laffon A. Assessment of inflammatory activity in rheumatoid arthritis: a comparative study of clinical evaluation with grey scale and power Doppler ultrasonography. Annals of the Rheumatic Diseases. 2005;64(3):375-81.
42. Horikoshi M, Suzuki T, Sugihara M, Kondo Y, Tsuboi H, Uehara T, et al. Comparison of low-field dedicated extremity magnetic resonance imaging with articular ultrasonography in patients with rheumatoid arthritis. Modern Rheumatology. 2010;20(6):556-60.
43. Zeman MN, Scott PJ. Current imaging strategies in rheumatoid arthritis. American journal of nuclear medicine and molecular imaging. 2012;2(2):174-220.
44. Boland EW. Medical progress: Rheumatoid arthritis: A review of recent literature. California Medicine. 1947;67(5):315-24.
45. Brook A, Corbett M. Radiographic changes in early rheumatoid disease. Annals of the Rheumatic Diseases. 1977;36(1):71.
46. van der Heijde DM, van Leeuwen MA, van Riel PL, Koster AM, van 't Hof MA, van Rijswijk MH, et al. Biannual radiographic assessments of hands and feet in a three-year prospective followup of patients with early rheumatoid arthritis. Arthritis and rheumatism. 1992;35(1):26-34.

47. McQueen FM, Stewart N, Crabbe J, Robinson E, Yeoman S, Tan PLJ, et al. Magnetic resonance imaging of the wrist in early rheumatoid arthritis reveals a high prevalence of erosions at four months after symptom onset. Annals of the Rheumatic Diseases. 1998;57(6):350.
48. Kaarela K. Prognostic factors and diagnostic criteria in early rheumatoid arthritis. Scandinavian journal of rheumatology Supplement. 1985;57:1-54.
49. Scott DL. Prognostic factors in early rheumatoid arthritis. Rheumatology. 2000;39 Suppl 1:24-9.
50. Larsen A. A radiological method for grading the severity of rheumatoid arthritis. Scandinavian Journal of Rheumatology. 1975;4(4):225-33.
51. Larsen A, Dale K, Eek M. Radiographic evaluation of rheumatoid arthritis and related conditions by standard reference films. Acta radiologica: diagnosis. 1977;18(4):481-91.
52. Sharp JT, Young DY, Bluhm GB, Brook A, Brower AC, Corbett M, et al. How many joints in the hands and wrists should be included in a score of radiologic abnormalities used to assess rheumatoid arthritis? Arthritis and rheumatism. 1985;28(12):1326-35.
53. Wolfe F, van der Heijde DM, Larsen A. Assessing radiographic status of rheumatoid arthritis: introduction of a short erosion scale. The Journal of rheumatology. 2000;27(9):2090-9.
54. van der Heijde D. Structural damage in rheumatoid arthritis as visualized through radiographs. Arthritis Research and Therapy. 2002;4(Suppl 2):S29-S33.
55. Taylor PC. The value of sensitive imaging modalities in rheumatoid arthritis. Arthritis Research and Therapy. 2003;5(5):210-3.
56. van der Heijde DM. Plain X-rays in rheumatoid arthritis: overview of scoring methods, their reliability and applicability. Bailliere's clinical rheumatology. 1996;10(3):435-53.
57. Brower AC. Use of the radiograph to measure the course of rheumatoid arthritis. The gold standard versus fool's gold. Arthritis and rheumatism. 1990;33(3):316-24.
58. Backhaus M, Kamradt T, Sandrock D, Loreck D, Fritz J, Wolf KJ, et al. Arthritis of the finger joints: a comprehensive approach comparing conventional radiography, scintigraphy, ultrasound, and contrast-enhanced magnetic resonance imaging. Arthritis and rheumatism. 1999;42(6):1232-45.
59. Ostergaard M, Pedersen SJ, Dohn UM. Imaging in rheumatoid arthritis--status and recent advances for magnetic resonance imaging, ultrasonography, computed tomography and conventional radiography. Best practice and research clinical rheumatology. 2008;22(6):1019-44.
60. Backhaus M, Burmester G, Sandrock D, Loreck D, Hess D, Scholz A, et al. Prospective two year follow up study comparing novel and conventional imaging procedures in patients with arthritic finger joints. Annals of the Rheumatic Diseases. 2002;61(10):895-904.
61. Kang T, Lanni S, Nam J, Emery P, Wakefield RJ. The evolution of ultrasound in rheumatology. Therapeutic advances in musculoskeletal disease. 2012;4(6):399-411.
62. Donald I, Macvicar J, Brown TG. Investigation of abdominal masses by pulsed ultrasound. Lancet. 1958;1(7032):1188-95.
63. Jacobson JA, van Holsbeeck MT. Musculoskeletal ultrasonography. The Orthopedic clinics of North America. 1998;29(1):135-67.

64. Cooperberg PL, Tsang I, Truelove L, Knickerbocker WJ. Gray scale ultrasound in the evaluation of rheumatoid arthritis of the knee. Radiology. 1978;126(3):759-63.
65. Gompels BM, Darlington LG. Septic arthritis in rheumatoid disease causing bilateral shoulder dislocation: diagnosis and treatment assisted by grey scale ultrasonography. Annals of the Rheumatic Diseases. 1981;40(6):609-11.
66. Koski JM. Ultrasonographic evidence of hip synovitis in patients with rheumatoid arthritis. Scandinavian Journal of Rheumatology. 1989;18(3):127-31.
67. Iagnocco A, Coari G, Zoppini A. Sonographic evaluation of femoral condylar cartilage in osteoarthritis and rheumatoid arthritis. Scandinavian Journal of Rheumatology. 1992;21(4):201-3.
68. Backhaus M, Ohrndorf S, Kellner H, Strunk J, Backhaus TM, Hartung W, et al. Evaluation of a novel 7-joint ultrasound score in daily rheumatologic practice: a pilot project. Arthritis and rheumatism. 2009;61(9):1194-201.
69. Grassi W. Clinical evaluation versus ultrasonography: who is the winner? The Journal of rheumatology. 2003;30(5):908-9.
70. Kane D, Balint PV, Sturrock RD. Ultrasonography is superior to clinical examination in the detection and localization of knee joint effusion in rheumatoid arthritis. The Journal of rheumatology. 2003;30(5):966-71.
71. Scheel AK, Hermann KGA, Ohrndorf S, Werner C, Schirmer C, Detert J, et al. Prospective 7 year follow up imaging study comparing radiography, ultrasonography, and magnetic resonance imaging in rheumatoid arthritis finger joints. Annals of the Rheumatic Diseases. 2006;65(5):595-600.
72. Witt M, Mueller F, Nigg A, Reindl C, Leipe J, Proft F, et al. Relevance of grade 1 gray-scale ultrasound findings in wrists and small joints to the assessment of subclinical synovitis in rheumatoid arthritis. Arthritis and rheumatism. 2013;65(7):1694-701.
73. Tang C, Liu Y, Kessler PS, Vaughan AM, Oram JF. The macrophage cholesterol exporter ABCA1 functions as an anti-inflammatory receptor. The Journal of Biological Chemistry. 2009;284(47):32336-43.
74. Kang T, Horton L, Emery P, Wakefield RJ. Value of Ultrasound in Rheumatologic Diseases. Journal of Korean Medical Science. 2013;28(4):497-507.
75. Martinoli C, Pretolesi F, Crespi G, Bianchi S, Gandolfo N, Valle M, et al. Power Doppler sonography: clinical applications. European journal of radiology. 1998;27 Suppl 2:S133-40.
76. Rubin JM, Bude RO, Carson PL, Bree RL, Adler RS. Power Doppler US: a potentially useful alternative to mean frequency-based color Doppler US. Radiology. 1994;190(3):853-6.
77. Elshabrawy HA, Chen Z, Volin MV, Ravella S, Virupannavar S, Shahrara S. The pathogenic role of angiogenesis in rheumatoid arthritis. Angiogenesis. 2015;18(4):433-48.
78. Brown AK. Using ultrasonography to facilitate best practice in diagnosis and management of RA. Nature Reviews Rheumatology. 2009;5(12):698-706.
79. Newman JS, Adler RS, Bude RO, Rubin JM. Detection of soft-tissue hyperemia: value of power Doppler sonography. American journal of roentgenology. 1994;163(2):385-9.
80. Schmidt WA, Volker L, Zacher J, Schlafke M, Ruhnke M, Gromnica-Ihle E. Colour Doppler ultrasonography to detect pannus in knee joint synovitis. Clinical and experimental rheumatology. 2000;18(4):439-44.

81. Szkudlarek M, Court-Payen M, Strandberg C, Klarlund M, Klausen T, Ostergaard M. Power Doppler ultrasonography for assessment of synovitis in the metacarpophalangeal joints of patients with rheumatoid arthritis: a comparison with dynamic magnetic resonance imaging. Arthritis and rheumatism. 2001;44(9):2018-23.
82. Foltz V, Gandjbakhch F, Etchepare F, Rosenberg C, Tanguy ML, Rozenberg S, et al. Power Doppler ultrasound, but not low-field magnetic resonance imaging, predicts relapse and radiographic disease progression in rheumatoid arthritis patients with low levels of disease activity. Arthritis and rheumatism. 2012;64(1):67-76.
83. Ruta S, Marin J, Acosta Felquer ML, Ferreyra-Garrot L, Rosa J, Garcia-Monaco R, et al. Utility of Power Doppler Ultrasound-detected Synovitis for the Prediction of Short-term Flare in Psoriatic Patients with Arthritis in Clinical Remission. The Journal of rheumatology. 2017.
84. Ohrndorf S, Backhaus M. Advances in sonographic scoring of rheumatoid arthritis. Annals of the Rheumatic Diseases. 2013;72 Suppl 2:ii69-75.
85. Wakefield RJ, Gibbon WW, Conaghan PG, O'Connor P, McGonagle D, Pease C, et al. The value of sonography in the detection of bone erosions in patients with rheumatoid arthritis: a comparison with conventional radiography. Arthritis and rheumatism. 2000;43(12):2762-70.
86. Szkudlarek M, Court-Payen M, Jacobsen S, Klarlund M, Thomsen HS, Ostergaard M. Interobserver agreement in ultrasonography of the finger and toe joints in rheumatoid arthritis. Arthritis and rheumatism. 2003;48(4):955-62.
87. Scheel AK, Hermann KG, Kahler E, Pasewaldt D, Fritz J, Hamm B, et al. A novel ultrasonographic synovitis scoring system suitable for analyzing finger joint inflammation in rheumatoid arthritis. Arthritis and rheumatism. 2005;52(3):733-43.
88. Naredo E, Gamero F, Bonilla G, Uson J, Carmona L, Laffon A. Ultrasonographic assessment of inflammatory activity in rheumatoid arthritis: comparison of extended versus reduced joint evaluation. Clinical and experimental rheumatology. 2005;23(6):881-4.
89. Ellegaard K, Torp-Pedersen S, Terslev L, Danneskiold-Samsoe B, Henriksen M, Bliddal H. Ultrasound colour Doppler measurements in a single joint as measure of disease activity in patients with rheumatoid arthritis--assessment of concurrent validity. Rheumatology. 2009;48(3):254-7.
90. Dougados M, Jousse-Joulin S, Mistretta F, d'Agostino MA, Backhaus M, Bentin J, et al. Evaluation of several ultrasonography scoring systems for synovitis and comparison to clinical examination: results from a prospective multicentre study of rheumatoid arthritis. Annals of the Rheumatic Diseases. 2010;69(5):828-33.
91. Hammer HB, Kvien TK. Comparisons of 7- to 78-joint ultrasonography scores: all different joint combinations show equal response to adalimumab treatment in patients with rheumatoid arthritis. Arthritis Research and Therapy. 2011;13(3):R78.
92. McQueen FM. Imaging in early rheumatoid arthritis. Best practice and research Clinical rheumatology. 2013;27(4):499-522.
93. Padovano I, Costantino F, Breban M, D'Agostino MA. Prevalence of ultrasound synovial inflammatory findings in healthy subjects. Annals of the Rheumatic Diseases. 2016;75(10):1819-23.
94. Berger A. Magnetic resonance imaging. BMJ : British Medical Journal. 2002;324(7328):35-.
95. Geva T. Magnetic resonance imaging: historical perspective. Journal of cardiovascular magnetic resonance. 2006;8(4):573-80.

96. Damadian R. Tumor detection by nuclear magnetic resonance. Science. 1971;171(3976):1151-3.
97. Gilkeson G, Polisson R, Sinclair H, Vogler J, Rice J, Caldwell D, et al. Early detection of carpal erosions in patients with rheumatoid arthritis: a pilot study of magnetic resonance imaging. The Journal of rheumatology. 1988;15(9):1361-6.
98. Sudoł-Szopińska I, Kontny E, Maśliński W, Prochorec-Sobieszek M, Warczyńska A, Kwiatkowska B. Significance of bone marrow edema in pathogenesis of rheumatoid arthritis. Polish Journal of Radiology. 2013;78(1):57-63.
99. Sudoł-Szopińska I, Ćwikła JB. Current imaging techniques in rheumatology: MRI, scintigraphy and PET. Polish Journal of Radiology. 2013;78(3):48-56.
100. Sudol-Szopinska I, Jurik AG, Eshed I, Lennart J, Grainger A, Ostergaard M, et al. Recommendations of the ESSR Arthritis Subcommittee for the Use of Magnetic Resonance Imaging in Musculoskeletal Rheumatic Diseases. Seminars in musculoskeletal radiology. 2015;19(4):396-411.
101. Woodworth TG, Morgacheva O, Pimienta OL, Troum OM, Ranganath VK, Furst DE. Examining the validity of the rheumatoid arthritis magnetic resonance imaging score according to the OMERACT filter-a systematic literature review. Rheumatology. 2017.
102. Ostergaard M, Bird P, Gandjbakhch F, Eshed I, Haugen IK, Haavardsholm EA, et al. The OMERACT MRI in Arthritis Working Group - Update on Status and Future Research Priorities. The Journal of rheumatology. 2015;42(12):2470-2.
103. Ostergaard M, Edmonds J, McQueen F, Peterfy C, Lassere M, Ejbjerg B, et al. An introduction to the EULAR-OMERACT rheumatoid arthritis MRI reference image atlas. Annals of the Rheumatic Diseases. 2005;64 Suppl 1:i3-7.
104. Boesen M, Ostergaard M, Cimmino MA, Kubassova O, Jensen KE, Bliddal H. MRI quantification of rheumatoid arthritis: current knowledge and future perspectives. European journal of radiology. 2009;71(2):189-96.
105. Tamai M, Kawakami A, Iwamoto N, Kawashiri SY, Fujikawa K, Aramaki T, et al. Comparative study of the detection of joint injury in early-stage rheumatoid arthritis by magnetic resonance imaging of the wrist and finger joints and physical examination. Arthritis care & research. 2011;63(3):436-9.
106. Wakefield RJ, Freeston JE, O'Connor P, Reay N, Budgen A, Hensor EM, et al. The optimal assessment of the rheumatoid arthritis hindfoot: a comparative study of clinical examination, ultrasound and high field MRI. Annals of the Rheumatic Diseases. 2008;67(12):1678-82.
107. Hetland ML, Ejbjerg B, Horslev-Petersen K, Jacobsen S, Vestergaard A, Jurik AG, et al. MRI bone oedema is the strongest predictor of subsequent radiographic progression in early rheumatoid arthritis. Results from a 2-year randomised controlled trial (CIMESTRA). Annals of the Rheumatic Diseases. 2009;68(3):384-90.
108. Ostergaard M, Stoltenberg M, Lovgreen-Nielsen P, Volck B, Jensen CH, Lorenzen I. Magnetic resonance imaging-determined synovial membrane and joint effusion volumes in rheumatoid arthritis and osteoarthritis: comparison with the macroscopic and microscopic appearance of the synovium. Arthritis and rheumatism. 1997;40(10):1856-67.
109. Ostendorf B, Peters R, Dann P, Becker A, Scherer A, Wedekind F, et al. Magnetic resonance imaging and miniarthroscopy of metacarpophalangeal joints: sensitive detection of morphologic changes in rheumatoid arthritis. Arthritis and rheumatism. 2001;44(11):2492-502.

110. Gaffney K, Cookson J, Blake D, Coumbe A, Blades S. Quantification of rheumatoid synovitis by magnetic resonance imaging. Arthritis and rheumatism. 1995;38(11):1610-7.
111. Tamai K, Yamato M, Yamaguchi T, Ohno W. Dynamic magnetic resonance imaging for the evaluation of synovitis in patients with rheumatoid arthritis. Arthritis and rheumatism. 1994;37(8):1151-7.
112. Wittoek R, Jans L, Lambrecht V, Carron P, Verstraete K, Verbruggen G. Reliability and construct validity of ultrasonography of soft tissue and destructive changes in erosive osteoarthritis of the interphalangeal finger joints: a comparison with MRI. Annals of the Rheumatic Diseases. 2011;70(2):278-83.
113. Taouli B, Guermazi A, Sack KE, Genant HK. Imaging of the hand and wrist in RA. Annals of the Rheumatic Diseases. 2002;61(10):867-9.
114. Vyas S, Bhalla AS, Ranjan P, Kumar S, Kumar U, Gupta AK. Rheumatoid Arthritis Revisited – Advanced Imaging Review. Polish Journal of Radiology. 2016;81:629-35.
115. Tan YK, Ostergaard M, Conaghan PG. Imaging tools in rheumatoid arthritis: ultrasound vs magnetic resonance imaging. Rheumatology. 2012;51 Suppl 7:vii36-42.
116. Perry D, Stewart N, Benton N, Robinson E, Yeoman S, Crabbe J, et al. Detection of erosions in the rheumatoid hand; a comparative study of multidetector computerized tomography versus magnetic resonance scanning. The Journal of rheumatology. 2005;32(2):256-67.
117. Dohn UM, Ejbjerg BJ, Court-Payen M, Hasselquist M, Narvestad E, Szkudlarek M, et al. Are bone erosions detected by magnetic resonance imaging and ultrasonography true erosions? A comparison with computed tomography in rheumatoid arthritis metacarpophalangeal joints. Arthritis Research and Therapy. 2006;8(4):R110.
118. Geijer M, Sihlbom H, Gothlin JH, Nordborg E. The role of CT in the diagnosis of sacro-iliitis. Acta radiologica. 1998;39(3):265-8.
119. Puhakka KB, Jurik AG, Egund N, Schiottz-Christensen B, Stengaard-Pedersen K, van Overeem Hansen G, et al. Imaging of sacroiliitis in early seronegative spondylarthropathy. Assessment of abnormalities by MR in comparison with radiography and CT. Acta radiologica. 2003;44(2):218-29.
120. McQueen FM. Bone marrow edema and osteitis in rheumatoid arthritis: the imaging perspective. Arthritis Research and Therapy. 2012;14(5):224.
121. Jaszczak RJ. The early years of single photon emission computed tomography (SPECT): an anthology of selected reminiscences. Physics in medicine and biology. 2006;51(13):R99-115.
122. Jansen FP, Vanderheyden JL. The future of SPECT in a time of PET. Nuclear medicine and biology. 2007;34(7):733-5.
123. Liberatore M, Clemente M, Iurilli AP, Zorzin L, Marini M, Di Rocco E, et al. Scintigraphic evaluation of disease activity in rheumatoid arthritis: a comparison of technetium-99m human non-specific immunoglobulins, leucocytes and albumin nanocolloids. European journal of nuclear medicine. 1992;19(10):853-7.
124. Sahin M, Bernay I, Basoglu T, Canturk F. Comparison of Tc-99m MDP, Tc-99m HSA and Tc-99m HIG uptake in rheumatoid arthritis and its variants. Annals of nuclear medicine. 1999;13(6):389-95.
125. de Bois MH, Arndt JW, Speyer I, Pauwels EK, Breedveld FC. Technetium-99m labelled human immunoglobulin scintigraphy predicts rheumatoid arthritis in patients with arthralgia. Scandinavian Journal of Rheumatology. 1996;25(3):155-8.

126. Fridkin M, Najjar VA. Tuftsin: its chemistry, biology, and clinical potential. Critical reviews in biochemistry and molecular biology. 1989;24(1):1-40.
127. Caveliers V, Goodbody AE, Tran LL, Peers SH, Thornback JR, Bossuyt A. Evaluation of 99mTc-RP128 as a potential inflammation imaging agent: human dosimetry and first clinical results. Journal of nuclear medicine. 2001;42(1):154-61.
128. Jamar F, Houssiau FA, Devogelaer JP, Chapman PT, Haskard DO, Beaujean V, et al. Scintigraphy using a technetium 99m-labelled anti-E-selectin Fab fragment in rheumatoid arthritis. Rheumatology. 2002;41(1):53-61.
129. Vanhagen PM, Markusse HM, Lamberts SW, Kwekkeboom DJ, Reubi JC, Krenning EP. Somatostatin receptor imaging. The presence of somatostatin receptors in rheumatoid arthritis. Arthritis and rheumatism. 1994;37(10):1521-7.
130. Reubi JC, Waser B, Markusse HM, Krenning EP, VanHagen M, Laissue JA. Vascular somatostatin receptors in synovium from patients with rheumatoid arthritis. European journal of pharmacology. 1994;271(2-3):371-8.
131. Marcus C, Thakur ML, Huynh TV, Louie JS, Leibling M, Minami C, et al. Imaging rheumatic joint diseases with anti-T lymphocyte antibody OKT-3. Nuclear medicine communications. 1994;15(10):824-30.
132. Malviya G, Anzola KL, Podesta E, Lagana B, Del Mastro C, Dierckx RA, et al. (99m)Tc-labeled rituximab for imaging B lymphocyte infiltration in inflammatory autoimmune disease patients. Molecular Imaging and Biology. 2012;14(5):637-46.
133. Barrera P, Oyen WJ, Boerman OC, van Riel PL. Scintigraphic detection of tumour necrosis factor in patients with rheumatoid arthritis. Annals of the Rheumatic Diseases. 2003;62(9):825-8.
134. Green CH. Technetium-99m production issues in the United Kingdom. Journal of Medical Physics. 2012;37(2):66-71.
135. Turkheimer FE, Rizzo G, Bloomfield PS, Howes O, Zanotti-Fregonara P, Bertoldo A, et al. The methodology of TSPO imaging with positron emission tomography. Biochemical Society transactions. 2015;43(4):586-92.
136. NHS. PET Scan. 2015 (accessed on 30th June). Available from: http://www.nhs.uk/conditions/PET-scan/pages/introduction.aspx
137. Nutt R. 1999 ICP Distinguished Scientist Award. The history of positron emission tomography. Molecular Imaging and Biology. 2002;4(1):11-26.
138. Buchbender C, Ostendorf B, Ruhlmann V, Heusch P, Miese F, Beiderwellen K, et al. Hybrid 18F-labeled Fluoride Positron Emission Tomography/Magnetic Resonance (MR) Imaging of the Sacroiliac Joints and the Spine in Patients with Axial Spondyloarthritis: A Pilot Study Exploring the Link of MR Bone Pathologies and Increased Osteoblastic Activity. The Journal of rheumatology. 2015;42(9):1631-7.
139. Miese F, Scherer A, Ostendorf B, Heinzel A, Lanzman RS, Kropil P, et al. Hybrid 18F-FDG PET-MRI of the hand in rheumatoid arthritis: initial results. Clinical rheumatology. 2011;30(9):1247-50.
140. Moses WW. Fundamental Limits of Spatial Resolution in PET. Nuclear instruments & methods in physics research Section A, Accelerators, spectrometers, detectors and associated equipment. 2011;648 Supplement 1:S236-s40.
141. Chaudhari AJ, Ferrero A, Godinez F, Yang K, Shelton DK, Hunter JC, et al. High-resolution (18)F-FDG PET/CT for assessing disease activity in rheumatoid and psoriatic arthritis: findings of a prospective pilot study. British Journal of Radiology. 2016;89(1063):20160138.
142. Gent YY, Weijers K, Molthoff CF, Windhorst AD, Huisman MC, Kassiou M, et al. Promising potential of new generation translocator protein tracers providing

enhanced contrast of arthritis imaging by positron emission tomography in a rat model of arthritis. Arthritis Research and Therapy. 2014;16(2):R70.
143. Garcia-Torano E, Medina VP, Ibarra MR. The half-life of 18F. Applied radiation and isotopes : including data, instrumentation and methods for use in agriculture, industry and medicine. 2010;68(7-8):1561-5; discussion 5.
144. Athanasou NA, Quinn J. Immunocytochemical analysis of human synovial lining cells: phenotypic relation to other marrow derived cells. Annals of the Rheumatic Diseases. 1991;50(5):311-5.
145. Takemura S, Braun A, Crowson C, Kurtin PJ, Cofield RH, O'Fallon WM, et al. Lymphoid neogenesis in rheumatoid synovitis. Journal of immunology. 2001;167(2):1072-80.
146. Koch AE. Review: angiogenesis: implications for rheumatoid arthritis. Arthritis and rheumatism. 1998;41(6):951-62.
147. Gent YY, Voskuyl AE, Kloet RW, van Schaardenburg D, Hoekstra OS, Dijkmans BA, et al. Macrophage positron emission tomography imaging as a biomarker for preclinical rheumatoid arthritis: findings of a prospective pilot study. Arthritis and rheumatism. 2012;64(1):62-6.
148. Yonemoto Y, Okamura K, Takeuchi K, Kaneko T, Kobayashi T, Okura C, et al. [18F]fluorodeoxyglucose uptake as a predictor of large joint destruction in patients with rheumatoid arthritis. Rheumatology international. 2016;36(1):109-15.
149. Gent YY, Ahmadi N, Voskuyl AE, Hoetjes N, van Kuijk C, Britsemmer K, et al. Detection of subclinical synovitis with macrophage targeting and positron emission tomography in patients with rheumatoid arthritis without clinical arthritis. The Journal of rheumatology. 2014;41(11):2145-52.
150. Lopci E, Nanni C, Castellucci P, Montini GC, Allegri V, Rubello D, et al. Imaging with non-FDG PET tracers: outlook for current clinical applications. Insights into imaging. 2010;1(5-6):373-85.
151. Chrapko BE, Chrapko M, Nocun A, Stefaniak B, Zubilewicz T, Drop A. Role of 18F-FDG PET/CT in the diagnosis of inflammatory and infectious vascular disease. Nuclear medicine review Central & Eastern Europe. 2016;19(1):28-36.
152. Loricera J, Blanco R, Hernandez JL, Martinez-Rodriguez I, Carril JM, Lavado C, et al. Use of positron emission tomography (PET) for the diagnosis of large-vessel vasculitis. Revista espanola de medicina nuclear e imagen molecular. 2015;34(6):372-7.
153. Dasgupta B, Borg FA, Hassan N, Alexander L, Barraclough K, Bourke B, et al. BSR and BHPR guidelines for the management of giant cell arteritis. Rheumatology. 2010;49(8):1594-7.
154. van der Laken CJ, Elzinga EH, Kropholler MA, Molthoff CF, van der Heijden JW, Maruyama K, et al. Noninvasive imaging of macrophages in rheumatoid synovitis using 11C-(R)-PK11195 and positron emission tomography. Arthritis and rheumatism. 2008;58(11):3350-5.
155. Watanabe T, Takase-Minegishi K, Ihata A, Kunishita Y, Kishimoto D, Kamiyama R, et al. (18)F-FDG and (18)F-NaF PET/CT demonstrate coupling of inflammation and accelerated bone turnover in rheumatoid arthritis. Modern Rheumatology. 2016;26(2):180-7.
156. Zhu Z, Yin Y, Zheng K, Li F, Chen X, Zhang F, et al. Evaluation of synovial angiogenesis in patients with rheumatoid arthritis using (6)(8)Ga-PRGD2 PET/CT: a prospective proof-of-concept cohort study. Annals of the Rheumatic Diseases. 2014;73(6):1269-72.

157. Batarseh A, Papadopoulos V. Regulation of translocator protein 18 kDa (TSPO) expression in health and disease states. Molecular and cellular endocrinology. 2010;327(1-2):1-12.
158. Li J, Hsu HC, Mountz JD. Managing macrophages in rheumatoid arthritis by reform or removal. Current rheumatology reports. 2012;14(5):445-54.
159. Czernin J, Satyamurthy N, Schiepers C. Molecular mechanisms of bone 18F-NaF deposition. Journal of nuclear medicine. 2010;51(12):1826-9.
160. Danks L, Sabokbar A, Gundle R, Athanasou NA. Synovial macrophage-osteoclast differentiation in inflammatory arthritis. Annals of the Rheumatic Diseases. 2002;61(10):916-21.
161. Tegler G, Sorensen J, Ericson K, Bjorck M, Wanhainen A. 4D-PET/CT with [(11)C]-PK11195 and [(11)C]-(D)-deprenyl does not identify the chronic inflammation in asymptomatic abdominal aortic aneurysms. European journal of vascular and endovascular surgery. 2013;45(4):351-6.
162. Danfors T, Bergström M, Feltelius N, Ahlström H, Westerberg G, Långström B. Positron Emission Tomography with 11C-D-deprenyl in Patients with Rheumatoid Arthritis. Scandinavian Journal of Rheumatology. 1997;26(1):43-8.
163. Zeisel SH. Choline phospholipids: signal transduction and carcinogenesis. FASEB. 1993;7(6):551-7.
164. Volchenkov R, Dung Cao M, Elgstoen KB, Goll GL, Eikvar K, Bjorneboe O, et al. Metabolic profiling of synovial tissue shows altered glucose and choline metabolism in rheumatoid arthritis samples. Scandinavian Journal of Rheumatology. 2016:1-2.
165. Guma M, Sanchez-Lopez E, Lodi A, Garcia-Carbonell R, Tiziani S, Karin M, et al. Choline kinase inhibition in rheumatoid arthritis. Annals of the Rheumatic Diseases. 2015;74(7):1399-407.
166. Walsh DA, Wade M, Mapp PI, Blake DR. Focally regulated endothelial proliferation and cell death in human synovium. The American journal of pathology. 1998;152(3):691-702.
167. Roivainen A, Hautaniemi S, Mottonen T, Nuutila P, Oikonen V, Parkkola R, et al. Correlation of 18F-FDG PET/CT assessments with disease activity and markers of inflammation in patients with early rheumatoid arthritis following the initiation of combination therapy with triple oral antirheumatic drugs. European Journal of Nuclear Medicine and Molecular Imaging. 2013;40(3):403-10.
168. Beckers C, Jeukens X, Ribbens C, Andre B, Marcelis S, Leclercq P, et al. (18)F-FDG PET imaging of rheumatoid knee synovitis correlates with dynamic magnetic resonance and sonographic assessments as well as with the serum level of metalloproteinase-3. European Journal of Nuclear Medicine and Molecular Imaging. 2006;33(3):275-80.
169. Palmer WE, Rosenthal DI, Schoenberg OI, Fischman AJ, Simon LS, Rubin RH, et al. Quantification of inflammation in the wrist with gadolinium-enhanced MR imaging and PET with 2-[F-18]-fluoro-2-deoxy-D-glucose. Radiology. 1995;196(3):647-55.
170. Polisson RP, Schoenberg OI, Fischman A, Rubin R, Simon LS, Rosenthal D, et al. Use of magnetic resonance imaging and positron emission tomography in the assessment of synovial volume and glucose metabolism in patients with rheumatoid arthritis. Arthritis and rheumatism. 1995;38(6):819-25.
171. Vijayant V, Sarma M, Aurangabadkar H, Bichile L, Basu S. Potential of (18)F-FDG-PET as a valuable adjunct to clinical and response assessment in rheumatoid

arthritis and seronegative spondyloarthropathies. World journal of radiology. 2012;4(12):462-8.
172. Beckers C, Ribbens C, Andre B, Marcelis S, Kaye O, Mathy L, et al. Assessment of disease activity in rheumatoid arthritis with (18)F-FDG PET. Journal of nuclear medicine. 2004;45(6):956-64.
173. Takata T, Taniguchi Y, Ohnishi T, Kohsaki S, Nogami M, Nakajima H, et al. (18)FDG PET/CT is a powerful tool for detecting subclinical arthritis in patients with psoriatic arthritis and/or psoriasis vulgaris. Journal of dermatological science. 2011;64(2):144-7.
174. Yamanaka H, Matsuda Y, Tanaka M, Sendo W, Nakajima H, Taniguchi A, et al. Serum matrix metalloproteinase 3 as a predictor of the degree of joint destruction during the six months after measurement, in patients with early rheumatoid arthritis. Arthritis and rheumatism. 2000;43(4):852-8.
175. Roivainen A, Parkkola R, Yli-Kerttula T, Lehikoinen P, Viljanen T, Mottonen T, et al. Use of positron emission tomography with methyl-11C-choline and 2-18F-fluoro-2-deoxy-D-glucose in comparison with magnetic resonance imaging for the assessment of inflammatory proliferation of synovium. Arthritis and rheumatism. 2003;48(11):3077-84.
176. Tran L, Huitema AD, van Rijswijk MH, Dinant HJ, Baars JW, Beijnen JH, et al. CD20 antigen imaging with (1)(2)(4)I-rituximab PET/CT in patients with rheumatoid arthritis. Human antibodies. 2011;20(1-2):29-35.
177. Edupuganti SR, Eder V, Ternant D, Courtehoux M, Tranquart F, Goupille P, et al. F-18 fluorodeoxyglucose positron emission tomography can detect early response to adalimumab, a tumor necrosis factor-alpha antagonist, in rheumatoid arthritis: A prospective pilot study. Joint Bone Spine. 2015;82(5):381-3.
178. Elzinga EH, van der Laken CJ, Comans EF, Boellaard R, Hoekstra OS, Dijkmans BA, et al. 18F-FDG PET as a tool to predict the clinical outcome of infliximab treatment of rheumatoid arthritis: an explorative study. Journal of nuclear medicine. 2011;52(1):77-80.
179. Goerres GW, Forster A, Uebelhart D, Seifert B, Treyer V, Michel B, et al. F-18 FDG whole-body PET for the assessment of disease activity in patients with rheumatoid arthritis. Clinical nuclear medicine. 2006;31(7):386-90.
180. Kubota K, Ito K, Morooka M, Mitsumoto T, Kurihara K, Yamashita H, et al. Whole-body FDG-PET/CT on rheumatoid arthritis of large joints. Annals of nuclear medicine. 2009;23(9):783-91.
181. Suto T, Okamura K, Yonemoto Y, Okura C, Tsushima Y, Takagishi K. Prediction of Large Joint Destruction in Patients With Rheumatoid Arthritis Using 18F-FDG PET/CT and Disease Activity Score. Medicine. 2016;95(7):e2841.
182. Bruijnen ST, van der Weijden MA, Klein JP, Hoekstra OS, Boellaard R, van Denderen JC, et al. Bone formation rather than inflammation reflects ankylosing spondylitis activity on PET-CT: a pilot study. Arthritis Research and Therapy. 2012;14(2):R71.
183. Elzinga EH, van der Laken CJ, Comans EF, Lammertsma AA, Dijkmans BA, Voskuyl AE. 2-Deoxy-2-[F-18]fluoro-D-glucose joint uptake on positron emission tomography images: rheumatoid arthritis versus osteoarthritis. Molecular Imaging and Biology. 2007;9(6):357-60.
184. Gent YY, Ter Wee MM, Voskuyl AE, den Uyl D, Ahmadi N, Dowling C, et al. Subclinical synovitis detected by macrophage PET, but not MRI, is related to short-term flare of clinical disease activity in early RA patients: an exploratory study. Arthritis Research and Therapy. 2015;17:266.

185. Snyder SH, Verma A, Trifiletti RR. The peripheral-type benzodiazepine receptor: a protein of mitochondrial outer membranes utilizing porphyrins as endogenous ligands. FASEB. 1987;1(4):282-8.
186. Braestrup C, Squires RF. Specific benzodiazepine receptors in rat brain characterized by high-affinity (3H)diazepam binding. Proceedings of the National Academy of Sciences of the United States of America. 1977;74(9):3805-9.
187. Papadopoulos V, Baraldi M, Guilarte TR, Knudsen TB, Lacapere JJ, Lindemann P, et al. Translocator protein (18kDa): new nomenclature for the peripheral-type benzodiazepine receptor based on its structure and molecular function. Trends in pharmacological sciences. 2006;27(8):402-9.
188. Park E, Gallezot JD, Delgadillo A, Liu S, Planeta B, Lin SF, et al. (11)C-PBR28 imaging in multiple sclerosis patients and healthy controls: test-retest reproducibility and focal visualization of active white matter areas. European Journal of Nuclear Medicine and Molecular Imaging. 2015;42(7):1081-92.
189. Roncaroli F, Su Z, Herholz K, Gerhard A, Turkheimer FE. TSPO expression in brain tumours: is TSPO a target for brain tumour imaging? Clinical and translational imaging. 2016;4:145-56.
190. Bonsack Ft, Alleyne CH, Jr., Sukumari-Ramesh S. Augmented expression of TSPO after intracerebral hemorrhage: a role in inflammation? Journal of neuroinflammation. 2016;13(1):151.
191. Toth M, Little P, Arnberg F, Haggkvist J, Mulder J, Halldin C, et al. Acute neuroinflammation in a clinically relevant focal cortical ischemic stroke model in rat: longitudinal positron emission tomography and immunofluorescent tracking. Brain structure & function. 2016;221(3):1279-90.
192. Papadopoulos V, Lecanu L, Brown RC, Han Z, Yao ZX. Peripheral-type benzodiazepine receptor in neurosteroid biosynthesis, neuropathology and neurological disorders. Neuroscience. 2006;138(3):749-56.
193. Papadopoulos V, Lecanu L. Translocator protein (18 kDa) TSPO: an emerging therapeutic target in neurotrauma. Experimental neurology. 2009;219(1):53-7.
194. Zavala F, Haumont J, Lenfant M. Interaction of benzodiazepines with mouse macrophages. European journal of pharmacology. 1984;106(3):561-6.
195. Canat X, Carayon P, Bouaboula M, Cahard D, Shire D, Roque C, et al. Distribution profile and properties of peripheral-type benzodiazepine receptors on human hemopoietic cells. Life sciences. 1993;52(1):107-18.
196. Raghavendra Rao VL, Dogan A, Bowen KK, Dempsey RJ. Traumatic brain injury leads to increased expression of peripheral-type benzodiazepine receptors, neuronal death, and activation of astrocytes and microglia in rat thalamus. Experimental neurology. 2000;161(1):102-14.
197. Chen MK, Guilarte TR. Translocator protein 18 kDa (TSPO): molecular sensor of brain injury and repair. Pharmacology & therapeutics. 2008;118(1):1-17.
198. Barron AM, Garcia-Segura LM, Caruso D, Jayaraman A, Lee JW, Melcangi RC, et al. Ligand for translocator protein reverses pathology in a mouse model of Alzheimer's disease. The Journal of neuroscience. 2013;33(20):8891-7.
199. Fujimura Y, Hwang PM, Trout Iii H, Kozloff L, Imaizumi M, Innis RB, et al. Increased peripheral benzodiazepine receptors in arterial plaque of patients with atherosclerosis: an autoradiographic study with [(3)H]PK 11195. Atherosclerosis. 2008;201(1):108-11.
200. Korkhov VM, Sachse C, Short JM, Tate CG. Three-dimensional structure of TspO by electron cryomicroscopy of helical crystals. Structure. 2010;18(6):677-87.

201. Delavoie F, Li H, Hardwick M, Robert JC, Giatzakis C, Peranzi G, et al. In vivo and in vitro peripheral-type benzodiazepine receptor polymerization: functional significance in drug ligand and cholesterol binding. Biochemistry. 2003;42(15):4506-19.
202. Banati RB, Middleton RJ, Chan R, Hatty CR, Kam WW, Quin C, et al. Positron emission tomography and functional characterization of a complete PBR/TSPO knockout. Nature communications. 2014;5:5452.
203. Wang H, Zhai K, Xue Y, Yang J, Yang Q, Fu Y, et al. Global Deletion of TSPO Does Not Affect the Viability and Gene Expression Profile. PloS one. 2016;11(12):e0167307.
204. Ruff MR, Pert CB, Weber RJ, Wahl LM, Wahl SM, Paul SM. Benzodiazepine receptor-mediated chemotaxis of human monocytes. Science. 1985;229(4719):1281-3.
205. Ostuni MA, Issop L, Péranzi G, Walker F, Fasseu M, Elbim C, et al. Overexpression of Translocator protein TSPO in inflammatory bowel disease: potential diagnostic and treatment value. Inflammatory bowel diseases. 2010;16(9):1476-87.
206. Matsumoto T, Ogata M, Koga K, Shigematsu A. Effect of peripheral benzodiazepine receptor ligands on lipopolysaccharide-induced tumor necrosis factor activity in thioglycolate-treated mice. Antimicrobial agents and chemotherapy. 1994;38(4):812-6.
207. Torres SR, Frode TS, Nardi GM, Vita N, Reeb R, Ferrara P, et al. Anti-inflammatory effects of peripheral benzodiazepine receptor ligands in two mouse models of inflammation. European journal of pharmacology. 2000;408(2):199-211.
208. Ching AS, Kuhnast B, Damont A, Roeda D, Tavitian B, Dolle F. Current paradigm of the 18-kDa translocator protein (TSPO) as a molecular target for PET imaging in neuroinflammation and neurodegenerative diseases. Insights into imaging. 2012;3(1):111-9.
209. Papadopoulos V, Amri H, Li H, Boujrad N, Vidic B, Garnier M. Targeted disruption of the peripheral-type benzodiazepine receptor gene inhibits steroidogenesis in the R2C Leydig tumor cell line. Journal of Biological Chemistry. 1997;272(51):32129-35.
210. Chung JY, Chen H, Midzak A, Burnett AL, Papadopoulos V, Zirkin BR. Drug ligand-induced activation of translocator protein (TSPO) stimulates steroid production by aged brown Norway rat Leydig cells. Endocrinology. 2013;154(6):2156-65.
211. Krueger KE, Papadopoulos V. Peripheral-type benzodiazepine receptors mediate translocation of cholesterol from outer to inner mitochondrial membranes in adrenocortical cells. Journal of Biological Chemistry. 1990;265(25):15015-22.
212. Midzak A, Denora N, Laquintana V, Cutrignelli A, Lopedota A, Franco M, et al. 2-Phenylimidazo[1,2-a]pyridine-containing ligands of the 18-kDa translocator protein (TSPO) behave as agonists and antagonists of steroidogenesis in a mouse leydig tumor cell line. European journal of pharmaceutical sciences. 2015;76:231-7.
213. Besman MJ, Yanagibashi K, Lee TD, Kawamura M, Hall PF, Shively JE. Identification of des-(Gly-Ile)-endozepine as an effector of corticotropin-dependent adrenal steroidogenesis: stimulation of cholesterol delivery is mediated by the peripheral benzodiazepine receptor. Proceedings of the National Academy of Sciences of the United States of America. 1989;86(13):4897-901.

214. Rone MB, Liu J, Blonder J, Ye X, Veenstra TD, Young JC, et al. Targeting and insertion of the cholesterol-binding translocator protein into the outer mitochondrial membrane. Biochemistry. 2009;48(29):6909-20.
215. Midzak A, Rone M, Aghazadeh Y, Culty M, Papadopoulos V. Mitochondrial Protein Import and the Genesis of Steroidogenic Mitochondria. Molecular and cellular endocrinology. 2011;336(1-2):70-9.
216. Morohaku K, Phuong NS, Selvaraj V. Developmental expression of translocator protein/peripheral benzodiazepine receptor in reproductive tissues. PloS one. 2013;8(9):e74509.
217. Tu LN, Morohaku K, Manna PR, Pelton SH, Butler WR, Stocco DM, et al. Peripheral benzodiazepine receptor/translocator protein global knock-out mice are viable with no effects on steroid hormone biosynthesis. Journal of Biological Chemistry. 2014;289(40):27444-54.
218. Lin R, Angelin A, Da Settimo F, Martini C, Taliani S, Zhu S, et al. Genetic analysis of dTSPO, an outer mitochondrial membrane protein, reveals its functions in apoptosis, longevity, and Ab42-induced neurodegeneration. Aging cell. 2014;13(3):507-18.
219. Azarashvili T, Grachev D, Krestinina O, Evtodienko Y, Yurkov I, Papadopoulos V, et al. The peripheral-type benzodiazepine receptor is involved in control of Ca2+-induced permeability transition pore opening in rat brain mitochondria. Cell calcium. 2007;42(1):27-39.
220. O'Rourke B. Pathophysiological and protective roles of mitochondrial ion channels. The Journal of physiology. 2000;529 Pt 1:23-36.
221. Bernardi P, Rasola A, Forte M, Lippe G. The Mitochondrial Permeability Transition Pore: Channel Formation by F-ATP Synthase, Integration in Signal Transduction, and Role in Pathophysiology. Physiological Reviews. 2015;95(4):1111-55.
222. Sutter AP, Maaser K, Hopfner M, Barthel B, Grabowski P, Faiss S, et al. Specific ligands of the peripheral benzodiazepine receptor induce apoptosis and cell cycle arrest in human esophageal cancer cells. International journal of cancer. 2002;102(4):318-27.
223. Zisterer DM, Campiani G, Nacci V, Williams DC. Pyrrolo-1,5-benzoxazepines induce apoptosis in HL-60, Jurkat, and Hut-78 cells: a new class of apoptotic agents. The Journal of pharmacology and experimental therapeutics. 2000;293(1):48-59.
224. Marginedas-Freixa I, Hattab C, Bouyer G, Halle F, Chene A, Lefevre SD, et al. TSPO ligands stimulate ZnPPIX transport and ROS accumulation leading to the inhibition of P. falciparum growth in human blood. Scientific reports. 2016;6:33516.
225. Palsson-McDermott EM, O'Neill LA. The Warburg effect then and now: from cancer to inflammatory diseases. BioEssays : news and reviews in molecular, cellular and developmental biology. 2013;35(11):965-73.
226. Wu C, Li F, Niu G, Chen X. PET Imaging of Inflammation Biomarkers. Theranostics. 2013;3(7):448-66.
227. Cuhlmann S, Gsell W, Van der Heiden K, Habib J, Tremoleda JL, Khalil M, et al. In vivo mapping of vascular inflammation using the translocator protein tracer 18F-FEDAA1106. Molecular imaging. 2014;13.
228. Pottier G, Bernards N, Dolle F, Boisgard R. [(1)(8)F]DPA-714 as a biomarker for positron emission tomography imaging of rheumatoid arthritis in an animal model. Arthritis Research and Therapy. 2014;16(2):R69.

229. Charbonneau P, Syrota A, Crouzel C, Valois JM, Prenant C, Crouzel M. Peripheral-type benzodiazepine receptors in the living heart characterized by positron emission tomography. Circulation. 1986;73(3):476-83.
230. Myers R, Manjil LG, Cullen BM, Price GW, Frackowiak RS, Cremer JE. Macrophage and astrocyte populations in relation to [3H]PK 11195 binding in rat cerebral cortex following a local ischaemic lesion. Journal of cerebral blood flow and metabolism. 1991;11(2):314-22.
231. Ramsay SC, Weiller C, Myers R, Cremer JE, Luthra SK, Lammertsma AA, et al. Monitoring by PET of macrophage accumulation in brain after ischaemic stroke. Lancet. 1992;339(8800):1054-5.
232. Banati RB, Newcombe J, Gunn RN, Cagnin A, Turkheimer F, Heppner F, et al. The peripheral benzodiazepine binding site in the brain in multiple sclerosis: quantitative in vivo imaging of microglia as a measure of disease activity. Brain : a journal of neurology. 2000;123 (Pt 11):2321-37.
233. Edison P, Archer HA, Gerhard A, Hinz R, Pavese N, Turkheimer FE, et al. Microglia, amyloid, and cognition in Alzheimer's disease: An [11C](R)PK11195-PET and [11C]PIB-PET study. Neurobiology of disease. 2008;32(3):412-9.
234. Gerhard A, Pavese N, Hotton G, Turkheimer F, Es M, Hammers A, et al. In vivo imaging of microglial activation with [11C](R)-PK11195 PET in idiopathic Parkinson's disease. Neurobiology of disease. 2006;21(2):404-12.
235. Wagner HN, Jr. A brief history of positron emission tomography (PET). Seminars in nuclear medicine. 1998;28(3):213-20.
236. Fonseca A, Wagner J, Yamaga LI, Osawa A, da Cunha ML, Scheinberg M. (18) F-FDG PET imaging of rheumatoid articular and extraarticular synovitis. Journal of clinical rheumatology. 2008;14(5):307.
237. Phelps ME, Huang SC, Hoffman EJ, Selin C, Sokoloff L, Kuhl DE. Tomographic measurement of local cerebral glucose metabolic rate in humans with (F-18)2-fluoro-2-deoxy-D-glucose: validation of method. Annals of neurology. 1979;6(5):371-88.
238. Townsend DW. Combined positron emission tomography-computed tomography: the historical perspective. Seminars in ultrasound, CT, and MR. 2008;29(4):232-5.
239. Owen DR, Piccini P, Matthews PM. Towards molecular imaging of multiple sclerosis. Multiple sclerosis. 2011;17(3):262-72.
240. Honer M, Gobbi L, Martarello L, Comley RA. Radioligand development for molecular imaging of the central nervous system with positron emission tomography. Drug discovery today. 2014;19(12):1936-44.
241. Keen M and MacDermot J. (Wharton J and Polak JM eds). Analysis of receptors by radioligand binding, in *Receptor Autoradiography: Principles and Practice*. Oxford University Press, Oxford, UK; 1993; pp. 23–56.
242. Valk PE, Delbeke D, Bailey DL, Townsend DW, Maisey MN. Positron Emission Tomography. 1st edition. London: Springer-Verlag London; 2006; pp 1-16.
243. University of Washington, Department of Nuclear Medicine. Introduction to PET physics. 2017 (accessed on 20th June 2017). Available from: https://depts.washington.edu/nucmed/IRL/pet_intro/intro_src/section2.html
244. Workman RB, Coleman RE. Fundamentals of PET and PET/CT imaging. In: PET/CT; Essentials for Clinical Practice. 1st edition: Springer-Verlag New York; 2006 2006; pp1-22.

245. Basu S, Kwee TC, Surti S, Akin EA, Yoo D, Alavi A. Fundamentals of PET and PET/CT imaging. Annals of the New York Academy of Sciences. 2011;1228:1-18.
246. Cherry SR, Dahlbom M (Edited by Phelps ME) PET: Physics, Instrumentation and Scanners. In: PET. 1st eduition. Springer-Verlag New York. 2006; p1-117.
247. Thie JA. Understanding the standardized uptake value, its methods, and implications for usage. Journal of nuclear medicine. 2004;45(9):1431-4.
248. Keyes JW, Jr. SUV: standard uptake or silly useless value? Journal of nuclear medicine. 1995;36(10):1836-9.
249. Huang SC. Anatomy of SUV. Standardized uptake value. Nuclear medicine and biology. 2000;27(7):643-6.
250. Zasadny KR, Wahl RL. Standardized uptake values of normal tissues at PET with 2-[fluorine-18]-fluoro-2-deoxy-D-glucose: variations with body weight and a method for correction. Radiology. 1993;189(3):847-50.
251. Laffon E, Cazeau AL, Monet A, de Clermont H, Fernandez P, Marthan R, et al. The effect of renal failure on 18F-FDG uptake: a theoretic assessment. Journal of nuclear medicine technology. 2008;36(4):200-2.
252. Dimitrakopoulou-Strauss A, Pan L, Strauss LG. Quantitative approaches of dynamic FDG-PET and PET/CT studies (dPET/CT) for the evaluation of oncological patients. Cancer imaging. 2012;12:283-9.
253. Kropholler MA, Boellaard R, Elzinga EH, van der Laken CJ, Maruyama K, Kloet RW, et al. Quantification of (R)-[11C]PK11195 binding in rheumatoid arthritis. European Journal of Nuclear Medicine and Molecular Imaging. 2009;36(4):624-31.
254. Zanotti-Fregonara P, Fadaili el M, Maroy R, Comtat C, Souloumiac A, Jan S, et al. Comparison of eight methods for the estimation of the image-derived input function in dynamic [(18)F]-FDG PET human brain studies. Journal of cerebral blood flow and metabolism. 2009;29(11):1825-35.
255. Fischer DR, Pfirrmann CW, Zubler V, Stumpe KD, Seifert B, Strobel K, et al. High bone turnover assessed by 18F-fluoride PET/CT in the spine and sacroiliac joints of patients with ankylosing spondylitis: comparison with inflammatory lesions detected by whole body MRI. European Journal of Nuclear Medicine and Molecular Imaging research. 2012;2(1):38.
256. Tateishi U, Imagawa T, Kanezawa N, Okabe T, Shizukuishi K, Inoue T, et al. PET assessment of disease activity in children with juvenile idiopathic arthritis. Pediatric radiology. 2010;40(11):1781-8.
257. The Turku PET Centte. Volume of Distribution. 2014 (accessed on 30th June 2017). Available from: http://turkupetcentre.net/petanalysis/model_distribution_volume.html
258. Mulherin D, Fitzgerald O, Bresnihan B. Synovial tissue macrophage populations and articular damage in rheumatoid arthritis. Arthritis and rheumatism. 1996;39(1):115-24.
259. Chauveau F, Boutin H, Van Camp N, Dolle F, Tavitian B. Nuclear imaging of neuroinflammation: a comprehensive review of [11C]PK11195 challengers. Eur J Nucl Med Mol Imaging. 2008;35(12):2304-19.
260. Suridjan I, Pollock BG, Verhoeff NP, Voineskos AN, Chow T, Rusjan PM, et al. In-vivo imaging of grey and white matter neuroinflammation in Alzheimer's disease: a positron emission tomography study with a novel radioligand, [18F]-FEPPA. Molecular psychiatry. 2015;20(12):1579-87.

261. Shao X, Wang X, English SJ, Desmond T, Sherman PS, Quesada CA, et al. Imaging of carrageenan-induced local inflammation and adjuvant-induced systemic arthritis with [(11)C]PBR28 PET. Nuclear medicine and biology. 2013;40(7):906-11.
262. Owen DR, Yeo AJ, Gunn RN, Song K, Wadsworth G, Lewis A, et al. An 18-kDa translocator protein (TSPO) polymorphism explains differences in binding affinity of the PET radioligand PBR28. Journal of cerebral blood flow and metabolism. 2012;32(1):1-5.
263. Fujita M, Imaizumi M, Zoghbi SS, Fujimura Y, Farris AG, Suhara T, et al. Kinetic analysis in healthy humans of a novel positron emission tomography radioligand to image the peripheral benzodiazepine receptor, a potential biomarker for inflammation. NeuroImage. 2008;40(1):43-52.
264. Kreisl WC, Fujita M, Fujimura Y, Kimura N, Jenko KJ, Kannan P, et al. Comparison of [(11)C]-(R)-PK 11195 and [(11)C]PBR28, two radioligands for translocator protein (18 kDa) in human and monkey: Implications for positron emission tomographic imaging of this inflammation biomarker. NeuroImage. 2010;49(4):2924-32.
265. Owen DR, Howell OW, Tang SP, Wells LA, Bennacef I, Bergstrom M, et al. Two binding sites for [3H]PBR28 in human brain: implications for TSPO PET imaging of neuroinflammation. Journal of cerebral blood flow and metabolism. 2010;30(9):1608-18.
266. Hulme EC, Trevethick MA. Ligand binding assays at equilibrium: validation and interpretation. British journal of pharmacology. 2010;161(6):1219-37.
267. Kennedy A, Fearon U, Veale DJ, Godson C. Macrophages in Synovial Inflammation. Frontiers in Immunology. 2011;2:52.
268. Canete JD, Celis R, Hernandez V, Pablos JL, Sanmarti R. Synovial immunopathological changes associated with successful abatacept therapy in a case of severe refractory psoriatic arthritis. Annals of the Rheumatic Diseases. 2010;69(5):935-6.
269. Kruithof E, De Rycke L, Vandooren B, De Keyser F, FitzGerald O, McInnes I, et al. Identification of synovial biomarkers of response to experimental treatment in early-phase clinical trials in spondylarthritis. Arthritis and rheumatism. 2006;54(6):1795-804.
270. Goedkoop AY, Kraan MC, Teunissen MB, Picavet DI, de Rie MA, Bos JD, et al. Early effects of tumour necrosis factor alpha blockade on skin and synovial tissue in patients with active psoriasis and psoriatic arthritis. Annals of the Rheumatic Diseases. 2004;63(7):769-73.
271. Scheel AK, Schmidt WA, Hermann KG, Bruyn GA, D'Agostino MA, Grassi W, et al. Interobserver reliability of rheumatologists performing musculoskeletal ultrasonography: results from a EULAR "Train the trainers" course. Annals of the Rheumatic Diseases. 2005;64(7):1043-9.
272. Baeten D, Van den Bosch F, Elewaut D, Stuer A, Veys EM, De Keyser F. Needle arthroscopy of the knee with synovial biopsy sampling: technical experience in 150 patients. Clinical rheumatology. 1999;18(6):434-41.
273. Saito N, Pulford KA, Breton-Gorius J, Masse JM, Mason DY, Cramer EM. Ultrastructural localization of the CD68 macrophage-associated antigen in human blood neutrophils and monocytes. The American journal of pathology. 1991;139(5):1053-9.
274. Fonseca JE, Edwards JC, Blades S, Goulding NJ. Macrophage subpopulations in rheumatoid synovium: reduced CD163 expression in CD4+ T lymphocyte-rich microenvironments. Arthritis and rheumatism. 2002;46(5):1210-6.

275. Kunisch E, Fuhrmann R, Roth A, Winter R, Lungershausen W, Kinne R. Macrophage specificity of three anti-CD68 monoclonal antibodies (KP1, EBM11, and PGM1) widely used for immunohistochemistry and flow cytometry. Annals of the Rheumatic Diseases. 2004;63(7):774-84.
276. Oliver JE, Worthington J, Silman AJ. Genetic epidemiology of rheumatoid arthritis. Current opinion in rheumatology. 2006;18(2):141-6.
277. Barton AC. Genetic epidemiology. Psoriatic arthritis. Arthritis research and therapy. 2002;4(4):247-51.
278. Wong FL, Wang MK, Boo NY, Hamidah NH, Ainoon BO. Rapid detection of the UGT1A1 single nucleotide polymorphism G211A using real-time PCR with Taqman minor groove binder probes. Journal of clinical laboratory analysis. 2007;21(3):167-72.
279. Mandl P, Balint PV, Brault Y, Backhaus M, D'Agostino MA, Grassi W, et al. Metrologic properties of ultrasound versus clinical evaluation of synovitis in rheumatoid arthritis: results of a multicenter, randomized study. Arthritis and rheumatism. 2012;64(4):1272-82.
280. Hartung W, Kellner H, Strunk J, Sattler H, Schmidt WA, Ehrenstein B, et al. Development and evaluation of a novel ultrasound score for large joints in rheumatoid arthritis: one year of experience in daily clinical practice. Arthritis care & research. 2012;64(5):675-82.
281. Owen DR, Guo Q, Kalk NJ, Colasanti A, Kalogiannopoulou D, Dimber R, et al. Determination of [(11)C]PBR28 binding potential in vivo: a first human TSPO blocking study. Journal of cerebral blood flow and metabolism. 2014;34(6):989-94.
282. Guo Q, Colasanti A, Owen DR, Onega M, Kamalakaran A, Bennacef I, et al. Quantification of the specific translocator protein signal of 18F-PBR111 in healthy humans: a genetic polymorphism effect on in vivo binding. Journal of nuclear medicine. 2013;54(11):1915-23.
283. Hilton J, Yokoi F, Dannals RF, Ravert HT, Szabo Z, Wong DF. Column-switching HPLC for the analysis of plasma in PET imaging studies. Nuclear medicine and biology. 2000;27(6):627-30.
284. Bancroft J. Theory and Practice of Histological Techniques: Elsevier Health Sciences; 2008.
285. Dakin SG, Martinez FO, Yapp C, Wells G, Oppermann U, Dean BJF, et al. Inflammation activation and resolution in human tendon disease. Science translational medicine. 2015;7(311):311ra173-311ra173.
286. Revu S, Neregard P, af Klint E, Korotkova M, Catrina AI. Synovial membrane immunohistology in early-untreated rheumatoid arthritis reveals high expression of catabolic bone markers that is modulated by methotrexate. Arthritis Research and Therapy. 2013;15(6):R205.
287. Scott DL, Antoni C, Choy EH, Van Riel PC. Joint counts in routine practice. Rheumatology. 2003;42(8):919-23.
288. Haringman JJ, Gerlag DM, Zwinderman AH, Smeets TJ, Kraan MC, Baeten D, et al. Synovial tissue macrophages: a sensitive biomarker for response to treatment in patients with rheumatoid arthritis. Annals of the Rheumatic Diseases. 2005;64(6):834-8.
289. Tak PP, Smeets TJ, Daha MR, Kluin PM, Meijers KA, Brand R, et al. Analysis of the synovial cell infiltrate in early rheumatoid synovial tissue in relation to local disease activity. Arthritis and rheumatism. 1997;40(2):217-25.

290. Nothdurfter C, Baghai TC, Schule C, Rupprecht R. Translocator protein (18 kDa) (TSPO) as a therapeutic target for anxiety and neurologic disorders. European archives of psychiatry and clinical neuroscience. 2012;262 Suppl 2:S107-12.
291. Smith MD. The Normal Synovium. The Open Rheumatology Journal. 2011;5:100-6.
292. Bustamante MF, Garcia-Carbonell R, Whisenant KD, Guma M. Fibroblast-like synoviocyte metabolism in the pathogenesis of rheumatoid arthritis. Arthritis Research and Therapy. 2017;19(1):110.
293. Bartok B, Firestein GS. Fibroblast-like synoviocytes: key effector cells in rheumatoid arthritis. Immunological reviews. 2010;233(1):233-55.
294. Firestein GS, Zvaifler NJ. How important are T cells in chronic rheumatoid synovitis? Arthritis and rheumatism. 1990;33(6):768-73.
295. Schett G. Cells of the synovium in rheumatoid arthritis. Osteoclasts. Arthritis Research and Therapy. 2007;9(1):203.
296. Veale D, Yanni G, Rogers S, Barnes L, Bresnihan B, Fitzgerald O. Reduced synovial membrane macrophage numbers, ELAM-1 expression, and lining layer hyperplasia in psoriatic arthritis as compared with rheumatoid arthritis. Arthritis and rheumatism. 1993;36(7):893-900.
297. Tran CN, Lundy SK, Fox DA. Synovial biology and T cells in rheumatoid arthritis. Pathophysiology. 2005;12(3):183-9.
298. Pitzalis C, Kelly S, Humby F. New learnings on the pathophysiology of RA from synovial biopsies. Current opinion in rheumatology. 2013;25(3):334-44.
299. Bugatti S, Manzo A, Bombardieri M, Vitolo B, Humby F, Kelly S, et al. Synovial tissue heterogeneity and peripheral blood biomarkers. Current rheumatology reports. 2011;13(5):440-8.
300. Dennis G, Holweg CTJ, Kummerfeld SK, Choy DF, Setiadi AF, Hackney JA, et al. Synovial phenotypes in rheumatoid arthritis correlate with response to biologic therapeutics. Arthritis Research and Therapy. 2014;16(2):R90-R.
301. Tak PP, Bresnihan B. The pathogenesis and prevention of joint damage in rheumatoid arthritis: advances from synovial biopsy and tissue analysis. Arthritis and rheumatism. 2000;43(12):2619-33.
302. Roberts CA, Dickinson AK, Taams LS. The Interplay Between Monocytes/Macrophages and CD4(+) T Cell Subsets in Rheumatoid Arthritis. Frontiers in Immunology. 2015;6:571.
303. Kinne RW, Stuhlmuller B, Burmester GR. Cells of the synovium in rheumatoid arthritis. Macrophages. Arthritis Research and Therapy. 2007;9(6):224.
304. Kim WU, Kang SS, Yoo SA, Hong KH, Bae DG, Lee MS, et al. Interaction of vascular endothelial growth factor 165 with neuropilin-1 protects rheumatoid synoviocytes from apoptotic death by regulating Bcl-2 expression and Bax translocation. Journal of immunology. 2006;177(8):5727-35.
305. Kawakami A, Eguchi K, Matsuoka N, Tsuboi M, Kawabe Y, Aoyagi T, et al. Inhibition of Fas antigen-mediated apoptosis of rheumatoid synovial cells in vitro by transforming growth factor beta 1. Arthritis and rheumatism. 1996;39(8):1267-76.
306. Seyler TM, Park YW, Takemura S, Bram RJ, Kurtin PJ, Goronzy JJ, et al. BLyS and APRIL in rheumatoid arthritis. Journal of Clinical Investigation. 2005;115(11):3083-92.
307. Laria A, Lurati A, Marrazza M, Mazzocchi D, Re KA, Scarpellini M. The macrophages in rheumatic diseases. Journal of Inflammation Research. 2016;9:1-11.

308. Martinez FO, Gordon S. The M1 and M2 paradigm of macrophage activation: time for reassessment. F1000prime reports. 2014;6:13.
309. Sica A, Mantovani A. Macrophage plasticity and polarization: in vivo veritas. The Journal of clinical investigation. 2012;122(3):787-95.
310. Murray PJ, Wynn TA. Protective and pathogenic functions of macrophage subsets. Nature Reviews Immunology. 2011;11(11):723-37.
311. Murray PJ, Allen JE, Biswas SK, Fisher EA, Gilroy DW, Goerdt S, et al. Macrophage activation and polarization: nomenclature and experimental guidelines. Immunity. 2014;41(1):14-20.
312. Vandooren B, Noordenbos T, Ambarus C, Krausz S, Cantaert T, Yeremenko N, et al. Absence of a classically activated macrophage cytokine signature in peripheral spondylarthritis, including psoriatic arthritis. Arthritis and rheumatism. 2009;60(4):966-75.
313. Batliwalla FM, Baechler EC, Xiao X, Li W, Balasubramanian S, Khalili H, et al. Peripheral blood gene expression profiling in rheumatoid arthritis. Genes and immunity. 2005;6(5):388-97.
314. Highton J, Carlisle B, Palmer DG. Changes in the phenotype of monocytes/macrophages and expression of cytokine mRNA in peripheral blood and synovial fluid of patients with rheumatoid arthritis. Clinical and experimental immunology. 1995;102(3):541-6.
315. Baeten D, Boots AM, Steenbakkers PG, Elewaut D, Bos E, Verheijden GF, et al. Human cartilage gp-39+,CD16+ monocytes in peripheral blood and synovium: correlation with joint destruction in rheumatoid arthritis. Arthritis and rheumatism. 2000;43(6):1233-43.
316. Kawanaka N, Yamamura M, Aita T, Morita Y, Okamoto A, Kawashima M, et al. CD14+,CD16+ blood monocytes and joint inflammation in rheumatoid arthritis. Arthritis and rheumatism. 2002;46(10):2578-86.
317. Ambarus CA, Noordenbos T, de Hair MJ, Tak PP, Baeten DL. Intimal lining layer macrophages but not synovial sublining macrophages display an IL-10 polarized-like phenotype in chronic synovitis. Arthritis Research and Therapy. 2012;14(2):R74.
318. Koning N, van Eijk M, Pouwels W, Brouwer MS, Voehringer D, Huitinga I, et al. Expression of the inhibitory CD200 receptor is associated with alternative macrophage activation. Journal of innate immunity. 2010;2(2):195-200.
319. Verreck FA, de Boer T, Langenberg DM, van der Zanden L, Ottenhoff TH. Phenotypic and functional profiling of human proinflammatory type-1 and anti-inflammatory type-2 macrophages in response to microbial antigens and IFN-gamma- and CD40L-mediated costimulation. Journal of Leukocyte Biology. 2006;79(2):285-93.
320. Martinez FO. Analysis of gene expression and gene silencing in human macrophages. Current protocols in immunology. 2012;Chapter 14:Unit 14.28.1-3.
321. Paramarta JE, Baeten D, De Rycke L. Synovial Tissue Response to Treatment with TNF Blockers in Peripheral Spondyloarthritis. The Open Rheumatology Journal. 2011;5:127-32.
322. Baum J, Duffy HS. Fibroblasts and Myofibroblasts: What are we talking about? Journal of cardiovascular pharmacology. 2011;57(4):376-9.
323. Filer A. The fibroblast as a therapeutic target in rheumatoid arthritis. Current opinion in pharmacology. 2013;13(3):413-9.
324. Fassbender HG. Specific and nonspecific structures developing in inflammatory rheumatic diseases. Acta pathologica japonica. 1970;20(4):409-22.

325. Chang SK, Gu Z, Brenner MB. Fibroblast-like synoviocytes in inflammatory arthritis pathology: the emerging role of cadherin-11. Immunological reviews. 2010;233(1):256-66.
326. Muller-Ladner U, Kriegsmann J, Franklin BN, Matsumoto S, Geiler T, Gay RE, et al. Synovial fibroblasts of patients with rheumatoid arthritis attach to and invade normal human cartilage when engrafted into SCID mice. The American journal of pathology. 1996;149(5):1607-15.
327. Kraan M, Haringman J, Weedon H, Barg E, Smith M, Ahern M, et al. T cells, fibroblast-like synoviocytes, and granzyme B+ cytotoxic cells are associated with joint damage in patients with recent onset rheumatoid arthritis. Annals of the Rheumatic Diseases. 2004;63(5):483-8.
328. Yamamoto T. Angiogenic and Inflammatory Properties of Psoriatic Arthritis. ISRN Dermatology. 2013;2013:630620.
329. Shigeyama Y, Pap T, Kunzler P, Simmen BR, Gay RE, Gay S. Expression of osteoclast differentiation factor in rheumatoid arthritis. Arthritis and rheumatism. 2000;43(11):2523-30.
330. McGettrick HM, Buckley CD, Filer A, Ed Rainger G, Nash GB. Stromal cells differentially regulate neutrophil and lymphocyte recruitment through the endothelium. Immunology. 2010;131(3):357-70.
331. Buckley CD, Pilling D, Lord JM, Akbar AN, Scheel-Toellner D, Salmon M. Fibroblasts regulate the switch from acute resolving to chronic persistent inflammation. Trends in Immunology. 2001;22(4):199-204.
332. Burger JA, Zvaifler NJ, Tsukada N, Firestein GS, Kipps TJ. Fibroblast-like synoviocytes support B-cell pseudoemperipolesis via a stromal cell-derived factor-1- and CD106 (VCAM-1)-dependent mechanism. The Journal of clinical investigation. 2001;107(3):305-15.
333. Filer A, Parsonage G, Smith E, Osborne C, Thomas AM, Curnow SJ, et al. Differential survival of leukocyte subsets mediated by synovial, bone marrow, and skin fibroblasts: site-specific versus activation-dependent survival of T cells and neutrophils. Arthritis and rheumatism. 2006;54(7):2096-108.
334. Buckley CD, Amft N, Bradfield PF, Pilling D, Ross E, Arenzana-Seisdedos F, et al. Persistent induction of the chemokine receptor CXCR4 by TGF-beta 1 on synovial T cells contributes to their accumulation within the rheumatoid synovium. Journal of immunology. 2000;165(6):3423-9.
335. Lefevre S, Knedla A, Tennie C, Kampmann A, Wunrau C, Dinser R, et al. Synovial fibroblasts spread rheumatoid arthritis to unaffected joints. Nature medicine. 2009;15(12):1414-20.
336. Klimiuk PA, Yang H, Goronzy JJ, Weyand CM. Production of cytokines and metalloproteinases in rheumatoid synovitis is T cell dependent. Clinical immunology (Orlando, Fla). 1999;90(1):65-78.
337. Hughes LB, Morrison D, Kelley JM, Padilla MA, Vaughan LK, Westfall AO, et al. The HLA–DRB1 Shared Epitope Is Associated With Susceptibility to Rheumatoid Arthritis in African Americans Through European Genetic Admixture. Arthritis and rheumatism. 2008;58(2):349-58.
338. Song YW, Kang EH. Autoantibodies in rheumatoid arthritis: rheumatoid factors and anticitrullinated protein antibodies. QJM: An International Journal of Medicine. 2010;103(3):139-46.
339. Cantaert T, De Rycke L, Bongartz T, Matteson EL, Tak PP, Nicholas AP, et al. Citrullinated proteins in rheumatoid arthritis: crucial...but not sufficient! Arthritis and rheumatism. 2006;54(11):3381-9.

340. Berner B, Wolf G, Hummel KM, Muller GA, Reuss-Borst MA. Increased expression of CD40 ligand (CD154) on CD4+ T cells as a marker of disease activity in rheumatoid arthritis. Annals of the Rheumatic Diseases. 2000;59(3):190-5.
341. Ruderman EM, Pope RM. The evolving clinical profile of abatacept (CTLA4–Ig): a novel co-stimulatory modulator for the treatment of rheumatoid arthritis. Arthritis Research and Therapy. 2005;7(Suppl 2):S21-S5.
342. Steiner G, Tohidast-Akrad M, Witzmann G, Vesely M, Studnicka-Benke A, Gal A, et al. Cytokine production by synovial T cells in rheumatoid arthritis. Rheumatology. 1999;38(3):202-13.
343. Rao DA, Gurish MF, Marshall JL, Slowikowski K, Fonseka CY, Liu Y, et al. Pathologically expanded peripheral T helper cell subset drives B cells in rheumatoid arthritis. Nature. 2017;542(7639):110-4.
344. Park H, Li Z, Yang XO, Chang SH, Nurieva R, Wang YH, et al. A distinct lineage of CD4 T cells regulates tissue inflammation by producing interleukin 17. Nature Immunology. 2005;6(11):1133-41.
345. Ehrenstein MR, Evans JG, Singh A, Moore S, Warnes G, Isenberg DA, et al. Compromised function of regulatory T cells in rheumatoid arthritis and reversal by anti-TNFalpha therapy. The Journal of experimental medicine. 2004;200(3):277-85.
346. Pilling D, Fan T, Huang D, Kaul B, Gomer RH. Identification of markers that distinguish monocyte-derived fibrocytes from monocytes, macrophages, and fibroblasts. PloS one. 2009;4(10):e7475.
347. Liu H, Shi B, Huang C-C, Eksarko P, Pope RM. Transcriptional diversity during monocyte to macrophage differentiation. Immunology letters. 2008;117(1):70-80.
348. Pap T, Müller-Ladner U, Gay RE, Gay S. Fibroblast biology: Role of synovial fibroblasts in the pathogenesis of rheumatoid arthritis. Arthritis research and therapy. 2000;2(5):361-7.
349. Turner JD, Filer A. The role of the synovial fibroblast in rheumatoid arthritis pathogenesis. Current opinion in rheumatology. 2015;27(2):175-82.
350. Maia M, de Vriese A, Janssens T, Moons M, van Landuyt K, Tavernier J, et al. CD248 and its cytoplasmic domain: a therapeutic target for arthritis. Arthritis and rheumatism. 2010;62(12):3595-606.
351. Del Rey MJ, Fare R, Izquierdo E, Usategui A, Rodriguez-Fernandez JL, Suarez-Fueyo A, et al. Clinicopathological correlations of podoplanin (gp38) expression in rheumatoid synovium and its potential contribution to fibroblast platelet crosstalk. PloS one. 2014;9(6):e99607.
352. Brennan FM, Chantry D, Jackson AM, Maini RN, Feldmann M. Cytokine production in culture by cells isolated from the synovial membrane. Journal of autoimmunity. 1989;2 Suppl:177-86.
353. Sivakumar B, Akhavani MA, Winlove CP, Taylor PC, Paleolog EM, Kang N. Synovial hypoxia as a cause of tendon rupture in rheumatoid arthritis. The Journal of hand surgery. 2008;33(1):49-58.
354. Zimmermann T, Kunisch E, Pfeiffer R, Hirth A, Stahl HD, Sack U, et al. Isolation and characterization of rheumatoid arthritis synovial fibroblasts from primary culture--primary culture cells markedly differ from fourth-passage cells. Arthritis research and therapy. 2001;3(1):72-6.
355. Neumann E, Riepl B, Knedla A, Lefevre S, Tarner IH, Grifka J, et al. Cell culture and passaging alters gene expression pattern and proliferation rate in rheumatoid arthritis synovial fibroblasts. Arthritis Research and Therapy. 2010;12(3):R83.

356. Stroncek DF, Fellowes V, Pham C, Khuu H, Fowler DH, Wood LV, et al. Counter-flow elutriation of clinical peripheral blood mononuclear cell concentrates for the production of dendritic and T cell therapies. Journal of Translational Medicine. 2014;12:241.
357. Berger TG, Strasser E, Smith R, Carste C, Schuler-Thurner B, Kaempgen E, et al. Efficient elutriation of monocytes within a closed system (Elutra) for clinical-scale generation of dendritic cells. Journal of immunological methods. 2005;298(1-2):61-72.
358. Schwanke U, Nabereit A, Moog R. Isolation of monocytes from whole blood-derived buffy coats by continuous counter-flow elutriation. Journal of clinical apheresis. 2006;21(3):153-7.
359. Banfalvi G. Cell cycle synchronization of animal cells and nuclei by centrifugal elutriation. Nature protocols. 2008;3(4):663-73.
360. Krausgruber T, Blazek K, Smallie T, Alzabin S, Lockstone H, Sahgal N, et al. IRF5 promotes inflammatory macrophage polarization and TH1-TH17 responses. Nature Immunology. 2011;12(3):231-8.
361. Ishida Y, Agata Y, Shibahara K, Honjo T. Induced expression of PD-1, a novel member of the immunoglobulin gene superfamily, upon programmed cell death. The EMBO journal. 1992;11(11):3887-95.
362. Swinehart DF. The Beer-Lambert Law. Journal of Chemical Education. 1962;39(7):333.
363. Glasel JA. Validity of nucleic acid purities monitored by 260nm/280nm absorbance ratios. BioTechniques. 1995;18(1):62-3.
364. Kubista M, Andrade JM, Bengtsson M, Forootan A, Jonak J, Lind K, et al. The real-time polymerase chain reaction. Molecular aspects of medicine. 2006;27(2-3):95-125.
365. Caradec J, Sirab N, Keumeugni C, Moutereau S, Chimingqi M, Matar C, et al. 'Desperate house genes': the dramatic example of hypoxia. British journal of cancer. 2010;102(6):1037-43.
366. Ledderose C, Heyn J, Limbeck E, Kreth S. Selection of reliable reference genes for quantitative real-time PCR in human T cells and neutrophils. BMC Research Notes. 2011;4:427-.
367. Bylund DB, Toews ML. Radioligand binding methods: practical guide and tips. The American journal of physiology. 1993;265(5 Pt 1):L421-9.
368. Dong C, Liu Z, Wang F. Radioligand saturation binding for quantitative analysis of ligand-receptor interactions. Biophysics Reports. 2015;1:148-55.
369. Imaizumi M, Briard E, Zoghbi SS, Gourley JP, Hong J, Fujimura Y, et al. Brain and Whole-body Imaging in Nonhuman Primates of [(11)C]PBR28, a Promising PET Radioligand for Peripheral Benzodiazepine Receptors. NeuroImage. 2008;39(3):1289-98.
370. Brown AK, Fujita M, Fujimura Y, Liow JS, Stabin M, Ryu YH, et al. Radiation dosimetry and biodistribution in monkey and man of 11C-PBR28: a PET radioligand to image inflammation. Journal of nuclear medicine. 2007;48(12):2072-9.
371. Foy JM, Schnieden H. Estimation of total body water (virtual tritium space) in the rat, cat, rabbit, guinea-pig and man, and of the biological half-life of tritium in man. The Journal of physiology. 1960;154:169-76.
372. Bocchini V, Mazzolla R, Barluzzi R, Blasi E, Sick P, Kettenmann H. An immortalized cell line expresses properties of activated microglial cells. Journal of neuroscience research. 1992;31(4):616-21.

373. Perry VH, Teeling J. Microglia and macrophages of the central nervous system: the contribution of microglia priming and systemic inflammation to chronic neurodegeneration. Seminars in Immunopathology. 2013;35(5):601-12.
374. Bae KR, Shim HJ, Balu D, Kim SR, Yu SW. Translocator protein 18 kDa negatively regulates inflammation in microglia. Journal of neuroimmune pharmacology. 2014;9(3):424-37.
375. Pilling D, Gomer RH. Differentiation of Circulating Monocytes into Fibroblast-Like Cells. Methods in molecular biology. 2012;904:191-206.
376. Franklin SL, Dean BJ, Wheway K, Watkins B, Javaid MK, Carr AJ. Up-regulation of Glutamate in Painful Human Supraspinatus Tendon Tears. The American journal of sports medicine. 2014;42(8):1955-62.
377. Murphy G, Nagase H. Reappraising metalloproteinases in rheumatoid arthritis and osteoarthritis: destruction or repair? Nature clinical practice Rheumatology. 2008;4(3):128-35.
378. Anholt RR, Pedersen PL, De Souza EB, Snyder SH. The peripheral-type benzodiazepine receptor. Localization to the mitochondrial outer membrane. Journal of Biological Chemistry. 1986;261(2):576-83.
379. Le Fur G, Perrier ML, Vaucher N, Imbault F, Flamier A, Benavides J, et al. Peripheral benzodiazepine binding sites: effect of PK 11195, 1-(2-chlorophenyl)-N-methyl-N-(1-methylpropyl)-3-isoquinolinecarboxamide. I. In vitro studies. Life sciences. 1983;32(16):1839-47.
380. Benavides J, Guilloux F, Rufat P, Uzan A, Renault C, Dubroeucq MC, et al. In vivo labelling in several rat tissues of 'peripheral type' benzodiazepine binding sites. European journal of pharmacology. 1984;99(1):1-7.
381. Janczar K, Su Z, Raccagni I, Anfosso A, Kelly C, Durrenberger PF, et al. The 18-kDa mitochondrial translocator protein in gliomas: from the bench to bedside. Biochemical Society transactions. 2015;43(4):579-85.
382. Gizinski AM, Fox DA. T cell subsets and their role in the pathogenesis of rheumatic disease. Current opinion in rheumatology. 2014;26(2):204-10.
383. Martinez FO, Gordon S, Locati M, Mantovani A. Transcriptional profiling of the human monocyte-to-macrophage differentiation and polarization: new molecules and patterns of gene expression. Journal of immunology. 2006;177(10):7303-11.
384. Croft AP, Naylor AJ, Marshall JL, Hardie DL, Zimmermann B, Turner J, et al. Rheumatoid synovial fibroblasts differentiate into distinct subsets in the presence of cytokines and cartilage. Arthritis Research and Therapy. 2016;18(1):270.
385. Antkiewicz-Michaluk L, Guidotti A, Krueger KE. Molecular characterization and mitochondrial density of a recognition site for peripheral-type benzodiazepine ligands. Molecular pharmacology. 1988;34(3):272-8.
386. Giatzakis C, Papadopoulos V. Differential utilization of the promoter of peripheral-type benzodiazepine receptor by steroidogenic versus nonsteroidogenic cell lines and the role of Sp1 and Sp3 in the regulation of basal activity. Endocrinology. 2004;145(3):1113-23.
387. De Souza EB, Anholt RR, Murphy KM, Snyder SH, Kuhar MJ. Peripheral-type benzodiazepine receptors in endocrine organs: autoradiographic localization in rat pituitary, adrenal, and testis. Endocrinology. 1985;116(2):567-73.
388. Anholt RR, De Souza EB, Oster-Granite ML, Snyder SH. Peripheral-type benzodiazepine receptors: autoradiographic localization in whole-body sections of neonatal rats. The Journal of pharmacology and experimental therapeutics. 1985;233(2):517-26.

389. Fan J, Papadopoulos V. Transcriptional Regulation of Translocator Protein (Tspo) via a SINE B2-Mediated Natural Antisense Transcript in MA-10 Leydig Cells. Biology of Reproduction. 2012;86(5):147.
390. de Hair MJ, van de Sande MG, Ramwadhdoebe TH, Hansson M, Landewe R, van der Leij C, et al. Features of the synovium of individuals at risk of developing rheumatoid arthritis: implications for understanding preclinical rheumatoid arthritis. Arthritis & rheumatology. 2014;66(3):513-22.
391. van de Sande MG, de Hair MJ, van der Leij C, Klarenbeek PL, Bos WH, Smith MD, et al. Different stages of rheumatoid arthritis: features of the synovium in the preclinical phase. Annals of the Rheumatic Diseases. 2011;70(5):772-7.
392. Hashimoto S, Takahashi Y, Tomita Y, Hayama T, Sawada S, Horie T, et al. Mechanism of calcium ionophore and phorbol ester-induced T-cell activation. Accessory cell requirement for T-cell activation. Scandinavian journal of immunology. 1991;33(4):393-403.
393. Riddell SR, Greenberg PD. The use of anti-CD3 and anti-CD28 monoclonal antibodies to clone and expand human antigen-specific T cells. Journal of immunological methods. 1990;128(2):189-201.
394. Spitzer MH, Nolan GP. Mass Cytometry: Single Cells, Many Features. Cell. 2016;165(4):780-91.
395. Costa B, Pini S, Gabelloni P, Da Pozzo E, Abelli M, Lari L, et al. The spontaneous Ala147Thr amino acid substitution within the translocator protein influences pregnenolone production in lymphomonocytes of healthy individuals. Endocrinology. 2009;150(12):5438-45.
396. Navegantes KC, de Souza Gomes R, Pereira PAT, Czaikoski PG, Azevedo CHM, Monteiro MC. Immune modulation of some autoimmune diseases: the critical role of macrophages and neutrophils in the innate and adaptive immunity. Journal of Translational Medicine. 2017;15:36.
397. Wynn TA, Chawla A, Pollard JW. Origins and Hallmarks of Macrophages: Development, Homeostasis, and Disease. Nature. 2013;496(7446):445-55.
398. Gautier EL, Shay T, Miller J, Greter M, Jakubzick C, Ivanov S, et al. Gene expression profiles and transcriptional regulatory pathways underlying mouse tissue macrophage identity and diversity. Nature immunology. 2012;13(11):1118-28.
399. Aderem A, Underhill DM. Mechanisms of phagocytosis in macrophages. Annual review of immunology. 1999;17:593-623.
400. Liddiard K, Rosas M, Davies LC, Jones SA, Taylor PR. Macrophage heterogeneity and acute inflammation. European journal of immunology. 2011;41(9):2503-8.
401. Root RK, Dale DC. Granulocyte colony-stimulating factor and granulocyte-macrophage colony-stimulating factor: comparisons and potential for use in the treatment of infections in nonneutropenic patients. The Journal of infectious diseases. 1999;179 Suppl 2:S342-52.
402. Laskin DL. Macrophages and Inflammatory Mediators in Chemical Toxicity: A Battle of Forces. Chemical research in toxicology. 2009;22(8):1376-85.
403. Unanue ER. Antigen-presenting function of the macrophage. Annual review of immunology. 1984;2:395-428.
404. Arango Duque G, Descoteaux A. Macrophage Cytokines: Involvement in Immunity and Infectious Diseases. Frontiers in Immunology. 2014;5:491.
405. Muraille E, Leo O, Moser M. Th1/Th2 Paradigm Extended: Macrophage Polarization as an Unappreciated Pathogen-Driven Escape Mechanism? Frontiers in Immunology. 2014;5:603.

406. Murray PJ, Wynn TA. Obstacles and opportunities for understanding macrophage polarization. Journal of Leukocyte Biology. 2011;89(4):557-63.
407. Mackaness GB. Cellular resistance to infection. The Journal of experimental medicine. 1962;116:381-406.
408. Pace JL, Russell SW, Schreiber RD, Altman A, Katz DH. Macrophage activation: priming activity from a T-cell hybridoma is attributable to interferon-gamma. Proceedings of the National Academy of Sciences of the United States of America. 1983;80(12):3782-6.
409. Celada A, Gray PW, Rinderknecht E, Schreiber RD. Evidence for a gamma-interferon receptor that regulates macrophage tumoricidal activity. The Journal of experimental medicine. 1984;160(1):55-74.
410. Mills CD, Kincaid K, Alt JM, Heilman MJ, Hill AM. M-1/M-2 Macrophages and the Th1/Th2 Paradigm. The Journal of Immunology. 2000;164(12):6166.
411. Mantovani A, Sica A, Sozzani S, Allavena P, Vecchi A, Locati M. The chemokine system in diverse forms of macrophage activation and polarization. Trends in Immunology. 2004;25(12):677-86.
412. Fleetwood AJ, Dinh H, Cook AD, Hertzog PJ, Hamilton JA. GM-CSF- and M-CSF-dependent macrophage phenotypes display differential dependence on type I interferon signaling. Journal of Leukocyte Biology. 2009;86(2):411-21.
413. Joshi S, Singh AR, Zulcic M, Bao L, Messer K, Ideker T, et al. Rac2 Controls Tumor Growth, Metastasis and M1-M2 Macrophage Differentiation In Vivo. PloS one. 2014;9(4):e95893.
414. Lawrence T, Natoli G. Transcriptional regulation of macrophage polarization: enabling diversity with identity. Nature Reviews Immunology. 2011;11(11):750-61.
415. Mosser DM, Edwards JP. Exploring the full spectrum of macrophage activation. Nature Reviews Immunology. 2008;8(12):958-69.
416. Stout RD, Suttles J. Functional plasticity of macrophages: reversible adaptation to changing microenvironments. Journal of Leukocyte Biology. 2004;76(3):509-13.
417. Edwards JP, Zhang X, Frauwirth KA, Mosser DM. Biochemical and functional characterization of three activated macrophage populations. Journal of Leukocyte Biology. 2006;80(6):1298-307.
418. Gratchev A, Kzhyshkowska J, Kannookadan S, Ochsenreiter M, Popova A, Yu X, et al. Activation of a TGF-beta-specific multistep gene expression program in mature macrophages requires glucocorticoid-mediated surface expression of TGF-beta receptor II. Journal of immunology. 2008;180(10):6553-65.
419. Gundra UM, Girgis NM, Ruckerl D, Jenkins S, Ward LN, Kurtz ZD, et al. Alternatively activated macrophages derived from monocytes and tissue macrophages are phenotypically and functionally distinct. Blood. 2014;123(20):e110-22.
420. Lang R, Patel D, Morris JJ, Rutschman RL, Murray PJ. Shaping gene expression in activated and resting primary macrophages by IL-10. Journal of immunology. 2002;169(5):2253-63.
421. Shirey KA, Cole LE, Keegan AD, Vogel SN. Francisella tularensis live vaccine strain induces macrophage alternative activation as a survival mechanism. Journal of immunology. 2008;181(6):4159-67.
422. Shirey KA, Lai W, Pletneva LM, Karp CL, Divanovic S, Blanco JC, et al. Role of the lipoxygenase pathway in RSV-induced alternatively activated macrophages leading to resolution of lung pathology. Mucosal immunology. 2014;7(3):549-57.

423. Shirey KA, Pletneva LM, Puche AC, Keegan AD, Prince GA, Blanco JC, et al. Control of RSV-induced lung injury by alternatively activated macrophages is IL-4R alpha-, TLR4-, and IFN-beta-dependent. Mucosal immunology. 2010;3(3):291-300.
424. Xue J, Schmidt SV, Sander J, Draffehn A, Krebs W, Quester I, et al. Transcriptome-based network analysis reveals a spectrum model of human macrophage activation. Immunity. 2014;40(2):274-88.
425. Walker JR, Su AI, Self DW, Hogenesch JB, Lapp H, Maier R, et al. Applications of a Rat Multiple Tissue Gene Expression Data Set. Genome Research. 2004;14(4):742-9.
426. Aitman TJ, Critser JK, Cuppen E, Dominiczak A, Fernandez-Suarez XM, Flint J, et al. Progress and prospects in rat genetics: a community view. Nature genetics. 2008;40(5):516-22.
427. Rawji KS, Yong VW. The benefits and detriments of macrophages/microglia in models of multiple sclerosis. Clinical & developmental immunology. 2013;2013:948976.
428. Hambardzumyan D, Gutmann DH, Kettenmann H. The role of microglia and macrophages in glioma maintenance and progression. Nature neuroscience. 2016;19(1):20-7.
429. Nayak D, Roth TL, McGavern DB. Microglia development and function. Annual review of immunology. 2014;32:367-402.
430. David S, Kroner A. Repertoire of microglial and macrophage responses after spinal cord injury. Nature reviews Neuroscience. 2011;12(7):388-99.
431. Scarf AM, Kassiou M. The translocator protein. Journal of nuclear medicine. 2011;52(5):677-80.
432. Morin D, Musman J, Pons S, Berdeaux A, Ghaleb B. Mitochondrial translocator protein (TSPO): From physiology to cardioprotection. Biochemical pharmacology. 2016;105:1-13.
433. Sandiego CM, Gallezot JD, Pittman B, Nabulsi N, Lim K, Lin SF, et al. Imaging robust microglial activation after lipopolysaccharide administration in humans with PET. Proceedings of the National Academy of Sciences of the United States of America. 2015;112(40):12468-73.
434. Banks WA, Gray AM, Erickson MA, Salameh TS, Damodarasamy M, Sheibani N, et al. Lipopolysaccharide-induced blood-brain barrier disruption: roles of cyclooxygenase, oxidative stress, neuroinflammation, and elements of the neurovascular unit. Journal of neuroinflammation. 2015;12:223.
435. Ransohoff RM, Perry VH. Microglial physiology: unique stimuli, specialized responses. Annual review of immunology. 2009;27:119-45.
436. Garcia-Cabezas MA, John YJ, Barbas H, Zikopoulos B. Distinction of Neurons, Glia and Endothelial Cells in the Cerebral Cortex: An Algorithm Based on Cytological Features. Frontiers in neuroanatomy. 2016;10:107.
437. Branley HM, du Bois RM, Wells AU, Jones HA. Peripheral-type benzodiazepine receptors in bronchoalveolar lavage cells of patients with interstitial lung disease. Nuclear medicine and biology. 2007;34(5):553-8.
438. Takaya S, Hashikawa K, Turkheimer FE, Mottram N, Deprez M, Ishizu K, et al. The lack of expression of the peripheral benzodiazepine receptor characterises microglial response in anaplastic astrocytomas. Journal of neuro-oncology. 2007;85(1):95-103.
439. Graham A. Mitochondrial regulation of macrophage cholesterol homeostasis. Free radical biology & medicine. 2015;89:982-92.

440. Auwerx J. The human leukemia cell line, THP-1: a multifacetted model for the study of monocyte-macrophage differentiation. Experientia. 1991;47(1):22-31.
441. Frede S, Stockmann C, Freitag P, Fandrey J. Bacterial lipopolysaccharide induces HIF-1 activation in human monocytes via p44/42 MAPK and NF-kappaB. The Biochemical journal. 2006;396(3):517-27.
442. Han J, Hajjar DP, Tauras JM, Feng J, Gotto AM, Jr., Nicholson AC. Transforming growth factor-beta1 (TGF-beta1) and TGF-beta2 decrease expression of CD36, the type B scavenger receptor, through mitogen-activated protein kinase phosphorylation of peroxisome proliferator-activated receptor-gamma. Journal of Biological Chemistry. 2000;275(2):1241-6.
443. Wong ML, Medrano JF. Real-time PCR for mRNA quantitation. BioTechniques. 2005;39(1):75-85.
444. Mahmood T, Yang PC. Western blot: technique, theory, and trouble shooting. North American journal of medical sciences. 2012;4(9):429-34.
445. Smith PK, Krohn RI, Hermanson GT, Mallia AK, Gartner FH, Provenzano MD, et al. Measurement of protein using bicinchoninic acid. Analytical biochemistry. 1985;150(1):76-85.
446. Narayan N, Mandhair H, Smyth E, Dakin SG, Kiriakidis S, Wells L, et al. The macrophage marker translocator protein (TSPO) is down-regulated on pro-inflammatory 'M1' human macrophages. PloS one. 2017;12(10):e0185767.
447. Lacerte P, Brunet A, Egarnes B, Duchêne B, Brown JP, Gosselin J. Overexpression of TLR2 and TLR9 on monocyte subsets of active rheumatoid arthritis patients contributes to enhance responsiveness to TLR agonists. Arthritis Research and Therapy. 2016;18:10.
448. Harberts E, Datta D, Chen S, Wohler JE, Oh U, Jacobson S. Translocator protein 18 kDa (TSPO) expression in multiple sclerosis patients. Journal of neuroimmune pharmacology. 2013;8(1):51-7.
449. Shi C, Pamer EG. Monocyte recruitment during infection and inflammation. Nature reviews Immunology. 2011;11(11):762-74.
450. Stansfield BK, Ingram DA. Clinical significance of monocyte heterogeneity. Clinical and Translational Medicine. 2015;4:5.
451. Rossol M, Kraus S, Pierer M, Baerwald C, Wagner U. The CD14(bright) CD16+ monocyte subset is expanded in rheumatoid arthritis and promotes expansion of the Th17 cell population. Arthritis and rheumatism. 2012;64(3):671-7.
452. Davies LC, Jenkins SJ, Allen JE, Taylor PR. Tissue-resident macrophages. Nature immunology. 2013;14(10):986-95.
453. Schweitzer PJ, Fallon BA, Mann JJ, Kumar JS. PET tracers for the peripheral benzodiazepine receptor and uses thereof. Drug discovery today. 2010;15(21-22):933-42.
454. Bernards N, Pottier G, Theze B, Dolle F, Boisgard R. In vivo evaluation of inflammatory bowel disease with the aid of muPET and the translocator protein 18 kDa radioligand [18F]DPA-714. Molecular Imaging and Biology. 2015;17(1):67-75.
455. Lamare F, Hinz R, Gaemperli O, Pugliese F, Mason JC, Spinks T, et al. Detection and quantification of large-vessel inflammation with 11C-(R)-PK11195 PET/CT. Journal of nuclear medicine. 2011;52(1):33-9.
456. Zavala F, Lenfant M. Peripheral benzodiazepines enhance the respiratory burst of macrophage-like P388D1 cells stimulated by arachidonic acid. International journal of immunopharmacology. 1987;9(3):269-74.

457. Taylor JM, Allen AM, Graham A. Targeting mitochondrial 18 kDa translocator protein (TSPO) regulates macrophage cholesterol efflux and lipid phenotype. Clinical science. 2014;127(10):603-13.
458. Tall AR, Yvan-Charvet L. Cholesterol, inflammation and innate immunity. Nature reviews Immunology. 2015;15(2):104-16.
459. Niyonzima N, Samstad EO, Aune MH, Ryan L, Bakke SS, Rokstad AM, et al. Reconstituted High-Density Lipoprotein Attenuates Cholesterol Crystal-Induced Inflammatory Responses by Reducing Complement Activation. Journal of immunology. 2015;195(1):257-64.
460. Fessler MB, Parks JS. Intracellular lipid flux and membrane microdomains as organizing principles in inflammatory cell signaling. Journal of immunology. 2011;187(4):1529-35.
461. Olsson S, Sundler R. The role of lipid rafts in LPS-induced signaling in a macrophage cell line. Molecular immunology. 2006;43(6):607-12.
462. Phillips MC. Molecular mechanisms of cellular cholesterol efflux. Journal of Biological Chemistry. 2014;289(35):24020-9.
463. Zhu X, Lee JY, Timmins JM, Brown JM, Boudyguina E, Mulya A, et al. Increased cellular free cholesterol in macrophage-specific Abca1 knock-out mice enhances pro-inflammatory response of macrophages. J Biol Chem. 2008;283(34):22930-41.
464. Yvan-Charvet L, Welch C, Pagler TA, Ranalletta M, Lamkanfi M, Han S, et al. Increased inflammatory gene expression in ABC transporter-deficient macrophages: free cholesterol accumulation, increased signaling via toll-like receptors, and neutrophil infiltration of atherosclerotic lesions. Circulation. 2008;118(18):1837-47.
465. Zhu X, Owen JS, Wilson MD, Li H, Griffiths GL, Thomas MJ, et al. Macrophage ABCA1 reduces MyD88-dependent Toll-like receptor trafficking to lipid rafts by reduction of lipid raft cholesterol. Journal of lipid research. 2010;51(11):3196-206.
466. Venkateswaran A, Laffitte BA, Joseph SB, Mak PA, Wilpitz DC, Edwards PA, et al. Control of cellular cholesterol efflux by the nuclear oxysterol receptor LXR alpha. Proceedings of the National Academy of Sciences of the United States of America. 2000;97(22):12097-102.
467. Allen AM, Taylor JM, Graham A. Mitochondrial (dys)function and regulation of macrophage cholesterol efflux. Clinical science. 2013;124(8):509-15.
468. Zheng J, Boisgard R, Siquier-Pernet K, Decaudin D, Dolle F, Tavitian B. Differential expression of the 18 kDa translocator protein (TSPO) by neoplastic and inflammatory cells in mouse tumors of breast cancer. Molecular pharmaceutics. 2011;8(3):823-32.
469. Miettinen H, Kononen J, Haapasalo H, Helen P, Sallinen P, Harjuntausta T, et al. Expression of peripheral-type benzodiazepine receptor and diazepam binding inhibitor in human astrocytomas: relationship to cell proliferation. Cancer research. 1995;55(12):2691-5.
470. Datta G, Colasanti A, Kalk N, Owen DR, Scott G, Rabiner EI, et al. [11C]PBR28 or [18F]PBR111 detect white matter inflammatory heterogeneity in multiple sclerosis. Journal of nuclear medicine. 2017.
471. Chaudhari AJ, Bowen SL, Burkett GW, Packard NJ, Godinez F, Joshi AA, et al. High-resolution (18)F-FDG PET with MRI for monitoring response to treatment in rheumatoid arthritis. European Journal of Nuclear Medicine and Molecular Imaging. 2010;37(5):1047.

472. The royal college of radiologists. Evidence Based Indications for the use of PET-CT in the UK 2016 (accessed 30th June 2017). Available from: https://rcr/ac/uk/publication/evidence-based-indications-use-pet-ct-united-kingdom-2016
473. Gordon S, Pluddemann A, Martinez Estrada F. Macrophage heterogeneity in tissues: phenotypic diversity and functions. Immunological reviews. 2014;262(1):36-55.
474. Leipold MD, Newell EW, Maecker HT. Multiparameter Phenotyping of Human PBMCs Using Mass Cytometry. Methods in molecular biology (Clifton, NJ). 2015;1343:81-95.
475. Roussel M, Ferrell PB, Jr., Greenplate AR, Lhomme F, Le Gallou S, Diggins KE, et al. Mass cytometry deep phenotyping of human mononuclear phagocytes and myeloid-derived suppressor cells from human blood and bone marrow. Journal of Leukocyte Biology. 2017.
476. Hatori A, Yui J, Yamasaki T, Xie L, Kumata K, Fujinaga M, et al. PET Imaging of Lung Inflammation with [(18)F]FEDAC, a Radioligand for Translocator Protein (18 kDa). PloS one. 2012;7(9):e45065.
477. Tabas I, Bornfeldt KE. Macrophage Phenotype and Function in Different Stages of Atherosclerosis. Circulation research. 2016;118(4):653-67.
478. Borthwick F, Taylor JM, Bartholomew C, Graham A. Differential regulation of the STARD1 subfamily of START lipid trafficking proteins in human macrophages. FEBS letters. 2009;583(7):1147-53.
479. Selvaraj V, Stocco DM, Tu LN. Minireview: Translocator Protein (TSPO) and Steroidogenesis: A Reappraisal. Molecular Endocrinology. 2015;29(4):490-501.
480. Wang D, Li Y, Liu Y, Shi G. The role of autoreactive T cell in the pathogenesis of rheumatoid arthritis and implications for T cell targeted vaccine therapy. Minerva medica. 2015;106(3):157-67.
481. Ahmed FE. Quantitative Real-time RT-PCR: Application to Carcinogenesis. Cancer Genomics-Proteomics. 2005;2(6):317-32.

APPENDIX

A1. Publications and Presentations

Publications:

***Narayan N**, Owen DR, Taylor PC.* Advances in positron emission tomography for the imaging of rheumatoid arthritis. *Rheumatology*. 2017 (epub ahead of print) https://www.ncbi.nlm.nih.gov/pubmed/28181650

Owen DR, **Narayan N***, Wells L, Healy L, Smyth E, Rabiner EA, Galloway D, Williams JB, Lehr J, Mandhair H, Peferoen LA, Taylor PC, Amor S, Antel JP, Matthews PM, Moore CS.* Pro-inflammatory activation of primary microglia and macrophages increases 18 kDa translocator protein expression in rodents but not humans. *J Cereb Blood Flow Metab* (epub ahead of print) https://www.ncbi.nlm.nih.gov/pubmed/28530125
*=joint first authors.

***Narayan N,** Mandhair H, Smyth E, Dakin SG, Kiriakidis S, Wells L, Owen D, Sabokbar A and Taylor PC.* The macrophage marker translocator protein (TSPO) is downregulated on pro-inflammatory 'M1' human macrophages. *PLoS One* 2017. 12(10); e0185767.
http://journals.plos.org/plosone/article?id=10.1371/journal.pone.0185767

***Nehal Narayan,** David R Owen, Harpreet Mandhair, Erica Smyth, Francesco Carlucci, Azeem Saleem, Roger N Gunn, Eugenii A. Rabiner, Lisa Wells, Stephanie G Dakin, Afsie Sabokbar, Peter C. Taylor.* Translocator protein as an imaging marker of macrophage and stromal activation in RA pannus. *Accepted for publication in J Nucl Med November 2017.*

Presentations:

***Narayan N,** Mandhair H, Coello C, Wells L, Owen D, Saleem A, Sabokbar A, Taylor PC.* Macrophage Targeted Positron Emission Tomography (PET) for the Imaging of Inflammatory arthritis; an in vivo and in vitro investigation of translocator protein (TSPO) tracer uptake and target expression in human pannus. Abstract accepted for EULAR 2017 (Madrid).

***Narayan N,** Saleem A, Mandhair H, Coello C, Sabokbar A, Taylor PC.* Poster presentation and poster tour at British Society of Rheumatology (BSR) 2017 (Birmingham): The translocator protein as an imaging biomarker of inflammatory arthritis

***Narayan N**, Carlucci F, Coello C, Wells L, Owen D, Sabokbar A and Taylor PC.* Poster presentation at Academy of Sciences Spring meeting 2017 for trainee academic clinicians (London) (poster competition); An investigation of the translocator protein as an imaging tool for arthritis.

***Narayan N,** Carlucci F, Coello C, Saleem A, Dakin S, Sabokbar A and Taylor PC.* Poster presentation at ACR 2016 (Washington): An investigation of the Translocator protein as a marker of disease activity in inflammatory arthritis.

Narayan N, *Coello C, Saleem A, Taylor PC.* Poster presentation at BSR 2016 (Glasgow): Macrophage targeted PET for rheumatoid arthritis; results of a pilot study.

A2. Summary of study design and approval processes

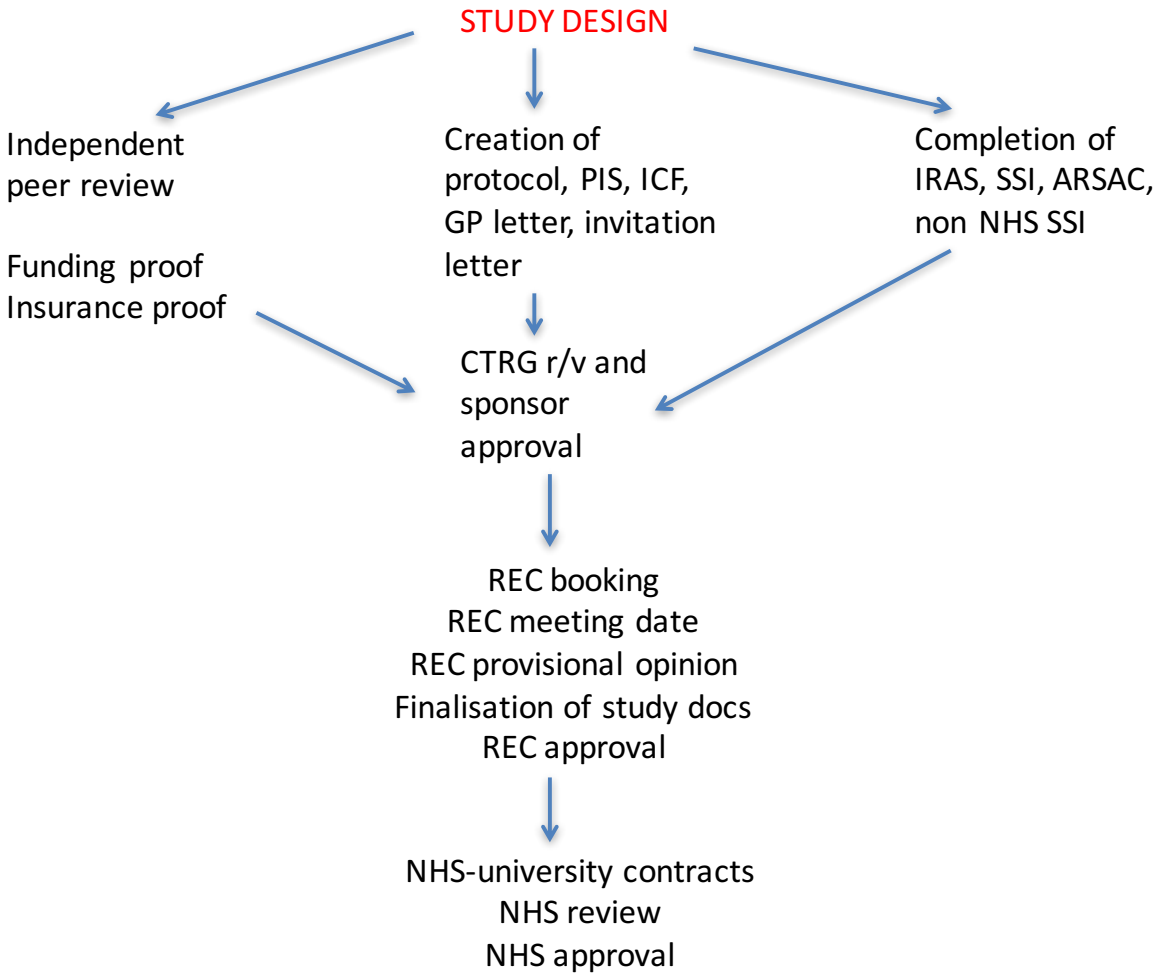

A3. Real-time PCR

The technique involves thermal cycling, consisting of cycles of rapid heating and cooling to optimal temperatures for the reaction for DNA melting and enzymatic replication. As PCR progresses, the DNA generated is itself acting as a template for replication, setting in motion a chain reaction in which the DNA template is exponentially amplified {Kubista, 2006 #131}. A PCR reaction requires a buffer containing deoxynucleotide triphosphates (dNTPs), one pair of primers specific to the DNA fragment to be amplified, DNA polymerase and the DNA strand of interest. Primers are oligonucleotides containing sequences complementary to the 3' end of each sense and antisense strand of the DNA of interest. Primers are required to initiate the generation of new DNA fragments. The DNA polymerase used is almost always heat stable. By using the separated single-stranded DNA of interest as a template, DNA polymerase enzymatically builds up a new complementary DNA strand from the dNTPs {Kubista, 2006 #131}.

In general, there are 3 stages in a PCR cycle:

1. *Denaturation*- the DNA strand of interest is heated to 95°C to separate the strands.
2. *Annealing*- specific primers will anneal into the complementary regions in the DNA of interest at a temperature calculated from the melting temperature, forming a double strand (usually between 50°C-60°C).
3. *Elongation*- a complementary DNA strand will be formed with a thermostable DNA polymerase at 72°C.

The entire cycle is then repeated by incubating the newly created DNA strands at 95°C to separate the DNA double strands (denaturation), followed by primers annealing and DNA elongation. With each cycle, there is exponential amplification of the target DNA sequence, which will then be used for further analysis.

Figure A1 represents a typical amplification plot of a real-time PCR reaction. This demonstrates a linear ground phase (initiation phase), which usually encompasses the first 15-20 cycles, which reflects background fluorescence, as during this time, the amount of PCR product is very small. Following this is an early exponential phase, where fluorescence reaches a threshold (usually 10 times the standard deviation of the baseline) as there is exponential production of the desired fragment. The cycle at which this occurs is known as the threshold cycle (C_t). This value reflects the starting copy number in the original template and is used to calculate the experiment results {AHMED, 2005 #133}. During the exponential phase, PCR reaches its optimal amplification potential, with the PCR product doubling after every cycle in ideal reaction conditions. The final plateau stage is reached when the reaction components then become limited, fall in polymerase activity, and competition with PCR products, so that the fluorescence intensity is no longer useful for data calculation.

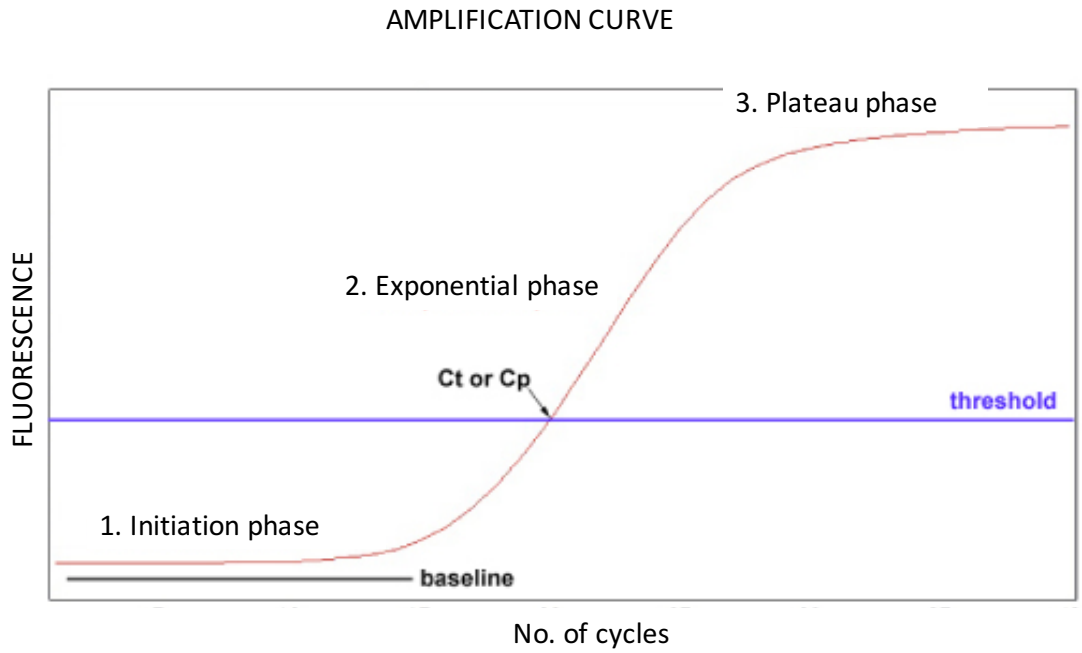

Figure A1: Demonstration of different phases of the PCR amplification plot; adapted from Ahmed *et al.* 2005 (481). C_t=cycle threshold.

Quantitative PCR can be used for absolute and relative DNA and RNA quantification. Absolute quantification uses serially diluted standards of known concentration to create a standard curve. This standard curve produces a linear relationship between C_t and initial amount of nucleic acid in order to determine absolute concentration. Therefore, measuring the C_t values of the study sample in parallel with the standards enables the determination of their absolute concentration. However, this method assumes that the standards and samples have approximately equal amplification efficiencies.

Relative quantification measures changes in sample gene expression in relation to a calibration, or reference sample (an untreated control, or time zero samples), and results are expressed as a target to reference ratio. In the case of this study, absolute nucleic acid concentrations are not particularly relevant; the change in expression relative to untreated or time zero samples is of interest. Hence we utilised a relative quantification method, always including an untreated or time zero control in our PCR plate with which to compare other samples.

In this study, the thermocycler ViiA^{TM} 7 Real-Time PCR System (Applied Biosystems, Paisley UK) was used to perform Real-Time quantitative PCR. The thermocycler uses a sensitive camera to detect the fluorescence in each well of the PCR plate during reaction. The fluorescence detection chemistry used was the SYBR® Green I, which emitted fluorescence when bound to dsDNA.

The fluorescence intensity increases proportionally to dsDNA concentration, which accumulates during the PCR. SYBR® Green I bound to any dsDNA and therefore was not specific to a particular DNA sequence. It has the advantage that one dye could be

used for various gene assays. However, its non-sequence specific property also has the disadvantage of being prone to false positives. Therefore, the end products were checked with dissociation curve analysis, where the presence of different PCR products was reflected in the number of first-derivative melting peaks. The dissociation curve analysis was performed automatically by the thermocycler.

A4 Positive controls for staining

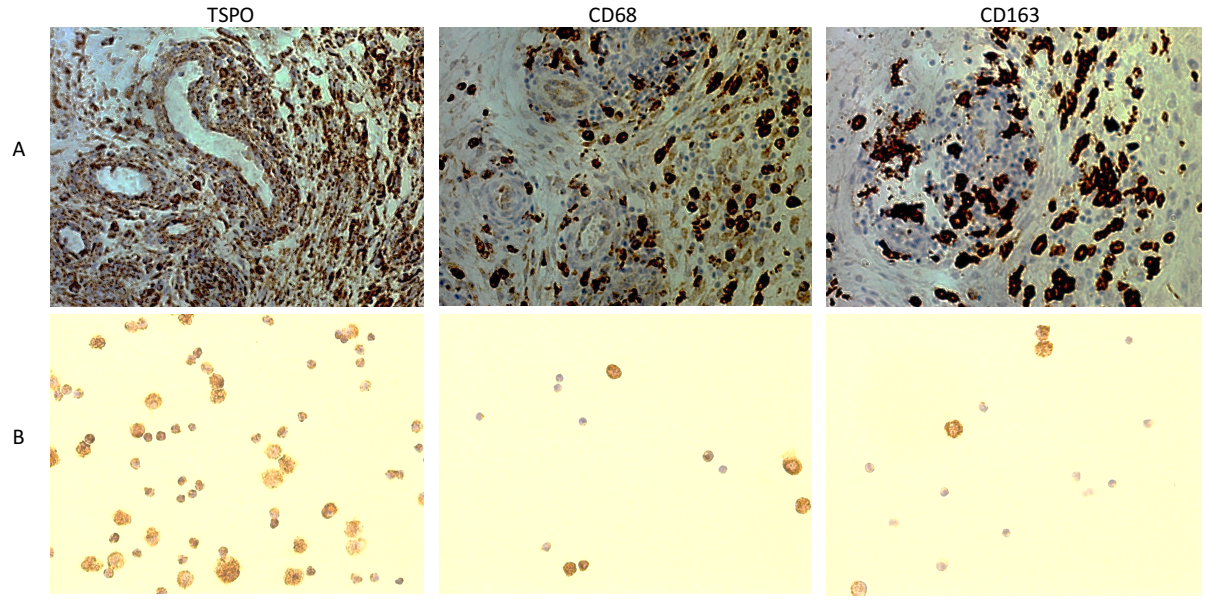

Figure A2: Positive control staining for TSPO (1:10,000), CD68 (1:4000), CD163 (1:2000) in **A**: knee synovial tissue from synovectomy of RA patient PET10 **B:** cytospin slides of macrophages generated *in vitro* (as described in **Chapter 4**) by culture of healthy monocytes with M-CSF for 7 days. X400 magnification

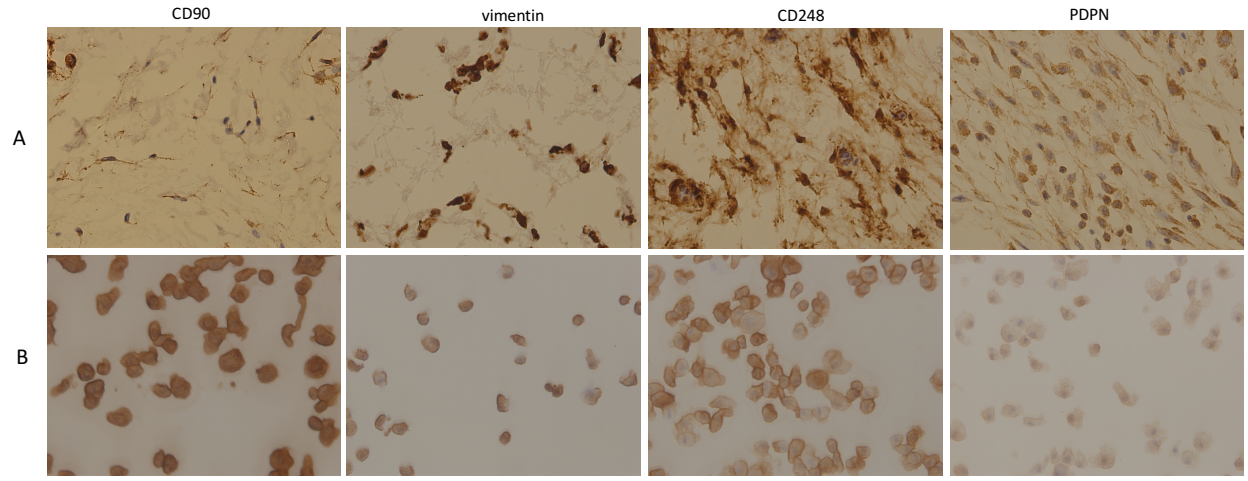

Figure A3: Positive control staining for CD90 (1:25), vimentin (1:800), CD248 (1:2000), PDPN (1:1000). **A**: knee synovial tissue from synovectomy of RA patient PET10 **B**: cytospin slides of unstimulated *in vitro* cultured FLS x400 magnification.

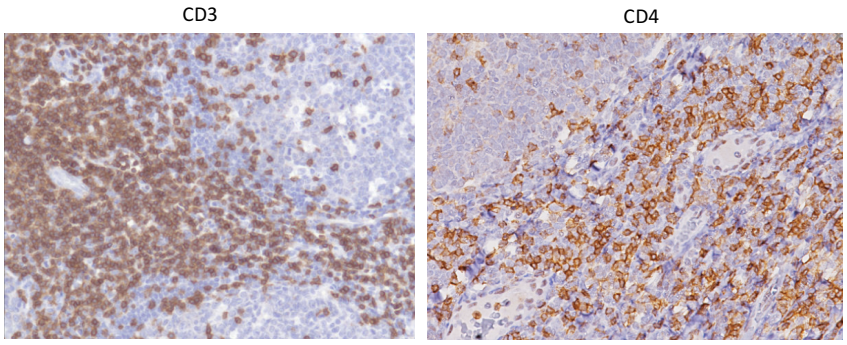

Figure A4: Positive control staining for CD3 (1:50) and CD4 (1:400), using healthy tonsillar tissue. X400 magnification

A5 Optimisation of autoradiography

Example of [^{3}H]PBR28 radioligand saturation binding curves, that estimated binding affinity K_d for macrophages, fibroblasts and lymphocytes, was used to identify a likely set of optimal [^{3}H]PBR28 concentrations to use for autoradiography.

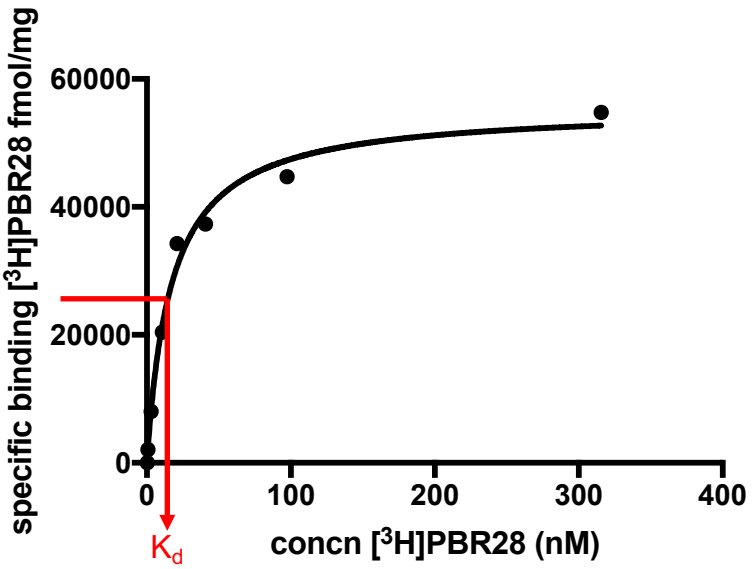

Figure A5: Representative example of radioligand saturation binding curve of in vitro data generated for macrophages, used along with radioligand saturation binding curves for FLS and lymphocytes to generate estimates for optimal radioligand concentration for synovial tissue autoradiography.